Rhodium(III) Supramolecular Complexes: Synthesis, DNA Binding and Biological Studies

UNIVERSITY OF BIRMINGHAM

Susana Ricardo Vitorino

A thesis submitted in partial fulfillment of the requirements for the degree of

Doctor of Philosophy in Chemistry

University of Birmingham, School of Chemistry

February 2011

To my parents, my Sister and to André, for their unconditional Love and support throughout this journey.

Aos meus pais, irmã e ao André pelo amor e apoio incondicional.

Acknowledgements

My first words of acknowledgment are dedicated to the ones without whom I would not have arrived here. To my parents, for my education, the unconditional love and support in each step of the way. A special thanks to my mum, for the endless phone calls and emails with words of strength and support, for sharing with me the happiness of each good achievement and the sadness and frustration of the non existent ones. For not allowing me to quit at any time and specially for reminding me that being strong and brave in life goes far beyond from finishing a PhD. To my sister, for always being there in each moment of my life in such a beautiful way with words of support, and for the infinite airport trips in these 4 years. A sweet word of acknowledgment to my grandparents that without understanding very well what was I doing all this time, were always present, supporting me no matter what. To my caring family in general that made each trip back home being always a great moment, to my aunt Getta a special thanks for the years of dedication and friendship. To Andre, beyond doubt my true Chemistry! For the fourteen years of love and dedication. For being my friend, my confident, for making me laugh when I so much needed it, for the many tough words of wisdom that made me grow up in so many ways, and simply for being there.

To Goncalo and Filipa, my Portuguese-Osforde best friends. Each moment of this PhD, definitely has a bit of each of you. For all the trips between Birmingham and Oxford, the dinners, the shopping moments, the naps on the sofa on sunday afternoons, the nonsense jokes, the chemistry discussions and advices, the phone calls, for bearing my hyperventilation moments, for being always so good with me in this ten years of friendship and for all the great moments spent together.

I would like to thank my supervisor Prof. Michael J. Hannon for letting me be part of his group. I am truly grateful for his guidance, enthusiasm, and support and for sharing ideas throughout these 4 years.

I consider myself very lucky for the opportunity I had to meet such amazing and good people here in Birmingham. To all of you, you know who you are, a special thanks for all the good moments shared. Nevertheless some of this people marked my life in a very special way. Lucia, for her true and amazing friendship, the good and the bad moments, the laughs and the tears, for being my cinema buddy and for the pasta….yes the pasta! Carlos, I am so happy your attempts to sell me failed, having you around was always such a comfort. My Cosimo, my dear sweet Cosimo, thank you for bearing me, making me believe in myself all the time, for your loyal friendship and for all we shared during your

stay in Birmingham, indeed, in fact was a pleasure! Luca, my friend, my "platonic Love" thanks for all the chemistry after the meals!!!! Alessio, always so positive and enthusiastic, thank you for all your help! Fran, for being such a nice and enthusiastic housemate and especially for her relentless friendship and all efforts to improve my knowledge of English vocabulary! My pipi Bene, Bick, Giorgio (Mr.PIA) and Pete, I could not have been luckier with my last flatmates during my final stay in Birmingham! Having you guys always around in these hard 6 months, all our meals, Bick's amazing oriental food, made this stage of the PhD so much bearable. Thank you so much for coping with me and for the joyful times! Antoine and Myrto, you were such a beautiful surprise in my life in this last year in Birmingham; Myrto your help in these last days was unbelievable precious! To Ornella for the immense support throughout this time.

I must also thank all the people in the Hannon group. To past members of the group, Dr. Anna Hotze and Dr. Dusan Drahonovsky for the several emails sharing ideas and valuable advises. A special thanks to Laura, Victoria and Cosimo for their kind collaboration in some parts of the work presented in this thesis. To "the girls" my sincere best wishes for concluding your PhD's.

I would like to thank all the people in the Analytical facilities at the School of Chemistry, a special word to Dr Neil Spencer and Peter Ashton, for their patience and availability to help and teach me. To Dr. Louise Male, for solving the X-ray structures presented in this thesis and for being always so helpful and supportive during my great fight for crystals! To Ian Bodfish, for standing me and my rush with the chemicals orders and all my Amazon cooking books purchases. To Graham Burns, not only for all he taught me about HPLC and his immense help and support but for all the nice countryside pubs lunches. Also, for together with Janet receiving me in their house, and making each dinner feel like home. No words to thank both of you for these last 4 years!

Big thanks to all my friends in Portugal, specially to Vanessa and Cajo, Susana, Claudia, Raquel, Sandra B., Alexandra and Antonio, for making me feeling always so welcome every time I went back. To Ze Beirao, my sweet absent but always there friend! To Regina and Ne for so many things!

Finally, I would like to thank to the EU DNAREC Marie Curie Training Site (MEST-CT-2005-020842, C.D. and A.L.) and the University of Birmingham for funding.

Declaration

The experimental work, observations and recommendations reported in this thesis are those of the author unless specifically stated and have not previously been submitted as part of a degree at the University of Birmingham or any other institution.

Contents

Chapter 2. Novel Rhodium (III) Complexes: *Design, Synthesis and Characterization.*

Chapter 3. DNA Binding Studies:

Chapter 4. Biological Activity and PCR Studies of Rh(III) Complexes

Chapter 5. Conclusions and Future Work

Abbreviations

3WJ	Three way junction
4WJ	Four way Junction
Å	Angstroms (1x10-10 m)
A2780	Ovarian Cancer Cell Line
bpy	2,2'-bipyridine
bp	base pairs
br	broaden
CD	Circular Dichroism
CD_3CN	Acetonitrile-*d3*
CD_3OD	Methyl-*d*3 alcohol-*d*
chrysi	Chrysene-5,6-quinone diimine
COSY	Correlation Proton Nuclear Magnetic Resonance
ct	calf thymus
d	doublet (in NMR data)
DCM	Dichloromethane
dd	double doublet (in NMR data)
DMEM	Dulbecco's modified Eagle's medium
DNA	Deoxyribonucleic acid
Δ	Delta- symmetry descriptor for chiral complexes
ε	Extinction coefficient ($dm^3\ mol^{-1}\ cm^{-1}$)
DIP	4,7-diphenyl- 1,10-phenanthroline
DMSO	Dimethyl sulfoxide
dppz	Dipyrido[3,2-a:2',3'-c]phenazine
dpq	dipyrido[3,2-d:2′,3′-f]quinoxaline
dpp	2,3'-bis(2-pyridyl)pyrazine
dppn	3,6-bis (2′-pyridyl) pyridazine
D_2O	Deuterium oxide
dt	double triplet
EDTA	Ethylenediaminetetracetic acid
EI-MS	Electronic Impact Mass Spectrometry

ESI-MS	Electrospray Ionisation Mass Spectrometry
Et_2O	Diethyl ether
EtOAc	Ethyl Acetate
EtOH	Ethanol
FBS	Foetal bovine serum
HEPES	4-(2-hydroxyethyl)-1-piperazineethanesulfonic acid
HSQC	Heteronuclear Single Quantum Coherence
Hz	Hertz
^{i}PrOH	Isopropanol
IC_{50}	Half maximal inhibitory concentration
ICD	Induced Circular Dichroism
ILD	Induced Linear Dichroism
J	NMR- coupling constant
° C	Degrees Celsius
λ_{max}	maximum of wavelength
LD	Linear Dichroism
Λ	Lambda- symmetry descriptor for chiral complexes
m	multiplet (in NMR data)
MDA-MB-231	Breast Cancer cell Line
MeOH	Methanol
MLCT	Metal to Ligand Charge Transfer
M	Molar (mol dm^{-3})
m/z	Mass spectrometry- mass/charge
mM	milli-molar concentration (1x10 mol dm^{-3})
MTT	3-(4,5-Dimethylthiazol-2-yl)-2,5-diphenyltetrazolium bromide
NMR	Nuclear Magnetic Resonance
phen	1,l0-phenanthroline
phi	9,l0-phenanthrenequinone diimine
phzi	benzo[*a*]phenazine-5,6-quinone diimine
PBS	Phosphate Buffered Saline
PCR	Polymerase Chain Reaction
PNA	Peptide Nucleic Acid
ppm	parts per million

pyr	pyridine
RNA	Ribonucleic acid
RP-HPLC	Reverse Phase High Performance Liquid Chromatography
rt	Room Temperature
RT	Retention time
s	singlet (NMR data)
t	triplet (in NMR data)
td	triple doublet (in NMR data)
tpy	2, 2'; 6',2''-terpyridine
TFA	Trifluoroacetic acid
TRISPHAT	*tris*(tetrachlorobenzenediolato) phosphate(V)
tpphz	tetrapyrido[3,2-a:2′,3′c:3″,2″,-h:2‴,3‴-j]phenazine)
UV-vis	Ultraviolet-visible spectroscopy
vt	variable temperature
δ	NMR- chemical shift

Abstract

The work described in this thesis concerns the synthesis, DNA binding and cytotoxicity studies of new Rh(III) supramolecular complexes.

Chapter 1 reviews DNA molecular recognition by synthetic agents; exploring the different DNA binding modes and their importance in the anticancer properties of several metallodrugs. Special attention is given to the exciting cylinder agents, which underpin the work in this thesis and to the work with rhodium complexes and their studies with DNA and as anticancer drugs.

Chapter 2 describes the synthesis, purification and characterization of Rh(III) mononuclear, dinuclear single, double and triple stranded complexes. NMR, MS, UV-Vis, elemental analyses and in some cases X-ray crystallography are discussed in detail.

In Chapter 3, DNA binding properties of the Rh(III) complexes are explored by CD and LD spectroscopy. Gel Electrophoresis experiments are also carried out using plasmid DNA (pBR322). The dinuclear complexes are found to bind to ct-DNA and to have more dramatic effects than the mononuclear analogues. In addition they were found to cleave plasmid DNA.

Chapter 4 presents cytotoxicity studies for some of the complexes synthesized against breast and ovarian cancer cell lines. A PCR study with the Rh(III) double stranded isomers is also carried out demonstrating that these complexes are able to inhibit and block DNA transactions as represented by PCR DNA replication.

Chapter 1

Introduction

Deoxyribonucleic acid (DNA) contains all the genetic information that codes for ribonucleic acid (RNA) and proteins that are essential for cell function.[1] The mechanism of how cells differentiate does not depend on the different information on the DNA contained in each cell but rather on the differences in how the information is read or accessed. Genetic information is accessed using ensembles of non-covalent binding interactions between proteins and DNA sites and leading to the regulation and further control of gene expression.[1-3] DNA binding and recognition has been widely investigated and explored as a means to control gene expression with the careful design of novel agents that can selectively bind to DNA allowing the discovery of new cancer therapeutics and diagnostic devices.

1.1 Deoxyribonucleic Acid Structure (DNA)

DNA is a polymer of nucleotide units consisting of a ribose sugar, a phosphate and a heterocyclic aromatic base. The information coded in the DNA polymer is displayed in the order or sequence of four different bases: guanine (G), adenine (A), cytosine (C) and thymine (T). Two of these polymeric structures are associated into a double helix via hydrogen bonds formed between the bases. Adenines are associated with thymines and guanines with cytosines in an arrangement referred as DNA base pairs, *Watson-Crick* base pairing (Figure 1.1).[1, 4]

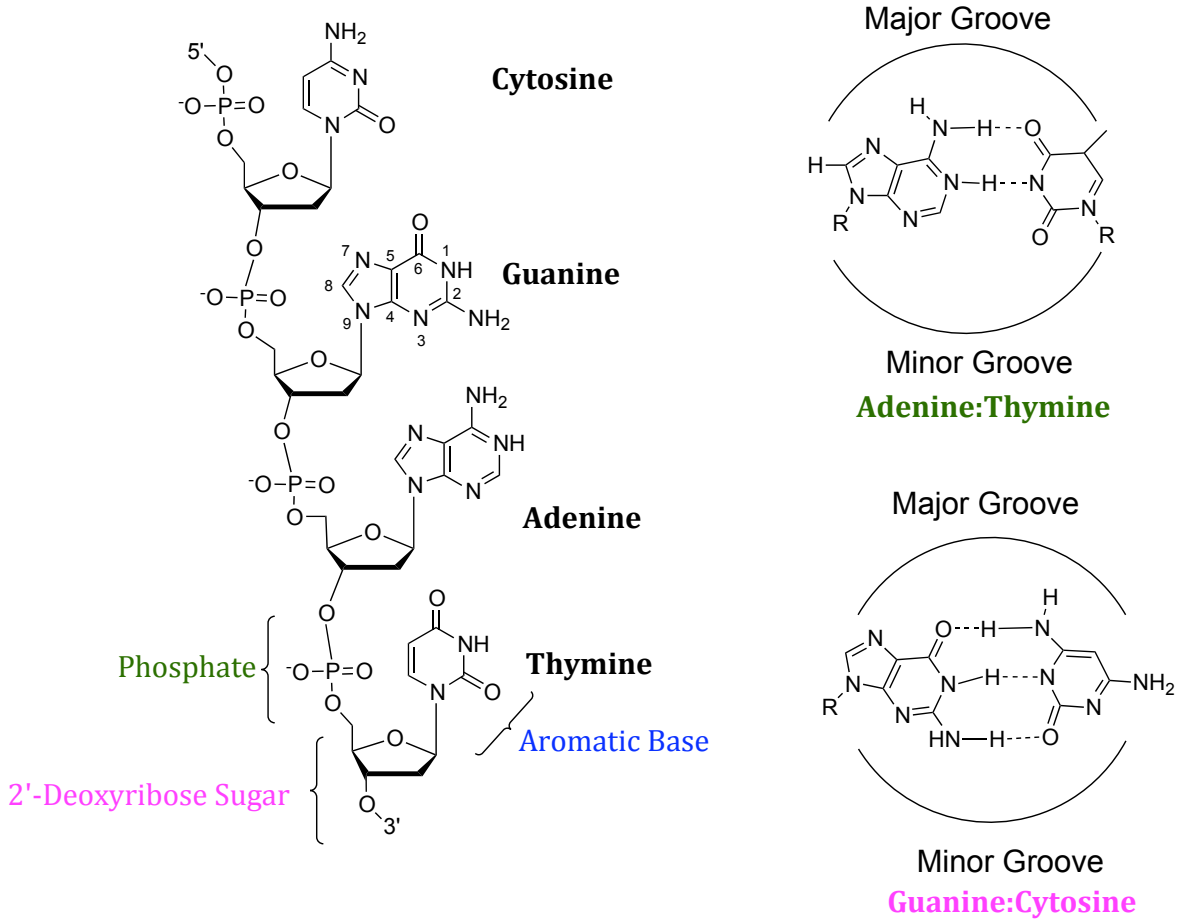

Figure 1.1 DNA building blocks between the DNA bases (left); Major and Minor groove sides of adenine:thymine and guanine:cytosine.

The base pairs are approximately perpendicular to the axis of the double helix and are stacked parallel to each other, forming π-π face-face interactions. In the B-DNA double helix, the base pair combine to form the so-called major and minor grooves (illustrated in Figure 1.1 right). The grooves are different in depth and size. The major groove is wide (12 Å wide) and deep and the minor groove, is deep but narrow (6 Å wide).[4]

There are three different crystallized forms of double helix DNA: A, B and Z-DNA (Figure 1.2).

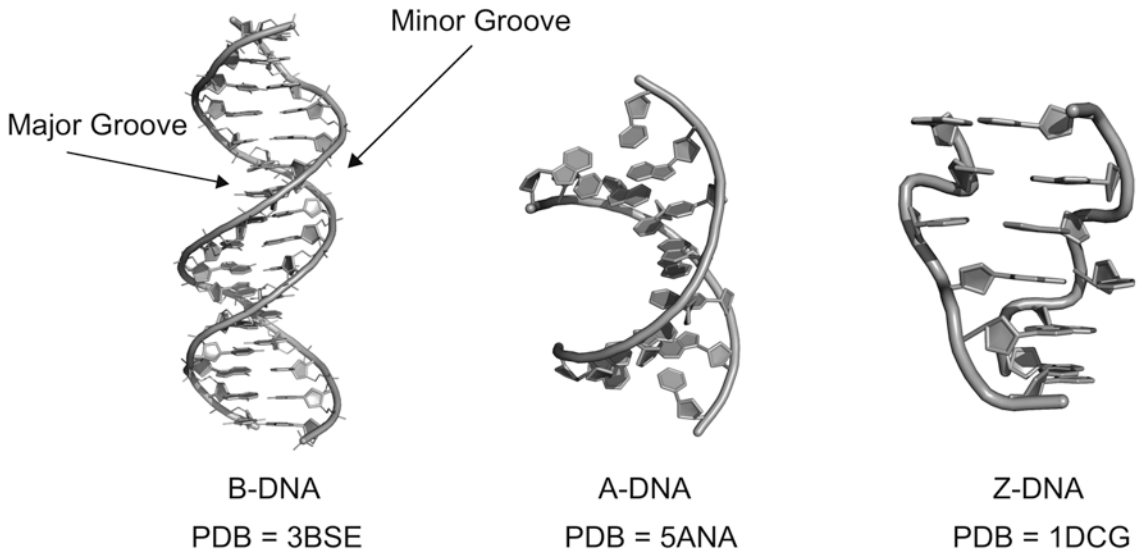

Figure 1.2 Three different double helix DNA structures: A, B and Z-DNA.

The A and B-DNA forms are right-handed helices whilst Z-DNA is left-handed. The B form of double helix DNA is the most prevalent in the biological systems being at least 90% of the DNA in living cells . Z-DNA can also be found in some living cells.[5-7]

Thus the B-DNA double stranded structure is the predominant form of DNA in biological systems. Nevertheless a number of secondary DNA structures different from the Watson-Crick double helix model are known.[5] DNA can adopt different conformations that may be recognized by a reporter molecule and each possess a unique biological role. Three-way and four-way junctions, Y-junctions, triplex and G-quadruplex DNA are some of the common conformations DNA can adopt.[8]

1.2 DNA Recognition

Molecules can recognize DNA by both covalent and non-covalent interactions. Five different modes in which molecules can interact with B-DNA exist. These different modes were recognized in the 60's: major and minor groove binding, intercalation, sugar-backbone binding and finally covalent binding.[2] More recently, a new DNA binding mode was reported: DNA junction binding.[9]

1.2.1 Minor and Major Groove Binding

Non-covalently bound molecules are usually groove binders or intercalators. Minor groove binding molecules possess a complementary size and shape to the minor groove and the binding process is promoted by van der Waals interactions and most of these molecules bind to A-T rich sequences.[10] Some good examples of minor groove binding molecules that were further developed as drugs include distamycin A, diarylamidines such as berenil (used in veterinary medicine), DAPI and pentamidine (Figure 1.3). Some diarylamidines have been shown to be therapeutically useful against protozoal diseases such as *Trypanosome Congolese*.[2, 10, 11] DAPI acts by inhibiting the DNA and RNA polymerase and binds specifically to AT-rich regions of double-stranded DNA (Figure 1.4). Its application *in vivo* is limited due to its side effects, but is commonly used as a blue-fluorescent stain for DNA *in vitro*.[2] Apart from antiprotozoal activity, minor groove binders can also exhibit antiviral and antibacterial properties with some also showing antitumor activity.[2, 10]

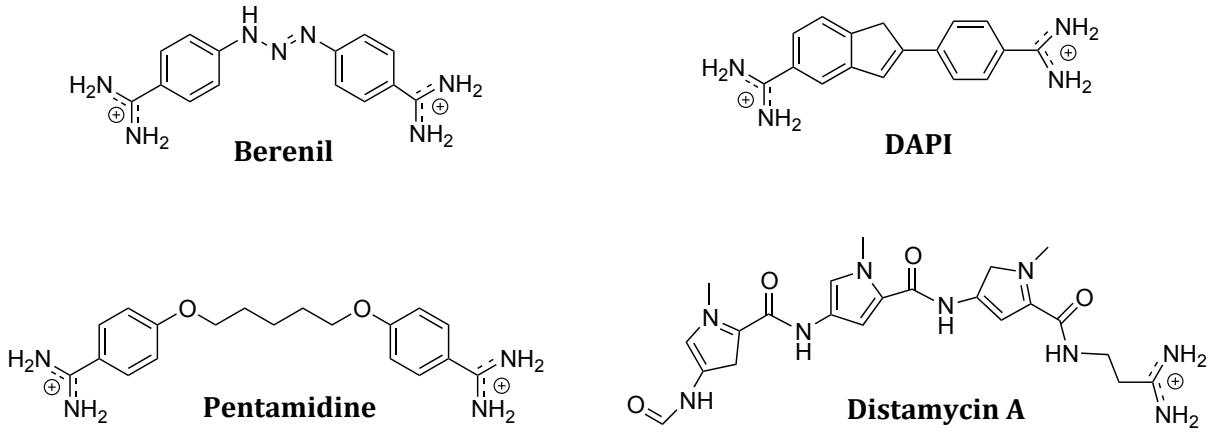

Figure 1.3 Chemical Structures of minor groove binding drugs: Berenil, DAPI Pentamidine and Distamycin A.

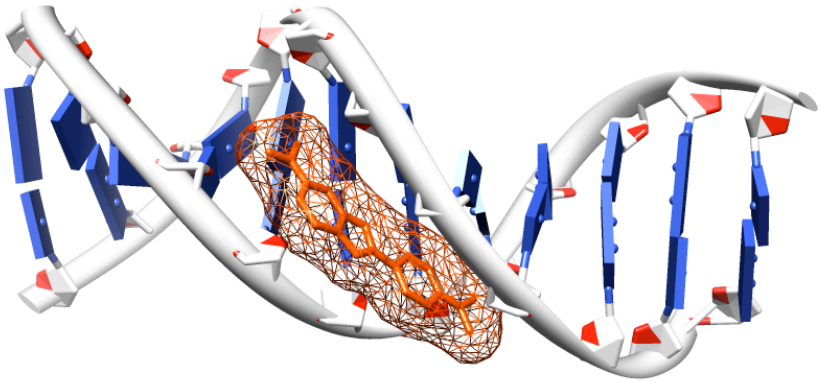

Figure 1.4 View of DAPI when bound to the DNA minor groove (PDB 1D30).

The majority of synthetic and natural drugs, which interact non-covalently with DNA, recognize the DNA minor groove. The major groove is in comparison with the minor groove too big and wide to facilitate a good close with small molecules. Although less studied, major groove recognition has been successfully achieved by synthetic protein motifs, synthetic biomolecules such as oligonucleotides and peptides, and in some cases in combination with minor groove binders.[2]

Most of the protein motifs that recognize DNA have a cylindrical shape and the recognition is usually based on an α helix motif (eg. Zinc fingers, Leucine Zippers or Helix-turn–Helix) that fit snugly into the DNA major groove.[12]

Oligonucleotides bind to DNA major groove forming hydrogen bonds with the purine nucleobases giving rise to pairing motifs named Hoogsteen or reverse Hoogsteen, that results in a triplex DNA. The downside of using synthetic oligonucleotides is related with their negative charge, which electrostatically is a barrier to binding to anionic DNA.

Peptide nucleic acids (PNAs), were first described by Nielsen in the 90's, in order to overcome the drawbacks of the synthetic oligonucleotides.[13] PNAs are synthetic neutral polymers where the sugar backbone of DNA is replaced by repeating N-(2-aminoethyl)-glycine units linked by peptide bonds. The various purine and pyrimidine bases are linked to the backbone by methylene carbonyl bonds (Figure 1.5).[2, 13]

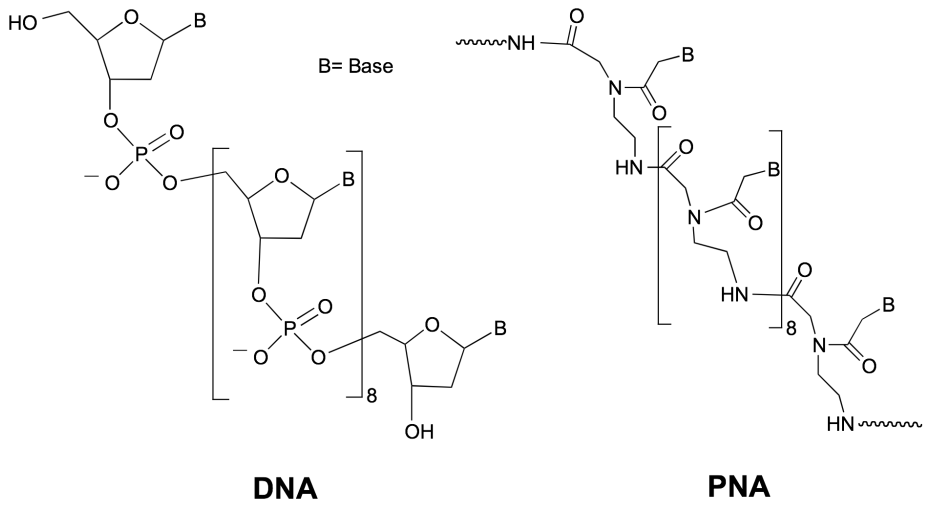

Figure 1.5 Chemical Structure of PNA in comparison with DNA (based on ref[13])

PNAs can bind in the DNA major groove forming triplex DNA. Structures like $(DNA)_2(PNA)$ are formed but the most common way they interact is through displacement of one DNA strands to form a stable $(DNA)(PNA)_2$. The ability of PNAs to bind DNA has been exploited and found many applications in the last two decades as biotechnological tools and in medicine (anticancer, antiviral and antibacterial agents). In addition PNAs have been used together with peptides and oligonucleotides in what remains one of the biggest challenges nowadays: to achieve full selective DNA recognition.[13, 14]

1.2.2 Intercalation

Another mode of DNA recognition is intercalation. It was first proposed by Lerman in the 60's, and it is arguably the most common mode used to design molecules that recognize DNA.[15, 16] This mode involves inserting a planar aromatic molecule between the base pairs forming face-face π-π interactions with the bases below and above. Intercalators can insert into DNA from the major or the minor groove, opening a gap between stacked base pairs causing DNA to unwind. An example of an intercalator molecule in clinical use is the antibiotic doxorubicin which belongs to the anthracycline family and has been widely used as anticancer agent (Figure 1.6 and 1.7).[17] Intercalators can be used as an anticancer agents and also as DNA stains. Ethidium bromide is one of the most important DNA stains used in molecular biology and shows an increase of fluorescence upon intercalation in between the DNA base pairs (Figure 1.6).

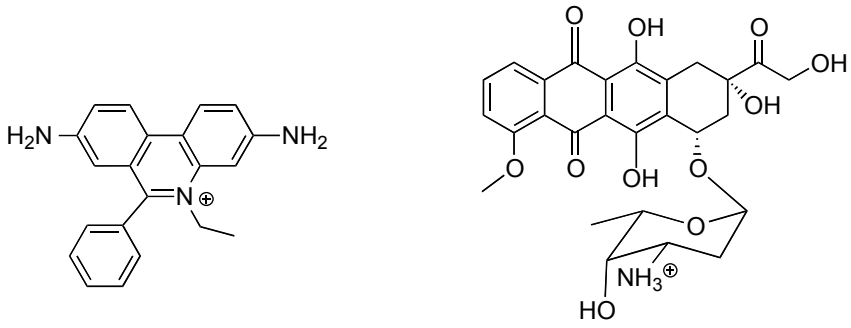

Ethidium **Doxorubicin**

Figure 1.6 Chemical Structures of intercalators: Ethidium and Doxorubicin.

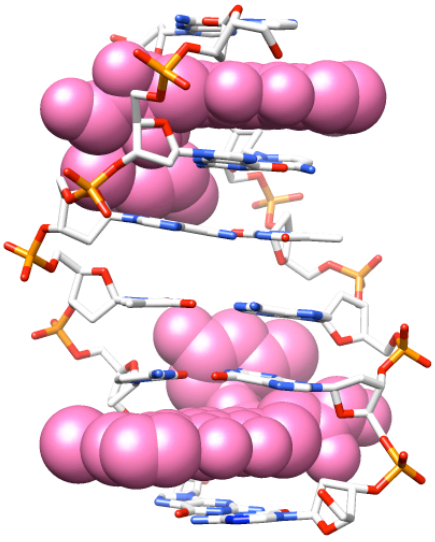

Figure 1.7 View of two molecules Doxorubicin intercalating between the DNA bases pairs (PDB 1D12).

These intercalating agents are normally cationic which enhances the interaction with the negatively charged sugar-phosphate backbone, with resulting electrostatic nteractions making an important contribution to the binding energy. A way to introduce positive charge into an intercalator is to incorporate a transition metal giving raise to a new class of drugs named metallo-intercalators, with the first one (terpyridine Pt(II) $[Pt(tpy)(SCH_2CH_2OH)]^+$) being reported by Lippard and co-workers.[18] Although initial

studies used metals only for charge reasons, soon it was realized that different metals could introduce other properties such as luminescence and DNA cleavage.[19-22]

Barton's group has explored metallo-intercalators containing rhodium and ruthenium centres where the intercalative functionalities are planar bidentate aromatic ligands (phen, phi, bpy, dppz) that can insert into the DNA (Figure 1.8). Figure 1.9 shows an example of a Rh(III) metallo-intercalator with phen as ancillary ligand and phi as the intercalating unit.

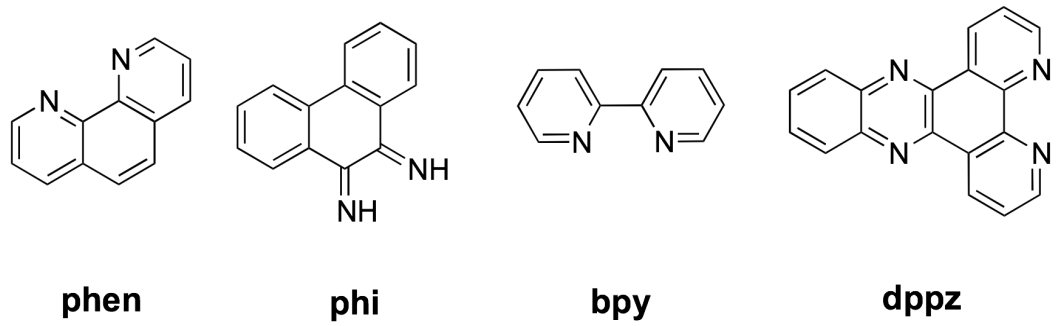

Figure 1.8 Chemical structures of polypyridyl ligands commonly used in metallo-intercalator complexes.

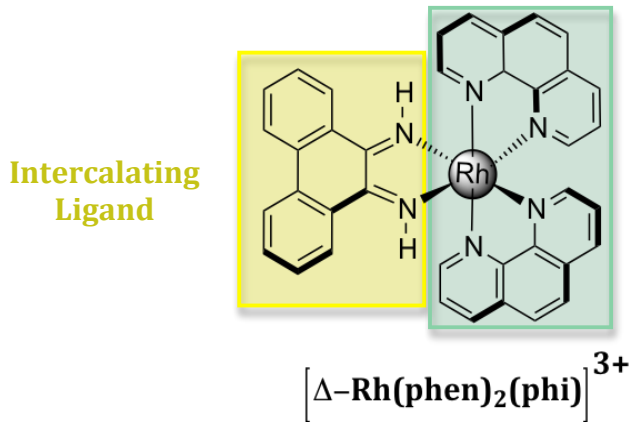

Figure 1.9 Chemical structure of an example of a Rh(III) metallo-intercalator: intercalating ligand highlited in yellow and the ancilliary ligands in green (based on ref[21]).

In these systems, the planar units insert into the DNA and the attached metal and the other co-ligands reside in the DNA grooves, either major or minor depending on the type

of complex.[1, 2, 21, 23] In addition, DNA-sequence specificity was achieved by attaching a peptide to the well known Rh(III) metallo-intercalator $[Rh(phi)_2(phen)]^{3+}$.[24] In this example, the metal complex provides the energy for the interaction with DNA in the major groove and the peptide provides the sequence specificity.[1, 25, 26] A more detailed discussion on metallo-intercalators and their function with DNA will be presented in section 1.4.

1.2.3 Coordinative Binding: *the role of Platinum Drugs*

Coordinative binding to DNA is an irreversible process that leads to inhibition of DNA processes and to cell death. The mechanism by which certain drugs bind coordinatively to DNA involves direct coordination of the N7 of G (Figure 1.1) and A bases located in the DNA major groove.[2, 11, 27]

Cisplatin, *cis*-$[PtCl_2(NH_3)_2]$ is the most famous example of a drug that binds coordinatively to DNA. It was discovered in 1960's and after its approval as a chemotherapeutic agent is still one of the world's best selling anticancer drug (Figure 1.10).[28, 29] It cures over 90% of cases of testicular cancer and it is fundamental for the treatment of different cancers such as ovarian, head and neck, bladder or cervical, melanomas and several lymphomas.[8, 30, 31] Despite its potent anticancer activity, resistance to cisplatin has been observed in certain tumours. In addition, therapeutic administration of cisplatin results in severe side effects including kidney toxicity and bone marrow suppression (leading to consequent leukemia). These drawbacks have prompted scientists to develop cisplatin drug derivatives that would reduce the side effects of cisplatin while maintaining its potent antitumor activity.[32] Oxaliplatin and

carboplatin are two of the cisplatin derivates produced that are used in the clinic across the world (Figure 1.10). Other derivates such as Nedaplatin, Lobaplatin and Heptaplatin are only used in certain specific countries (Figure 1.10).[8]

It was back in the 1970's when Rosenberg and co-workers established DNA as the biological target of cisplatin, which acts by formation of covalent adducts via ligand exchange.[33] The major adducts formed by cisplatin with DNA are bifunctional GG intrastand crosslinks. This results from replacement of the chloride ligands coordinated to the Pt(II) centre by the nitrogen of the purine bases, usually the nitrogen atom N7 of the adjacent guanine base residues (Figure 1.11).[11, 34-36]

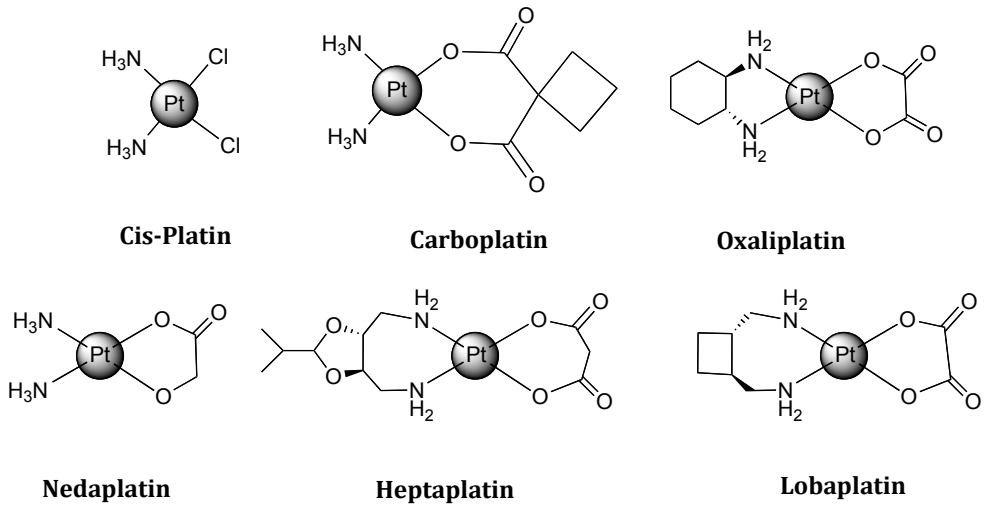

Figure 1.10 Chemical structures of cisplatin and derivates used in clinic.

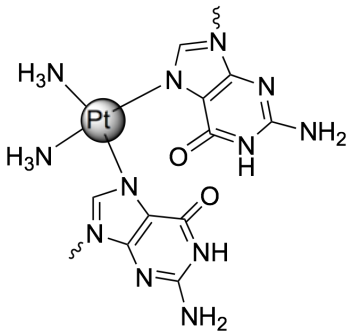

Figure 1.11 Cisplatin coordinated to two guanine bases.

Several cisPt-DNA adducts can be observed: 1,2-intrastrand GG (~ 65%) and 1,2-intrastrand AG crosslinks (25%) are the major ones.[37] The binding process causes a lesion that forces the double strand to unwind by 13° and bend the DNA by 45° near the coordination site (Figure 1.12, A).[38]

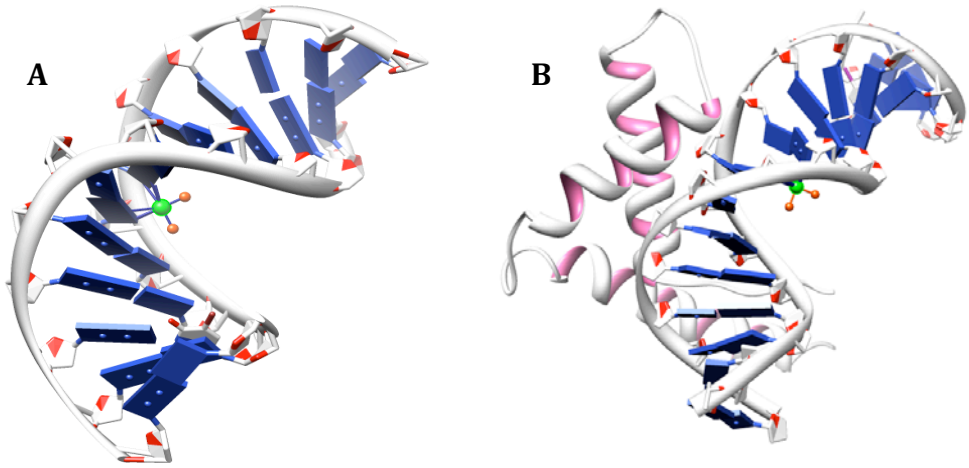

Figure 1.12 (A) View of cisplatin when bound to DNA (PDB 1AIO).[39] (B) DNA-cisplatin adduct recognized by the HMG protein (Pink) (PDB1CKT).[40]

The bent DNA is recognized by the High Mobility Group proteins (HMG's) (Figure 1.12, B) and the damaged DNA is no longer repaired leading to inhibition of transcription and replication and consequent cell apoptosis at the G2 phase of the cell cycle.[11, 35, 37, 41-43]

Although cisplatin is highly effective as an anticancer drug, it is important to underline that it also shows cytotoxicity in non-cancer cells. Achieving DNA sequence-selective interactions by new metallo-drugs, using different transition metals remains a major challenge in organometallic drug development.

1.2.4 Sugar-Phosphate Backbone Binding

Another mode of DNA binding is sugar-phosphate backbone binding. The DNA backbone offers a rich polyanionic surface that allows drugs and natural proteins to interact by both electrostatics and hydrogen bonding. Farrell and co-workers reported what is to date the most representative family of multinuclear Pt(II) backbone binding drugs: in these complexes all Pt(II) centres are coordinated to inert amine ligands to avoid Pt-DNA covalent bonding as it happens with Pt-Cl based drugs (eg. cisplatin). A representation of the chemical structure of a trinuclear platinum (II) compound backbone bonder is shown in Figure 1.13.

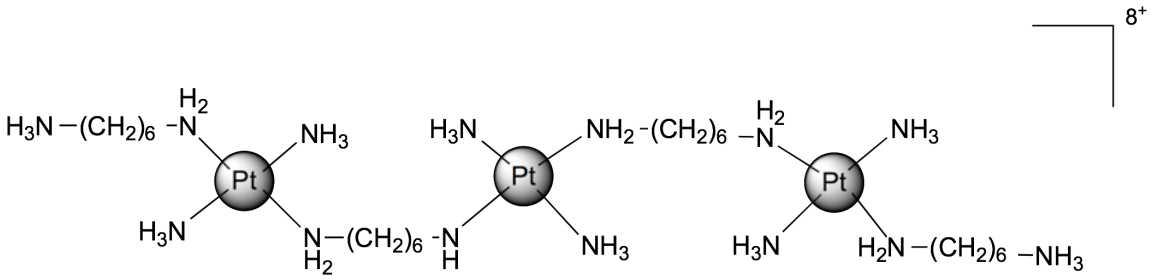

Figure 1.13 Chemical structures of trinuclear platinum (II) compound, TrisplatinNC.

This trinuclear platinum (II) complex binds non- covalently to DNA via hydrogen bonding and electrostatic interactions.[2, 44] Komeda[45] and co-workers have reported a X-ray crystal structure that reveals that the complex forms hydrogen bonds between two *cis* amine groups and one oxygen phosphate of the DNA (NH----O----HN), the so-called phosphate clamps (Figure 1.14). Importantly this complex was shown to have good activity in certain cancer cell lines.[46]

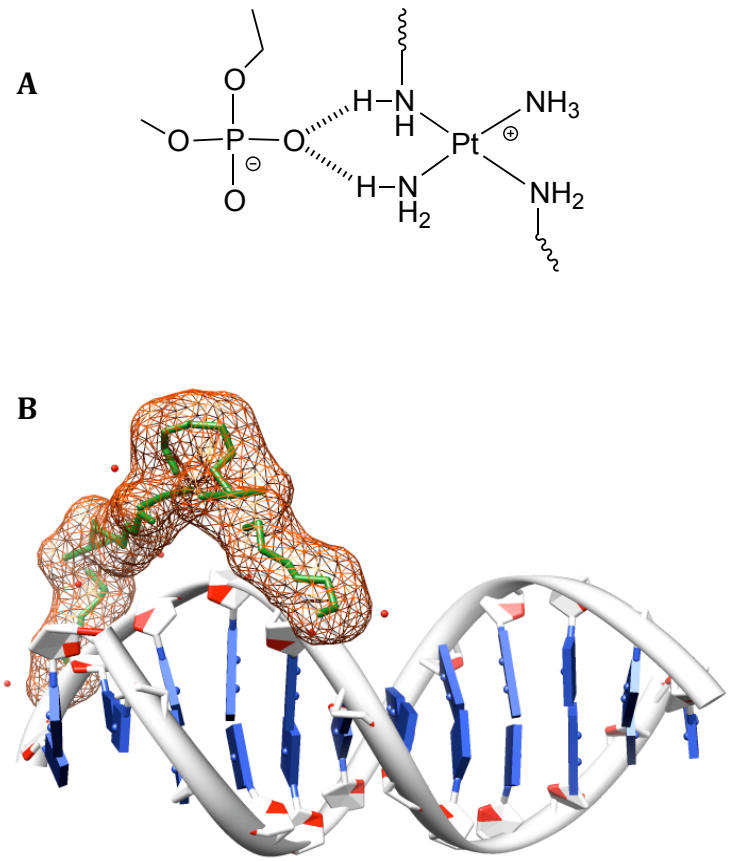

Figure 1.14 (A) Schematic representation of a Phosphate clamp;[45] (B) View of platinum (II) compound, TrisplatinNC when bound to the DNA phosphate backbone (PDB 2DYW).

1.2.5 Binding to DNA Junction and Other Unusual DNA Structures

DNA junctions are unique branched structures that consist of several double strands converging at one point. Four-way junctions (4WJ) are the best characterized and are known as Holliday junctions.[47, 48] Three-way junctions (3WJ) are simpler but their role in Biology is less well studied. They occur in DNA and in RNA. For instance, three way junctions are found in some abnormal DNA structures related with genetic diseases such as myotonic dystrophy type 1 and Huntington's disease.[9, 49] In RNA they are involved in splicing and translation but normally contain bulges rather than being perfect 3WJs. In

DNA a related Y shaped fork structure (a 3WJ in which a strand is not joined up) is found in its replication process. The Hannon group in collaboration with the Coll laboratory was able to crystallise and structurally characterize the interaction between a palindromic hexanucleotide DNA 3WJ with an iron(II) supramolecular cylinder (Figure 1.15).[9]

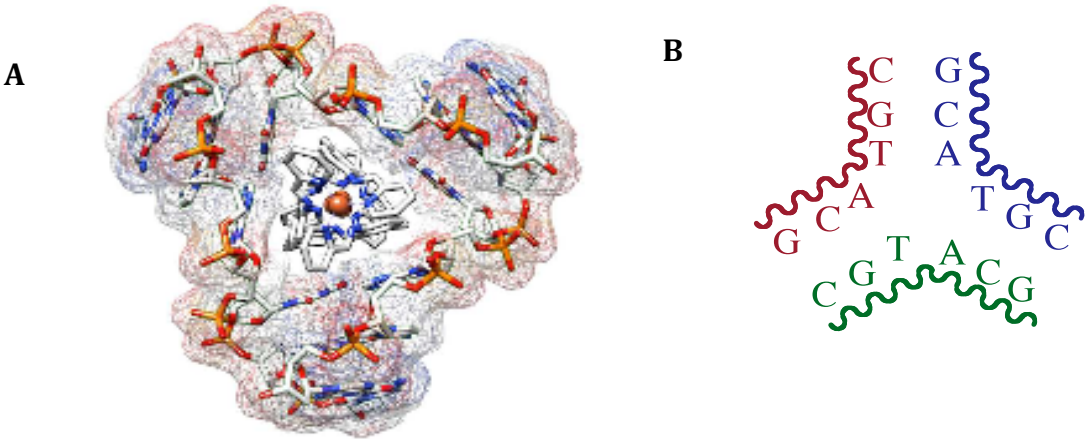

Figure 1.15 (A) Crystal structure of the interaction between the iron cylinder and a DNA 3WJ structure (PDB 2ETO); (B) Example of a DNA palindromic 3WJ structure.

This constitutes the first new DNA binding mode discovered in the last forty years.[9] As well as binding to the DNA major groove, the cylinder binds to DNA three way junctions (3WJ) and also to other Y shaped junctions (Figure 1.15).[9, 50, 51]

NMR and gel electrophoresis studies confirmed the observations detected in the crystalline state.[50, 51] The cylinder possesses a high positive charge due to the two Fe^{2+} ions axially located at both ends of the complex and displays large hydrophobic surfaces due to the presence of the 12 aromatic rings. These are driving forces for the non-covalent recognition of DNA junction by the helicate. The electrostatic-dipole interaction occurs between the positive charge of the supramolecule and the negatively charged DNA phosphates. Additionally, the phenyl rings at the centre of the helicate form

extensive π-stacking interactions with the thymine and adenine bases at the junctions. Recent experiments showed that this cylinder binds stronger to 3WJs than to double strand DNA from the fact that palindromic induces 3WJ. The unprecedented binding mode of this synthetic cylinder to three way and Y shaped junctions opened a window to explore and achieve DNA structure based specificity.

As mentioned above, another higher-order structure commonly found in DNA is the 4WJ (Figure 1.16).[47] 4WJs are branch points generated by the interconnections of four helices by strand exchange.[47, 52] Their importance is directly related with the role they play in several biological processes such as replication and recombination, DNA repair, restart of failed replication forks and viral integration.[53] Increased attention has been given to developing small molecules which can target such structures and either stabilize or disrupt them and exploring how this can be useful for therapeutics.[53, 54]

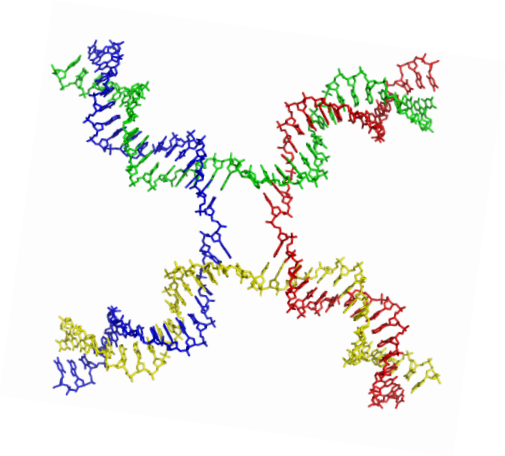

Figure 1.16 Example of a four-way junction structure.[47]

Molecules that target 4WJs are primarily based on agents that recognize two B-DNA arms of the structure. Lowe's bis-acridines, rigid bis-intercalators, and Sasaki's bis-Hoechst agents target 4WJs in this way but with different motifs (Figure 1.17).[55-57]

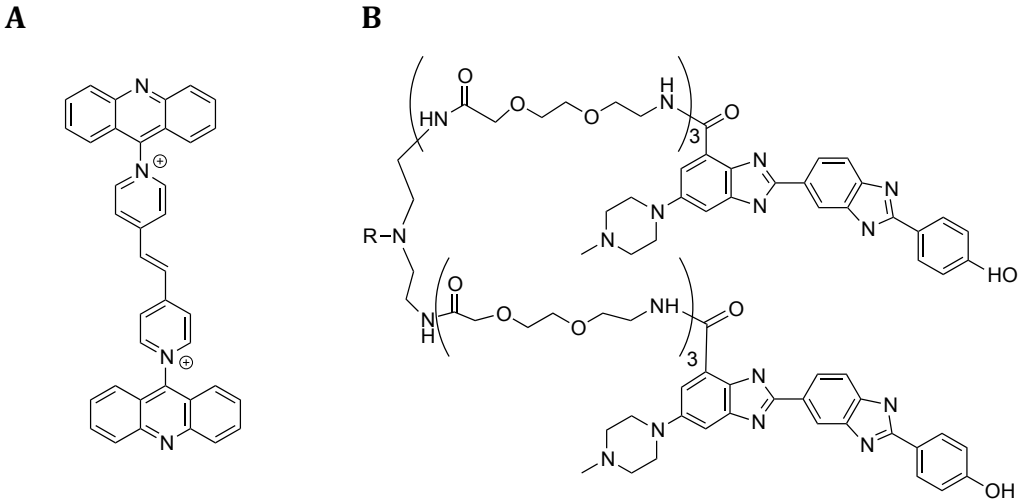

Figure 1.17 (A) Example of a Lowe's acridine; (B) Sasaki's bis-Hoechst agent.

Searcey and co-workers have also been exploring the synthesis of intercalator molecules to target 4WJs.[54] The two acridine moieties act as intercalators which are separated by a spacer with the right distance for insertion at the two distant sites. The molecule binds across the centre of a Holliday junction and the two adenines are replaced by the acridine chromophores either side of the crossover.[48, 57] An example of such a molecule is shown in Figure 1.18 as well as a schematic representation of its interaction with DNA at the crossover region.[48]

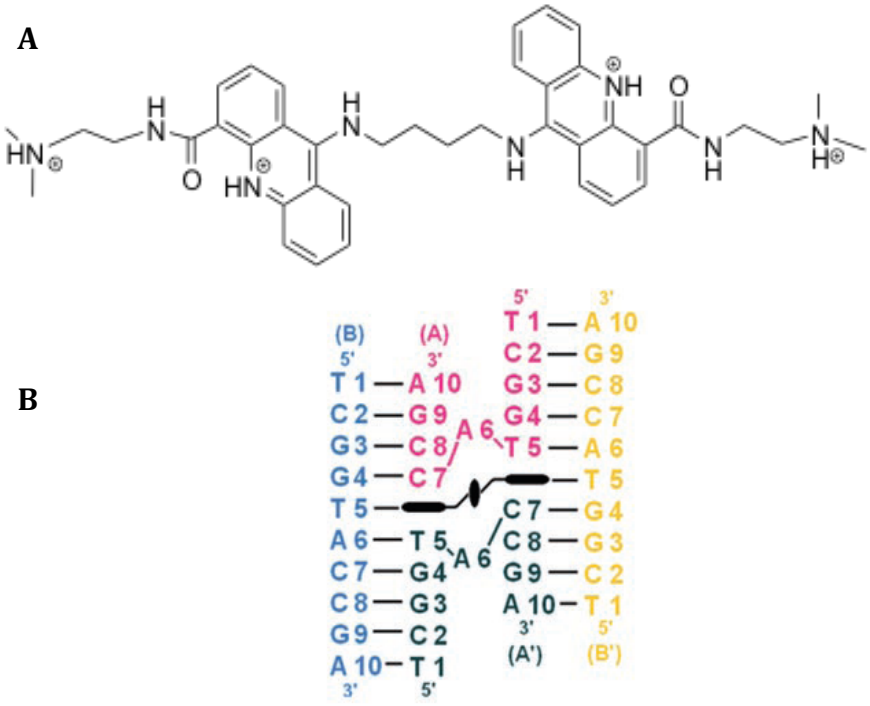

Figure 1.18 (A) Chemical structure of a bis-acridine compound to target a four-way junction; (B) Schematic representation of the target nucleotide where the compound can be seen in black in he crossover region.[48]

G-quadruplexes are other possible DNA structures that might be targets for drug recognition. They are formed by a square construction of guanine (G) residues held together through Hoogsteen hydrogen bonding. These structures are stabilized by a central monovalent cation in most cases potassium but sodium or lithium can also be found (Figure 1.19).[8, 58]

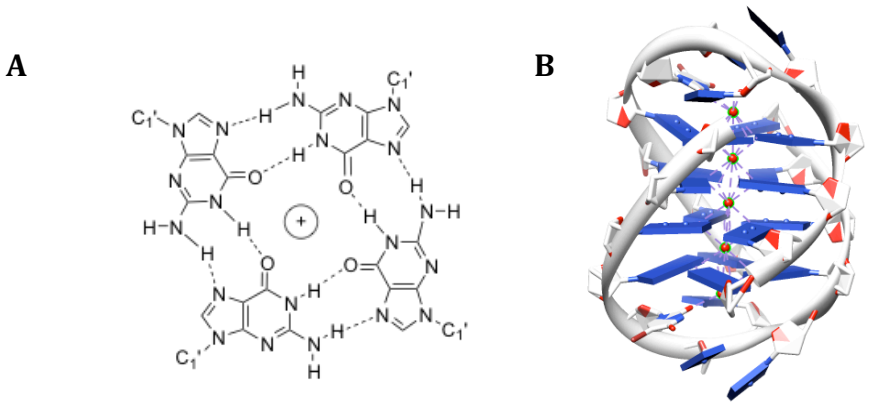

Figure 1.19 (A) Chemical structure of G-quadruplex; (B) G-quadruplex X-ray structure with G bases in a square arrangement stabilized by five central potassium cations (PDB 1JPQ).[59]

The identification of G-quadruplexes *in vivo* in telomeric DNA (Figure 1.20) made a tremendous impact and prompted the scientific community to try further understand the structural arrangements and properties of these structures.[60, 61] G-quadruplexes are present at the end of every human chromosome and telomerase, an enzyme which is overexpressed in ~ 85% of cancer cells, is inhibited if single telomeric DNA is folded into quadruplexes.[62]

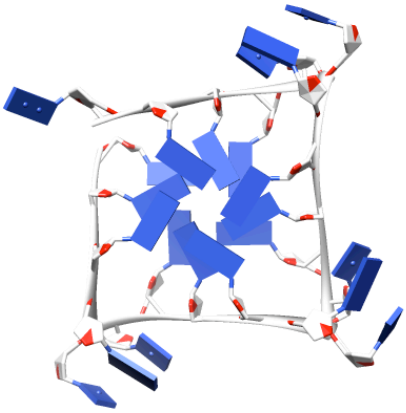

Figure 1.20 Top view of the X-ray crystal structure of human telomeric quadruplex DNA (PDB 1KF1).

Furthermore promoter regions of some oncogenes such as *c-myc* and *c-kit* are G rich, and the formation of quadruplexes in these regions is responsible for regulating oncogene's transcription.[63] Over the past few years, many studies have reported molecules that are able to induce the formation and to stabilize quadruplexes as a new strategy in cancer therapy.[64] Specific molecules can interact with G-quadruplex DNA and inhibit telomerase regulating the transcription of certain oncogenes.[53, 60, 62, 65]

Recently, it was reported that a Fe(II) cylinder can stabilize G quadruplex DNA[66] suggesting that tetraplexes do not compete for binding with duplexes and raising questions of a proposed tetraplex binding mode that remains to be clarified.

1.3 Metallo-Supramolecular Chemistry

Metallo-supramolecular chemistry harnesses coordination chemistry approaches to supramolecular design. It is based on the use of ligand-metal ion interactions using ligands containing multiple metal binding sites. The donor sets are matched to the coordination geometric requirements of specific metals so as to give rise to multi-stranded arrays. One of the most studied and developed types of supramolecular architecture are the helicates, pioneered by Jean Marie-Lehn.[67, 68]

Helicates are formed when one or more organic, covalent strands are wrapped around metal ions defining the helical axis. The design of these structures involves consideration of a number of factors: the ligand must be flexible enough for multiple strands to wrap or bridge around two or more metal centres while also being rigid enough to control the architecture formed.[69] The compounds are usually formed by self-assembly, with high selectivity, into a well-defined, discrete supramolecular architecture. Helicates can be classified as homotopic or heterotopic and this last type can exist in two isomeric forms. If the coordinated ligand strands contain similar binding sites, a homotopic helicate is formed. If the ligand strands hold different binding sites the final helicate produced will be heterotopic (Figure 1.21).

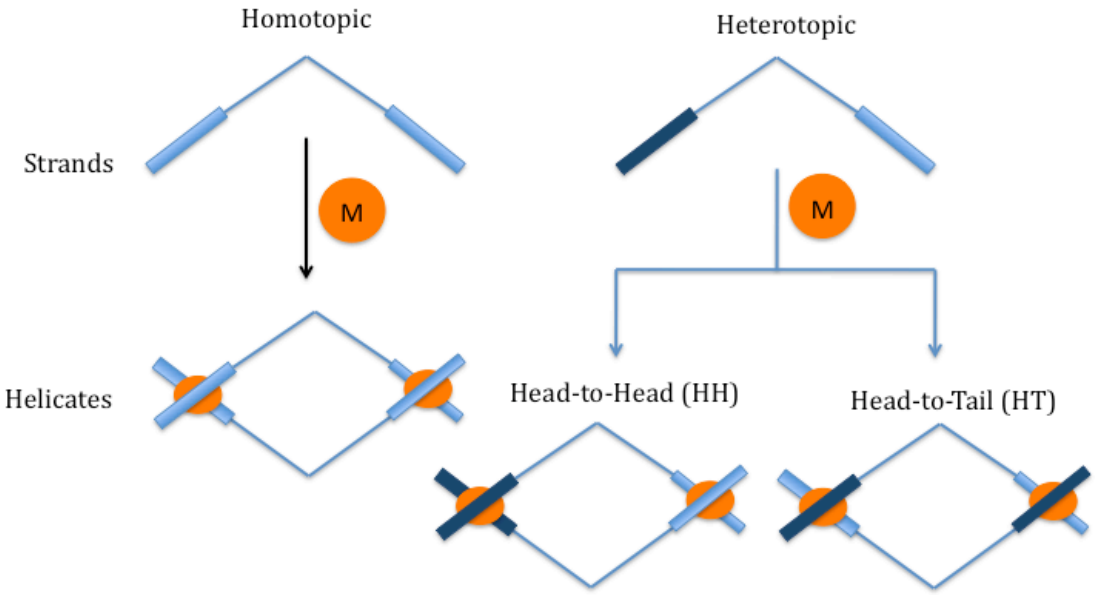

Figure 1.21 Schematic representation of Homotopic and Heterotopic helicates.[68]

With precise design, supramolecular helicates can be prepared as mimics of α-Helix protein motifs, with similar size and cylindrical shape.[2, 70] The presence of metal centres in these supramolecular systems imparts a cationic charge to the structure, which contributes to the interaction with the negatively charged DNA molecule. The choice of the metal is important as it can impart further properties too (eg. Platinum, Ruthenium, Rhodium)

The Hannon group pioneered the use of helicates to recognize the DNA major groove. The key helicate is termed cylinder and is based on a ligand (L_{im}) that incorporates two pyridylimine binding sites separated by a spacer (Figure 1.22).[71]

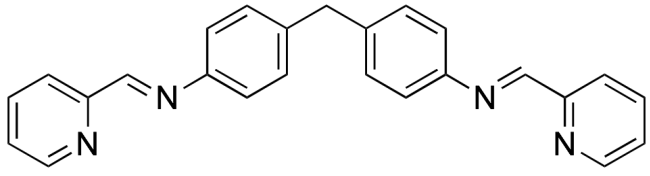

Figure 1.22 Chemical structure of the bispyridylimine Ligand (L_{im})

Many cylinders containing different metals have been synthesized, such as Fe(II), Co(II), Ni(II), Zn(II) and more recently Ru(II).[70-72] In all cases, coordination results in the formation of a tetracationic dinuclear triple stranded helicate $[M_2(L_{im})_3]^{4+}$ in which the three strands of the ligands are wrapped around the metal centres. The most representative one is $[Fe_2(L_{im})_3]^{4+}$. This cylinder is easily synthesized starting with $FeCl_2.H_2O$ with the correct amount of L_{im} in a one-pot synthesis (Scheme 1.1)

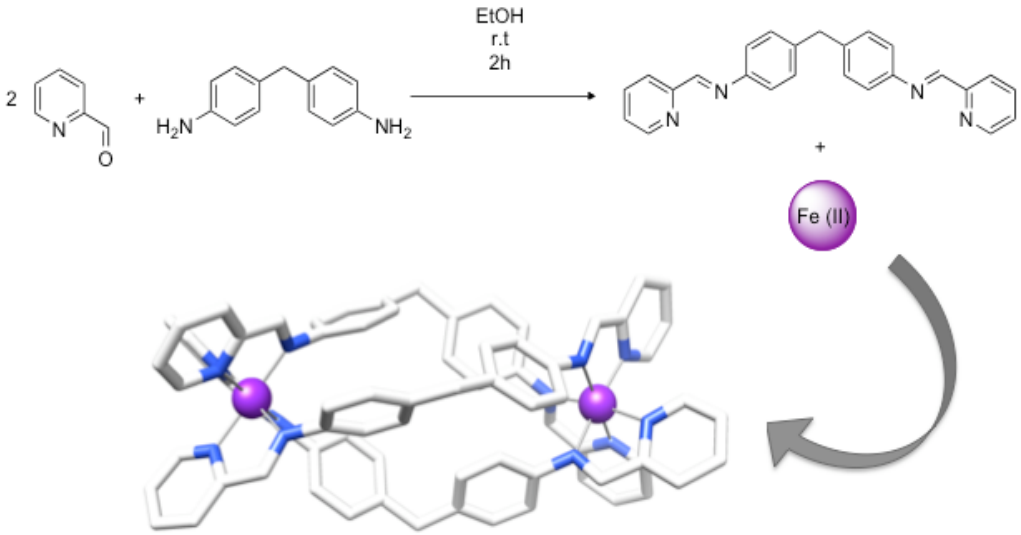

Scheme 1.1 Scheme showing the synthesis of the L_{im} and the Fe(II) cylinder and respective crystal structure (Hydrogens and counter ions omitted for clarity).[73, 74]

X-ray studies showed that this cylinder has the correct size (2 nm length, 1 nm diameter) and shape to fit in the B-DNA major groove just like DNA binding protein motifs.[75] The fact that the octahedral sphere around the metal is fully saturated by the six nitrogen atoms of the bidentate ligands excludes any possibility of coordination to the DNA base pairs. The surface of the spacer of L_{im} allows π-stacking interactions (face to face or more likely face to edge) with the DNA bases. Spectroscopic studies, circular dichroism (CD), linear dichroism (LD) and UV-Visible absorption showed that the Fe(II)

cylinder binds to B-DNA (calf thymus and other smaller oligonucleotides) even at low concentrations of complex and in a single binding mode up to 5:1 DNA:complex. Atomic Force Microscopy (AFM) studies showed that the complex causes linear DNA to bend at low concentrations followed by a cooperative coiling of the DNA around the cylinder (Figure 1.23).[9, 70, 76]

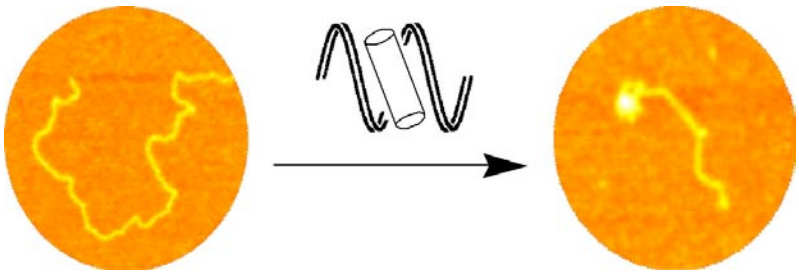

Figure 1.23 AFM images of plasmid DNA before and after interaction with Fe(II) cylinder.[70]

The synthesis of this complex results in a racemic mixture that can be resolved to afford a chiral complex. After the resolution of the mixture (using cellulose column chromatography) both M (minus, ligands wrapped anticlockwise) and P (plus, ligands wrapped clockwise) enantiomers showed binding and coiling abilities by CD and LD. The M enantiomer was shown to bind more strongly and to be more effective at DNA coiling than the P enantiomer.[77]

In light of the exciting and highly promising results with $[Fe_2L_3]^{4+}$, the design of new helicates with improved stability is a longstanding challenge. Particular attention has been given to the development of ruthenium (II) cylinders. The synthesis of such cylinders is more complicated than that of the iron analogues with extremely low yield (~ 1%). Nevertheless replacing the metal centre with a less labile metal improved the overall stability of the complex. The complex survives different conditions needed for

some biological experiments without showing any signs of decomposition (as e.g. PCR). The complex $[Ru_2L_3]^{4+}$ was prepared, fully characterized and X-Ray studies revealed a similar structure to that obtained for the Fe(II) in size and shape. CD and LD studies showed that the Ru(II) cylinder binds to B-DNA in a comparable way as observed for the iron analogue (both with K_b in the order of 10^7 M^{-1}).[73, 78] In addition introducing ruthenium into the system imparted luminescence and photocleavage properties to the cylinder, and a small enhancement of luminescence could be detected upon binding to DNA.[72, 79] Such an array of properties enabled cell uptake and localization studies and also artificial DNA cleavage activity by photoactivation of the metal centres. Recently, it has been shown that the Ru(II) cylinder dramatically inhibits DNA amplification at low concentrations and fully blocks the polymerase chain reaction (PCR) with displacement of the Taq DNA polymerase from DNA.[80] Analogous studies using the Fe(II) cylinder, showed that this cylinder is an even stronger Taq polymerase displacer though this cylinder has insufficient chemical stability to undergo PCR experiment conditions.[80]

The Rh(III) supramolecular complexes whose design and synthesis are the focus of this thesis are quickly synthesized and in particular the reaction of the formation of a Rh(III) triple helicate seems to be quicker and obtained in higher yields in comparison with Ru(II) analogues.

An important step for the iron and ruthenium cylinders involved the study of their behaviour in biological systems. Cytotoxic activity of both Fe(II) and Ru(II) complexes in breast cancer cell lines, HBL-100 and T47D, showed activity 5 fold lower than that of cisplatin. The activity of these cylinders is however comparable with carboplatin a related platinum drug derivate. The Fe(II) cylinder acts by causing G0/G1 arrest followed by apoptosis. An Ames bacterial mutagenicity test proved that the Fe(II)

cylinder is neither mutagenic nor genotoxic which is a clinical drawback of cisplatin (raised probability of subsequent cancer, especially Leukemia).[72, 81]

Many other similar cylinders were synthesized with substituted ligands but most seem to be less effective DNA binders. More recently, a new procedure was established to conjugate amino acids and short peptides to the edges of the L_{im} based cylinders. These conjugates exhibited DNA binding features comparable with the ones reported for the unconjugated ones. In addition they have comparable or higher cytotoxicity.[14]

Another approach involved the synthesis of double stranded complexes. For example, a Cu(I) cylinder as shown in Figure 1.24, that showed lower binding affinities to DNA but has the capacity to act has an artificial nuclease which can cleave DNA in the presence of hydrogen peroxide.[82]

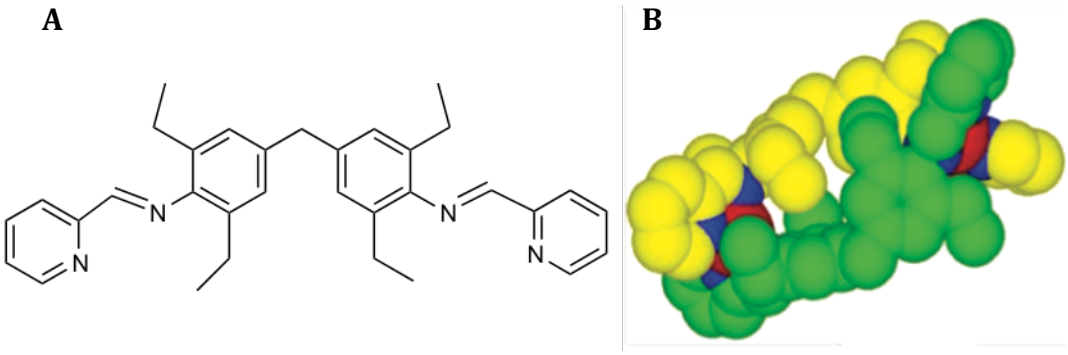

Figure 1.24 (A) Byspyridylimine Ligand with ethyl groups in the spacer for the formation of the di-Cu(I) double stranded cylinder with helical architecture (B). [83]

The peptide conjugated Cu(I) double stranded helicate exhibited the same artificial nuclease ability although less than the unconjugated one.[14, 82]

An important step on these designs and an alternative to the di- Ru(II) cylinder described before was the design, synthesis and separation of a set of five different Ru(II)

double stranded helicates. These architectures were inspired by the work performed on dichlorobis(2-phenylazopyridine)ruthenium(II) complexes, $[Ru(L_{azpy})_2Cl_2]$. Reedijk and co-workers have intensively studied this family of mononuclear complexes, due to their cytotoxic activity in different human tumour cell lines. In particular, the α (Figure 1.25) configuration is the most active isomer with good stability and reasonable solubility.[84-86]

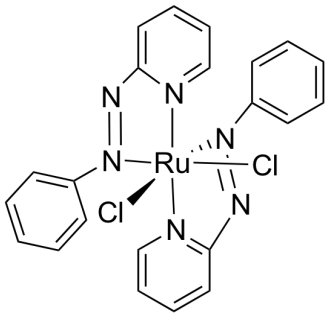

Figure 1.25 Schematic representation of the compound α-$[Ru\text{-}(L_{azpy})_2Cl_2]$.

The aim behind the synthesis of the dinuclear Ru(II) double stranded complexes was to create a unsaturated helicate with similar size and cylindrical shape to the Ru(II) cylinder but with vacant coordination positions that could offer an additional possibility of the metal centre interacting directly with DNA.[87] These double stranded complexes are based on a dinucleating bisazopyridine ligand (Figure 1.26), analogous to the mononucleating 2-phenylazopyridine ligand in Figure 1.25.

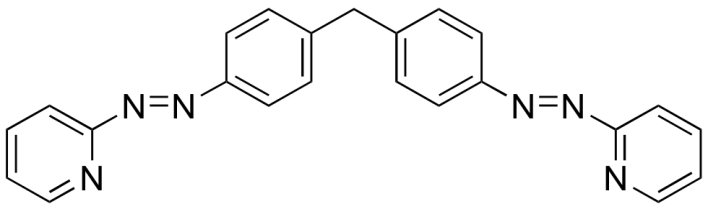

Figure 1.26 Chemical structure of the Bispyridylazo Ligand (L_{azo})

Each ruthenium centre can have one of three possible configurations: α (N_{pyr} ring *trans*, N_{azo} bond *cis* and Cl *cis*), β (N_{pyr} ring *cis*, N_{azo} *cis* and Cl *cis*) and γ (N_{pyr} ring *cis*, N_{azo} bond *cis* and Cl *trans*) according with the scheme of Figure 1.27.

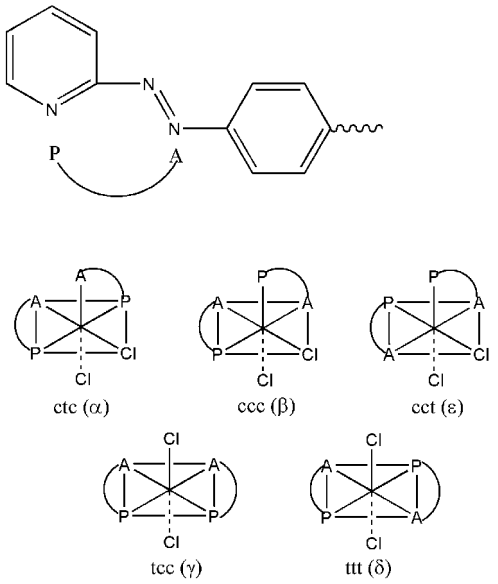

Figure 1.27 Schematic representations of the five possible isomers considering each metal centre. P (N of the pyr), A (N of the azo bond), Cl (Chloride ligands). [88]

Five isomers, γγ, γα, γβ, αα, and ββ of $[Ru(L_{azo})_2Cl_2]$ (Figure 1.28) were isolated, fully characterized and further studied.[87]

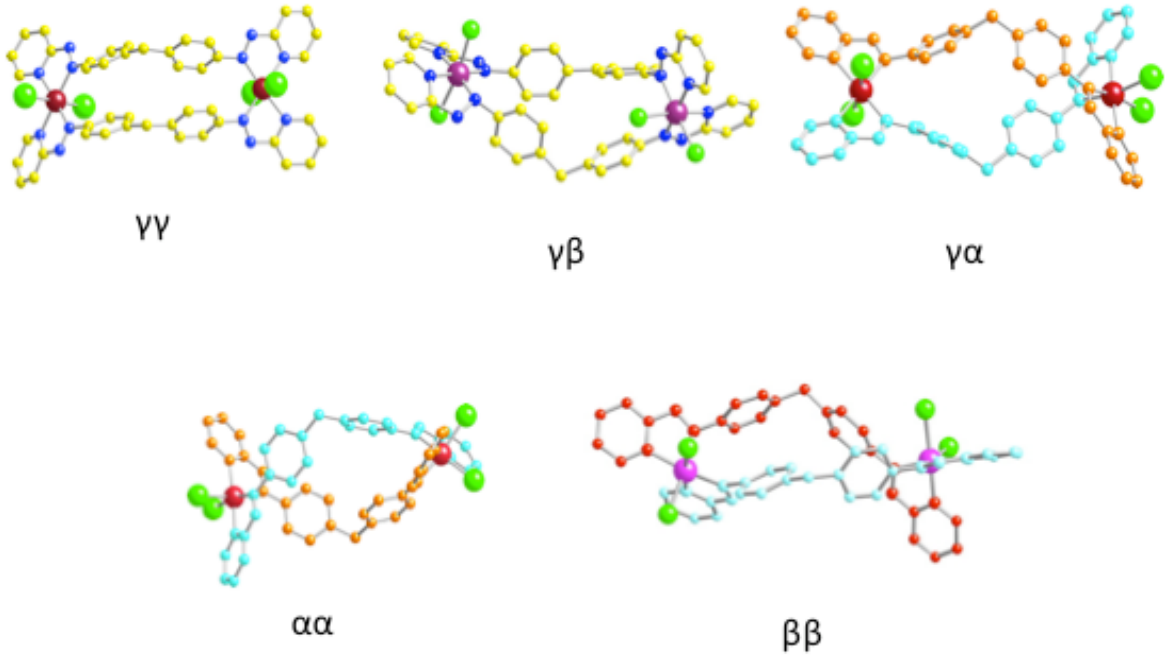

Figure 1.28 X-Ray Structures of the five isomers of $[Ru(L_{azo})_2Cl_2]$. [87]

The five different isomers show different levels of cytotoxicity with the γγ and γα exhibiting 36 and 8 times higher activity than cisplatin in A2780 cell line and 300 and 4 times higher than cisplatin when in A2780cisR (cisplatin resistant cell line). Bacterial mutagenicity tests and Comet assays corroborate the fact that they are not mutagenic or genotoxic.[89] The different levels of activity between the five isomers show that the configuration and the architecture of the molecule itself it is of high importance for the biological activity. Also, the fact that the Ru(II) cylinder (saturated triple helicate) is much less active than these double stranded unsaturated helicates, strongly suggests that the Ru centres may be involved in the binding to DNA. Despite the exciting biological properties, their low solubility did not allow studies on their DNA binding abilities.

1.4 Metal Complexes as Anticancer Agents

Although the discovery of the anticancer properties of cisplatin was a remarkable achievement, many efforts have been made to prepare other transition metal complexes, which could then circumvent cisplatin drawbacks. Transition metals offer a wide range of advantages for designing and preparing new compounds that can be biologically active:[21, 90, 91] for example, different available oxidation states and possible geometries, tune ability of the thermodynamics and kinetics of ligand substitution and a range of structural diversity.[91] For DNA binding and recognition, transition metal complexes are appealing as the metal centre can work as an anchor which holds a rigid and stable three dimensional structure while the ligands may bear recognition elements.[21, 61] Groove binding and intercalation are with no doubt the most common way of a metal complex to recognize DNA. Intercalation is well documented, Lerman[15] in his report about intercalation also proposed a third non-covalent DNA binding mode: *insertion*. As intercalation may apply to metal complexes (metallo-intercalators) also the same happens for insertion (metallo-insertor) (Figure 1.29).[21]

The difference between a metallo-intercalator and a metallo-insertor is that the first one unwinds the DNA and inserts the planar ligand in between two intact base-pairs while a metallo-insertor ejects the bases of a single base-pair with the planar ligand and acts as a π-stacking replacement in the DNA base stack (Figure 1.29).[21]

Barton and co-workers pioneered the discovery of a family of metallo-insertors when investigating and designing specific complexes to target mismatch-DNA sequences (this subject will be further explored in section 1.4.3).[21, 92, 93]

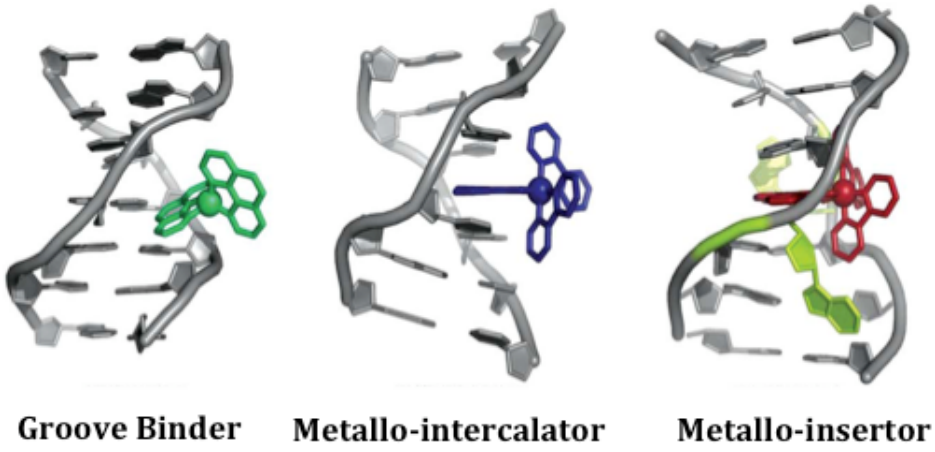

Figure 1.29 Three different binding modes of metal complexes to DNA (from ref[21]).

Transition metals with rich photophysical and photochemistry properties extend the use of the complexes beyond molecular recognition.[21, 94, 95] There is growing interest in the use of transition metal complexes that can be used for photodynamic therapy (PDT), such agents can cleave double stranded DNA upon irradiation and there have been several recent reports on such complexes of Ru(II)[19], Rh(III)[96], Re(I)[97], di-rhodium(II-II)[98, 99] and trinuclear Ru(II)-Rh(III)-Ru(II)[20, 100].

PDT provides the possibility of activating an anti-cancer drug (photosensitizer) in a specific location (cancerous area) through specific irradiation.[101] This methodology results in greater specificity of drug action and control of side effects. Four compounds have passed clinical trials and are currently used as PDT agents (eg. Photofrin®, Foscan®, Levulan® and Melvix®).[102, 103]

1.4.1 Ruthenium Anticancer Agents: NAMI-A and KP1019

Pentaammine(purine)ruthenium (III) was reported by Clarke and co-workers in the 70's as the first ruthenium complex showing *in vitro* activity against carcinoma cells. From this point a growing interest in ruthenium complexes as potential anticancer drugs has emerged.[104] Among several new ruthenium compounds, two of them are in clinical trials: *trans*-[tetrachlorobis(1H-indazole)ruthenate(III)] (KP1019)[105] and imidazolium *trans*-imidazoledimethylsulfoxidetetrachlororuthenate (NAMI-A) which just completed phase I clinical trials (Figure 1.30).[106]

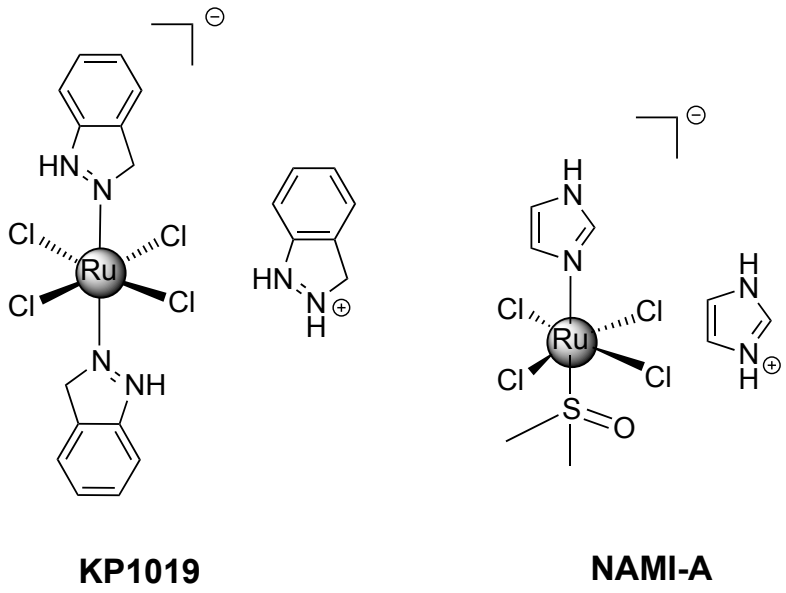

Figure 1.30 Chemical structure of KP1019 and NAMI-A.

Although similar in structure, NAMI-A is active against metastases while KP1019 is active against primary tumours. Due to water solubility of KP1019 the drug is administered as a sodium salt (KP1339) and is now passing from phase I to phase II clinical trails.[107] The drug undergoes activation *in vivo* through reduction from Ru(III) to Ru(II) interacting with biomolecules after labilization of the Ru(II)-Cl bonds.[8, 108] It

was recently showen that KP1019 binds strongly to serum proteins like albumin and transferrin, which are very important for the drug accumulation inside the tumour, which occurs via transferrin pathway.[105, 107]

The anti-metastatic mechanism of NAMI-A remains unclear but there are clear evidences that the metal centre plays a crucial role in interacting with the cell surface and extracellular components like collagen.[106, 108, 109]

1.4.2 Ruthenium Polypyridyl Complexes

Ruthenium(II) complexes with polypyridyl ligands have been intensively studied for their exciting photophysical properties and DNA binding.[110] Some of the complexes belonging to this family have been investigated as nucleic acid probes, for DNA mediated electron transfer, DNA footprinting, DNA sequence-specific cleavage and as anticancer drugs.[21, 111, 112]

Several ruthenium(II) mononuclear and dinuclear complexes have been intensively studied.[72, 112-114] The initial DNA binding studies made with octahedral complexes were focused on $[Ru(phen)_3]^{2+}$ and $[Ru(bpy)_3]^{2+}$ which were introduced by Barton and co-workers. The octahedral complex $[Ru(phen)_3]^{2+}$ (Figure 1.31, Left) binds to DNA inserting one of the phen ligands into the DNA base pair stacks. One important feature of this complex is that it possesses two distinct DNA binding modes depending on the enantiomer.[21, 113, 115] Later experiments led to the synthesis of similar complexes, fusing a dppz ligand (Figure 1.31, Right) which possess an increases aromatic surface, to the phen ligand. This complex was revealed to bind much stronger to DNA due to the extended aromatic surface of the intercalation ligand dppz in comparison with phen. In

this case, the Δ enantiomer showed to have affinity to AT sequences and a slightly higher affinity for calf tymus-DNA (ct-DNA) when compared with the Λ enantiomer.[113]

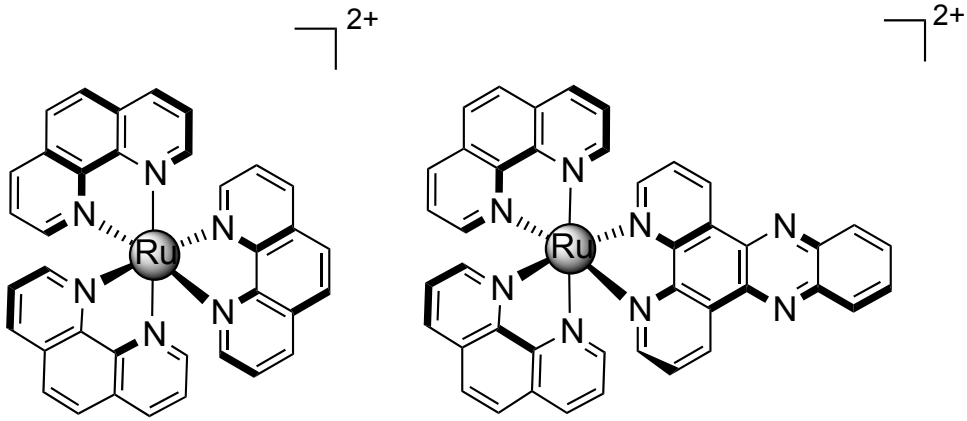

Λ–[Ru(phen)$_3$]$^{2+}$ **[Ru(phen)$_2$(dppz)]$^{2+}$**

Figure 1.31 Chemical structure of ruthenium(II) metallo-intercalators.

An exciting property of [Ru(phen)$_2$(dppz)]$^{2+}$ is its ability to work as a molecular light switch once bound to DNA. The dppz ligand when intercalated into DNA is protected from water molecules and becomes luminescent.[21, 110] Later Turro and co-workers[116] reported that intercalation was not a necessary requirement for DNA light-switch behaviour, showing that the non intercalating bimetallic Ru(II) complex [(bpy)$_2$Ru(tpphz)Ru(bpy)$_2$] (Figure 1.32) behaves as a light switch.[116]

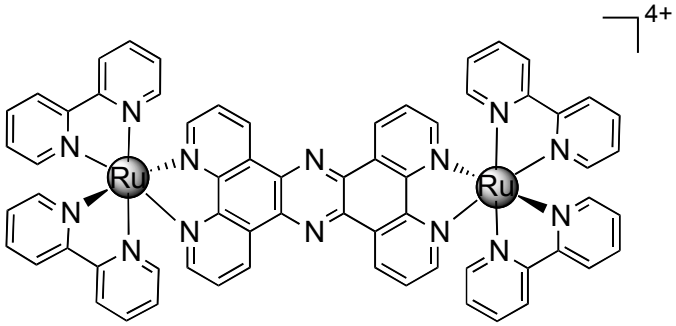

[(bpy)$_2$Ru(tpphz)Ru(bpy)$_2$]$^{4+}$

Figure 1.32 Chemical structure of a ruthenium(II) non-intercalator light switch.

Another example of a tris(chelate) complex is $[Ru(bpy)_3]^{2+}$ (Figure 1.33) which binds to DNA merely by electrostatic interactions once its bpy ligands do not have enough aromatic surface to π-stack with DNA bases. Nevertheless this complex possesses DNA cleavage properties upon visible irradiation.[117] In addition when cells are treated with the complex and light the formation of singlet oxygen ($^1O_2$) causes cell apoptosis.[118]

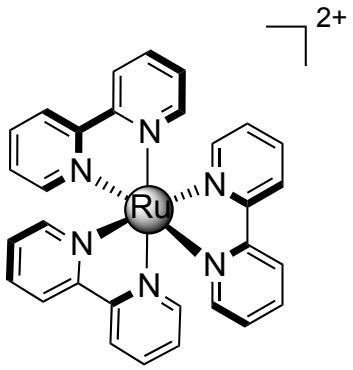

$[Ru(bpy)_3]^{2+}$

Figure 1.33 Chemical structure of $[Ru(bpy)_3]^{2+}$

Cellular uptake and localization studies of Ru(II) polypyridyl complexes have been investigated.[101, 114, 119-121] Barton and co-workers reported a flow cytometry and confocal microscopy study where the ruthenium luminescent metallo-intercalators $[Ru(DIP)_2(dppz)]^{2+}$ and $[Ru(bpy)_2(dppz)]^{2+}$ (Figure 1.34) were found inside HeLa cells.[119, 122] The first complex was showen to be more readily taken up than the complex with bpy ligands, suggesting that hydrophobicity of the complex is more important than size for achieving entry into the cell.[120, 122]

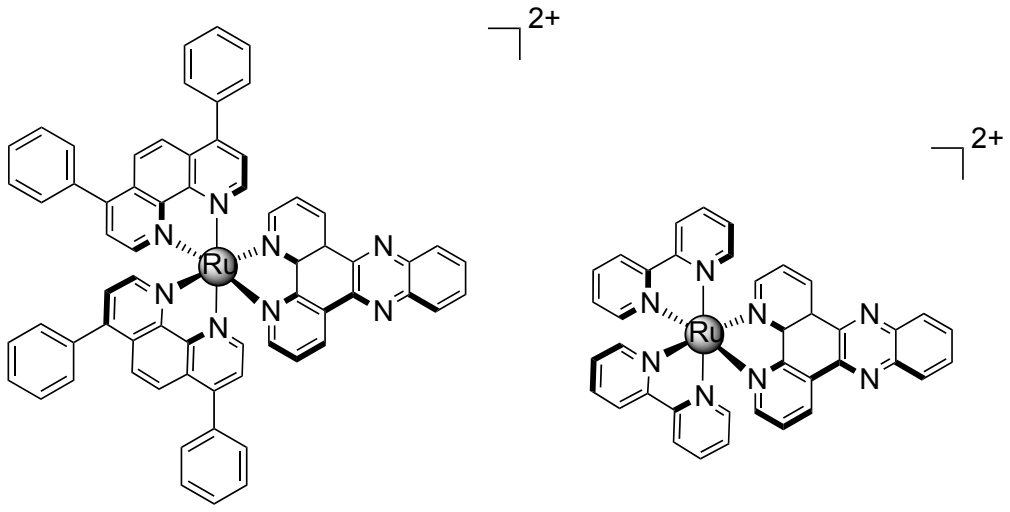

$[Ru(DIP)_2(dppz)]^{2+}$ **$[Ru(bpy)_2(dppz)]^{2+}$**

Figure 1.34 Chemical structure of $[Ru(DIP)_2(dppz)]^{2+}$ and $[Ru(bpy)_2(dppz)]^{2+}$.

Some studies have been presented showing how Ru(II) complexes are also able to interact with telomeric DNA. More recently a trinuclear Ru(II) (Figure 1.35) polypyridyl complex was synthesized and CD studies showed that it is able to induce conformational changes of human telomeric DNA and in addition it is also able to stabilize G-quadruplexes.[111]

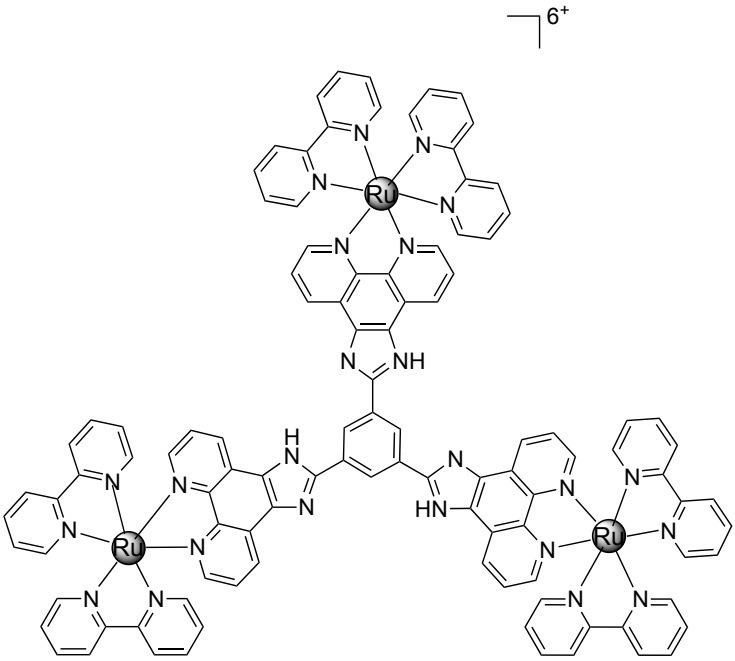

Figure 1.35 Chemical structure of a trinuclear Ru(II) polypyridyl complex which stabilizes telomeric quadruplexes.

1.4.3 Rhodium Complexes as Anticancer Agents

Several groups have explored the photochemical and photophysical properties of rhodium compounds. In particular, Rh(III) complexes with nitrogen aromatic ligands are of importance for their DNA recognition and cleavage features.[101] However, anticancer properties of rhodium complexes have not attracted as much attention as other metals, like platinum or ruthenium. Recent interest has been growing in the use of rhodium complexes for biological and medicinal purposes.[91, 123]

As anticancer compounds, special attention was given to the dirhodium (II,II) carboxylate complexes studied by Kim Dunbar's research group in the 70's. They reported a family of dirhodium (II,II) complexes $Rh_2(\mu\text{-}O_2CR_4)$ (Figure 1.36) which

exhibit significant *in vivo* antitumor activity against L1210 tumours, Ehrlich ascites, sarcoma 180 and P388 tumour lines.[90]

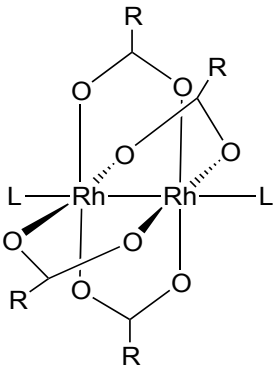

R=Me, Et, Pr, CF_3

dirhodium carboxylates

Figure 1.36 Chemical structure of $Rh_2(\mu\text{-}O_2CR_4)$.

These complexes are believed to bind to DNA and inhibit DNA replication and protein synthesis in a similar way to cisplatin.[124-127]

In a joint collaboration, Dunbar and Turro's research laboratories developed a new family of di-rhodium(II,II) carboxylate complexes that hold an intercalating ligand. These complexes exhibit antitumor properties and can be potent agents for photochemotherapy.[98, 99, 128, 129] Recently they have synthesized a series of complexes of dirhodium (II,II) of the type *cis*-$[Rh_2(\mu\text{-}O_2CCH_3)(dppn)(L)]^{2+}$ (Figure 1.37) and their photocleavage properties were further explored.[130]

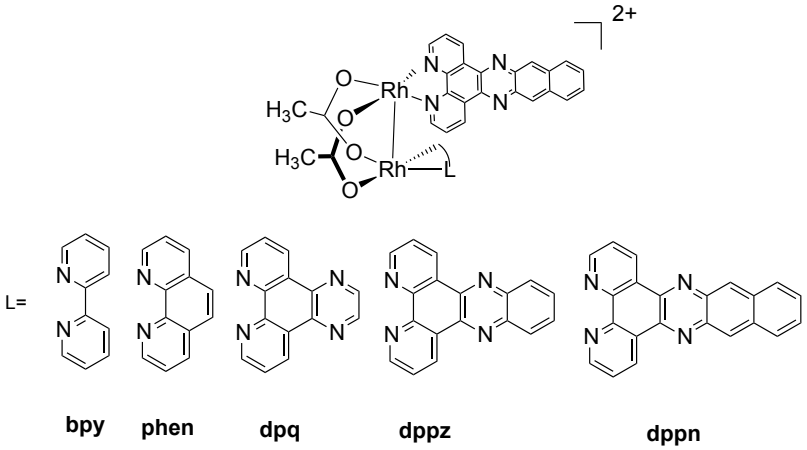

Figure 1.37 Chemical structure of *cis*-[$Rh_2(\mu\text{-}O_2CCH_3)(dppn)(L)]^{2+}$

For example, when L=bpy, the complex does not intercalate between the DNA base pairs and DNA photocleavage proceeds via both oxygen dependent and independent mechanisms. In addition, the complex exhibits similar light and lower dark toxicity to a known PDT agent (hematoporphyrin).[98]

The importance of new complexes for PDT was already addressed before. In this context, Morrison and co-workers developed an important work with the studies on rhodium (III) *cis*-dichloride complexes. The *cis*-[$Rh(phen)_2Cl_2$] (Bisphen)(Figure 1.38, Left) when irradiated binds covalently to nucleic acids primarily to G, cross-links RNA and inactivates viral DNA.[131, 132]

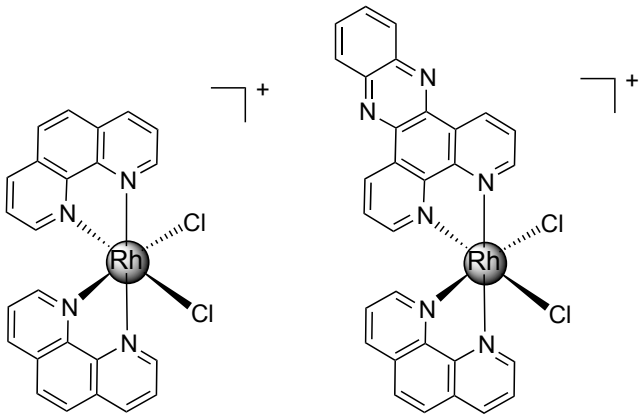

Bisphen **Dppzphen**

Figure 1.38 Chemical structure of Rh(III) photoactivated complexes: *cis*-$[Rh(phen)_2Cl_2]$ (Bisphen) and $[Rh(phen)(dppz)Cl_2]$ (Dppzphen).

In dark conditions this complex shows minimal affinity with DNA once it lacks a ligand with intercalation abilities.[133] To overcome this situation, they have synthesized a similar complex bearing a dppz ligand instead of one of the phen ligands (Dppzphen) (Figure 1.38, Right), which is capable to penetrate tumour cell membranes and in addition it displays phototoxic activity towards tumour cells and to alphavirus Sindbis. Upon irradiation with light $\lambda_{irradiation}$ >330 nm, it binds covalently to ct-DNA.[133] An important feature of Dppzphen is its ability to be photoactivated by an oxygen-independent mechanism, which makes it a very promising PDT candidate, as tumour cells are very often hypoxic.[133, 134]

More recently Sheldrick and co-workers have been investigating the cytotoxicity of mononuclear Rh(III) polypyridyl complexes and, exploring different ligands, they have been trying to establish structure activity relationships (SAR's) among several complexes.[135, 136] They showed that the meridional rhodium(III) polypyridyl complexes

of the type *mer*-[RhX_3(DMSO)(pp)] (X=Cl, Br) (Figure 1.39) where pp can be bpy, phen, dpq or dppz are potent cytostatic agents for treatment of lymphoma and leukemia.

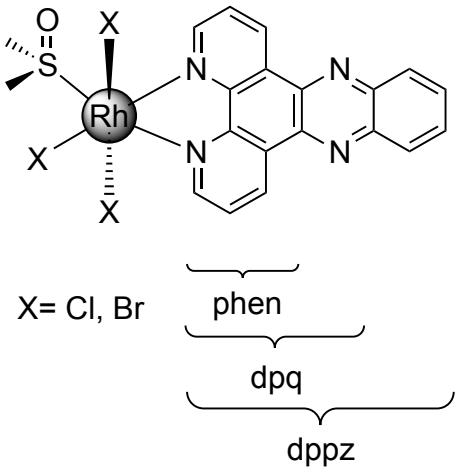

Figure 1.39 Meridional rhodium(III) complexes *mer*-[RhX_3(DMSO)(pp)].[135]

They showed that the cytotoxicity of these complexes is directly correlated with the size of the polypyridyl ligand with complexes of dppz and dpq having lower IC_{50} than the ones with phen and bpy.[137] It was also shown that *mer*-[RhX_3(DMSO)(pp)] (pp=dpq and dppz) complexes induce apoptosis via the intrinsic mitochondrial pathway. In addition the Rh(III) meridional complexes are more cytotoxic when compared with the facial geometry. Analogous studies performed with Ru(II) and Ir(III) complexes, showed that these last ones are less cytotoxic towards the same cell lines which can be explained by differences in the rate of DMSO/H_2O exchange.

Complexes of the type *mer*-[$RhCl_3$(tpy)] and [Rh(Im)$(tpy)_2$]$Cl_3.3H_2O$ (lm= imidazole) are also known to possess high cytotoxic activity towards HCV29T tumour cells.[138, 139]

Brewer and co-workers, synthesized mixed-metal supramolecules $[\{(bpy)_2Ru(dpp)\}_2RhCl_2]Cl_5$ and $[\{(bpy)_2Os(dpp)\}_2RhCl_2]Cl_5$ (Figure 1.40) which are able to photocleave supercoiled circular plasmid DNA when irradiated with light $\lambda_{irradiation}$ >450 nm in presence and absence of molecular oxygen.[20, 140-142]

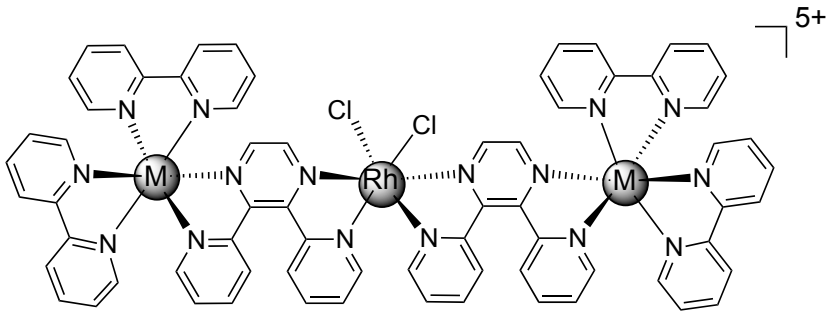

$[\{(bpy)_2M(dpp)\}_2RhCl_2]^{5+}$
M=Ru(II) or Os(II)

Figure 1.40 Mixed-metal supramolecules $[\{(bpy)_2M(dpp)\}_2RhCl_2]^{5+}$ used for photobiology studies where M can be either Ru(II) or Os(II).

A photochemical study was reported using these two supramolecules on African green monkey (*Chlorocebus sabaceus*) kidney (Vero) cells. They showed that when cells were treated with both molecules and exposed to light there was an inhibition of cell growth and replication which did not happen under total dark conditions.[134] The mixed supramolecule bearing ruthenium metal centres apart from causing cell growth inhibition showed evidence of cell death as well, while the complex with osmium only showed inhibition of cell growth.[134]

Barton's research group has done much work on Rh(III) metallo-intercalators [21, 143] containing ligands such as phi and dppz used as intercalating units. Intercalation of the metal complexes was first demonstrated using photophysical and NMR studies. A high-

resolution crystal structure of a Rh(III) intercalator with DNA oligonucleotide has been obtained and allows more precise details about this DNA binding mode (Figure 1.41). This metallo-intercalator enters the DNA double helix from the major groove with the intercalating moiety acting as a new base pair, resulting in a widening of the major groove at the binding site.[21, 144, 145]

While it is known that ruthenium dppz based metallo-intercalators have the ability to work as DNA light switch molecules, rhodium intercalators are efficient DNA photocleavage agents allowing the identification and characterization of the intercalation site (DNA Footprinting). Most of these studies rely on complexes of phi ligands like $[Rh(bpy)_2(phi)]^{3+}$, $[Rh(phen)_2(phi)]^{3+}$ $[Rh(phi)_2(bpy)]^{3+}$.[21, 96]

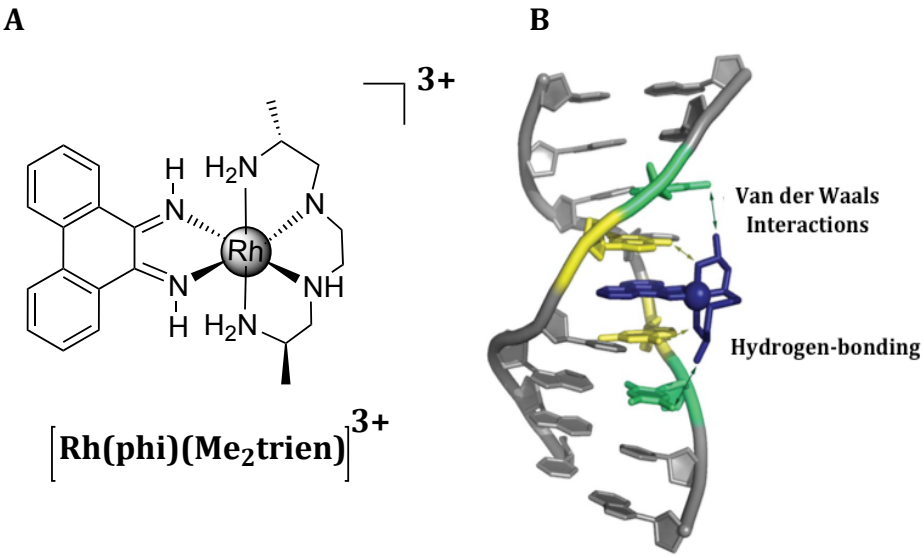

Figure 1.41 (A) Chemical structure of Δ-α-[Rh{(*R,R*)-Me_2trien}(phi)]$^{3+}$; (B) Crystal structure of the Rh(III) metallo-intercalator Δ-α-[Rh{(*R,R*)-Me_2trien}(phi)]$^{3+}$ bound to a target sequence, 5'-TGCA-3' (from ref[21]).

An approach to achieve selectivity in DNA binding is to conjugate complexes to structures, which possess DNA selectivity; one example is peptides. A bifunctional

metallo-intercalator where a metal-coordinating peptide is covalently attached to $[Rh(phi)_2(bpy')]^{3+}$ (Figure 1.42), was designed and synthesized.[24] The intercalator moiety acts as a coordination vector, which directs the peptide to the DNA backbone and the peptide promotes DNA hydrolytic cleavage. Studies showed that this conjugate could act as an artificial nuclease (Figure 1.42).[21, 24]

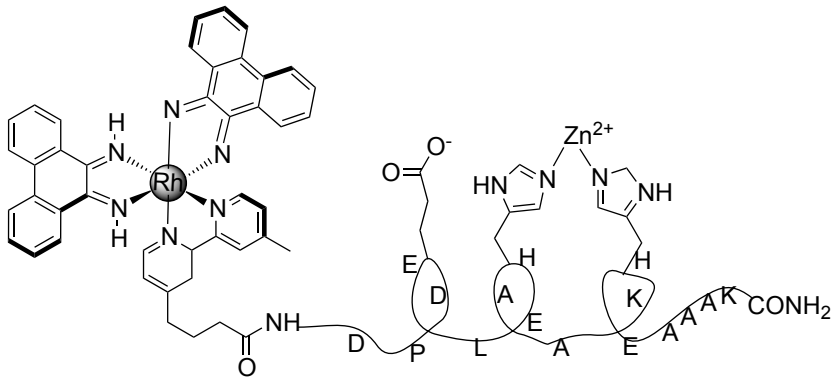

Figure 1.42 Chemical structure of a rhodium complex with a peptide chimera.

More recently, some rhodium(III) and also ruthenium(II) intercalators have been specifically designed to target DNA mismatches.[21, 146-149] During the DNA replication and recombination process some errors might commonly occur: deletion, erroneous insertion and mis-incorporation of bases. This can happen through polymerase errors, and damage can also occur by exposure to genotoxic chemicals or UV or ionizing radiation.[8, 145, 150] Targeting DNA base pair mismatch sequences is a new challenge for chemotherapeutics: it is known that many cancers are associated with a deficiency in DNA mismatch repair.[92, 151]

The premise of this approach is that bulky rhodium intercalators are too wide to insert into B-DNA matched sequences and instead they preferentially target the bulged mispaired sites. The $[Rh(bpy)_2(chrysi)]^{3+}$ was synthesized and reported to bind

selectively to a mismatch DNA duplex containing two AC mismatches (Figure 1.43).[152] A crystal structure of the complex bound to a mismatched DNA allowed structural characterization revealing that the compound intercalates at the mismatch site, ejecting the mismatched bases and replacing the pair with the aromatic four-ring system of one of the ligands (insertion) while the remaining part of the ligand resides in the minor groove.[21, 152] The complex binds and cleaves 80% of mismatch DNA sites, with the Δ-enantiomer being far more effective than the Λ-enantiomer, which is almost inactive.[21, 153, 154] Also a correlation was found between the metal complex and the stability of the mismatch site: the higher the stability of the mismatch the stronger and tighter the binding. Of note is the fact that the insertion of the bulky metallo-insertor causes minor distortions on the duplex DNA structure.[155]

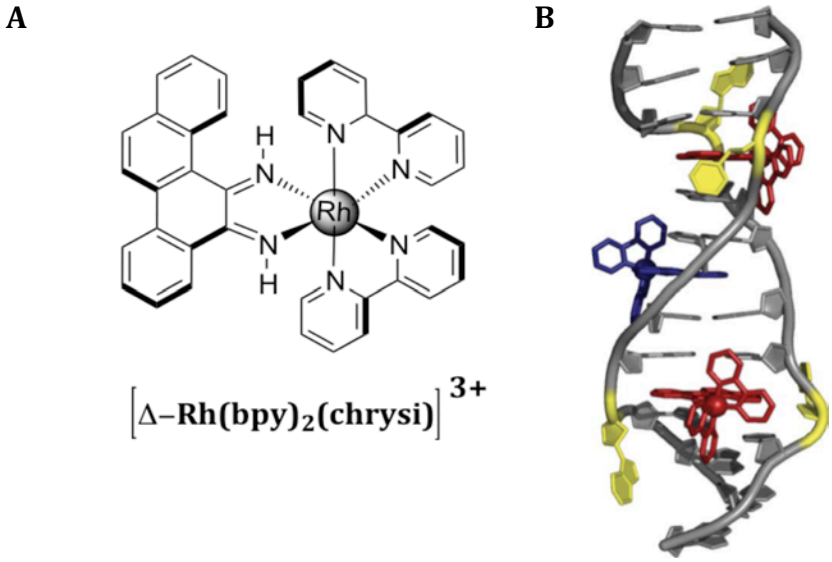

Figure 1.43 (A) Chemical structure of Δ-$[Rh(bpy)_2(chrysi)]^{3+}$; (B) Crystal structure of the Rh(III) metalllo-intercalator Δ-$[Rh(bpy)_2(chrysi)]^{3+}$ bound to a target mismatch AC DNA sequence 5'-CGGA*A*ATT*C*CCG-3' (from ref[21]).

When studied in cells $[Rh(bpy)_2(chrysi)]^{3+}$ (Figure 1.43) selectively inhibits cellular proliferation in mismatch repair deficient cells when compared with cells which are

mismatch proficient. More interestingly, this process seems to be enantioselective as the Δ-enantiomer once again showing a higher anti-proliferative effect when compared with the Λ-enantiomer meaning that DNA is the biological target.[156]

A conjugate of this bulge intercalator with a fluorophore (Oregon Green) was designed to create a fluorescent probe to study and characterize mismatch recognition sites. [146, 150, 157] The rhodium-fluorophore complex (Figure 1.44) selectively binds and photocleaves DNA mismatches with an enhanced fluorescence upon binding.[21, 101, 150]

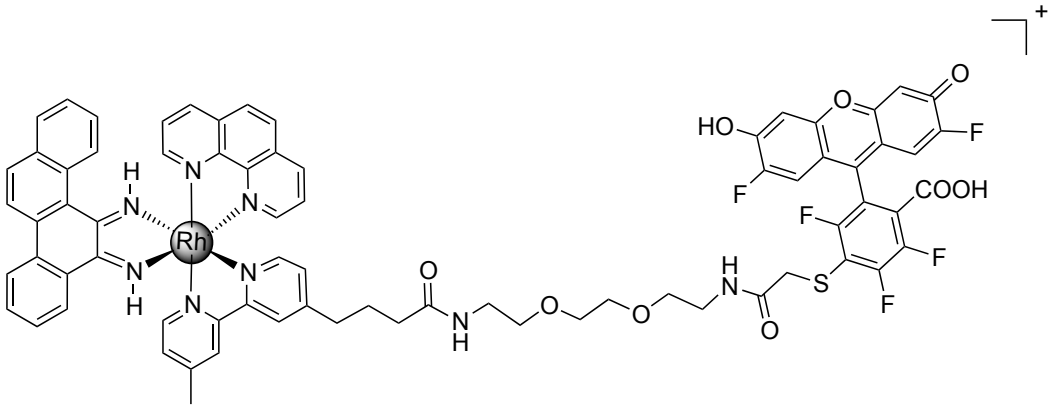

Rhodium-Oregon Green Conjugate

Figure 1.44 Rhodium-Oregon Green Conjugate, Luminescent probe for mismatch detection.

1.5 Final Remarks and Thesis Aims

As has been seen, DNA binding and recognition is being widely explored. Transition metal complexes are attractive for such agents not only for the cationic charge they afford but as metal centres and ligands can be changed in a relatively easy way to allow different properties to be incorporated (cleavage, fluorescence, etc.). This has made possible to create new pathways for DNA binding selectivity.

Among the most exciting new design for DNA binding are the supramolecular cylinders developed by the Hannon group.

This thesis aims to exploit the great properties of rhodium metal centres, discussed in this chapter, and combine them with the remarkable supramolecular designs developed by Hannon's group in the last decade to achieve powerful DNA binders with photo and cleavage activity.

Several Rh(III) molecules will be designed and synthetic conditions will be explored. DNA binding and preliminary cytotoxic studies in cancer cell lines will be reported.

1.6 References

[1] T. W. Johann, J. K. Barton, *Philosophical Transactions of the Royal Society of London Series a-Mathematical Physical and Engineering Sciences* **1996**, *354*, 299.

[2] M. J. Hannon, *Chemical Society Reviews* **2007**, *36*, 280.

[3] M. H. Werner, A. M. Gronenborn, G. M. Clore, *Science* **1996**, *271*, 778.

[4] J. D. Watson, F. H. C. Crick, *Nature* **1953**, *171*, 964.

[5] G. L. Wang, L. A. Christensen, K. M. Vasquez, *Proc. Natl. Acad. Sci. U. S. A.* **2006**, *103*, 2677.

[6] M. Balaz, M. De Napoli, A. E. Holmes, A. Mammana, K. Nakanishi, N. Berova, R. Purrello, *Angew. Chem., Int. Ed.* **2005**, *44*, 4006.

[7] J. R. Bothe, K. Lowenhaupte, H.M.Al-Hashimi, *J. Am. Chem. Soc.* **2011**, *133*, 2016.

[8] N. V. Hud, *Nucleic Acid-Metal Ion Interactions*, RCS Publishing, **2009**.

[9] A. Oleksi, A. G. Blanco, R. Boer, I. Uson, J. Aymami, A. Rodger, M. J. Hannon, M. Coll, *Angew. Chem., Int. Ed.* **2006**, *45*, 1227.

[10] P. G. Baraldi, A. Bovero, F. Fruttarolo, D. Preti, M. A. Tabrizi, M. G. Pavani, R. Romagnoli, *Med. Res. Rev.* **2004**, *24*, 475.

[11] M. J. Hannon, *Pure Appl. Chem.* **2007**, *79*, 2243.

[12] S.Neidle, *Principle of nucleic acid structure*, Elsevier Inc., London, **2008**.

[13] P. E. Nielsen, M. Egholm, R. H. Berg, O. Buchardt, *Science* **1991**, *254*, 1497.

[14] L. Cardo, M. J. Hannon, *Inorg. Chim. Acta* **2009**, *362*, 784.

[15] L. S. Lerman, *J. Mol. Biol.* **1961**, *3*, 18.

[16] K. W. Jennette, J. T. Gill, J. A. Sadownick, S. J. Lippard, *J. Am. Chem. Soc.* **1976**, *98*, 6159.

[17] R. Martinez, L. Chacon-Garcia, *Curr. Med. Chem.* **2005**, *12*, 127.

[18] P. J. Bond, Langridge, R., Jennette, K. W., Lippard, S.J., *Proc. Natl. Acad. Sci. U. S. A.* **1975**, *72*, 4825.

[19] P. K. L. Fu, P. M. Bradley, C. Turro, *Inorg. Chem.* **2003**, *42*, 878.

[20] S. Swavey, K. J. Brewer, *Inorg. Chem.* **2002**, *41*, 6196.

[21] B. M. Zeglis, V. C. Pierre, J. K. Barton, *Chem. Commun.* **2007**, 4565.

[22] R. E. Holmlin, J. A. Yao, J. K. Barton, *Inorg. Chem.* **1999**, *38*, 174.

[23] K. E. Erkkila, D. T. Odom, J. K. Barton, *Chem.Rev.* **1999**, *99*, 2777.

[24] M. P. Fitzsimons, J. K. Barton, *J. Am. Chem. Soc.* **1997**, *119*, 3379.

[25] J. K. Barton, M. Fitzsimons, N. Y. Sardesai, *Abstracts of Papers of the American Chemical Society* **1996**, *212*, 179.

[26] J. Brunner, J. K. Barton, *Biochemistry* **2006**, *45*, 12295.

[27] M. Galanski, B. K. Keppler, *Anti-Cancer Agents Med. Chem.* **2007**, *7*, 55.

[28] Rosenber.B, E. Renshaw, L. Vancamp, J. Hartwick, J. Drobnik, *J. Bacteriol.* **1967**, *93*, 716.

[29] B. Lippert, *Cisplatin, Chemistry and Biochemistry of a Leading Anti-Cancer Drug*, Wiley-VCH, Weinheim, **1999**.

[30] A. M. Pizarro, P. J. Sadler, *Biochimie* **2009**, *91*, 1198.

[31] B.Lippert, *Cisplatin Chemistry and Biochemistry of a Leading Anticancer Drug*, Wiley-VCH, **1999**.

[32] D. Wang, G. Y. Zhu, X. H. Huang, S. J. Lippard, *Proc. Natl. Acad. Sci. U. S. A.* **2010**, *107*, 9584.

[33] E. R. Jamieson, S. J. Lippard, *Chem.Rev.* **1999**, *99*, 2467.

[34] R. E. Mahnken, M. A. Billadeau, E. P. Nikonowicz, H. Morrison, *J. Am. Chem. Soc.* **1992**, *114*, 9253.

[35] C. Sanchez-Cano, M. Huxley, C. Ducani, A. E. Hamad, M. J. Browning, C. Navarro-Ranninger, A. G. Quiroga, A. Rodger, M. J. Hannon, *Dalton Trans.* **2010**, *39*, 11365.

[36] M. Huxley, C. Sanchez-Cano, M. J. Browning, C. Navarro-Ranninger, A. G. Quiroga, A. Rodger, M. J. Hannon, *Dalton Trans.* **2010**, *39*, 11353.

[37] W. H. Ang, M. Myint, S. J. Lippard, *J. Am. Chem. Soc.* **2010**, *132*, 7429.

[38] S. F. Bellon, J. H. Coleman, S. J. Lippard, *Biochemistry* **1991**, *30*, 8026.

[39] P. M. Takahara, A. C. Rosenzweig, C. A. Frederick, S. J. Lippard, *Nature* **1995**, *377*, 649.

[40] U. M. Ohndorf, M. A. Rould, Q. He, C. O. Pabo, S. J. Lippard, *Nature* **1999**, *399*, 708.

[41] C. Sanchez-Cano, M. J. Hannon, *Dalton Trans.* **2009**, 10702.

[42] R. N. Bose, *Proc. Natl. Acad. Sci. U. S. A.* **2008**, *105*, 18314.

[43] R. N. Bose, L. Maurmann, R. J. Mishur, L. Yasui, S. Gupta, W. S. Grayburn, H. Hofstetter, T. Milton, *Proc. Natl. Acad. Sci. U. S. A.* **2008**, *105*, 18314.

[44] A. Harris, Y. Qu, N. Farrell, *Inorg. Chem.* **2005**, *44*, 1196.

[45] S. Komeda, T. Moulaei, K. K. Woods, M. Chikuma, N. P. Farrell, L. D. Williams, *J. Am. Chem. Soc.* **2006**, *128*, 16092.

[46] J. B. Mangrum, N. P. Farrell, *Chem. Commun.* **2010**, *46*, 6640.

[47] D. M. J. Lilley, *Q. Rev. Biophys.* **2000**, *33*, 109.

[48] A. L. Brogden, N. H. Hopcroft, M. Searcey, C. J. Cardin, *Angew. Chem., Int. Ed.* **2007**, *46*, 3850.

[49] R. R. Sinden, *Nature* **2001**, *411*, 757.

[50] L. Cerasino, M. J. Hannon, E. Sletten, *Inorg. Chem.* **2007**, *46*, 6245.

[51] J. Malina, M. J. Hannon, V. Brabec, *Chem.Eur. J.* **2007**, *13*, 3871.

[52] D. M. J. Lilley, *Biochem. Soc. Trans.* **2010**, *38*, 399.

[53] L. A. Howell, M. Searcey, *ChemBioChem* **2009**, *10*, 2139.

[54] L. A. Howell, R. Gulam, A. Mueller, M. A. O'Connell, M. Searcey, *Bioorg. Med. Chem. Lett.* **2010**, *20*, 6956.

[55] M. Tanada, S. Tsujita, S. Sasaki, *J. Org. Chem.* **2006**, *71*, 125.

[56] M. L. Carpenter, G. Lowe, P. R. Cook, *Nucleic Acids Res.* **1996**, *24*, 1594.

[57] G. T. Song, J. S. Ren, *Chem. Commun.* **2010**, *46*, 7283.

[58] A. K. Todd, M. Johnston, S. Neidle, *Nucleic Acids Res.* **2005**, *33*, 2901.

[59] S. Haider, G. N. Parkinson, S. Neidle, *J. Mol. Biol.* **2002**, *320*, 189.

[60] S. N. Georgiades, N. H. Abd Karim, K. Suntharalingam, R. Vilar, *Angew. Chem., Int. Ed.* **2010**, *49*, 4020.

[61] K. L. Haas, K. J. Franz, *Chem.Rev.* **2009**, *109*, 4921.

[62] K. Suntharalingam, A. J. P. White, R. Vilar, *Inorg. Chem.* **2010**, *49*, 8371.

[63] S. Rankin, A. P. Reszka, J. Huppert, M. Zloh, G. N. Parkinson, A. K. Todd, S. Ladame, S. Balasubramanian, S. Neidle, *J. Am. Chem. Soc.* **2005**, *127*, 10584.

[64] G.W.Collie, S. Sparapani, G.N.Parkinson, S. Neidle, *J. Am. Chem. Soc.* **2011**.

[65] K. M. Rahman, A. P. Reszka, M. Gunaratnam, S. M. Haider, P. W. Howard, K. R. Fox, S. Neidle, D. E. Thurston, *Chem. Commun.* **2009**, 4097.

[66] H. J. Yu, X. H. Wang, M. L. Fu, J. S. Ren, X. G. Qu, *Nucleic Acids Res.* **2008**, *36*, 5695.

[67] J. M. Lehn, *Science* **1993**, *260*, 1762.

[68] C. Piguet, G. Bernardinelli, G. Hopfgartner, *Chem.Rev.* **1997**, *97*, 2005.

[69] R. Kramer, J. M. Lehn, A. Marquisrigault, *Proc. Natl. Acad. Sci. U. S. A.* **1993**, *90*, 5394.

[70] M. J. Hannon, V. Moreno, M. J. Prieto, E. Moldrheim, E. Sletten, I. Meistermann, C. J. Isaac, K. J. Sanders, A. Rodger, *Angew. Chem., Int. Ed.* **2001**, *40*, 880.

[71] M. J. Hannon, C. L. Painting, A. Jackson, J. Hamblin, W. Errington, *Chem. Commun.* **1997**, 1807.

[72] G. I. Pascu, A. C. G. Hotze, C. Sanchez-Cano, B. M. Kariuki, M. J. Hannon, *Angew. Chem., Int. Ed.* **2007**, *46*, 4374.

[73] J. C. Peberdy, J. Malina, S. Khalid, M. J. Hannon, A. Rodger, *Journal of Inorganic Biochemistry* **2007**, *101*, 1937.

[74] J. M. C. A. Kerckhoffs, J. C. Peberdy, I. Meistermann, L. J. Childs, C. J. Isaac, C. R. Pearmund, V. Reudegger, S. Khalid, N. W. Alcock, M. J. Hannon, A. Rodger, *Dalton Trans.* **2007**, 734.

[75] M. J. Hannon, L. J. Childs, *Supramol. Chem.* **2004**, *16*, 7.

[76] S. Khalid, M. J. Hannon, A. Rodger, P. M. Rodger, *Chem.Eur. J.* **2006**, *12*, 3493.

[77] I. Meistermann, V. Moreno, M. J. Prieto, E. Moldrheim, E. Sletten, S. Khalid, P. M. Rodger, J. C. Peberdy, C. J. Isaac, A. Rodger, M. J. Hannon, *Proc. Natl. Acad. Sci. U. S. A.* **2002**, *99*, 5069.

[78] J. Malina, M. J. Hannon, V. Brabec, *Nucleic Acids Res.* **2008**, *36*, 3630.

[79] J. Malina, M. J. Hannon, V. Brabec, *Chem.Eur. J.* **2008**, *14*, 10408.

[80] C. Ducani, A. Leczkowska, N. J. Hodges, M. J. Hannon, *Angew. Chem. Int. Ed* **2010**, *49*, 1.

[81] A. C. G. Hotze, N. J. Hodges, R. E. Hayden, C. Sanchez-Cano, C. Paines, N. Male, M. K. Tse, C. M. Bunce, J. K. Chipman, M. J. Hannon, *Chemistry & Biology* **2008**, *15*, 1258.

[82] L. J. Childs, J. Malina, B. E. Rolfsnes, M. Pascu, M. L. Prieto, M. L. Broome, P. M. Rodger, E. Sletten, V. Moreno, A. Rodger, M. J. Hannon, *Chem.Eur. J.* **2006**, *12*, 4919.

[83] L. J. Childs, M. Pascu, A. J. Clarke, N. W. Alcock, M. L. Hannon, *Chem.Eur. J.* **2004**, *10*, 4291.

[84] A. C. G. Hotze, E. P. L. van der Geer, H. Kooijman, A. L. Spek, J. G. Haasnoot, J. Reedijk, *Eur. J. Inorg. Chem.* **2005**, 2648.

[85] A. C. G. Hotze, E. P. L. van der Geer, S. E. Caspers, H. Kooijman, A. L. Spek, J. G. Haasnoot, J. Reedijk, *Inorg. Chem.* **2004**, *43*, 4935.

[86] A. C. G. Hotze, A. H. Velders, F. Ugozzoli, M. Biagini-Cingi, A. M. Manotti-Lanfredi, J. G. Haasnoot, J. Reedijk, *Inorg. Chem.* **2000**, *39*, 3838.

[87] A. C. G. Hotze, B. M. Kariuki, M. J. Hannon, *Angew. Chem., Int. Ed.* **2006**, *45*, 4839.

[88] A. H. Velders, K. van der Schilden, A. C. G. Hotze, J. Reedijk, H. Kooijman, A. L. Spek, *Dalton Trans.* **2004**, 448.

[89] A.Pope, *Supramolecular Anticancer Agents and Their Effects on Cells and Biomelecules, PhD Thesis*, University of Birmingham, Birmingham, **2010**.

[90] H. T. Chifotides, K. R. Dunbar, *Acc. Chem. Res.* **2005**, *38*, 146.

[91] S. H. van Rijt, P. J. Sadler, *Drug Discovery Today* **2009**, *14*, 1089.

[92] H. Junicke, J. R. Hart, J. Kisko, O. Glebov, I. R. Kirsch, J. K. Barton, *Proc. Natl. Acad. Sci. U. S. A.* **2003**, *100*, 3737.

[93] B. A. Jackson, J. K. Barton, *Biochemistry* **2000**, *39*, 6176.

[94] N. J. Farrer, L. Salassa, P. J. Sadler, *Dalton Trans.* **2009**, 10690.

[95] M. Y. Berezin, S. Achilefu, *Chem. Rev.* **2010**, *110*, 2641.

[96] A. Sitlani, E. C. Long, A. M. Pyle, J. K. Barton, *J. Am. Chem. Soc.* **1992**, *114*, 2303.

[97] C. A. Mitsopoulou, C. Dagas, *Bioinorg. Chem. Appl.* **2010**.

[98] A. M. Angeles-Boza, P. M. Bradley, P. K. L. Fu, M. Shatruk, M. G. Hilfiger, K. R. Dunbar, C. Turro, *Inorg. Chem.* **2005**, *44*, 7262.

[99] A. M. Angeles-Boza, H. T. Chifotides, J. D. Aguirre, A. Chouai, P. K. L. Fu, K. R. Dunbar, C. Turro, *J. Med. Chem.* **2006**, *49*, 6841.

[100] D. F. Zigler, J. Wang, K. J. Brewer, *Inorg. Chem.* **2008**, *47*, 11342.

[101] U. Schatzschneider, *Eur. J. Inorg. Chem.* **2010**, 1451.

[102] M. R. Detty, S. L. Gibson, S. J. Wagner, *J. Med. Chem.* **2004**, *47*, 3897.

[103] D. E. J. G. J. Dolmans, D. Fukumura, R. K. Jain, *Nat. Rev. Cancer* **2003**, *3*, 380.

[104] Y. K. Yan, M. Melchart, A. Habtemariam, P. J. Sadler, *Chem. Commun.* **2005**, 4764.

[105] C. G. Hartinger, M. A. Jakupec, S. Zorbas-Seifried, M. Groessl, A. Egger, W. Berger, H. Zorbas, P. J. Dyson, B. K. Keppler, *Chem. Biodiversity* **2008**, *5*, 2140.

[106] M. M. Liu, Z. J. Lim, Y. Y. Gwee, A. Levina, P. A. Lay, *Angew. Chem., Int. Ed.* **2010**, *49*, 1661.

[107] P. Heffeter, K. Bock, B. Atil, M. A. R. Hoda, W. Korner, C. Bartel, U. Jungwirth, B. K. Keppler, M. Micksche, W. Berger, G. Koellensperger, *Journal of Biological Inorganic Chemistry* **2010**, *15*, 737.

[108] A. Bergamo, G. Sava, *Dalton Trans.* **2007**, 1267.

[109] G. Sava, S. Zorzet, C. Turrin, F. Vita, M. Soranzo, G. Zabucchi, M. Cocchietto, A. Bergamo, S. DiGiovine, G. Pezzoni, L. Sartor, S. Garbisa, *Clinical Cancer Research* **2003**, *9*, 1898.

[110] C. Metcalfe, J. A. Thomas, *Chem. Soc. Rev.* **2003**, *32*, 215.

[111] L. Xu, G. L. Liao, X. A. Chen, C. Y. Zhao, H. Chao, L. N. Ji, *Inorg. Chem. Commun.* **2010**, *13*, 1050.

[112] X. L. Liang, L. F. Tan, *Aust. J. Chem.* **2010**, *63*, 1453.

[113] P. Nordell, F. Westerlund, L. M. Wilhelmsson, B. Norden, P. Lincoln, *Angew. Chem., Int. Ed.* **2007**, *46*, 2203.

[114] M. R. Gill, J. Garcia-Lara, S. J. Foster, C. Smythe, G. Battaglia, J. A. Thomas, *Nature Chem.* **2009**, *1*, 662.

[115] J. K. Barton, A. T. Danishefsky, J. M. Goldberg, *J. Am. Chem. Soc.* **1984**, *106*, 2172.

[116] D. A. Lutterman, A. Chouai, Y. Liu, Y. Sun, C. D. Stewart, K. R. Dunbar, C. Turro, *J. Am. Chem. Soc.* **2008**, *130*, 1163.

[117] Q. X. Zhou, W. H. Lei, Y. Sun, J. R. Chen, C. Li, Y. J. Hou, X. S. Wang, B. W. Zhang, *Inorg. Chem.* **2010**, *49*, 4729.

[118] J. W. Dobrucki, *Journal of Photochemistry and Photobiology B-Biology* **2001**, *65*, 136.

[119] C. A. Puckett, J. K. Barton, *J. Am. Chem. Soc.* **2007**, *129*, 46.

[120] C. A. Puckett, R. J. Ernst, J. K. Barton, *Dalton Trans.* **2010**, *39*, 1159.

[121] V. Fernandez-Moreira, F. L. Thorp-Greenwood, M. P. Coogan, *Chem. Commun.* **2010**, *46*, 186.

[122] C. A. Puckett, J. K. Barton, *J. Am. Chem. Soc.* **2009**, *131*, 8738.

[123] R. F. M. Frade, N. R. Candeias, C. M. M. Duarte, V. Andre, M. T. Duarte, P. M. P. Gois, C. A. M. Afonso, *Bioorg. Med. Chem. Lett.* **2010**, *20*, 3413.

[124] H. T. Chifotides, P. K. L. Fu, K. R. Dunbar, C. Turro, *Inorg. Chem.* **2004**, *43*, 1175.

[125] K. Sorasaenee, P. K. L. Fu, A. M. Angeles-Boza, K. R. Dunbar, C. Turro, *Inorg. Chem.* **2003**, *42*, 1267.

[126] H. T. Chifotides, J. M. Koomen, M. J. Kang, S. E. Tichy, K. R. Dunbar, D. H. Russell, *Inorg. Chem.* **2004**, *43*, 6177.

[127] D. V. Deubel, H. T. Chifotides, *Chem. Commun.* **2007**, 3438.

[128] J. D. Aguirre, A. M. Angeles-Boza, A. Chouai, C. Turro, J. P. Pellois, K. R. Dunbar, *Dalton Trans.* **2009**, 10806.

[129] J. D. Aguirre, H. T. Chifotides, A. M. Angeles-Boza, A. Chouai, C. Turro, K. R. Dunbar, *Inorg. Chem.* **2009**, *48*, 4435.

[130] L. E. Joyce, J. D. Aguirre, A. M. Angeles-Boza, A. Chouai, P. K. L. Fu, K. R. Dunbar, C. Turro, *Inorg. Chem.* **2010**, *49*, 5371.

[131] T. Mohammad, *Toxicol. in Vitro* **2004**, *18*, 45.

[132] D. Loganathan, H. Morrison, *Curr. Opin. Drug Discovery Dev.* **2005**, *8*, 478.

[133] E. L. Menon, R. Perera, M. Navarro, R. J. Kuhn, H. Morrison, *Inorg. Chem.* **2004**, *43*, 5373.

[134] A. A. Holder, D. F. Zigler, M. T. Tarrago-Trani, B. Storrie, K. J. Brewer, *Inorg. Chem.* **2007**, *46*, 4760.

[135] M. Harlos, I. Ott, R. Gust, H. Alborzinia, S. Wolfl, A. Kromm, W. S. Sheldrick, *J. Med. Chem.* **2008**, *51*, 3924.

[136] M. Dobroschke, Y. Geldmacher, I. Ott, M. Harlos, L. Kater, L. Wagner, R. Gust, W. S. Sheldrick, A. Prokop, *ChemMedChem* **2009**, *4*, 177.

[137] M. A. Scharwitz, I. Ott, Y. Geldmacher, R. Gust, W. S. Sheldrick, *J. Organomet. Chem.* **2008**, *693*, 2299.

[138] U. Sliwinska, F. P. Pruchnik, I. Pelinska, S. Ulaszewski, A. Wilczok, A. Zajdel, *Journal of Inorganic Biochemistry* **2008**, *102*, 1947.

[139] F. P. Pruchnik, P. Jakimowicz, Z. Ciunik, J. Zakrzewska-Czerwinska, A. Opolski, J. Wietrzyk, E. Wojdat, *Inorg. Chim. Acta* **2002**, *334*, 59.

[140] A. A. Holder, S. Swavey, K. J. Brewer, *Inorg. Chem.* **2004**, *43*, 303.

[141] D. F. Zigler, M. T. Mongelli, M. Jeletic, K. J. Brewer, *Inorg. Chem. Commun.* **2007**, *10*, 295.

[142] M. Elvington, K. J. Brewer, *Inorg. Chem.* **2006**, *45*, 5242.

[143] M. J. Hannon, *Coord. Chem. Rev.* **1997**, *162*, 477.

[144] C. L. Kielkopf, K. E. Erkkila, B. P. Hudson, J. K. Barton, D. C. Rees, *Nature Structural Biology* **2000**, *7*, 117.

[145] R. J. Ernst, H. Song, J. K. Barton, *J. Am. Chem. Soc.* **2009**, *131*, 2359.

[146] A. Petitjean, J. K. Barton, *J. Am. Chem. Soc.* **2004**, *126*, 14728.

[147] B. M. Zeglis, J. K. Barton, *Nat. Protoc.* **2007**, *2*, 357.

[148] B. M. Zeglis, V. C. Pierre, J. T. Kaiser, J. K. Barton, *Biochemistry* **2009**, *48*, 4247.

[149] B. M. Zeglis, J. A. Boland, J. K. Barton, *Biochemistry* **2009**, *48*, 839.

[150] B. M. Zeglis, J. K. Barton, *J. Am. Chem. Soc.* **2006**, *128*, 5654.

[151] A. Duval, R. Hamelin, *Cancer Res.* **2002**, *62*, 2447.

[152] V. C. Pierre, J. T. Kaiser, J. K. Barton, *Proc. Natl. Acad. Sci. U. S. A.* **2007**, *104*, 429.

[153] B. A. Jackson, J. K. Barton, *J. Am. Chem. Soc.* **1997**, *119*, 12986.

[154] A. H. Krotz, B. P. Hudson, J. K. Barton, *J. Am. Chem. Soc.* **1993**, *115*, 12577.

[155] C. Cordier, V. C. Pierre, J. K. Barton, *J. Am. Chem. Soc.* **2007**, *129*, 12287.

[156] J. R. Hart, O. Glebov, R. J. Ernst, I. R. Kirsch, J. K. Barton, *Proc. Natl. Acad. Sci. U. S. A.* **2006**, *103*, 15359.

[157] U. Schatzschneider, J. K. Barton, *J. Am. Chem. Soc.* **2004**, *126*, 8630.

Chapter 2

Novel Rhodium(III) Complexes:

Design, Synthesis and Characterization

2.1 Introduction

The remarkable work and results concerning the metallo-supramolecular cylinders as DNA binding drugs, discussed in Chapter 1, together with known physical properties of Rh(III) diimine complexes (photoactivity and photophysical) encouraged the idea of combining the bidentate cylinder ligands with Rh(III). Studies with Rh(III) complexes in biological systems are scarce when compared with for example Ru(II) either for their DNA binding properties or for their biological activity. Examples of some mononuclear Rh(III) complexes and polypyridyl ligands have been reported[1-3] but not much attention has been given to the potential of dinuclear Rh(III) complexes. The aim of this work is to explore whether it is possible to synthesize new Rh(III) complexes whose molecular properties would be of interest for DNA binding and cytotoxicity studies.

In this chapter, new mononuclear complexes and several dinuclear (single, double and triple stranded) are designed and methodology for their synthesis explored. The synthesis of a novel class of Rh(III) complexes is established, including purification, methodology and characterization.

2.2 Molecular Design of New Dinuclear Single Stranded and Mononuclear Rh(III) Complexes

The desired initial molecule was a dinuclear single stranded Rh(III) complex consisting of two metal centres linked by a bis-bidentate cylinder-type ligand and attached diimine ligands (phen or bpy), to impart photophysical properties, and/or chloride ligands, for displacement by DNA. An example of such molecular structure is shown in Figure 2.1.

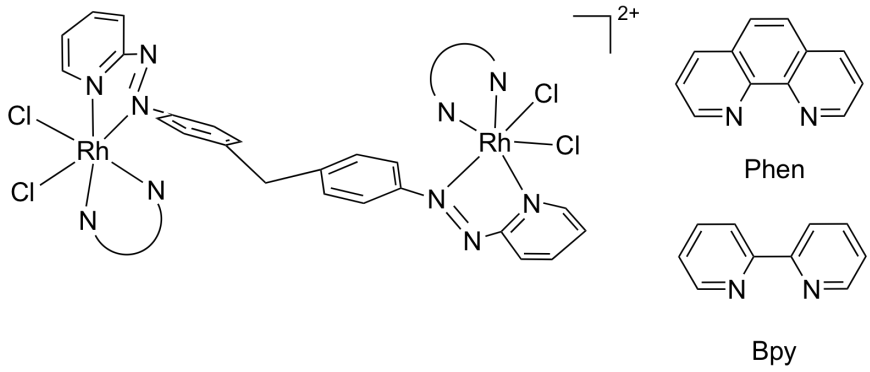

Figure 2.1 Structure of the Rh(III) dinuclear single stranded complexes designed.

Additionally, mononuclear complexes analogous to the dinuclear shown above were designed (Figure 2.2). Instead of the bidentate ligand, the mononuclear complexes display the 2-phenylazopyridine ligand (L_{azpy}), which resembles half of the L_{azo} used for the dinuclear single stranded complex. These mononuclear complexes are also novel.

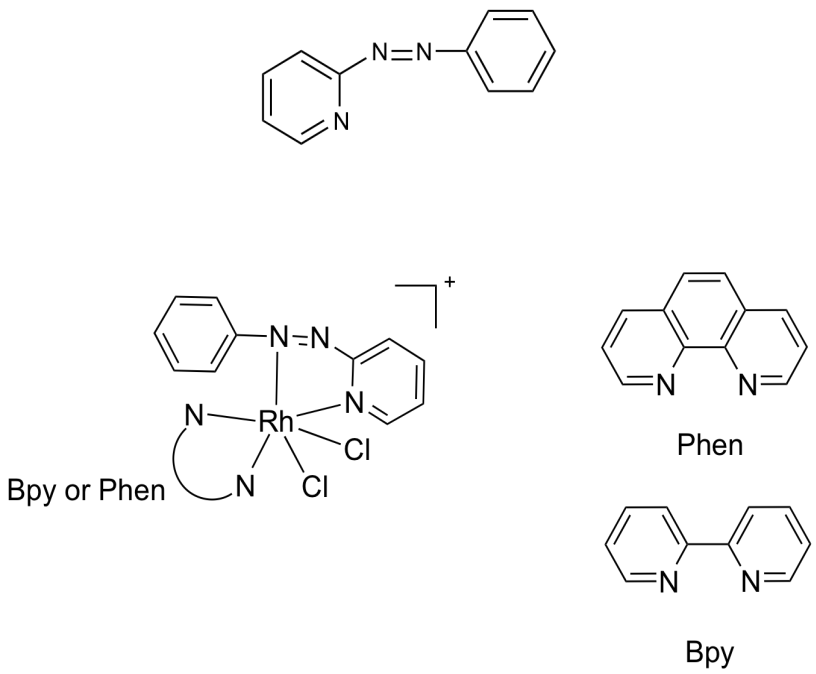

Figure 2.2 (Top) Structure of the 2- phenylazopyridine Ligand (L_{azpy}); (Bottom) Structure of both mononuclear complexes $[Rh(L_{azpy})(phen)Cl_2]^+$ and $[Rh(L_{azpy})(bpy)Cl_2]^+$.

The bidentate ligand L_{azo} was chosen instead of the analogous imine ligand (L_{im}) more usually used in the Fe (II)[4] and Ru(II)[5] cylinders, because of its greater stability. Attempts to use L_{im} (various conditions) were unsuccessful probably due to the lability of the imine bond in aqueous conditions.

The inert nature of rhodium (III) makes its chemistry more complicated when compared to other metals and finding ideal reaction conditions, as well as purification methods proved a challenging process.

Initial attempts to use $(H_3O)[Rh(phen)Cl_4]$ as a starting material and reacting with L_{azo} (in different alcohols) following a similar approach used by Barton[6] for the synthesis of $[Rh(phi)(phen)(NH_3)_2]^{3+}$ were unsuccessful.

A different approach using Sheldrick's Rh(III) neutral mononuclear complex $[Rh(DMSO)Cl_3(pp)]$[7] as starting material (where pp could be several polypyridyl ligands like phen or bpy) was then explored. This was more successful and a synthetic

procedure was developed for the synthesis of the first Rh(III) single stranded complexes based on these starting materials.

2.3 Synthesis of the Dinuclear Single Stranded Complexes

2.3.1 Synthesis of the Bisphenylazopyridine (L_{azo})

The bisphenylazopyridine ligand (L_{azo}) was synthesized from 2-nitrosopyridine and 4,4'-methylenedianiline.[8] For the synthesis of the ligand a diamine spacer was added to 2-nitrosopyridine in a ratio of 1 to 2.5 (Scheme 2.1).

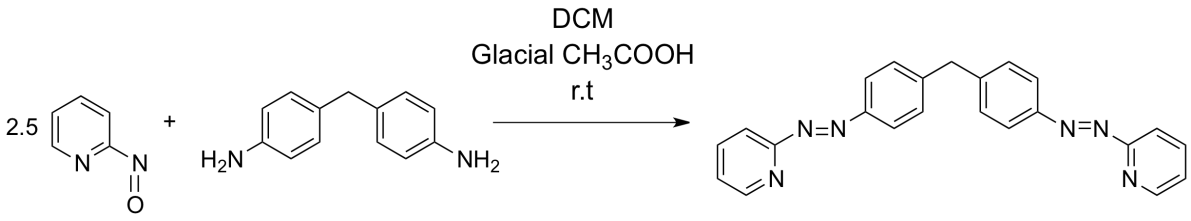

Scheme 2.1 Synthetic route for the preparation of the Bisphenylazopyridine ligand (L_{azo}).

The reaction was carried out at room temperature for 24 hours in DCM with 1 drop of glacial acetic acid. The reaction proceeds through a condensation step with loss of water (dehydration) to afford N=N bond. 2-Nitrosopyridine is not available commercially but can be synthesized following a two-step literature procedure.[9] An excess of 2-nitrosopyridine is required in the ligand synthesis reaction to avoid the formation of half ligand (condensation of only one NH_2 of the diamine to the 2-nitrosopyridine) as a side product. The ligand L_{azo} can be purified by column chromatography on silica gel, but improved purity can be obtained by RP- HPLC using a C_{18} silica column with an isocratic elution method using MeOH:water (90:10). The fact that this ligand can be purified by

chromatography shows the higher stability in comparison with the imine ligand, which cannot be readily purified by chromatography method due to hydrolysis of the imine bond. The orange ligand was obtained in 65% yield and characterized by MS and elemental analysis, which were in accordance with the synthesis of $[C_{23}H_{18}N_6]$. MS spectrum showed fragments corresponding to the species $[C_{23}H_{18}N_6 + H^+]^+$ and $[C_{23}H_{18}N_6 + Na^+]^+$. The ^{1}H-NMR revealed one set of nine resonances consistent with the formation of a symmetrical molecule.

2.3.2 Synthesis of the Complexes

The desired single stranded complexes were synthesized according to scheme 2.2. The starting materials $[Rh(DMSO)Cl_3(pp)]$ (pp is phen or bpy) were synthesized in two steps starting from the commercially available $RhCl_3.H_2O$ via the *mer*-$[RhCl_3(DMSO)_3]$ using a literature procedure with one equivalent of the appropriate pp ligand.[7] While the synthesis of pure *fac* isomer was reported[7] for $[Rh(DMSO)Cl_3(pp)]$, we instead obtained a 1:1 mixture of the *fac* and *mer* isomers. The two isomers were found to be separable by HPLC with an isocratic elution method using EtOAc 100% as eluent in a C_{18} silica column. However when each separated isomer was reacted with L_{azo}, an identical crude mixture was obtained. Therefore, we decided to use the initial mixture of the *fac* and *mer* isomers in the reaction with the L_{azo} ligand without prior separation/purification. The Rh(III) dinuclear complexes were obtained from the reaction of 5 equivalents of the yellow solid $[Rh(DMSO)Cl_3(pp)]$ with L_{azo} ligand in a mixture of propanol:water (2:1) under reflux. The use of a lower excess of $[Rh(DMSO)Cl_3(pp)]$ led to the co-formation of a mononuclear product. During the reaction, the solution becomes light brown (15 minutes after refluxing) and then dark green, indicating the coordination of the metal to the ligand corresponding

to the RhN_4Cl_2 chromophore.[10, 11] After 40 minutes, the reaction was cooled to room temperature and a dark green complex precipitated after addition of an aqueous saturated solution of NH_4PF_6.

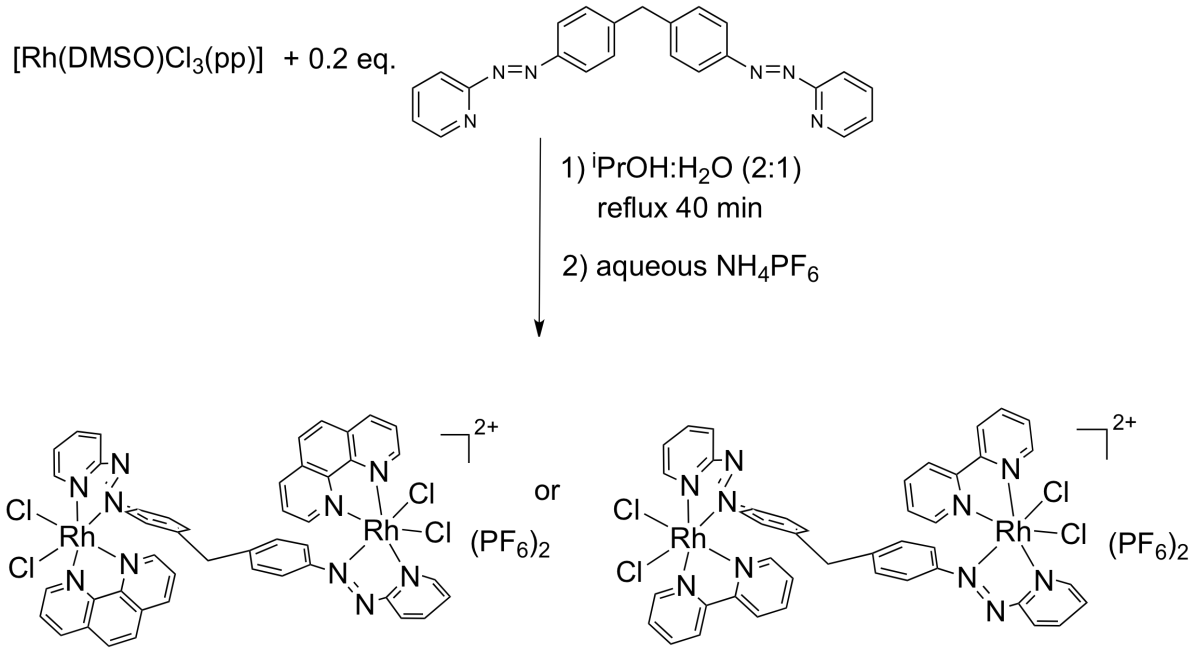

Scheme 2.2 Synthetic route for the preparation of the dinuclear single stranded complexes.

Prolonged reaction times (up to 3 hours) led to the formation of a black insoluble material that could be removed by filtration but resulted in a lower yield of the desired product. This is in accordance with previous observations reported by Brewer and co-workers during the synthesis of mixed metal Rh(III) containing supramolecular complexes.[12]

While mass spectrometry analysis of the crude mixtures revealed the presence of only the desired complex with peaks corresponding to $[Rh_2(L_{azo})(phen)_2Cl_4]^{2+}$ (*m/z* = 543) and $[Rh_2(L_{azo})(phen)_2Cl_4](PF_6)^+$ (*m/z* = 1231) or to $[Rh_2(L_{azo})(bpy)_2Cl_4]^{2+}$(*m/z* = 518) and $[Rh_2(L_{azo})(bpy)_2Cl_4](PF_6)^+$ (*m/z* = 1180) with the correct isotopic pattern, the ^{1}H-NMR spectra indicated the presence of more than one species. Broad peaks in the

region of the CH_2 of the ligand suggested overlapping species as well as several broad and overlapped peaks in the aromatic region (Figure 2.3 and 2.4)

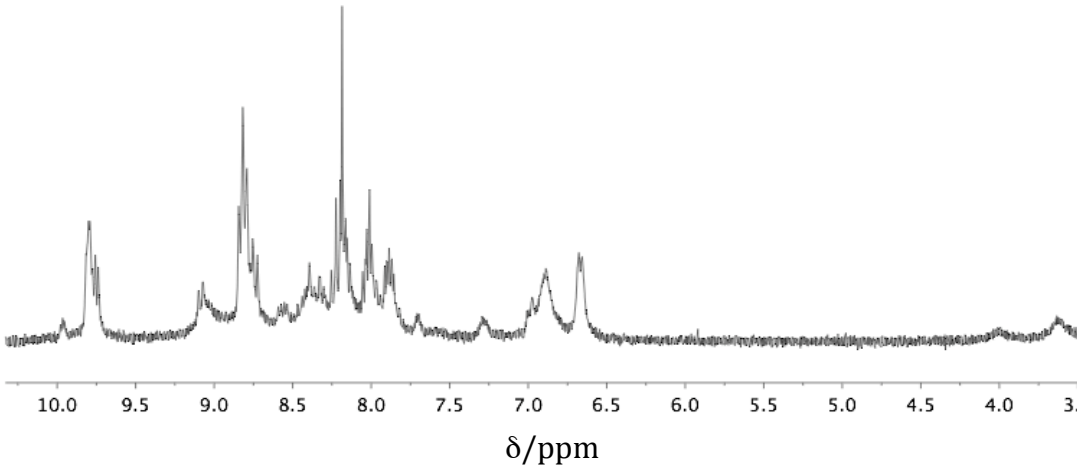

Figure 2.3 ^{1}H-NMR (300 MHz, 25 °C) spectrum of crude mixture of $[Rh_2(L_{azo})(phen)_2Cl_4](PF_6)_2$ in CD_3CN.

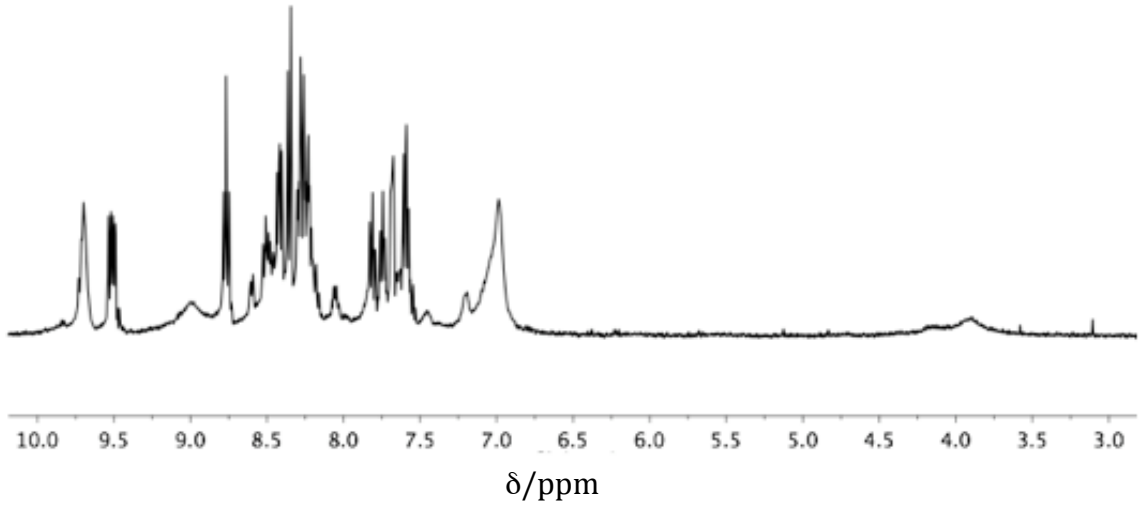

Figure 2.4 ^{1}H-NMR (300 MHz, 25 °C) spectrum of crude mixture of $[Rh_2(L_{azo})(bpy)_2Cl_4](PF_6)_2$ in CD_3CN.

The formation of different isomers was not unexpected since the design incorporates chloride ions and phen or bpy ligands at each metal centre. Three geometric isomers are possible at each metal centre: one with the chlorides in *cis* configuration and the pyr ring *trans* to a phen ring; another with the chlorides in a *cis* configuration and the pyr ring *cis* to both rings and a third one with the chlorides in *trans* configuration. The two configurations with the chlorides in a *cis* configuration would exist as two enantiomers.

The presence of the two metal centres in the molecule affords seven potential isomers, four of which have enantiomers. The ^{1}H-NMR spectra indicate that a smaller subset of the possible seven are present.

Initial attempts to separate the isomers on alumina or silica columns using a number of eluents including organic solvents, mixtures of organic solvents and water, aqueous solutions of NaCl, NH_4PF_6 or KNO_3 were unsuccessful. Eventually a HPLC chromatography method was established which enabled successful separation of two of the different isomers.

2.3.3 Separation of the Isomers by HPLC

HPLC proved to be a more useful technique than flash chromatography and after many attempts and different methods including several organic solvent mixtures ratios, a method for the separation of the isomers was established. An isocratic method using a solution of 85% acetonitrile: 15% of a 2% aqueous solution of KNO_3 was used on HPLC silica column at a flow rate of 1 ml/min. The analytical chromatogram obtained for the crude mixture of $[Rh_2(L_{azo})(phen)_2Cl_4](PF_6)_2$ showed the presence of three peaks with different retention times (detection at a wavelength of 400 nm) (Figure 2.5). A more concentrated solution of the crude mixture in acetonitrile was injected on the analytical column and the collected peaks were concentrated enough to be analyzed by MS. Three different peaks were obtained corresponding to three isomers, each showed the presence of a doubly charged peak with *m/z* = 543 for the phen complexes and *m/z* = 518 for the bpy ones. A preparative separation was optimized, by using an HPLC preparative silica column with readjusted flow rates (20 ml/min) and injection size. The

loading sample size was found to be critical to achieve separation. The optimal load injection found was of 10 mg of solid dissolved in 1 ml of acetonitrile.

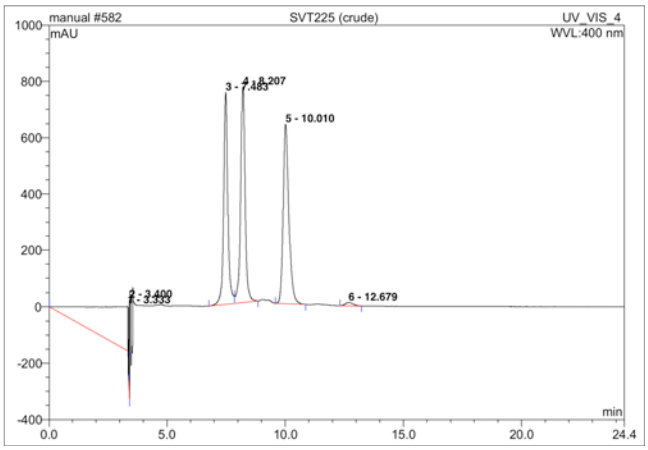

No.	Ret.Time min	Peak Name	Height mAU	Area mAU*min	Rel.Area %	Amount	Type
1	3.33	n.a.	159.986	259.589	33.68	n.a.	BMB
2	3.40	n.a.	335.106	4.885	0.63	n.a.	BMB
3	7.48	n.a.	751.212	156.168	20.26	n.a.	BM
4	8.21	n.a.	766.063	168.613	21.88	n.a.	MB
5	10.01	n.a.	637.146	176.997	22.97	n.a.	BMB
6	12.68	n.a.	11.682	4.413	0.57	n.a.	BMB
Total:			2661.194	770.667	100.00	0.000	

Figure 2.5 Analytical HPLC chromatogram of a crude sample for $[Rh_2(L_{azo})(phen)_2Cl_4](PF_6)_2$ showing the separation for the three isomers with the isocratic method 85:15 (CH_3CN:Aqueous KNO_3 2%).

Each peak was collected, the solutions concentrated in vacuo to remove excess of acetonitrile, and the complexes were precipitated with a methanolic solution of NH_4PF_6. Although this method allowed separation of the isomers of $[Rh_2(L_{azo})(phen)_2Cl_4](PF_6)_2$ in sufficient quantity for preliminary characterization, the method could not always be reproduced due to physical damages in the column. This problem gave rise to a decrease in the resolution and further loss of separation. Meanwhile, a separation method for other complexes was accomplished (see section 2.6.2). Molecular similarities of such complexes with the ones described here prompted us to explore the same separation method. A new preparative C_{18} reverse phase silica HPLC column was used instead of the silica one. The method involves a gradient of acetonitrile: water (0.01% TFA) with a flow rate of 2 ml/min for analytical HPLC and 15 ml/min for preparative. After several

attempts to optimize the method, successful separation was achieved. An advantage is that it was possible to maintain the preparative HPLC column always under the same experimental conditions allowing reproducible results for all the separations. The optimal conditions were achieved by injecting each time approximately 10 mg of crude product in 0.7 ml of acetonitrile containing 0.01 % of TFA. The TFA improved the resolution and resulted in sharper peaks. The preparative chromatogram for the final separation is shown in Figure 2.6.

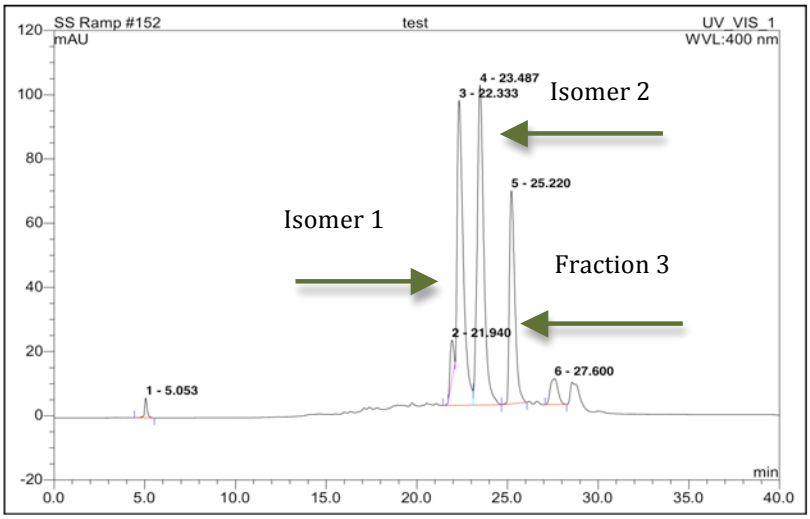

No.	Ret.Time min	Peak Name	Height mAU	Area mAU*min	Rel.Area %	Amount	Type
1	5.05	n.a.	6.223	1.022	0.90	n.a.	BMB
2	21.94	n.a.	12.400	2.718	2.39	n.a.	Ru
3	22.33	n.a.	94.966	40.671	35.82	n.a.	BM
4	23.49	n.a.	99.664	42.200	37.16	n.a.	MB
5	25.22	n.a.	66.409	22.958	20.22	n.a.	BMB
6	27.60	n.a.	8.104	3.983	3.51	n.a.	BMB
Total:			287.767	113.552	100.00	0.000	

Figure 2.6 Preparative HPLC chromatogram of a crude sample for $[Rh_2(L_{azo})(phen)_2Cl_4](PF_6)_2$ showing the final separation for the three isomers with the gradient method CH_3CN (0.01% TFA) and water (0.01% TFA).

The retention time for the first isomer was 22.3 minutes and for the second isomer 23.5 minutes. A third peak at 25.2 minutes was also collected but the ^{1}H-NMR of the compound shows the existence of more than one isomer (for ^{1}H-NMR and COSY of fraction 3 see Appendix A.1).

After the preparative separation, a minimum amount of purified compound was re-dissolved in acetonitrile with 0.01% TFA and re-injected in the analytical column under the same conditions and method to verify the purity (for chromatograms of each peak after separation see A.2). The first isomer was always collected with a high degree of purity (100%) in comparison with the second isomer that even with careful collection contained a 1 to 1.5% contaminant of the first isomer. The third isomer, that had a longer retention time, was never obtained as a single isomer, with the chromatogram showing the presence of the first isomers plus the presence of a shoulder peak, which suggests the overlapping of another species. In order to try to obtain the last isomer with enough purity for characterization and further studies different separation conditions were used. For example, changing the gradient of solvents to increase the retention of the complexes in the column, but this proved to be unsuccessful.

The same separation method was used for the final separation of the single stranded complexes with bpy ligands, $[Rh_2(L_{azo})(bpy)_2Cl_4](PF_6)_2$. The separation was achieved with success for these complexes and the chromatogram for the preparative separation is presented in Figure 2.7. The retention time for the first isomer was 21.7 minutes and for the second isomer 22.9 minutes. The third peak shows clearly the overlapping of two different species, which again were unable to be separated. Several efforts were made to allow separation and purification of this fraction: collecting the mixture of two compounds followed by re-injecting onto a semi-preparative HPLC column using a method that results in prolonged retention times and improved separation was not successful.

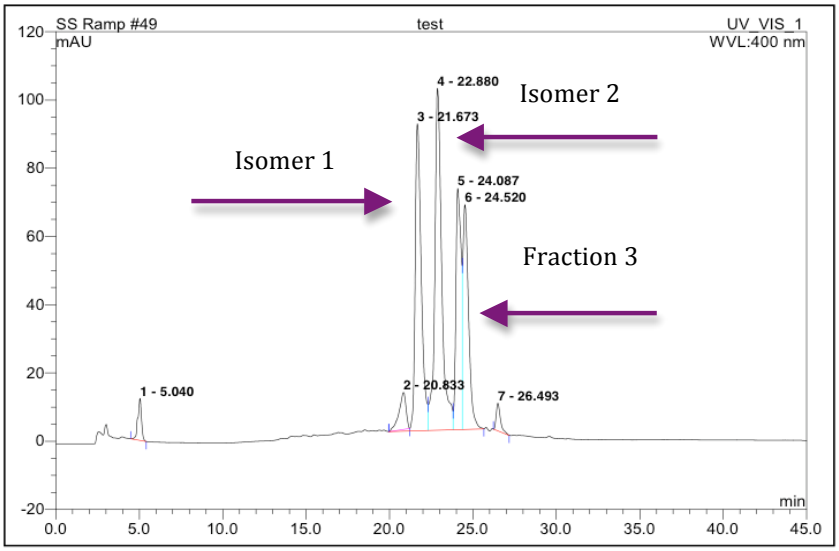

No.	Ret.Time min	Peak Name	Height mAU	Area mAU*min	Rel.Area %	Amount	Type
1	5.04	n.a.	12.305	3.107	2.08	n.a.	BMB
2	20.83	n.a.	10.828	5.238	3.50	n.a.	Ru
3	21.67	n.a.	89.923	38.440	25.72	n.a.	BM
4	22.88	n.a.	100.170	48.609	32.52	n.a.	M
5	24.09	n.a.	70.650	25.750	17.23	n.a.	M
6	24.52	n.a.	65.831	25.966	17.37	n.a.	MB
7	26.49	n.a.	8.063	2.348	1.57	n.a.	BMB
Total:			357.771	149.458	100.00	0.000	

Figure 2.7 Preparative HPLC chromatogram of a crude sample for $[Rh_2(L_{azo})(bpy)_2Cl_4](PF_6)_2$ showing the final separation for the three isomers with the gradient method CH_3CN (0.01 %TFA) and water (0.01 %TFA).

Isomers 1 and 2 for $[Rh_2(L_{azo})(phen)_2Cl_4](PF_6)_2$ will be named complexes **1** and **2** and Isomers 1 and 2 for $[Rh_2(L_{azo})(bpy)_2Cl_4](PF_6)_2$ will be named **3** and **4**.

These four complexes were isolated and further characterized by MS, ^{1}H-NMR, elemental analysis and UV-Vis.

Complex **1** was obtained with a final yield of 20% and **2** with 18%. The elemental analysis for **1** and **2** support a $[Rh_2(L_{azo})(phen)_2Cl_4](PF_6)_2$ formulation. The ESI-MS spectra of the complexes (acetonitrile, low cone voltage of 5 eV) of both complexes **1** and **2** were dominated by a doubly charged peak with the correct pattern for $[Rh_2(L_{azo})(phen)_2Cl_4]^{2+}$ (m/z = 543) as well singly charged species $[Rh_2(L_{azo})(phen)_2Cl_4]^+$ and $[Rh_2(L_{azo})(phen)_2Cl_4](PF_6)^+$ m/z = 1086 and m/z = 1231.

In the absorption spectra recorded in acetonitrile, the visible region of **1** and **2** is dominated by an MLCT transition at 399 nm (ε_{399} = 15 500 $dm^3\ mol^{-1}\ cm^{-1}$ for **1** and ε_{399} = 20 800 $dm^3\ mol^{-1}\ cm^{-1}$ for **2**) while the UV region is dominated by strong π-π* ligand transitions at 274 nm (ε_{274} = 49 600 $dm^3\ mol^{-1}\ cm^{-1}$ for **1** and ε_{274} = 66 400 $dm^3\ mol^{-1}\ cm^{-1}$ for **2**). These data are in accordance with those for similar complexes such as $[Rh(phen)_2Cl_2]$.[13]

Complexes **3** and **4** were obtained in similar yields to **1** and **2**. The elemental analysis data for **3** and **4** support the $[Rh_2(L_{azo})(bpy)_2Cl_4](PF_6)_2$ formulation and the MS for both complexes (under the same conditions as for **1** and **2**) is again dominated by the doubly charged species $[Rh_2(L_{azo})(bpy)_2Cl_4]^{2+}$ (*m/z* = 518) with the correct isotopic pattern and minor singly charged species $[Rh_2(L_{azo})(bpy)_2Cl_4]^{+}$ and $[Rh_2(L_{azo})(bpy)_2Cl_4](PF_6)^{+}$ with *m/z* = 1036 and *m/z* = 1180. The absorption spectra recorded in acetonitrile show that the visible region of **3** and **4** is dominated by an MLCT transition at 390 nm (ε_{390}=13 520 $dm^3\ mol^{-1}\ cm^{-1}$ for **3** and ε_{390} = 18 230 $dm^3\ mol^{-1}\ cm^{-1}$ for **4**) while the UV region is dominated by strong π-π* transitions at 250 nm (ε_{250} = 42 320 $dm^3\ mol^{-1}\ cm^{-1}$ for **3** and ε_{250} = 50 312 $dm^3\ mol^{-1}\ cm^{-1}$ for **4**).

The PF_6 salts of the complexes (**1**, **2**, **3** and **4**) are highly soluble in acetonitrile, acetone and nitromethane and on exchanging the counter ion using a Dowex ion exchange column chloride salts were afforded which possess high water solubility.

For each compound two main isomers have been formed. Before turning to consider in detail the ^{1}H-NMR spectra of these isomers it became apparent that it would be beneficial to explore what happens when a single metal centre reacts with this type of ligand as this might provide the key to confirming the identity of the dinuclear isomers.

The discussion about these four isomers and characterization will be further discussed in section 2.5.2.

2.4 Synthesis of Mononuclear Analogous Complexes

2.4.1 Synthesis of Azophenylpyridine Ligand (L_{azpy})

The azophenylpyridine ligand (L_{azpy}) was synthesized modifying the method used by Krause & Krause[14] which involves the use of benzene as a solvent. The ligand was synthesized from 2-nitrosopyridine and aniline in a 1:1 ratio according with scheme 2.3 in similar experimental conditions as for the L_{azo}.

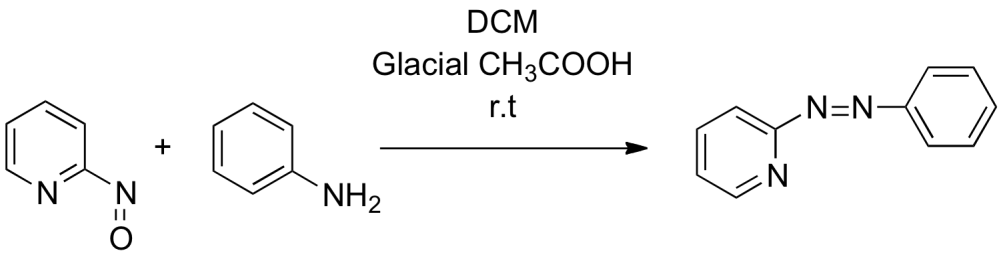

Scheme 2.3 Synthetic route for the preparation of the azophenylpyridine ligand (L_{azpy}).

The ligand was obtained as a red orange oil that crystallized after days when left standing in 78% yield. The ligand was characterized by MS and the EI spectrum is in accordance with the synthesis of $[C_{11}H_9N_3]^+$. ^{1}H-NMR reveals resonances for the pyridine ring and for the phenyl ring as expected. The ligand was used without any further purification.

2.4.2 Synthesis of the Mononuclear Complexes

To prepare the mononuclear complexes, analogous routes and reaction conditions to those used for the dinuclear complexes were employed. The starting material and L_{azpy} were heated under reflux in a 1:1 ratio in propanol:water (2:1) for 90 minutes according with scheme 2.4. A light green solid was obtained for both complexes on addition of an aqueous solution of NH_4PF_6 and used without any further purification.

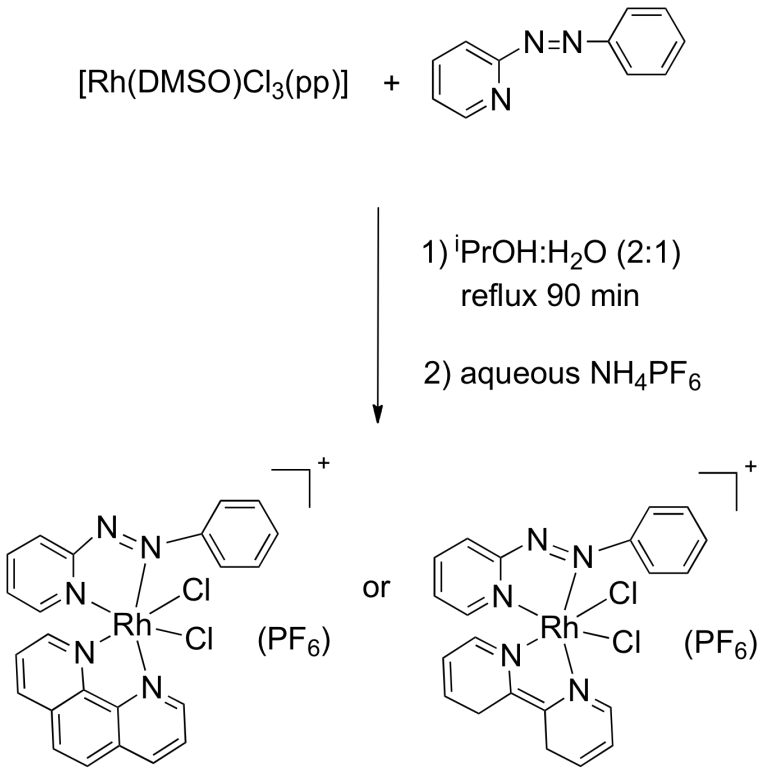

Scheme 2.4 Synthetic route for the preparation of the Mononuclear complexes $[Rh(L_{azpy})(phen)Cl_2](PF_6)$ (**5**) and $[Rh(L_{azpy})(bpy)Cl_2](PF_6)$ (**6**).

The complexes were obtained in 49% and 44% yields for **5** and **6** respectively. Elemental analyses for **5** and **6** were consistent with the synthesis of $[Rh(L_{azpy})(phen)Cl_2](PF_6)$ and $[Rh(L_{azpy})(bpy)Cl_2](PF_6)$ and the ESI-MS of both solids was

dominated by the singly charged species at *m/z* = 536 corresponding to $[Rh(L_{azpy})(phen)Cl_2]^+$ or *m/z* = 512 corresponding to $[Rh(L_{azpy})(bpy)Cl_2]^+$.

The UV-Vis spectra of **5** and **6** are similar to those of the dinuclear analogues as expected. The absorption spectrum of **5** is dominated by two UV transitions assigned as π-π* transitions of the ligand at 227 nm (ε_{227} = 45 230 $dm^3\ mol^{-1}\ cm^{-1}$) and π-π* transitions of the phen ligand at 274 nm (ε_{274} = 33 133 $dm^3\ mol^{-1}\ cm^{-1}$). The MLCT transition is blue shifted (375 nm with ε_{375} = 9 985 $dm^3\ mol^{-1}\ cm^{-1}$) in comparison with the dinuclear analogues **1** and **2**. The UV-Vis spectrum of **6** has two UV transitions assigned as π-π* transitions of the ligand at 227 nm (ε_{227} = 27 033 $dm^3\ mol^{-1}\ cm^{-1}$) and π-π* transitions of the bpy ligand at 312 nm (ε_{312} = 12 833 $dm^3\ mol^{-1}\ cm^{-1}$). The MLCT transition positioned at 361 nm (ε_{361} = 7 900 $dm^3\ mol^{-1}\ cm^{-1}$) is similarly blue shifted compared to complexes **3** and **4**. A comparison between the transitions of the six complexes with known analogues $Rh(phen)_2Cl_2$ and $Rh(bpy)_2Cl_2$ in the literature is presented in the Table 2.1.

The red shift of the MLCT band in the dinuclear isomers (compared with the mononuclear analogues) is a little surprising, given that such an effect is not observed in the $Ru(bpy)_2$ complexes of the pyridylimine version of the ligand.[15]

The PF_6 salts of both mononuclear complexes (**5** and **6**) are soluble in acetonitrile, and the counter ion which was also exchanged using Dowex ion exchange column led to the respective chloride salts which were highly soluble in water.

Table 2.1 Wavelengths and assignment of UV-Vis transitions for complexes **1** to **6** in acetonitrile.

UV-Vis Transitions	π-π*	MLCT
1	274	399
2	274	399
3	250	390
4	250	390
5	227, 274	357, 375
6	227, 312	361
$Rh(phen)_2Cl_2$†	275	337, 355
$Rh(bpy)_2Cl_2$††	300, 311	380

† UV-vis spectrum recorded at r.t in acetonitrile.[13]

†† UV-vis spectrum recorded at r.t in ethanol:methanol.[13].

2.5 X-Ray and ^{1}H-NMR Characterization of the Complexes

2.5.1 X-Ray and ^{1}H-NMR Characterization of 5 and 6

Crystals of complex **5** and **6** were obtained from slow diffusion of diethyl ether into a solution of the pure PF_6 salts of the complexes complex in acetonitrile.

The X-ray structure of **5** (Figure 2.8) confirms the formation of a Rh(III) mononuclear complex. The metal centre occupies a six-coordinated octahedral environment with the Rh-N bonds all with similar length (2.01-2.05 Å) as well as the Rh-Cl bonds, both with 2.33 Å. Selected bond lengths for **5** are shown in Table 2.2. This is in agreement with reported data for other Rh(III) complexes.[7, 10, 11] The structure contains the chloride atoms in a *cis* configuration and the pyr *trans* to a phen ring. The phenyl ring is twisted with respect to the phenylazo unit by -42.8 (4)° and is placed above the central ring of the phen with an intramolecular π-π stacking inter-planar distance of 3.7 Å. The crystal packing of $[Rh(L_{azpy})(phen)Cl_2](PF_6)$ in Figure 2.9 shows that the molecules engage in intermolecular π-π stacking interactions with each rhodium complex connected to two others via inter-molecular π-π stacking interactions between the phen units and the phenyl rings (inter-planar separation of 3.7 Å).

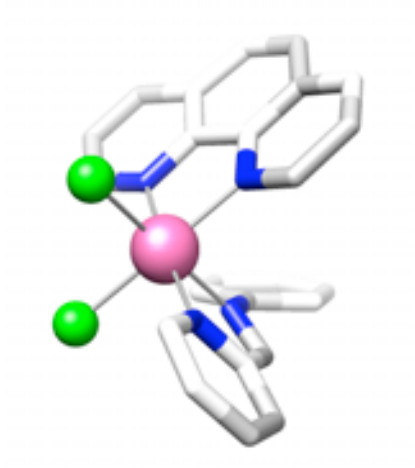

Figure 2.8 Crystal structure of *cis*-[Rh(L_{azpy})(phen)Cl_2](PF_6)(**5**) in acetonitrile. Hydrogen atoms have been omitted for clarity. For crystallographic data and refinement details see Appendix A.3 Table 1.

Table 2.2 Selected Bond lengths for complex **5** (Å).

Metal	**M-Cl**	**M-N_{azo}**	**M-N_{pyr}**	**M-N_{phen}**	**N=N**
Rh	2.3313(8) 2.3326(8)	2.014(3)	2.010(3)	2.036(3) 2.048(2)	1.265(4)

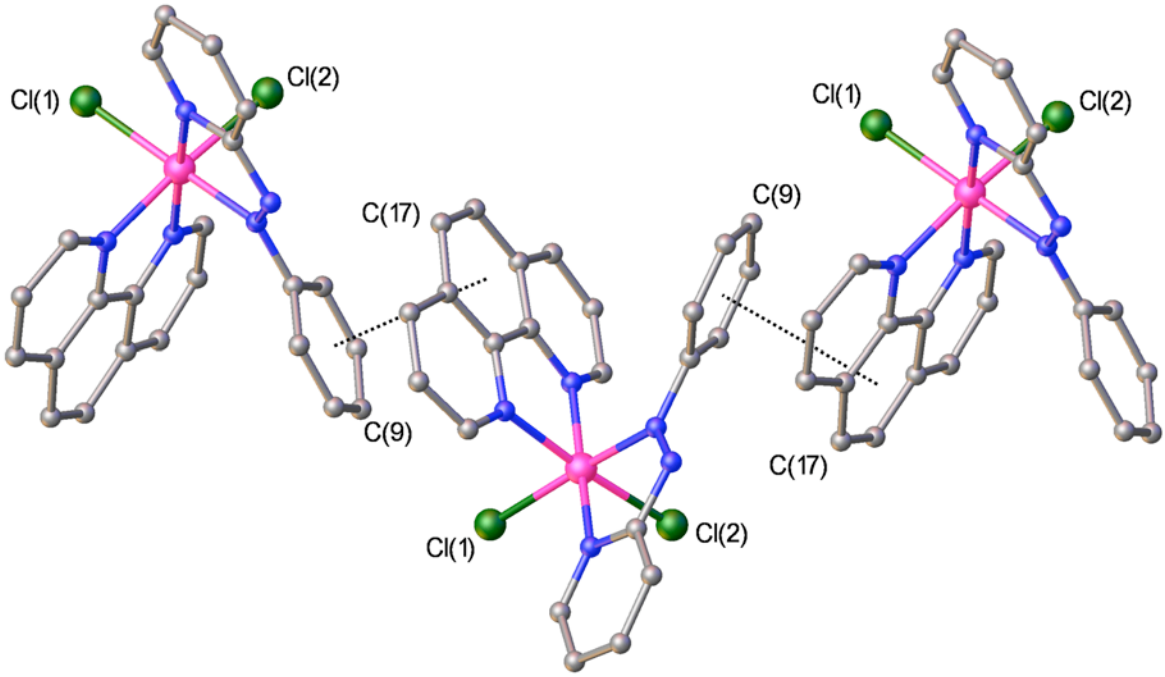

Figure 2.9 Crystal packing of **5.** Each rhodium complex of **5** is connected to two others via an inter-molecular π-π stacking interaction. PF_6 anions and all hydrogen atoms have been omitted for clarity. Carbon atoms are shown in grey, rhodium in pink, chlorine in green and nitrogen in blue, while π-π stacking interactions are indicated by black dotted lines.

A different polymorph was obtained from slow diffusion of diethyl ether into methanol:acetonitrile (1:1). The structure in Figure 2.10 contains two crystallographically-independent rhodium complexes both of which have the same molecular conformation as the previous polymorph, but which pack differently. Stacking through phen-phen π-π interactions (inter-planar separation of 3.5 Å) is observed in Figure 2.11.

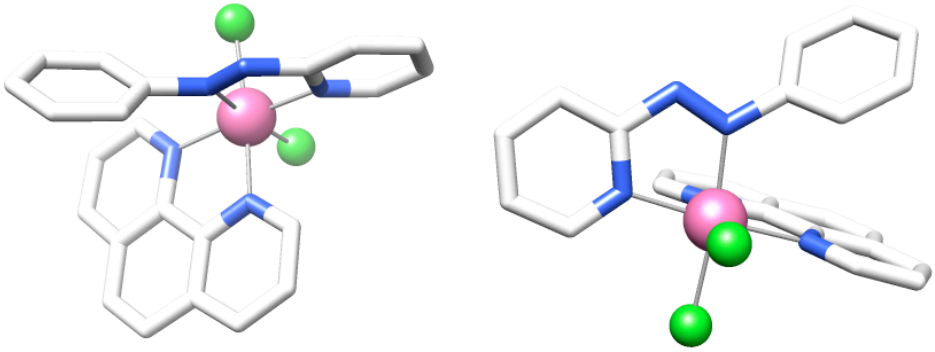

Figure 2.10 Crystal structure of polymorph of *cis*-[Rh(L_{azpy})(phen)Cl_2](PF_6) (**5**) in methanol:acetonitrile. Hydrogen atoms have been omitted for clarity. For crystallographic data and refinement details see Appendix A.3 Table 1.

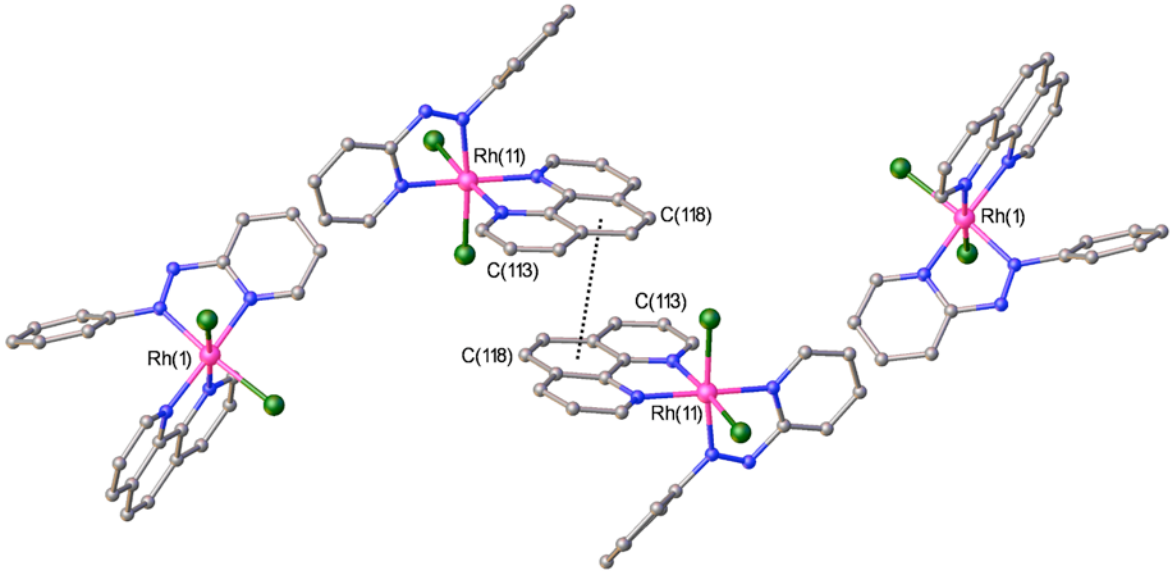

Figure 2.11 Crystal packing of polymorph of **5.** Each rhodium complex of **5** is connected to one other via an inter-molecular π-π stacking. PF_6 anions and all hydrogen atoms have been omitted for clarity. Carbon atoms are shown in grey, rhodium in pink, chlorine in green and nitrogen in blue, while π-π stacking interactions are indicated by black dotted lines.

The ^{1}H-NMR spectrum of **5** at room temperature (Figure 2.12) shows broad peaks for the pyr ring and for the protons of the phenyl ring. The broad peaks may be due to sterically hindered rotations of the phenyl ring. Cooling of the sample during the NMR experiment can slow this rotation on the NMR time scale and help to distinguish the

different resonances. At -20 °C it is possible to observe twelve well-resolved resonances including the ones for the phenyl ring with the expected multiplicity. The resonances were fully assigned with support of COSY and NOE experiments (Appendix A.4). Importantly the ^{1}H-NMR spectrum reveals the presence of just one species (whitin the detection limits of NMR). There are two particularly noticeable resonances that aid assignment of the structure. Both H_6 of the pyr and H_2 of the phen are found at high chemical shift. This high shift is typical of such a pyridine-like proton pointing directly at a *cis* chloride environment.[16] This can only happen in the *cis* chlorides, N_{azo} *trans* to the chloride configuration confirming that the structure in solution is the same as the solid state structure.

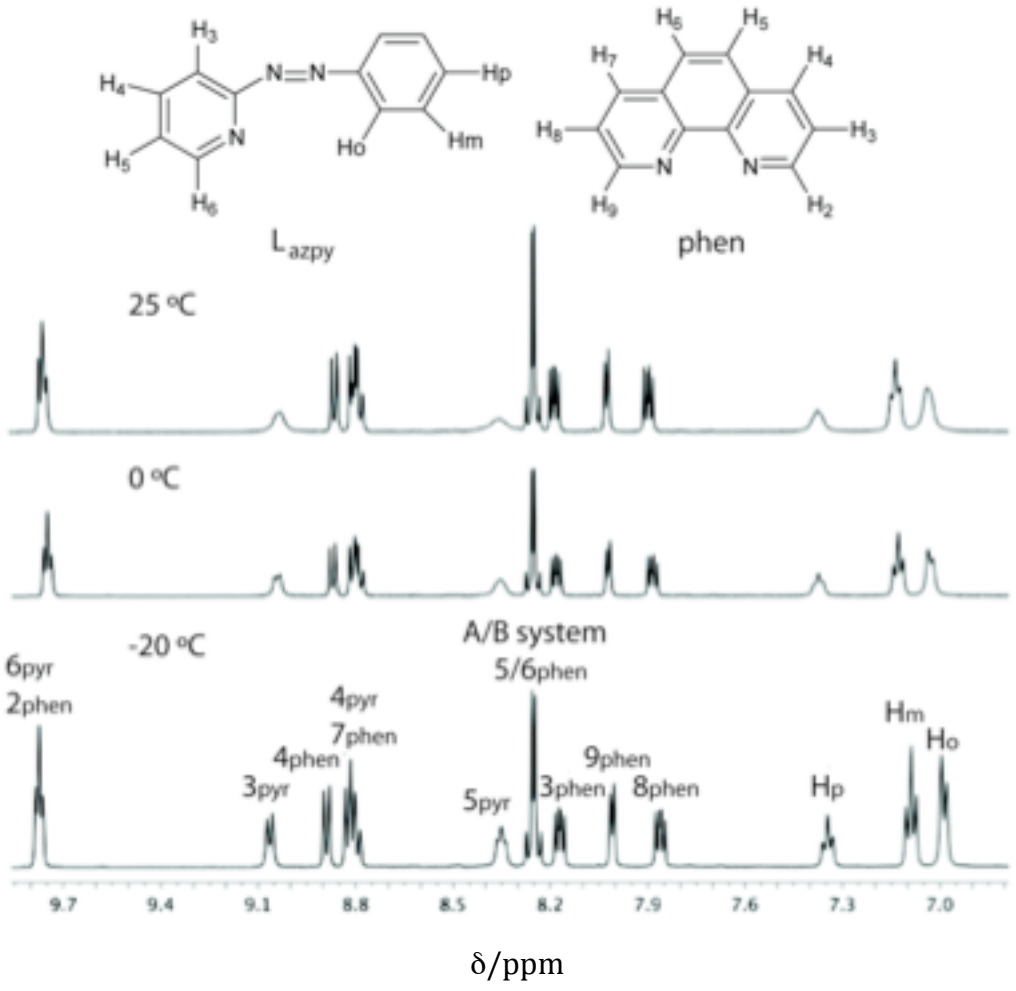

Figure 2.12 ^{1}H-NMR (500 MHz, 25, 0 and -20 °C) spectra of **5** in CD_3CN.

The X-ray structure of **6** (Figure 2.13) confirms the formation of a Rh(III) mononuclear complex. The metal centre occupies a six-coordinated octahedral environment with the Rh-N bonds all with similar length (2.03-2.04 Å) and similar to the previous structure **5** as well as the Rh-Cl bonds, both with 2.33 Å. Selected bond lengths for **6** are shown in Table 2.3. Additionally, the structure confirms that the chloride atoms are coordinated to the metal centre in *cis* configuration and the pyr in *trans* configuration to the bpy ring as in **5**. The phenyl ring is twisted with respect to the phenylazo unit of -35.1 (6)° and is placed above the central ring of the bpy but the distances are too long (and the ring not sufficient coplanar) to propose strong intramolecular π-π stacking interaction.

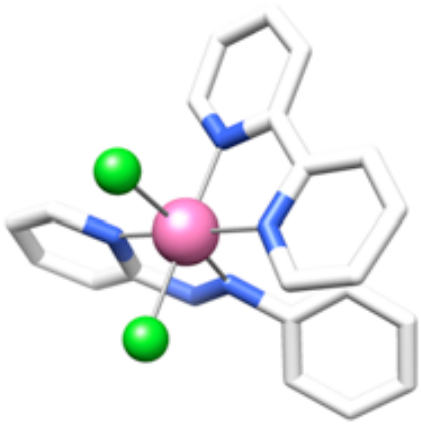

Figure 2.13 Crystal structure of *cis*-[Rh(L_{azpy})(bpy)Cl_2](PF_6) (**6**) in acetonitrile. Hydrogen atoms have been omitted for clarity. For crystallographic data and refinement details see Appendix A.5 Table 2.

Table 2.3 Selected Bond lengths for complex **6** (Å).

Metal	**M-Cl**	**M-N_{azo}**	**M-N_{pyr}**	**M-N_{bpy}**	**N=N**
Rh	2.327(11) 2.335(11)	2.031(4)	2.031(4)	2.042(4) 2.032(4)	1.259(5)

The crystal packing of *cis*-[Rh(L_{azpy})(bpy)Cl_2](PF_6) (Figure 2.14) shows each rhodium complex of **6** is connected to two others via inter-molecular π-π stacking interactions between two pyr rings of the bpy containing C(13) with an inter-planar separation of 3.5 Å and between two pyr rings containing C(20), with an inter-planar separation of 3.4 Å.

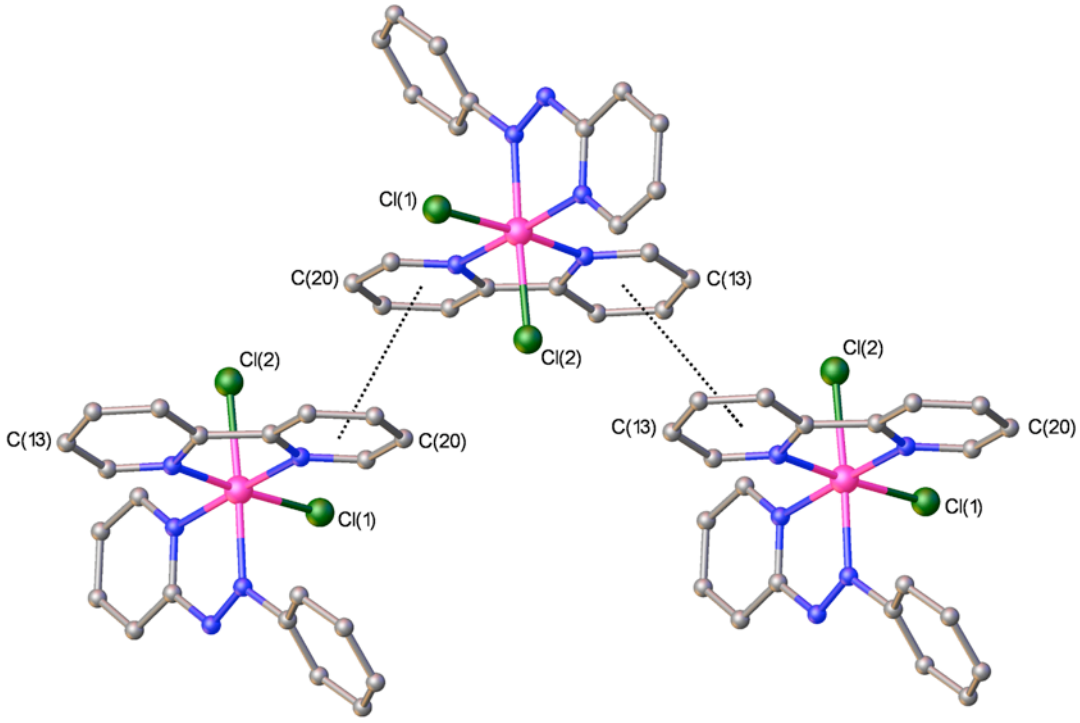

Figure 2.14 Crystal packing of **6.** Each rhodium complex of **6** is connected to two others via inter-molecular π-π stacking interactions. PF_6 anions and all hydrogen atoms have been omitted for clarity. Carbon atoms are shown in grey, rhodium in pink, chlorine in green and nitrogen in blue, while π-π stacking interactions are indicated by black dotted lines.

The ^{1}H-NMR spectrum of **6** at room temperature (Figure 2.15) shows seventeen well-resolved resonances, assigned by a COSY experiment (Appendix A.6). In contrast with complex **5**, the ^{1}H-NMR of **6** shows sharp peaks at room temperature with the smaller bpy ligand allowing free rotation of the phenyl at room temperature and thus no broadening of the peaks as seen in **5**. As in **5** the high chemical shifts of H_6 of pyr and H_6 of the bpy confirm that the structure seen in the solid state is retained in solution. Again just one species is observed.

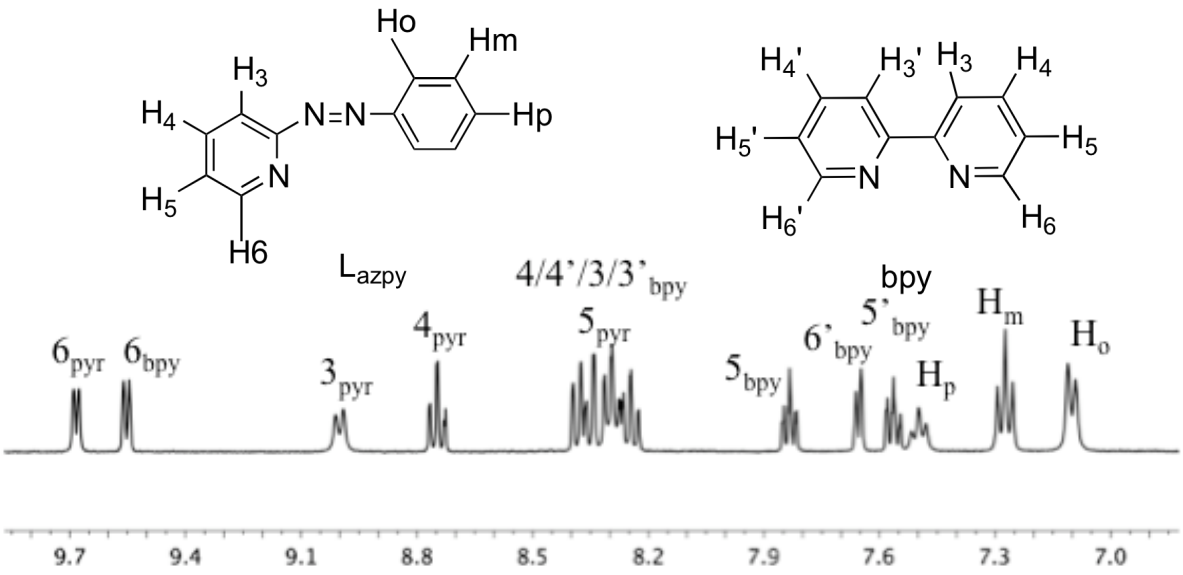

Figure 2.15 ^{1}H-NMR (400 MHz, 25 °C) spectrum of **6** in CD_3CN.

2.5.2 X-Ray and ^{1}H-NMR Characterization of 1 and 2

The reactions with the mononucleating ligands have demonstrated that the rhodium starting materials react with this type of ligand donor set to give predominantly the *cis* chlorides, N_{azo} *trans* to a chloro isomer.

Moreover it was seen that this isomer could be identified in solution by characteristic proton shifts on the phen/bpy and of the azopyridine ligands.

Armed with this information it is now pertinent to return to the isomers of the dinuclear single stranded complexes to assess their structure.

The ^{1}H-NMR spectra of isomers **1** and **2** (Figure 2.16) was measured at room temperature and fully assigned achieved using COSY spectra (Appendix A.7 and A.8). Although both isomers have similar NMR shifts, it was possible to clearly distinguish signals of each of them. Both complexes show a high symmetry meaning that the metal

centres of the dinuclear molecule have the same geometric configuration. **1** shows twelve resonances and **2** ten, with some appearing as multiplets due to overlap of resonances.

For both isomers the striking feature is the high chemical shifts of H_6 of the pyr and H_2 of the phen. As for compound **5** this confirms that the metal centres have a *cis* chloride N_{azo} *trans* to a chloride structure. Taking this into account, the two isomers must correspond to a *Rac* (ΔΔ,ΛΛ) and a *Meso* (ΔΛ) isomer, which would be in agreement with similarities of observed in both NMR spectra.

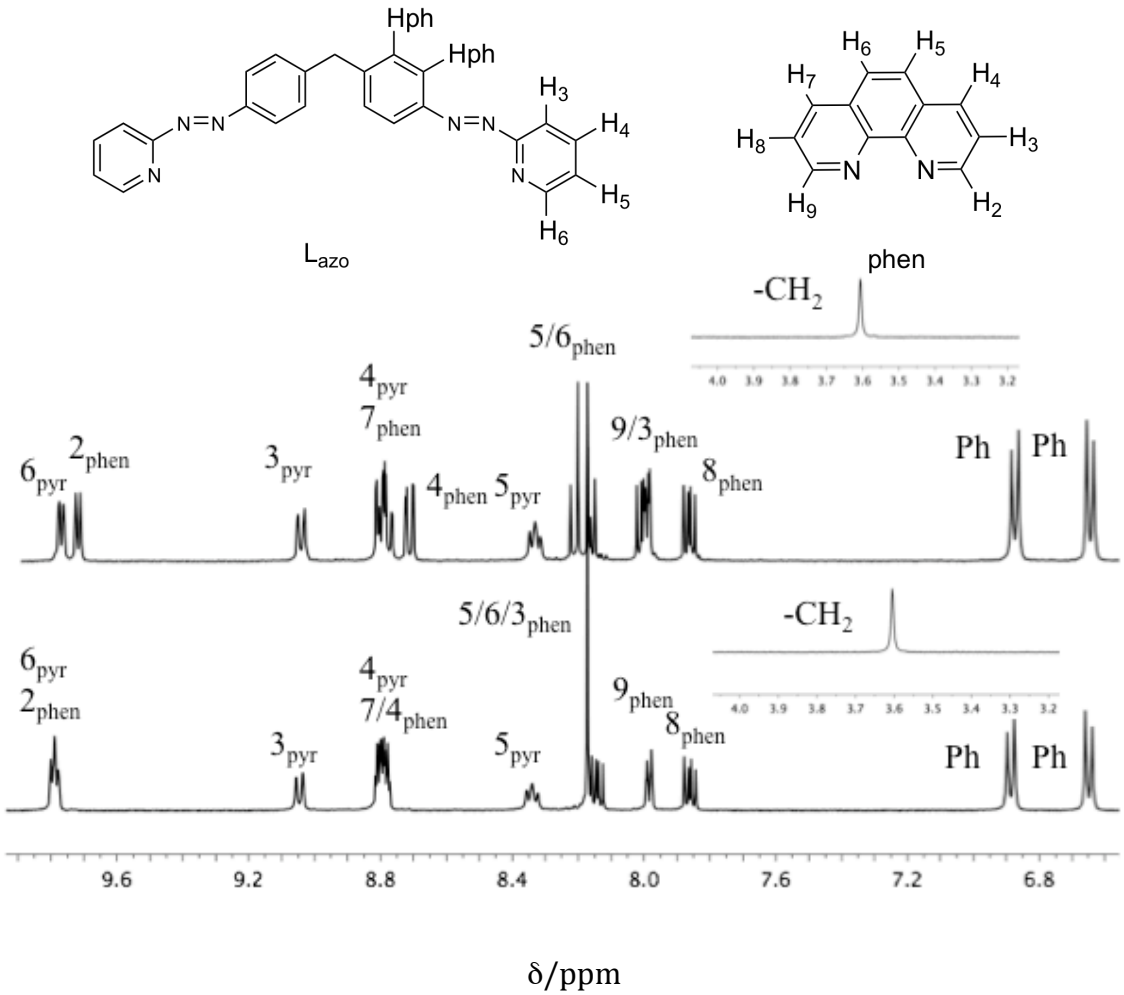

Figure 2.16 ^{1}H-NMR (400 MHz, 25 °C) spectra of **1** (top) and **2** (bottom) in CD_3CN.

Crystals of **1** were obtained from slow diffusion of diethyl ether into a solution of pure complex in nitromethane.

The molecular structure of **1** (Figure 2.17) was determined by X-ray diffraction analysis and the crystal structure reveals this dinuclear complex to be the *Rac* (ΔΔ,ΛΛ) isomer. Each Rh(III) centre has an octahedral geometry as before, with Rh-N bonds distances all with close lengths (2.01-2.05 Å). The structure shows the chlorides in a *cis* position in each metal centre and the pyr ring of the L_{azo} in *trans* configuration to the phen ligand, as anticipated from the ^{1}H-NMR. The configuration of the ligands in each metal centre in **1** is similar to **5**. All of the four Rh-Cl bonds have lengths in between 2.31-2.33 Å, which is equivalent to the ones obtained for **5**. Selected bond lengths for **1** are shown in Table 2.4. The Rh-Rh distance is 10.2 Å which although similar to, is slightly smaller than the metal-metal distance observed for the Fe(II) (11.4 Å) and Ru(II) triple (11.3 Å) stranded helicates and for the Ru(II) double stranded helicates (12.1-12.5 Å, for different isomers).[4, 5, 8]

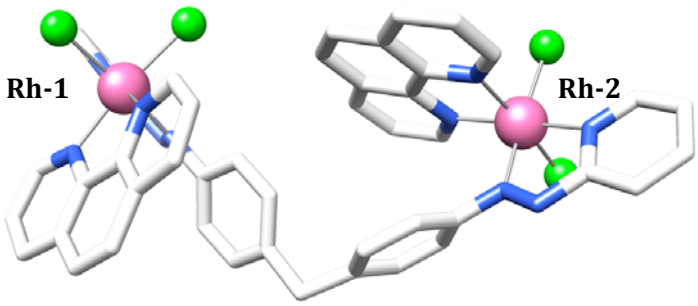

Figure 2.17 Crystal structure of ΔΔ,ΛΛ-$[Rh_2(L_{azo})(phen)_2Cl_4](PF_6)_2$ (**1**). The PF_6 anions and acetonitrile molecules and all hydrogen atoms have been omitted for clarity. For crystallographic data and refinement details see Appendix A.9 Table 3.

Although no intramolecular π-π stacking interactions are observed, intermolecular π-π interactions were found as shown in Figure 2.18. Both enantiomers of this chiral complex are found in the solid state structure.

Table 2.4 Selected Bond lengths for complex **1** (Å).

Metal	**M-Cl**	**M-N_{azo}**	**M-N_{pyr}**	**M-N_{phen}**	**N=N**
Rh-1	2.321(4) 2.335(4)	2.017(12)	2.017(12)	2.041(12) 2.046(11)	1.253(16)
Rh-2	2.311(4) 2.333(4)	2.021(12)	2.005(13)	2.042(14) 2.076(14)	1.237(17)

From the crystal packing of **1** (Figure 2.18), each rhodium complex of **1** is connected to three others via inter-molecular π-π stacking interactions as follows: the phen unit containing C(38) forms an interaction with another phen unit containing C(38) with an inter-planar separation of 3.3 Å; the phenyl ring containing C(30) forms an interaction with the rings containing C(6) and C(11) with an inter-planar separation of 3.5 Å. The pyridine ring containing C(16) forms an interaction with another pyridine ring containing C(16) with an inter-planar separation of 3.6 Å.

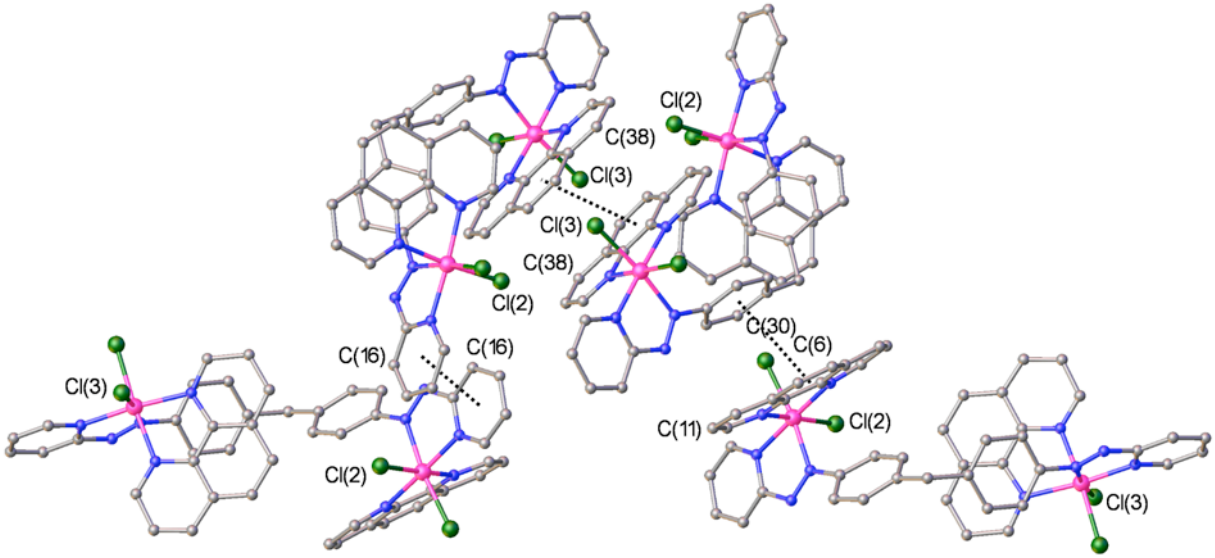

Figure 2.18- Crystal packing of **1**. Each rhodium complex **1** is connected to three others via inter-molecular π-π stacking interactions. PF_6 anions, nitromethane and acetonitrile molecules and all hydrogen atoms have been omitted for clarity. Carbon atoms are shown in grey, rhodium in pink, chlorine in green and nitrogen in blue, while π-π stacking interactions are indicated by black dotted lines.

Implicit in this structure is that if **1** is the *rac* isomer, **2** must be the *meso* isomer. Unfortunately multiple attempts to grow crystals of **2** have been unsuccessful.

2.5.3 X-Ray and ^{1}H-NMR Characterization of 3 and 4

The ^{1}H-NMR spectra of **3** and **4** (Figure 2.19) were recorded at room temperature and full assignment was achieved using COSY spectra (Appendix A.10 and A.11). As with **1** and **2** the molecules exhibit high symmetry with both metals centres displaying the same geometry. The ^{1}H-NMR spectra are very similar indeed. Once again the spectra feature H_6 of the pyr and H_2 of the bpy at high chemical shift confirming the *cis* chlorides, N_{azo} *trans* to chlorides conformation at the metal centres and thus that the two isomers are again the *rac* and *meso* isomers.

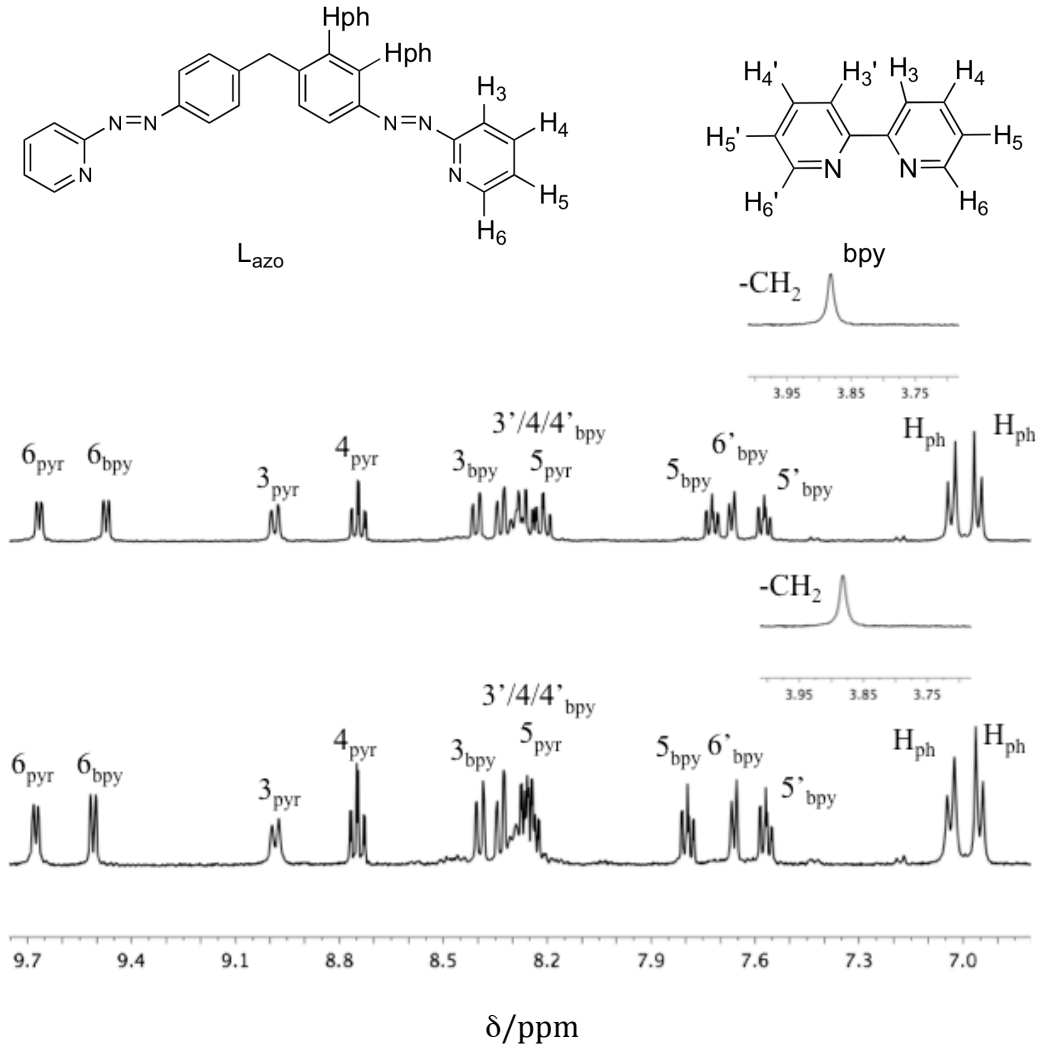

Figure 2.19 ^{1}H-NMR (400 MHz, 25 °C) spectra of **3** (top) and **4** (bottom) in CD_3CN.

Crystals of **3** were obtained from slow diffusion of diethyl ether into a solution of pure complex in nitromethane. As with **2** numerous attempts to grow X-ray quality crystals of **4** were unsuccessful.

The molecular structure of **3** (Figure 2.20) was determined by X-ray diffraction analysis and the crystal structure reveals the dinuclear complex to be the *Rac* (ΔΔ,ΛΛ) isomer.

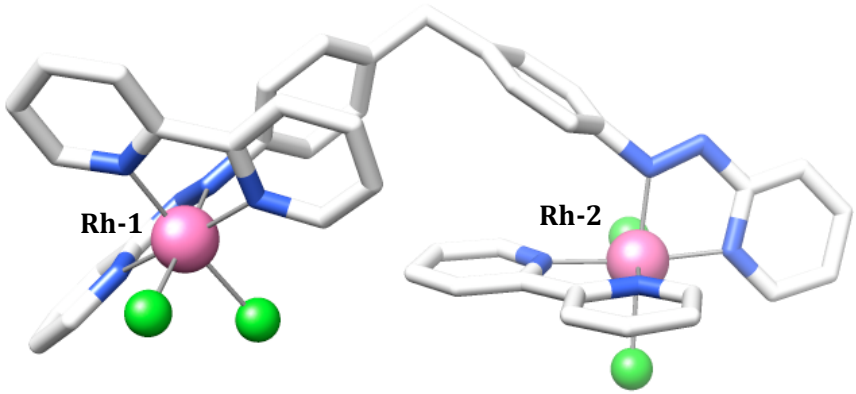

Figure 2.20 Crystal structure of ΔΔ,ΛΛ-$[Rh_2(L_{azo})(bpy)_2Cl_4](PF_6)_2$ (**3**). The PF_6 anions and acetonitrile molecules and all hydrogen atoms have been omitted for clarity. For crystallographic data and refinement details see Appendix A.12 Table 4.

Each Rh(III) centre has an octahedral geometry with Rh-N bonds distances all with lengths in between 1.98-2.04 Å. The structure shows the chlorides in a *cis* position in each metal centre and the pyr ring of the L_{azo} in *trans* configuration to the bpy ligand as anticipated from the ^{1}H-NMR spectrum. The configuration of the ligands in each metal centre in **3** is similar to what it occurs in the mononuclear analogue **6** as well as in **1** and **5**. All of the four Rh-Cl bonds have similar lengths (2.33-2.34 Å), which are equivalent to the ones obtained for **6** as well as for **1** and **5**. Selected bond lengths for **3** are shown in Table 2.5. The Rh-Rh distance is slightly smaller than in **1** (9.8 Å). Although no intramolecular π-π stacking interactions are observed, intermolecular π-π interactions were found as shown in Figure 2.21.

Table 2.5 Selected Bond lengths for complex **3** (Å).

Metal	M-Cl	M-N_{azo}	M-N_{pyr}	M-N_{bpy}	N=N
Rh-1	2.345(2) 2.336(2)	1.985(6)	2.031(6)	2.0249(6) 2.029(7)	1.263(9)
Rh-2	2.329(2) 2.336(2)	2.014(7)	2037(7)	2.021(7) 2.027(6)	1.269(9)

Each rhodium complex of **3** is connected to one other via inter-molecular π-π stacking interactions between two pyridine rings containing C(22) with an inter-planar separation of 3.3 Å.

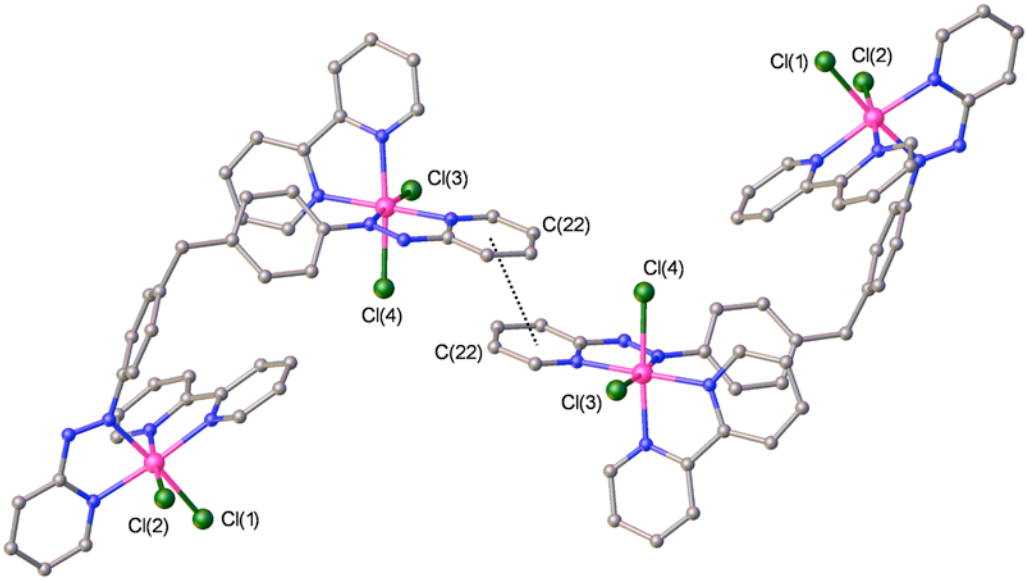

Figure 2.21 Crystal packing of **3.** Each rhodium complex **3** is connected to one other via inter-molecular π-π stacking interactions. PF_6 anions, acetonitrile groups and all hydrogen atoms have been omitted for clarity. Carbon atoms are shown in grey, rhodium in pink, chlorine in green and nitrogen in blue, while π-π stacking interactions are indicated by black dotted lines.

2.6 Rh(III) Double Stranded Complexes $[Rh_2(L_{azo})_2Cl_4]^{2+}$

The synthesis of the Rh(III) double stranded helicates proved to be particularly difficult. Initial attempts to synthesize such complexes using a similar approach as for the Ru(II) analogue[8] were unfruitful. Using $Rh(DMSO)_3Cl_3$ as a starting material, heating under reflux in the presence of ligand in a variety of different organic solvents (different alcohols, acetonitrile, ethyleneglycol, acetone, methoxyethanol) for different periods of time failed. In all cases, such conditions led to insoluble brown/black mixtures, assumed to be polymeric materials and from which the desired product could not be isolated. Taking $Rh(DMSO)_3Cl_3$ in a mixture of acetonitrile:water 25:1 refluxing for 5 hours led as well to a solution contaminated with polymeric material but from where a double charged peak with *m/z* = 552 indicating the presence of the desired compound, could be identified in ESI-MS. Nevertheless the ^{1}H-NMR spectrum exhibited a broad peak in the aromatic region impeding assignment of the peaks. In an attempt to control and reduce the formation of the polymeric material different reaction times, concentrations and temperatures were used including placing the reaction in a warm ultrasound bath for 6 hours. These last conditions afforded a compound that could be analysed by ^{1}H-NMR. The spectrum indicated the presence of the double stranded complex in a mixture of isomers. Nevertheless, the amount of polymeric material, was still fairly high and when separated from the product by filtration led to a very low amount of the desired material.

Eventually, by using $RhCl_3.3H_2O$ directly as a starting material and varying the reaction conditions (temperature, concentration and time), a procedure was found for the synthesis of Rh(III) double stranded complexes. A first method used a mixture of

ethanol:water in a 2:1 ratio, but difficulties in the ESI-MS analysis due to the persistent adduct of 46 Da. attributed to ethanol prompt us to change the alcohol from ethanol to isopropanol, which was finally the solvent of choice.

2.6.1 Synthesis of the Rh(III) Double stranded Complexes

$RhCl_3.3H_2O$ was heated under reflux with the ligand (L_{azo}) in a 1:1 ratio in a mixture of propanol:water (2:1) according to scheme 2.5. The optimal reaction time to form the double stranded compound was found to be 20 minutes. Longer reactions (up to 90 minutes) gave lower yield of the desired compound and increased the formation of the undesired insoluble side products.

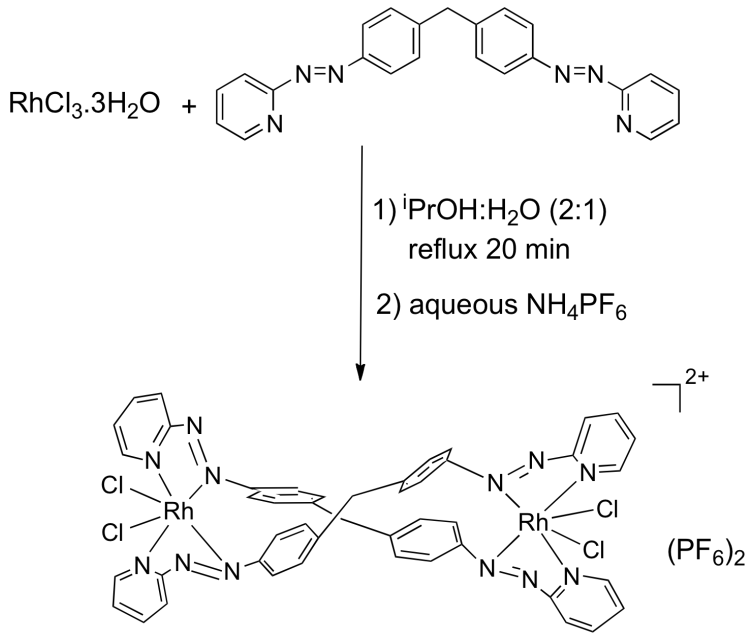

Scheme 2.5 Synthetic route for the preparation of the Rh(III) Double Stranded complex.

The ligand goes into solution after the reaction mixture starts to reflux, and after 5 minutes the mixture changes from orange to light brown, and then dark brown. After 20

minutes, the mixture turns to a very strong yellow/green colour. The warm crude mixture is filtered through celite to separate the compound from the insoluble black polymer. After cooling to room temperature, the green complex is obtained as a PF_6 salt by the addition of a concentrated aqueous NH_4PF_6 solution. The ESI-MS of the crude mixture is dominated by the doubly charged peak of the species $[Rh_2(L_{azo})_2Cl_4]^{2+}$ with *m/z* = 552 and a singly charged peak for the species $[Rh_2(L_{azo})_2Cl_4](PF_6)^+$ (*m/z* = 1248). Once again readjustments of the conditions (low cone voltage and spray solvent) for the ESI-MS spectrum had to be made in order to be able to observe these peaks, as with the single stranded complexes. Elemental analysis of the mixture was consistent with the formation of $[Rh_2(L_{azo})_2Cl_4](PF_6)_2$. The ^{1}H-NMR spectrum of the crude reaction (Figure 2.22) showed sharp and well resolved peaks for what would be two predominant isomers, a major and a minor one. This is suggested by the overlapping singlets around 4 ppm characteristic of the CH_2 group of the ligand. Longer reaction times did not lead to the formation of additional isomers with the ^{1}H-NMR spectrum exhibiting constantly the same pattern, although it led to a decrease on the yield as already discussed.

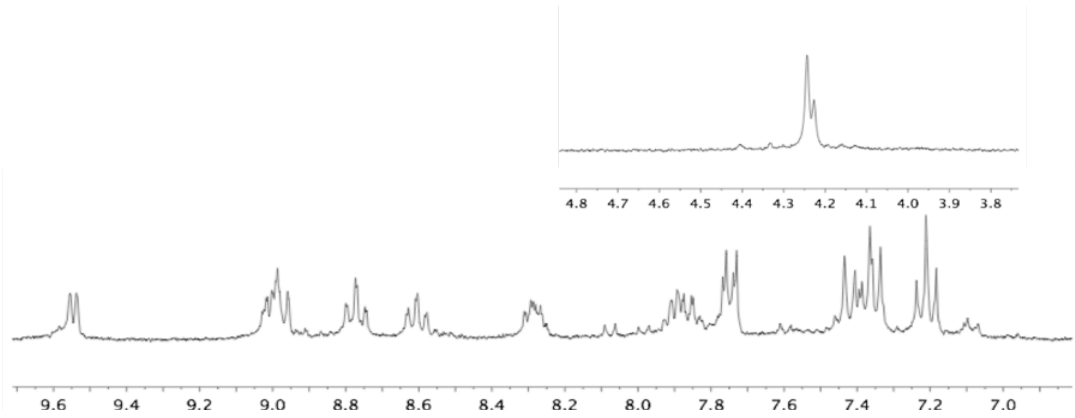

Figure 2.22 ^{1}H-NMR (300 MHz, 25 °C) spectrum of crude mixture of $[Rh_2(L_{azo})_2Cl_4](PF_6)_2$ in CD_3CN.

2.6.2 Separation of Rh(III) Double Stranded Complexes

The separation/purification of these isomers was a challenge. Initial attempts for the separation involved alumina columns using a variety of different organic solvents, mixtures of organic solvents with concentrated aqueous solutions of KNO_3 or aqueous solutions with a range of different concentrations of salts such as NaCl or NH_4PF_6 as eluents.

The complex had high affinity for alumina (it sticks), but the little product that could be collected showed a mixture of different doubly charged peaks in the MS spectrum. This observation suggested the replacement of the chlorides by some of the anionic species of the salts used during purification. Attempts to use cation exchange sephadex C_{25} columns with a different concentration range of $MgCl_2$ were made in order to collect the double charged species, but those attempts failed as the entire compound remained stuck on the column. Silica columns proved to be slightly better and again several conditions were explored: eluting the compounds with a mixture of acetonitrile:water (6:1) with 5 mM concentration of NH_4PF_6 or using acetonitrile:water: KNO_3 (saturated solution) (40:2:1) allowed the enrichment of one of the isomers to >75%, along with the presence of some of the second isomer (Figure 2.23). The fact that the two isomers have the same colour and identical RF value on TLC, makes the separation process by column chromatography a complicated process. Attempts to re-column to further enrich the major isomer using the same conditions were unsuccessful in part because the amount of solid obtained before was already low.

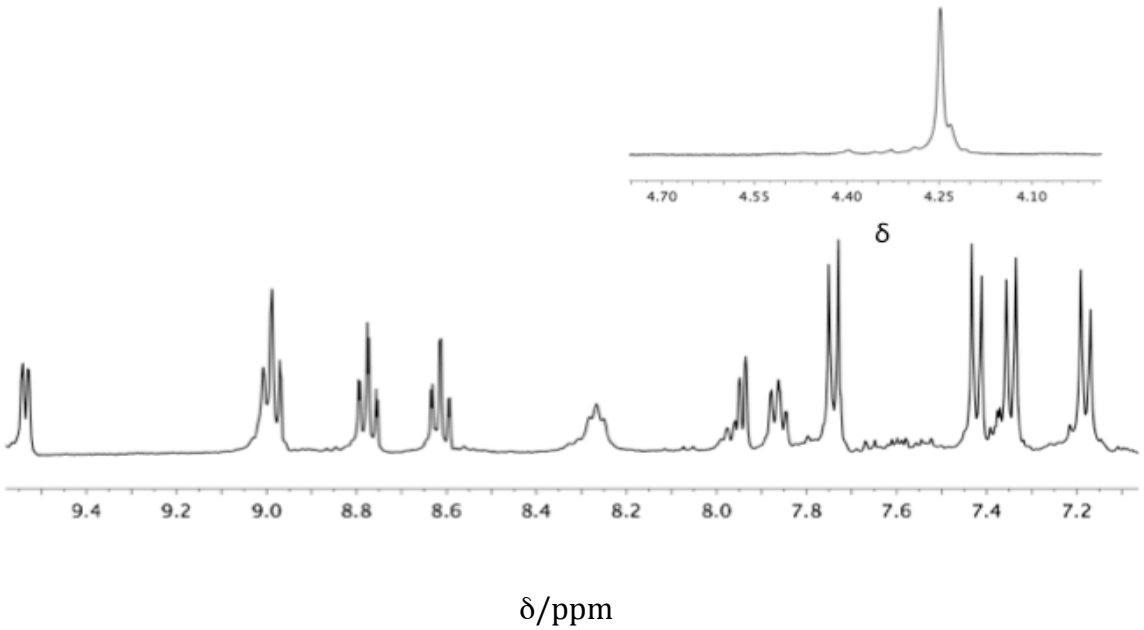

Figure 2.23 ^{1}H-NMR (300 MHz, 25 °C) spectrum of major isomer of $[Rh_2(L_{azo})_2Cl_4](PF_6)_2$ in CD_3CN separated by column chromatography using a silica gel column and eluted using a mixture of acetonitrile:water: KNO_3 (saturated solution) (40:2:1).

Separation of the two isomers was however accomplished by an HPLC 45 minutes gradient method using a C_{18} preparative column. This final method utilises a reverse phase C_{18} preparative column and starts with a mixture of water (0.01% TFA): acetonitrile (0.01% TFA) (85:15) that runs for a period of 5 minutes, after which time the ratio of (0.01% TFA) is increased to 30% over a period of 20 minutes, staying at (70:30) water (0.01% TFA):acetonitrile (0.01% TFA) for a period of 15 minutes and finally going back to the initial ratio of 85:15 and running for 5 minutes.

The method achieved for the separation of these isomers was then applied for the separation of the complexes discussed in section 2.3.3. After analytical HPLC separation the fractions were analyzed by ESI-MS, and for each it was possible to observe the doubly charged peak corresponding to the complex. Preparative HPLC was carried out, and the two main isomers could be successfully separated (Figure 2.24) with a retention time of 27.3 minutes for the minor isomer and 28.4 minutes for the major one. After

separation and purification, the major isomer was obtained with a 2% yield and the minor one with 1%. While the yields for these two isomers were low, these are the first examples of double stranded Rh(III) supramolecular complexes and the quantities obtained were enough for characterization and biological evaluation.

After HPLC separation and purification the complexes were isolated and characterized by ESI-MS, ^{1}H-NMR, elemental analysis and UV-Vis spectroscopy. The first isomer collected, the minor one, will be named complex **7** and the major isomer complex **8**. Elemental analysis data for **7** and **8** support a $[Rh_2(L_{azo})_2Cl_4](PF_6)_2$ formulation and the ESI-MS of both complexes is dominated by a peak with the correct pattern for $[Rh_2(L_{azo})_2Cl_4]^{2+}$ (*m/z* = 552) as well singly charged species $[Rh_2(L_{azo})_2Cl_4]^{+}$ (*m/z* = 1104) and $[Rh_2(L_{azo})_2Cl_4](PF_6)^{+}$ with *m/z* = 1248. In the absorption spectra of both isomers, the visible region is dominated by an MLCT transition centred at 408 nm (ε_{408} = 58 750 dm^3 $mol^{-1}cm^{-1}$ (**7**) and 60 606 dm^3 $mol^{-1}cm^{-1}$ (**8**)). The third peak was also collected and identified by MS as a third isomer, although it was difficult to collect enough material for a ^{1}H-NMR spectrum. Several HPLC injections of additional amounts of crude from different reactions allowed collecting the third peak in a sufficient quantity to perform ^{1}H-NMR spectroscopy (Appendix A.13). The spectrum showed a different pattern (new isomer) than the isomers separated before, nevertheless it was still not enough material to be properly characterized and therefore we decided to not pursue with isolation of the compound.

The PF_6 salts of the complexes **7** and **8**, showed good solubility in acetonitrile, acetone and nitromethane. Exchange of the counter ion to chloride using a Dowex ion exchange column led to water soluble complexes.

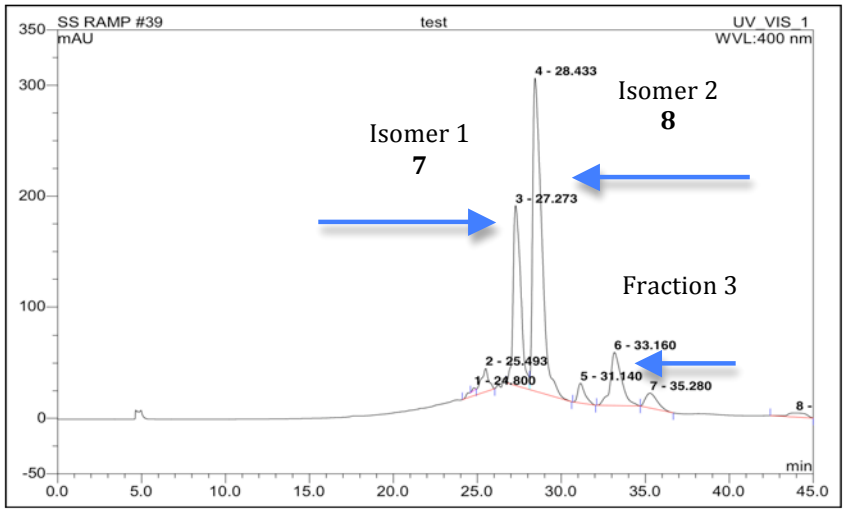

No.	Ret.Time min	Peak Name	Height mAU	Area mAU*min	Rel.Area %	Amount	Type
1	24.80	n.a.	2.406	0.461	0.14	n.a.	Ru
2	25.49	n.a.	20.944	13.717	4.09	n.a.	BMB
3	27.27	n.a.	161.813	85.544	25.52	n.a.	BM
4	28.43	n.a.	281.956	173.538	51.77	n.a.	MB
5	31.14	n.a.	17.910	8.903	2.66	n.a.	BMB
6	33.16	n.a.	48.046	37.271	11.12	n.a.	BMB
7	35.28	n.a.	13.379	11.004	3.28	n.a.	BMB
8	43.99	n.a.	3.708	4.777	1.43	n.a.	BMB
Total:			550.162	335.216	100.00	0.000	

Figure 2.24 Preparative HPLC chromatogram of a crude sample for $[Rh_{2(}L_{azo})_2Cl_4](PF_6)_2$ showing the final separation for the three isomers with the gradient method CH_3CN (0.01 %TFA) and water (0.01 %TFA).

To date, unfortunately, no crystals of any of the isomers isolated were obtained. Despite the use of different conditions, the crystals grown did not have size or sufficient quality to enable X-ray characterization even on the Diamond Synchrotron beam line.

2.6.3 ^{1}H-NMR Characterization of Complexes (7) and (8)

The ^{1}H-NMR spectra of **7** and **8** are similar (Figure 2.25 and 2.26). Diluted samples showed the same pattern on the ^{1}H-NMR spectra confirming that the two spectra are genuinely of different species. When comparing the ^{1}H-NMR spectrum of the crude with the isolated isomers (Figure 2.25), at 4 ppm (singlet of the CH_2 of the spacer of L_{azo}) the difference in the shift for each isomer is clear, with the singlet for **8** (highlighted in green) being shifted downfield in comparison with the one for **7** (highlighted in pink). In addition the peaks between 7.5-7.1 ppm characteristic of the phenyl rings of the spacer of the L_{azo} are different for the two isomers. The ^{1}H-NMR spectra in CD_3CN for **7** and **8**, show eight pyr signals and four signals from the phenyl rings. The two sets of pyr rings and the phenyl rings of the L_{azo} for each complex were assigned with aid of COSY and NOE experiments (Appendix A.14 and A.15). The fact that the molecules show eight pyr signals is important as it rules out the highly symmetrical $\alpha\alpha$ and $\gamma\gamma$ isomers, and excludes the $\beta\alpha$ and $\beta\gamma$ isomers which would have three different pyr environments (see Figure 1.27 in Chapter 1, section 1.3). Assuming that the β, α and γ are the only conformations that can be sustained in a dinuclear double stranded structure (by analogy with the Ru(II) counterparts)[8] this leaves just $\beta\beta$ and $\alpha\gamma$ as possibilities. $\beta\beta$ could have *meso* and *rac* isomers, although only *rac* was observed for the ruthenium ones. However, the remarkable similarity of the two spectra does seem inconsistent with the two isomers being one $\beta\beta$ and the other one $\alpha\gamma$. In addition the CH_2 signal in the $\alpha\gamma$ isomer would be expected to be two doublets, although it might happen that they fall at the same chemical shift and will appear as a singlet.

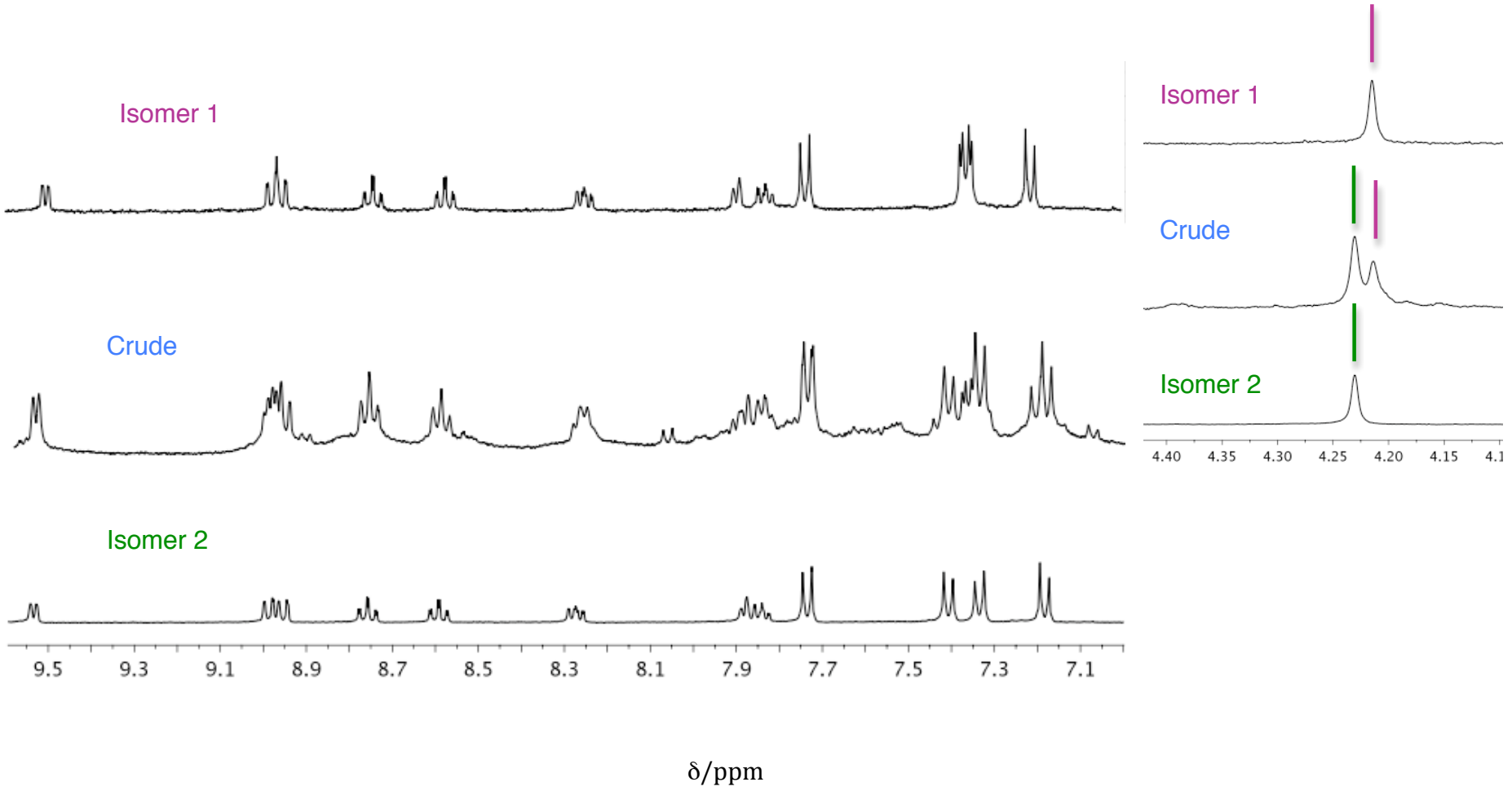

Figure 2.25 ^{1}H-NMR (400 MHz, 25 °C) spectra of the $[Rh_2(L_{azo})_2Cl_4](PF_6)_2$ Isomer 1 (**7**) (top), Crude mixture (middle) and Isomer 2 (**8**) (bottom) in CD_3C

In the NOE experiment, when H_6 of one of the pyr rings is excited a NOE cross peak is observed for $H_{6'}$ which is consistent with a ββ geometry. This is observed in both NOE experiments (for both **7** and **8**) and this implies that the two complexes are the *meso* and *rac* ββ isomers of Rh(III) double stranded complexes.

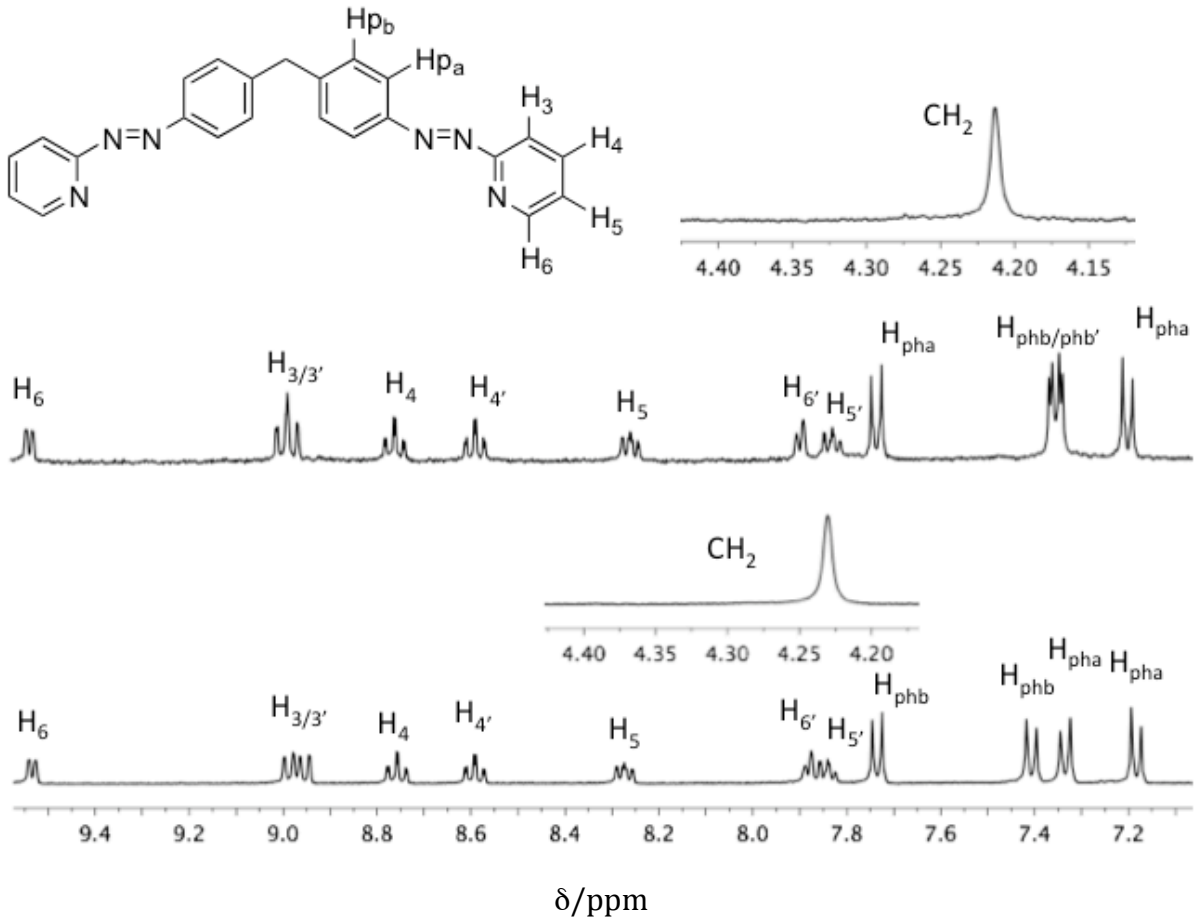

Figure 2.26 ^{1}H-NMR (400 MHz, 25 °C) spectra of the $[Rh_2(L_{azo})_2Cl_4](PF_6)_2$ (**7**) (top), and (**8**) (bottom) in CD_3CN.

In the absence of X-Ray structures, to explore the chiral aspects of the molecular structure of each double stranded isomer, a ^{1}H-NMR experiment using TRISPHAT was carried out. Tris(tetrachlorobenzenediolato)phosphate(V), so called TRISPHAT (Figure 2.27), is a chiral NMR shift anion that exists in two enantiomeric forms. It was first proposed by Lacour and co-workers who were able to separate the Δ and the Λ-TRISPHAT. The tetrabutylammonium salt of the Δ form is commercially available.[17] It

has been demonstrated that one specific isomer of TRISPHAT can preferentially interact with a specific isomer of mono or dinuclear coordination complexes giving rise to differences in the NMR shifts of the protons, which are directly involved in the interaction.[18, 19]

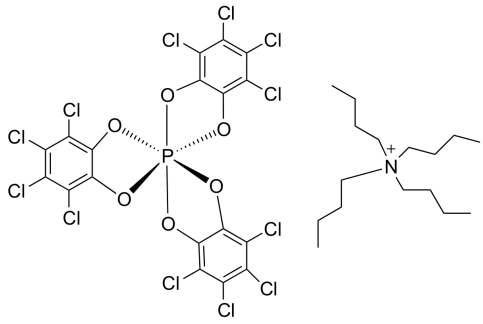

Figure 2.27 Δ-TRISPHAT, [Tris(tetrachlorobenzenediolato)phosphate(V)].

The tetrabutylammonium salt of Δ-TRISPHAT is soluble in acetonitrile and the experiment was carried by addition of an equivalent of Δ-TRISPHAT to a sample of the PF_6 salt of each double stranded isomer (**7** and **8**). This experiment aimed to understand in detail the coordination of each metal centre of the dinuclear complex. On comparing the ^{1}H-NMR spectrum of each isomer after adding Δ-TRISPHAT (Figure 2.28) it is clear that there are differences between them. It is possible to observe that the singlet of the methyl proton of the spacer unit for **8** is split in a 1:1 ratio suggesting that one or more of the centres of the dinuclear complexes is chiral and is interacting with the the Δ-TRISPHAT. This effect is confirmed by the splitting of the phenyl resonances. Taking in consideration the information before, this corroborates the idea of a ββ *rac* isomer, which is a mixture of two enantiomeric species.

When performing the same experiment now for **7**, the CH_2 of the spacer remains as a singlet and the aromatic region of the spectrum does not change significantly, being consistent with a ββ *meso* isomer.

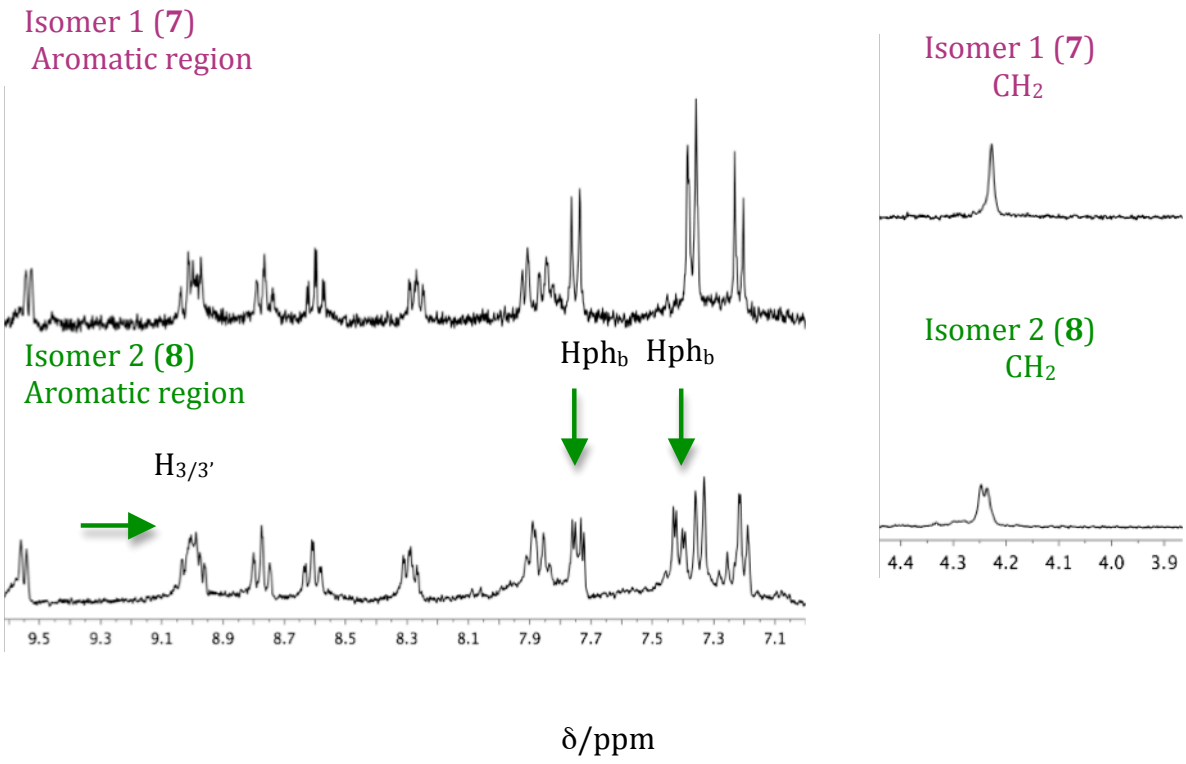

Figure 2.28- ^{1}H-NMR (500 MHz, 25 °C) spectra in CD_3CN of the $[Rh_2(L_{azo})_2Cl_4](PF_6)_2$ Isomer 1 (**7**) (top), and Isomer 2 (**8**) (bottom) with one equivalent of Δ-TRISPHAT.

An X-ray structure of an analogous mononuclear $[Rh(L_{azpy})_2Cl_2]ClO_4$ complex α isomer is available, but no ^{1}H-NMR data was reported.[11] This is an isolated example, and to the best of our knowledge no other structures have been reported. In addition, the work performed with the α-$[Rh(L_{azpy})_2Cl_2]ClO_4$ was focused on the redox properties of the complex rather than into its biological features. Because of this we thought it would be of importance to synthesize the mononuclear analogue for comparison in future biological studies.

Using the same method as for the synthesis of the dinuclear Rh(III) double stranded complexes, the $[Rh(L_{azpy})_2Cl_2]PF_6$, (compound **9**) was synthesized from $RhCl_3.3H_2O$ with two equivalents of the L_{azpy} in a system of propanol:water (2:1) refluxing for 3 hours. The PF_6 salt was isolated and the elemental analysis of the yellow/green solid was

consistent with the formulation of $[Rh(L_{azpy})_2Cl_2]PF_6$. The MS was dominated by the singly charged peak corresponding to $[Rh(L_{azpy})_2Cl_2]^+$ with *m/z* = 539. The UV-Vis spectrum of the complex in acetonitrile is dominated an MLCT transition at 363 nm (ε_{363} = 24 470 $dm^3\ mol^{-1}cm^{-1}$. ^{1}H-NMR (Figure 2.29) and COSY experiments (Appendix A.16) showed one set of resonances for the protons of the pyridine ring and a set of resonances for the protons of the phenyl ring.

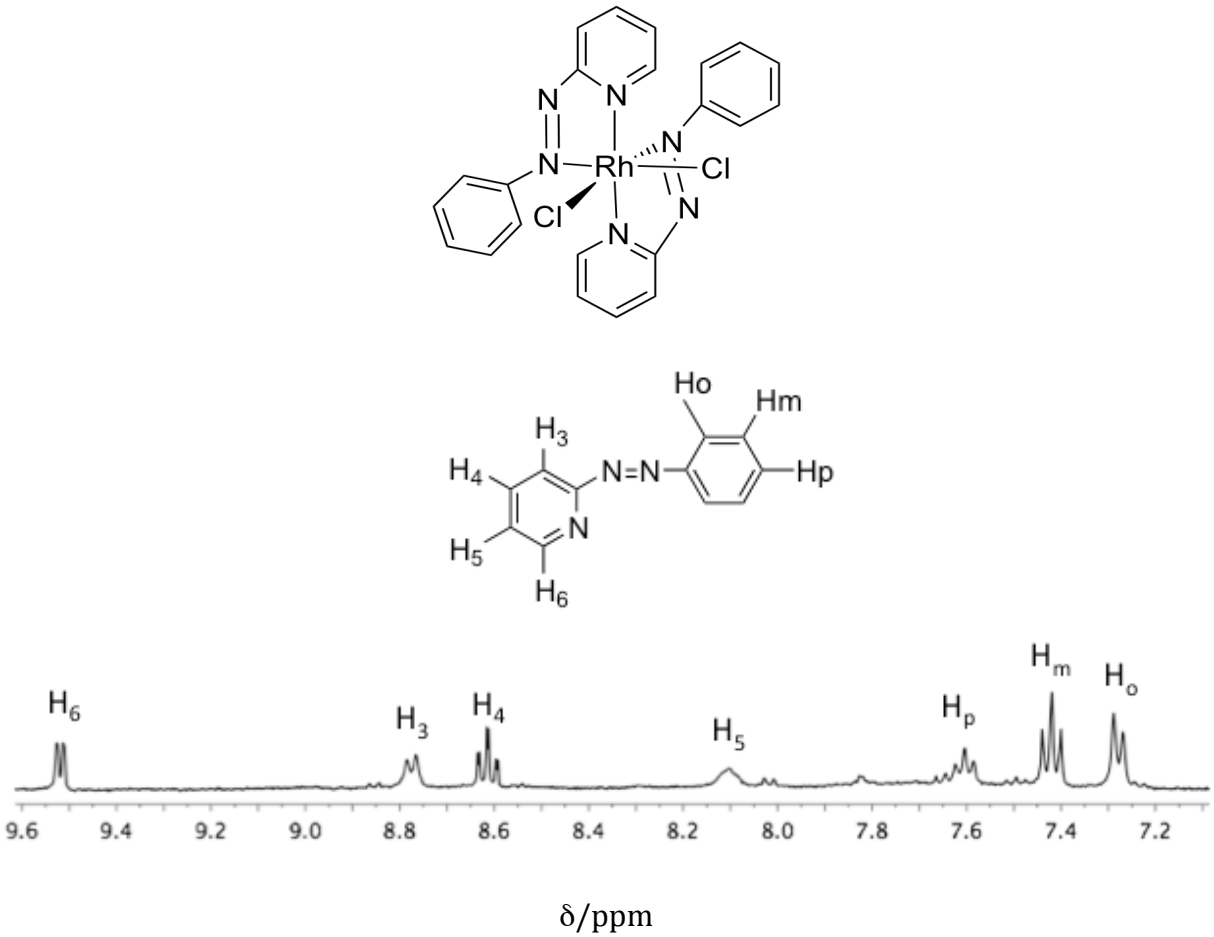

Figure 2.29 ^{1}H-NMR (400 MHz, 25 °C) spectrum of the $[Rh(L_{azpy})_2Cl_2](PF_6)$ (**9**) (top) in CD_3CN.

This indicates that the complex is symmetrical and that the ligands are coordinated in the same configuration.

2.7 Towards the Synthesis of Rh(III) Triple Stranded Complex

As mentioned before, the DNA binding studies in Hannon's group have focused on the Fe(II) and Ru(II) tetracationic helicates which are formed by three L_{im} ligands wrapped around the two metal centres. These cylinders are triple stranded helicates with a high positive charge (4+), which enhances their binding affinities to the negatively charged DNA. Thermal stability problems of the Fe(II) cylinder were overcome by using the Ru(II) analogue. The aim of synthesizing a Rh(III) cylinder was not only to obtain a complex with increased stability when compared with the Fe(II) one but also to study the increase on the overall charge and to probe its effect on the DNA binding and cytotoxicity.

The synthesis of the Ru(II) cylinder was rather more complicated than for the Fe(II) complex which is easily formed.[4, 20] The Ru(II) triple stranded helicate is synthesised from *cis*-$Ru(DMSO)_4Cl_2$ with L_{im} over a period of 5 days in ethylene glycol under nitrogen atmosphere. The complex is finally precipitated from a methanolic solution of NH_4PF_6 and an extensive column purification process is required.[5]

The synthesis of the Rh(III) triple stranded complex was also not straightforward. Initially $RhCl_3.3H_2O$ was explored as a starting material in a ratio of 1 to 1.5 with the L_{azo} and L_{im} ligands using solvents and mixtures of solvents as for the synthesis the previously described single and double stranded complexes. After heating under reflux these reaction mixtures for periods of time, the products were analysed by MS or ^{1}H-NMR but in no case was the desired triple stranded species observed. Attempts to use $Rh(DMSO)_3Cl_3$ and $Rh(DMSO)_4Cl_2$ as starting materials were similarly unfruitful. Replacing the chloride ligands in the starting material $RhCl_3.3H_2O$ with $AgNO_3$ in a

refluxing mixture of ethanol:water (2:1), led to the precipitation of AgCl and upon hot filtration, 1.5 equivalents of L_{azo} were added to the mixture and refluxed for 1 extra hour. The MS of the crude reaction mixture was analyzed and showed a set of peaks that suggested the formation of the desired complex along with several other peaks indicating the presence of other species formed by the non-total substitution of the chloride ligands by the nitrates. As a consequence, new efforts were made starting from the commercial available Rhodium (III) nitrate ($Rh(NO_3)_3.xH_2O$). The use of this starting material with nitrates and water ligands as good leaving groups, would lead to a water soluble complex which can be used directly for DNA binding and biological studies.

2.7.1 Synthesis of Rh(III) Triple Stranded Complex

The starting material $Rh(NO_3)_3.xH_2O$ is hygroscopic, so it was handled rapidly and carefully kept under vacuo. For this reason, initial attempts made in a ratio of 1:1.5 (Rhodium to ligand) always led to an excess of ligand in the crude reaction mixture as observed by ^{1}H-NMR. Therefore the reaction stoichiometry was readjusted to a ratio of 1:1. A sample of $Rh(NO_3)_3.xH_2O$ and L_{azo} were added to an argon purged solution of propanol:water (2:1) and heated under reflux for 40 minutes under an argon atmosphere (scheme 2.6). The solution very quickly changed (five minutes after the start of the reflux) from bright intense orange to dark orange/brown and the reaction was allowed to reflux for an additional 35 minutes. The reaction was monitored each five minutes (by ESI-MS), to follow the consumption of ligand and formation of new species. The reaction mixture was filtered to remove some of the black insoluble material formed. After cooling to room temperature the dark orange/brown complex was obtained as a PF_6 salt by the addition of a concentrated aqueous NH_4PF_6 solution.

The MS of the Rh(III) triple helicate complex when the PF_6 salt was dissolved in acetonitrile (MS, 5 eV, injected via syringe pump in acetonitrile) was dominated by a doubly charged peak corresponding to $[Rh_2(L_{azo})_3]^{2+}$ with *m/z* = 670, and triply and four charged peaks $[Rh_2(L_{azo})_3]^{3+}$,$[Rh_2(L_{azo})_3]^{4+}$ with *m/z* = 446 and *m/z* = 335, respectively. Also a singly charged peak was observed for the species $[Rh_2(L_{azo})_3](PF_6)^{+}$ at *m/z* = 1486 (Figure 2.30).

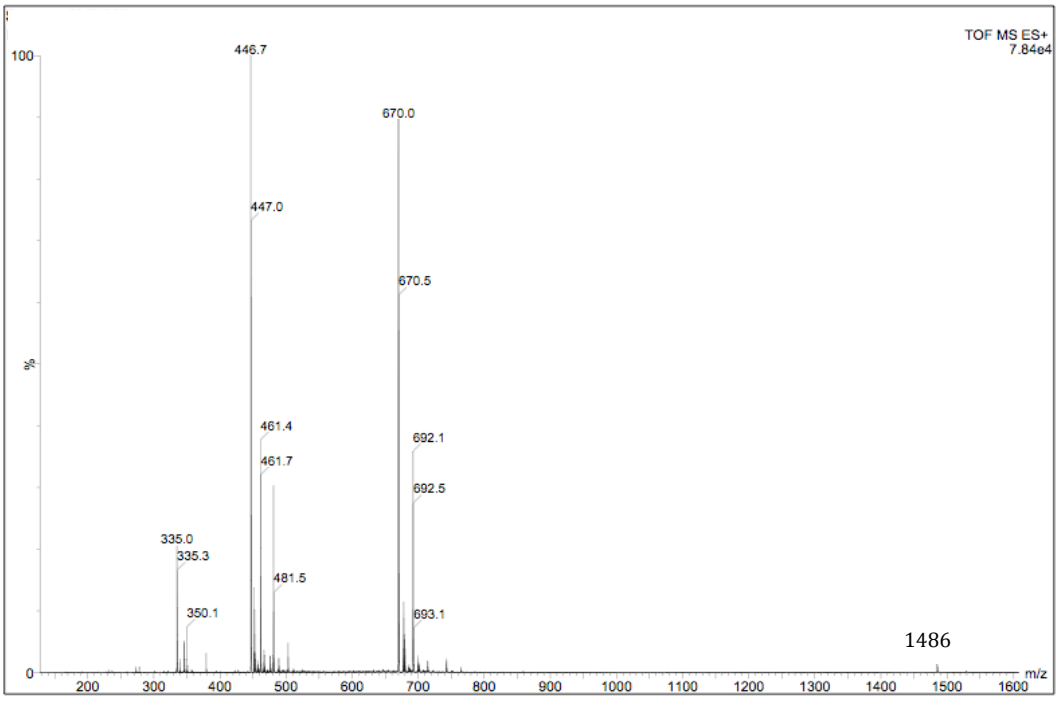

Figure 2.30 ESI-MS of Rh(III) triple stranded complex dissolved in CH_3CN and recorded at 5 eV using as spray solvent CH_3CN.

Although these successive reduction peaks seem unexpected, a reported dinuclear rhodium (III) complex $[(tpyRh(tpy\text{-}AB\text{-}tpy)Rhtpy)]^{6+}$ (AB- azobenzene bridge), showed the same behaviour in the ESI mass spectrum with the reduction peaks being dependent on the counter ion of the final complex.[21]

The ^{1}H-NMR spectrum of this solid in CD_3CN (Figure 2.31) exhibited a species with peaks as expected in the aromatic region of the spectrum as well as in the aliphatic region with the singlet of the CH_2 group of the spacer being shifted with respect to the free ligand in the same solvent. However the complex showed broad and overlapped peaks suggesting the presence of impurities (polymer materials and/or excess of L_{azo}). The purification methods attempted (columns and HPLC) were unsuccessful and the ^{1}H-NMR spectrum never improved; on the contrary the spectrum became more complicated suggesting that the complex was suffering degradation under the conditions used for purification.

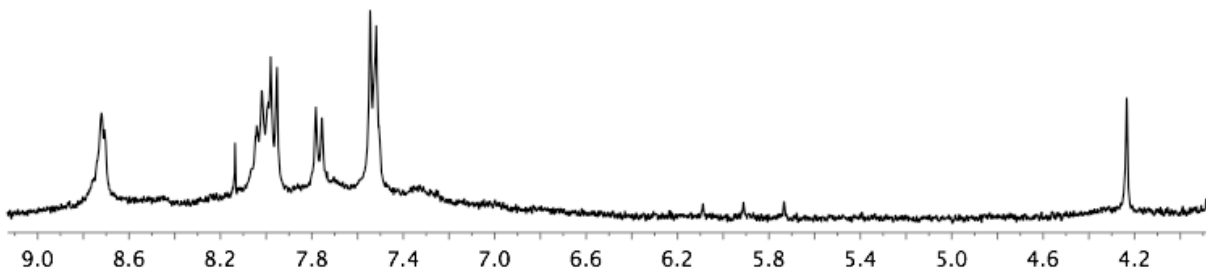

Figure 2.31 ^{1}H-NMR (400 MHz, 25 °C) spectrum of $[Rh_2(L_{azo})_3](PF_6)_6$ in CD_3CN.

On cooling to room temperature the reaction mixture was evaporated to dryness obtaining as final product a nitrate salt, the ^{1}H-NMR spectrum of which showed a purer species with the ESI-MS showing peaks for the same doubly charged species already observed for the PF_6 salt and a singly charged peak.

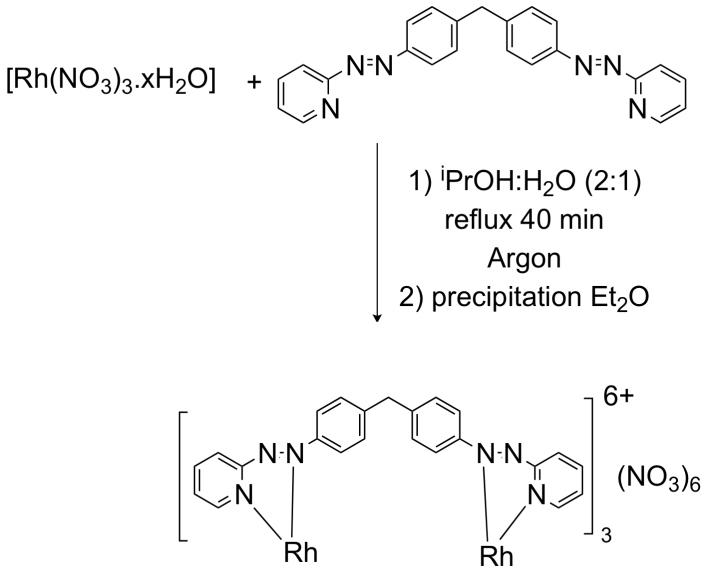

Scheme 2.6 Synthetic route for the preparation o the Rh(III) triple stranded complex.

The nitrate solid is highly soluble in water and also in methanol. The MS of the complex when dissolved in methanol (MS, 5 eV, injected via syringe pump in acetonitrile) was dominated by a doubly charged peak corresponding to $[Rh_2(L_{azo})_3]^{2+}$ with *m/z* = 670, and a singly charged peak for the species $[Rh_2(L_{azo})_3]^{+}$ with m/z = 1340 and with one nitrate counter ion at *m/z* = 1402 for $[Rh_2(L_{azo})_3](NO_3)^{+}$. The MS is shown in Figure 2.32. This complex will be named complex number **10**.

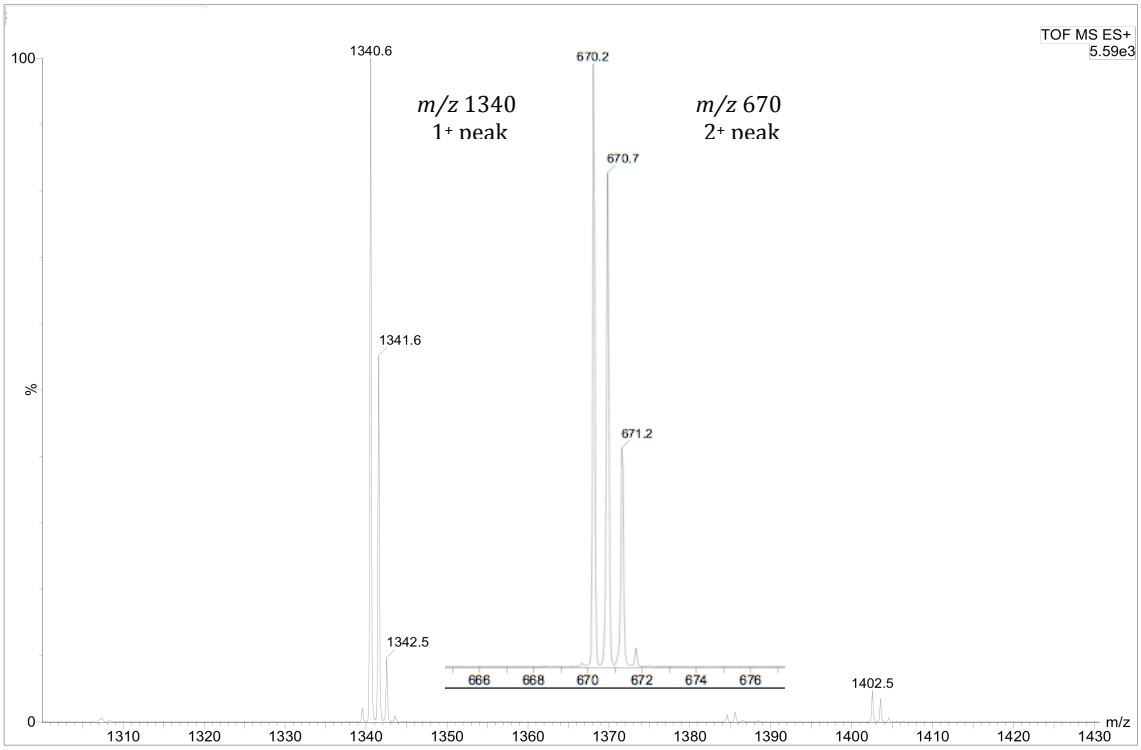

Figure 2.32 ESI-MS of $[Rh_2(L_{azo})_3](NO_3)_6$, dissolved in MeOH (spray solvent CH_3CN, 5eV).

The ^{1}H-NMR spectrum of **10** in MeOD displays one aliphatic and six aromatic proton resonances, which indicates the formation of a symmetric compound. Each resonance was assigned with help of a COSY experiment (Appendix A.17). The helical arrangement of the strands of the ligands wrapped around the Rh(III) metal centres axis is indicated by the singlet resonances of the CH_2 of the central spacer at 4.29 ppm showing that both protons are equivalent (Figure 2.33). The high symmetry in the ^{1}H-NMR can just indicate the presence of a triple stranded or an αα- double stranded system, although a double stranded geometry would not be consistent with the MS shown in Figure 2.32 with the peaks corresponding to a mass of three coordinated L_{azo}. Also, in the MS there are no peaks with NO_3 adducts that could suggest the coordination of such ligands to the metal

centres. The triple stranded complex can exist in two forms, *rac* and *meso* isomers, to date for the Ru(II) analogue[5] just the *rac* form was observed, although the ruthenium triple stranded complex is obtained in very poor yield from a large mixture of several reaction side products and the *meso* form may as well exist. The ^{1}H-NMR spectrum of the Ru(II) helicate shows very high symmetry like the one for the Rh(II) complex shown in Figure 2.33.

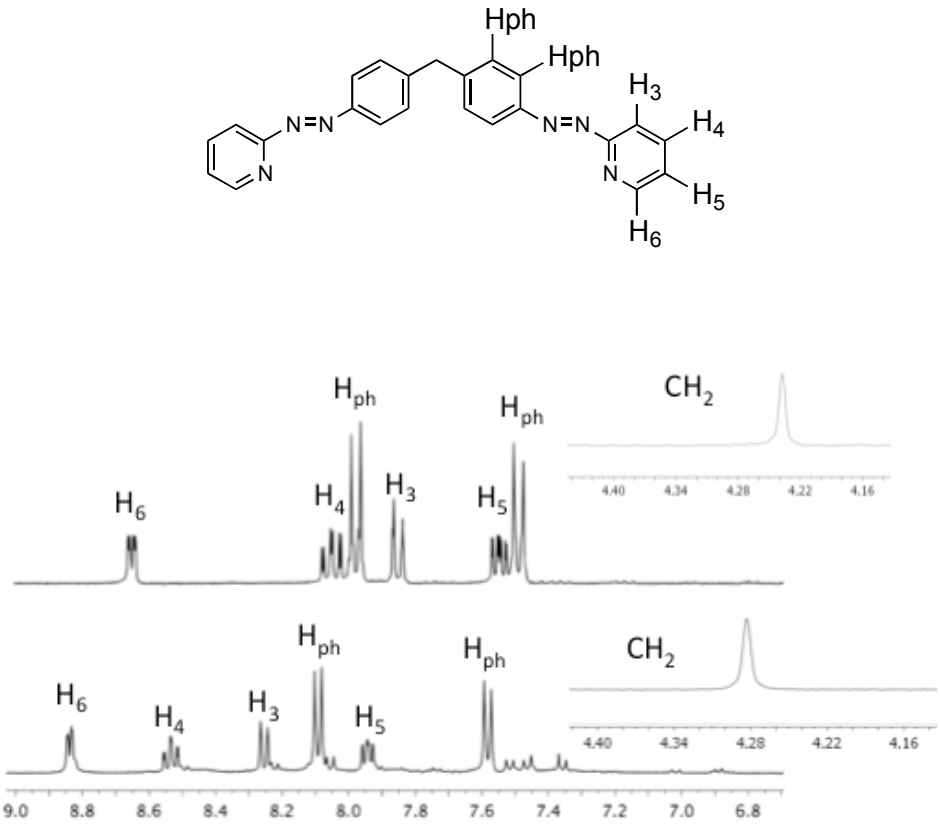

Figure 2.33 ^{1}H-NMR spectrum (400 MHz, 25 °C) in CD_3OD of the L_{azo} (top), and $[Rh_2(L_{azo})_3](NO_3)_6$ (**10**) (bottom).

As the phenyl rings of the spacer are freely rotating in solution the corresponding protons appear as two sharp doublets at 8.09 and 7.58 ppm. The coordination of the ligand to the metal is confirmed by the large downfield shift of all the aromatic protons

of the complex in comparison with the free ligand in the same solvent and conditions. The same happens for the singlet of the spacer, which is shifted downfield by 0.07 ppm.

The ^{1}H-NMR spectrum indicates the presence of an impurity, which according to the MS may be presence of ligand (Figure 2.32, *m/z* = 401 L_{azp}+Na^{+}). Several attempts were made to purify this complex but due to its high charge and strong affinity with columns (silica or alumina) the purification repeatedly led to high loss of complex in the columns independently of the solvent system used. High polarity solvents with high concentration of salts were used but the complex was never obtained with higher purity than the original crude product. In addition washing of the complex to remove the amount of salt used led to lower yields. During the elution of the complex through silica columns it was possible to observe an extra band with a reddish colour. This band was analyzed by MS, which showed several doubly charged peaks of an unidentified species perhaps suggesting that the main compound was decomposing during the purification.

Attempts to wash the complex with some other organic solvents in which the ligand is very soluble (DCM, $CHCl_3$) did not improve purity. The complex is quite stable in methanol and water for days and as well in the presence of light. To verify this, a ^{1}H-NMR study was carried out during 3 days but no detectable differences were observed between the sample exposed to daylight and the one kept in the dark. The synthetic procedure could always be reproduced but always with presence of ~ 10% of impurity. Because it did not prove possible to develop a purification method, the complex was used as obtained and without further purification.

The UV-Vis absorption spectrum reveals a broad band with two absorption maxima centred at 387 nm ((ε_{387} = 37 766 $dm^3\ mol^{-1}cm^{-1}$) and 420 nm (ε_{420} = 34 833 $dm^3\ mol^{-}$

$^{1}cm^{-1}$) and a less intense band in the visible region at 530 nm (ε_{530} = 12 633 dm^3 $mol^{-1}cm^{-1}$).

Numerous attempts were made to grow X-ray quality crystals of this complex, but unfortunately such efforts were unsuccessful.

With the aim to explore the emission properties of complex **10**, experiments were carried out in water with a different range of excitation wavelengths. This study showed that the complex emits poorly at room temperature under these conditions. This result was not totally unexpected because complexes like $[Rh(phen)_3]^{3+}$ and $[Rh(bpy)_2Cl_2]^{+}$ show weak emission at room temperature and with emission properties explored at 77 Kelvin in ethanol-methanol glass.[13, 22, 23]

2.8 New Mononuclear *Facial* Isomer of Rh(III)

The ruthenium complexes of L_{azpy} are well studied and the meridional (*mer*) isomer of $[Ru(L_{azpy})_3]^{2+}$ was synthesized and fully characterized by Hotze and co-workers. They show that even with the replacement of the two chloride ligands of the α-$[Ru\text{-}(L_{azpy})_2Cl_2]$ by another L_{azpy}, the final complex still exhibits moderate cytotoxicity in some particular cancer cell lines.[24] This encouraged us to attempt the synthesis of a new mononuclear complex $[Rh(L_{azpy})_3]^{3+}$, that could be further studied for its DNA binding and cytotoxicity.

2.8.1 Synthesis of a New Mononuclear *fac*- $[Rh(L_{azpy})_3]^{3+}$

$Rh(NO_3)_3.xH_2O$ and L_{azpy} were added to an argon purged solution of propanol:water (2:1) and heated under reflux for 40 minutes under an argon atmosphere (scheme 2.7). The solution changed very quickly (five minutes after reflux commenced) from bright intense orange to dark orange/brown (indicating the presence of the same chromophore as in complex **10**) and it was allowed to reflux for an additional 35 minutes. The reaction mixture was cooled to room temperature, evaporated to dryness and freeze dried to remove excess water. The dark orange/brown crude product was then taken up into a minimum amount of methanol and precipitated with diethyl ether to give a dark orange/brown solid, which was dried in vacuum overnight. $[Rh(L_{azpy})_3]^{3+}$ theoretically exists in two different geometric isomeric forms (ie. disregarding enantiomers) the *mer* and *fac* isomers (scheme 2.7).

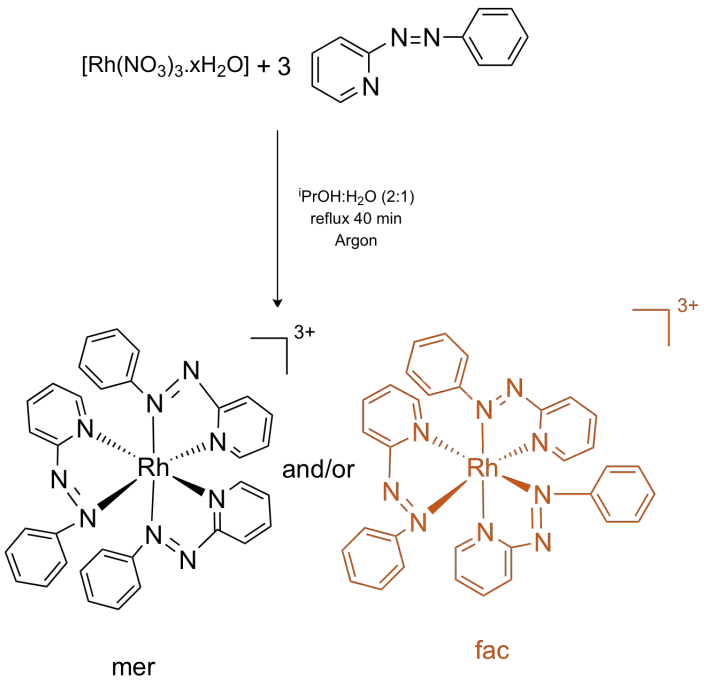

Scheme 2.7 Synthetic route for the preparation of the complex $[Rh(L_{azpy})_3]^{3+}$ *mer* and *fac*-$[Rh(L_{azpy})_3]^{3+}$ (Δ form shown).

The symmetry properties of the two isomers (*mer* and *fac*) are noticeably different. The *fac*-$[Rh(L_{azpy})_3]^{3+}$ belongs to a C_3 point group having three equivalents ligands L_{azpy}. The *mer* -$[Rh(L_{azpy})_3]^{3+}$ belongs to a C_1 symmetry group where all the L_{azpy} ligands are inequivalent. The ^{1}H-NMR in MeOD (Figure 2.34) of the of the brown solid obtained displays one set of resonances with nine protons being assigned that are consistent with the formation of a single isomer, and that isomer being the *fac* isomer. Each resonance was assigned with help of a COSY experiment (Appendix A.18). The *fac* isomer seems to be less likely to form in comparison with the *mer* isomer due to the crowding of the three phenyl groups. The ^{1}H-NMR spectrum of the complex (Figure 2.34 bottom) is markedly different from the ^{1}H-NMR of the free ligand (Figure 2.34 top). The protons of the pyridine rings (H_6, H_4, H_3 and H_5) are significantly shifted downfield upon coordination.

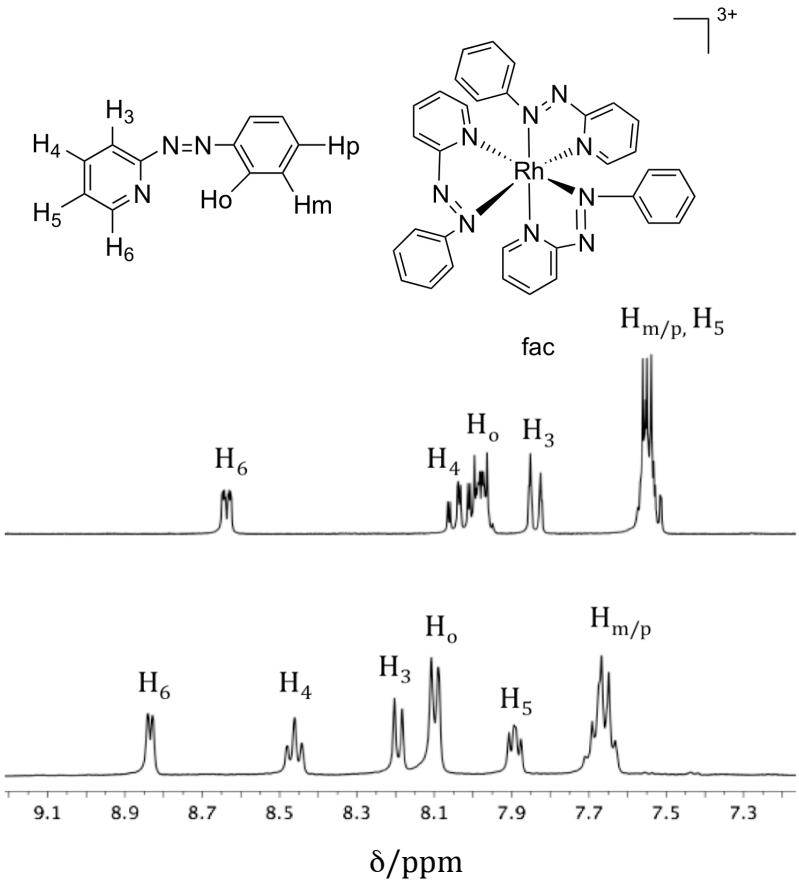

Figure 2.34 ^{1}H-NMR spectra (400 MHz, 25 °C) in CD_3OD of the L_{azpy} (top), and $[Rh_2(L_{azo})_3](NO_3)_3$ (**11**) (bottom).

In addition, there are close similarities between the ^{1}H-NMR spectrum of the dinuclear triple stranded complexes, $[Rh_2(L_{azo})_3](NO_3)_6]$ (**10**) and the ^{1}H-NMR of *fac*-$[Rh(L_{azpy})_3](NO_3)_3$ which once again supports the helical arrangement of the strands of the di-nucleating L_{azo} around the Rh(III) metal centres, being consistent with a Rh(III) triple stranded helicate.

The *fac*-$[Rh(L_{azpy})_3](NO_3)_3$ UV-Vis absorption spectrum reveals a band with absorption maximum at 321 nm (ε_{321} = 30 100 dm^3 mol^{-1}cm^{-1}) and a shoulder at 370 nm (ε_{370} = 16 066 dm^3 mol^{-1}cm^{-1}) and a much less intense band in the visible region at 509 nm (ε_{509} = 3 100 dm^3 mol^{-1}cm^{-1}).

The MS is dominated by a singly charged peak with *m/z* = 531 corresponding to $[Rh(L_{azpy})_2](NO_3)$ and another singly charged peak with m/z = 469 corresponding to the same species but with the loss of the counter ion $[Rh(L_{azpy})_2]^+$. Although these MS peaks may imply the presence of a square planar Rh(I) complex, it is known in the literature that the complex $[Rh(bpy)_2]^+$ for example, is purple and very unstable to air and it rapidly oxidizes to Rh(III).[25] Several ^{1}H-NMR spectra were recorded over a period of 4 days and no changes were observed, meaning that the complex remained stable in methanol at room temperature and exposed to air.

Several attempts to grow X-ray quality crystals of this complex were made. Unfortunately these efforts were unfruitful.

2.9 Conclusions

In this chapter, the synthesis and characterisation of ten new Rhodium (III) complexes has been described. The mononucleating and dinucleating (L_{azpy} and L_{azo}) ligands were successfully used in the synthesis of three novel Rh(III) mononuclear, four dinuclear single stranded, two dinuclear double stranded and one dinuclear triple stranded complex. Attempts to use the L_{im} ligand under the same reaction conditions failed.

A general synthetic procedure using propanol:water (2:1) was established for the synthesis of all complexes with the reactions of the mononuclear complexes leading to pure complexes without the requirement of any additional purification. For the single and double stranded complexes a general HPLC method was developed for the separation of the different isomers. All the reactions afforded the desired complexes in a short period of time with reaction times varying from 20 to 90 minutes.

The aim of this work was to synthesize mononuclear and dinuclear new complexes of Rh(III) with potential DNA binding affinity. In chapter 3, DNA binding studies of these new complexes using Circular and Linear Dichroism (CD and LD) and Gel Electrophoresis are reported.

2.10 Experimental

2.10.1 Materials and Methods

All chemicals and solvents were purchased from Sigma–Aldrich, Fisher, Alfa Aesar, or Fluorochem and used as received. Deuterated solvents for NMR were supplied by Goss Scientific. Silica high performance liquid chromatography (HPLC) analyses and purifications were performed on Dionex Summit HPLC systems with Chromeleon software, using HPLC grade solvents, supplied by Fisher. Analytical HPLC data was acquired with the aid of a Summit P580 quaternary low pressure gradient pump with built in vacuum degasser while, for the preparative HPLC, a high pressure gradient pump was employed. A Dionex UVD 170s UV-Vis multichannel detector was used on both instruments. Phenomenex Luna Silica HPLC columns were used for analytical (250 x 4.6 mm) and preparative (250 x 21.2 mm) separations. NMR spectra were recorded on Bruker AVIII300 (operating at 300 MHz for ^{1}H and 75 MHz for ^{13}C), on AVIII400 (operating at 400 MHz for ^{1}H and 100 MHz for ^{13}C) and on a DRX500 (operating at 500 MHz for ^{1}H and 125 MHz for ^{13}C), using standard Bruker software. Electrospray Ionisation (MS) analyses were performed on a Waters LCT Time of Flight Spectrometer equipped with ESI-MS probe. For the Rhodium (III) final complexes with PF_6 counter ion the samples were dissolved in acetonitrile and introduced using a syringe pump operating at a flow rate of 50 μl/min. The desolvation temperature was 300 °C and the source temperature of 130 °C. The cone voltage used was of 5 eV. For the L_{azo} and other starting materials the samples were diluted in methanol and run under the same conditions and using a cone voltage of 30 eV. For the L_{azpy}, the sample was dissolved in methanol and run by Electronic Impact (EI) in a VG ZabSpec mass spectrometer equipped with EI/CI source. Samples were introduced via direct insertion probe using a

temperature ramp from 50 °C to 350 °C. Source operated at 180 °C and spectrometer scanned at 1 sec/decade over a mass range of 600-300 amu.

Microanalyses of the compounds were performed on a CE Instruments EA1110 elemental analyzer. UV-Vis spectra were performed in a Varian Cary 5000 UV-Vis spectrometer. X-ray crystal analyses were performed by the X-ray Diffraction Facility Officer of the School of Chemistry, University of Birmingham (Dr. Louise Male). Suitable crystals were selected and a dataset for *cis*-[$Rh(L_{azpy})(phen)Cl_2][PF_6]$ (**5**) (in CH_3CN) was measured on a Bruker KappaCCD diffractometer and for *cis*-[$Rh(L_{azpy})(phen)Cl_2][PF_6]$ (MeOH:CH_3CN), for *cis*-[$Rh(L_{azpy})(bpy)Cl_2][PF_6]$ (**6**), *rac*-[$Rh_2(L_{azo})(phen)_2Cl_4](PF_6)_2$ (**1**) and *rac*-[$Rh_2(L_{azo})(bpy)_2Cl_4](PF_6)_2$ (**3**) on a Bruker APEXII CCD diffractometer both at the windows of a Bruker FR591 rotating anode ($\lambda_{Mo\text{-}K_\alpha}$ = 0.71073 Å) at 120 K by the EPSRC National Crystallography Service at the University of Southampton. The data collections were driven by COLLECT and processed by DENZO. Absorption corrections were applied using SADABS. The structures of **5**, polymorph of **5** and **3** were solved in SHELXS-97, **6** was solved in SIR92 and **1** was solved in SIR2004 and all five structures were refined by a full-matrix least-squares procedure on F^2 in SHELXL-97. All non-hydrogen atoms were refined with anisotropic displacement parameters. All hydrogen atoms were added at calculated positions and refined by use of a riding model with isotropic displacement parameters based on the equivalent isotropic displacement parameter (U_{eq}) of the parent atom. Figures were produced using Chimera Software for Macintosh.

2.10.2 Synthesis of [Rh(DMSO)(phen)Cl_3][7]

[Rh(DMSO)(phen)Cl_3] was synthesized according to a literature procedure.[7] *mer*-[$RhCl_3$(DMSO-*κO*)(DMSO-*κS*)$_2$] (0.200 g, 0.45 mmol) was dissolved in 10 ml of a 1:1 mixture of methanol and water. After addition of 1,10′-phenanthroline (0.070 g, 0.45 mmol), the reaction mixture was stirred for 2 hours at 75 °C and left standing at 4 °C for further 24 hours. The resulting yellow precipitate was filtered off, washed with 1 ml of methanol, dried with diethyl ether and kept in vacuum (0.130 g, 60%).

Positive-ion ESI (30 eV, DMSO): *m/z* (%) = 465 [$Rh(CH_3SOCH_3)(C_{12}H_8N_2)Cl_3]^+$ (100).
Elemental analysis calcd (%) for [$Rh(CH_3SOCH_3)(C_{12}H_8N_2)Cl_3$] C: 36.0, H: 3.0, N: 6.0; Found C: 35.8; H:2.6; N:6.0

^{1}H NMR (300 MHz, d-DMSO, 25 °C, TMS): δ = 10.05 (d, 1H, *J* = 5.4 Hz, H_9), 9.96 (d, 1H, *J* = 4.9 Hz, H_2), 9.62 (dt, 2H, *J* = 5.4, 1.1 Hz, $H_{9/2}$ *fac* and *mer*,), 9.10-8.96 (m, 4H, $H_{5/6}$ *fac* and *mer*), 8.45-8.32 (m, 5H, $H_{7/4}$, *fac* and *mer*, H_3), 8.26 (ddd, 3H, *J* = 8.5, 5.5, 3.1 Hz $H_{3/8}$ *fac* and *mer*), 3.69 (s, 6H, H-$_{DMSO}$), 3.11 (6H, s, H-$_{DMSO}$).

2.10.3 Synthesis of [Rh(DMSO)(bpy)Cl_3][7]

[Rh(DMSO)(bpy)Cl_3] was synthesized according to the same literature procedure.[7] *mer*-[$RhCl_3$(DMSO-*κO*)(DMSO-*κS*)$_2$] (0.200 g, 0.45 mmol) was dissolved in 10 ml of a 1:1 mixture of methanol and water. After addition of 2,2'-bypyridine (0.070 g, 0.45 mmol), the reaction mixture was stirred for 2 hours at 75 °C and left standing at 4 °C for further 24 hours. The resulting yellow precipitate was filtered off, washed with 1 ml of methanol and dried with diethyl ether and kept in vacuum (0.100 g, 50 %).

Positive-ion ESI (30 eV, DMSO): *m/z* (%) = 443 [$Rh(CH_3SOCH_3)(C_{10}H_8N_2)Cl_3]^+$ (100). Elemental analysis calcd (%) for [$Rh(CH_3SOCH_3)(C_{10}H_8N_2)Cl_3$] C: 32.5, H: 3.2, N: 6.3; Found C: 32.8; H: 2.8; N: 6.3.

^{1}H NMR (300 MHz, d-DMSO, 25 °C, TMS): δ= 9.79 (d, 1H, *J* = 5.8 Hz, H_9), 9.76-9.72 (m, 1H, H_2), 8.84-8.75 (m, 2H, $H_{5/6}$), 8.44 (td, 1H, *J* = 7.5, 1.4 Hz, H_7), 8.38-8.32 (m, 1H, H_4), 7.99 (ddd, 1H, *J* = 7.5, 5.8, 1.4 Hz, H_8), 7.90 (ddd, 1H, *J* = 7.5, 5.8, 1.4 Hz, H_3), 3.61 (s, 6H, H_{DMSO}).

2.10.4 Synthesis of L_{azo}

The L_{azo} was synthesized according to the procedure established previously in the Hannon group.[8, 26] 2-Nitrosopyridine was synthesized according to a literature procedure.[9] 2- Aminopyridine (9.545 g, 101.5 mmol) and dimethyl sulfide (8 ml) were dissolved in dichloromethane (100 ml). *N*-chlorosuccinimide (13.300 g, 100 mmol) was dissolved in dichloromethane (250 ml) and added drop wise to the aminopyridine solution over a period of 1 hour whilst maintaining the temperature at -20 °C. The reaction mixture was then stirred at -20 °C for 1 hour and then for 1 hour at room temperature during which time the colour changed from a pale yellow to a pale green. A solution of sodium methoxide in methanol (4.050 g, 170 mmol in 75 ml of methanol) was added and stirred for 10 minutes. Water (150 ml) was added and the mixture was allowed to stir overnight. The organic layer was separated extracted with water (2 x 50 ml). The combined organic portions were washed with water (50 ml), dried using $MgSO_4$ and evaporated to produce yellow/brown oil that was kept in the fridge overnight. All the oil product (*S,S*-Dimethyl-*N*-(2-pyridyl)sulfilimine) was dissolved in dry dichloromethane (100 ml). This was added to a solution of m-chloroperbenzoic acid (20.000 g, 116 mmol) in dry dichloromethane (500 ml) cooled to 0 °C. The reaction mixture was stirred at 0-5 °C for 90 minutes followed by addition of dimethyl sulfide (4 ml). After stirring for 30 minutes, a saturated aqueous sodium carbonate solution (500 ml) was added to the reaction mixture. The green organic layer was separated and washed with water (25 ml), dried with $MgSO_4$ and evaporated to dryness to give a light brown solid. The solid was then recrystallized from ethanol to provide yellow crystals. 2- Nitrosopyridine (2.000 g, 18.52 mmol) and 4,4'-methylenedianiline (1.470 g, 7.41

mmol) were dissolved in 25 ml of dichloromethane. Glacial acetic acid (2 drops) was added to the mixture and the resulting orange solution was stirred at room temperature for 24 hours. The final orange solution was then evaporated to dryness to provide the L_{azo} as an orange solid (3.46 g, 65%).

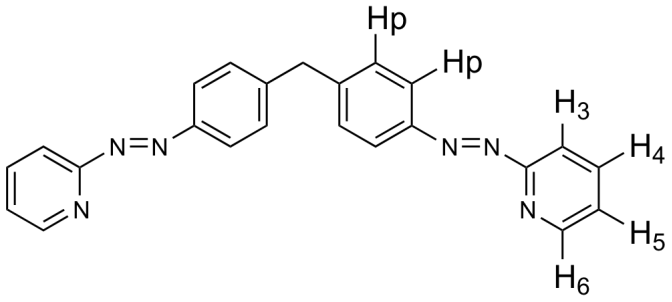

Positive-ion ESI (30 eV, $CHCl_3$): *m/z* (%) 379 [L_{azo}+H^+] (100), 401 [L_{azo}+Na^+] (70);

Elemental analysis calcd (%) for $C_{23}H_{18}N_6.0.5H_2O$: C:71.3; H:4.9; N:21.7; found: C:71.1; H:4.5; N:22.1.

^{1}H NMR (300 MHz, $CDCl_3$, 25 °C, TMS): δ = 8.74 (ddd, 1H, *J* = 4.8, 1.7, 0.8 Hz, H_6); 8.07-8.00 (m, 2H, $H_{ph\ system}$); 7.95-7.87 (m, 1H, H_4); 7.82 (dt, 1H, *J* = 8.0, 0.8 Hz, H_3); 7.43-7.37 (m, 3H, H_5, H_{ph}); 4.16 (s, 1H, CH_2).

UV-Vis (CH_3OH) λ_{max} (ε_{max}/dm^3 mol^{-1} cm^{-1}) 227 (22 766), 334 (44 033), 350 (39 133), 447 (2 600) nm.

^{13}C NMR (100 MHz, $CDCl_3$, 25 °C, TMS): δ= 163.0 ($C_{2/7/10}$), 157.1 ($C_{2/7/10}$), 151.1 (C_6), 146.7 ($C_{2/7/10}$), 139.9 ($C_{8/9}$), 130.2(C_5), 125.3 ($C_{8/9}$), 119.6 (C_4), 117.5 (C_3), 43.3 (C_{13}).

2.10.5 Synthesis of $[Rh_2(L_{azo})(phen)_2Cl_4](PF_6)_2$

$[Rh(DMSO)(phen)Cl_3]$ (0.200 g, 0.43 mmol) and L_{azo} (0.032 g, 0.09 mmol) were suspended in a mixture of propanol:water (2:1) (70 ml) and heated under reflux for a period of 40 minutes. The starting orange solution becomes light brown and after 15 minutes of reflux the solution becomes green and is left refluxing for an extra 25 minutes. The reaction mixture was cooled down to room temperature and the complex precipitated as a PF_6 salt by addition of a concentrated aqueous solution of NH_4PF_6. The resulting dark green precipitate was washed with 1 ml of water to remove the excess of salt and dried with diethyl ether (2 ml). The complex was re-dissolved in a minimum amount of acetonitrile and precipitated with diethyl ether (0.100 g).

Positive-ion ESI (5 eV, CH_3CN,): *m/z* (%) 543 $[Rh_2(L_{azo})(phen)_2Cl_4]^{2+}$ (100), 1086 $[Rh_2(L_{azo})(phen)_2Cl_4]^{+}$ (10), 1231 $[Rh_2(L_{azo})(phen)_2Cl_4][PF_6]^{+}$ (10).

2.10.6 Separation of the Isomers by Preparative HPLC

Although a first isocratic method using silica HPLC column was achieved to separate the three isomers (as mentioned in the discussion), herein only details for the final method that enabled the separation and purification of these complexes as well as double stranded complexes is described. The final method utilises a reverse phase C_{18} preparative column and starts with a mixture of water (0.01% TFA): acetonitrile (0.01% TFA) (85:15) that runs for a period of 5 minutes, after which time the ratio of (0.01%

TFA) is increased to 30% over a period of 20 minutes, staying at (70:30) water (0.01% TFA):acetonitrile (0.01% TFA) for a period of 15 minutes and finally going back to the initial ratio of 85:15 and running for 5 minutes.

Retention time for ΔΔ,ΛΛ-$[Rh_2(L_{azo})(Phen)_2Cl_4](PF_6)_2$] **(1)**: 22.3 minutes.

Retention time for ΔΛ-$[Rh_2(L_{azo})(Phen)_2Cl_4](PF_6)_2$] **(2)**:: 23.5 minutes.

In both cases the solutions containing the complexes after collections were concentrated in vacuo to remove the excess of acetonitrile and the yellow/green product was re-precipitated from a concentrated methanolic solution of NH_4PF_6 (excess).

2.10.7 ΔΔ,ΛΛ-$[Rh_2(L_{azo})(phen)_2Cl_4](PF_6)_2$ (1)

Positive-ion ESI (5 eV; CH_3CN,): *m/z* (%) 543 $[Rh_2(L_{azo})(phen)_2Cl_4]^{2+}$ (100), 1086 $[Rh_2(L_{azo})(phen)_2Cl_4]^{+}$ (10), 1231 $[Rh_2(L_{azo})(phen)_2Cl_4][PF_6]^{+}$ (10).

Crystals suitable for X-ray diffraction measurements were obtained by slow diffusion of ether into a nitromethane solution of a pure sample of complex.

Elemental analysis calcd (%) for $[Rh_2(C_{23}H_{18}N_6)(C_{12}H_8N_2)_2Cl_4(PF_6)_2]$: C:41.0; H:2.5; N:10.2; found: C:40.8; H:2.2; N:10.1.

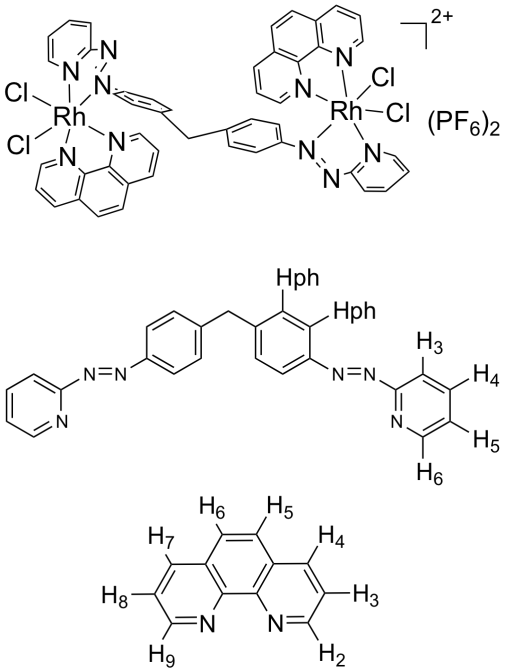

^{1}H NMR (400 MHz, CD_3CN, 25 °C, TMS) δ= 9.77 (d, 1H, *J* = 6.2 Hz, H_{6pyr}); 9.73 (d, 1H, *J* = 5.4 Hz, H_{2phen}); 9.05 (d, 1H, *J* = 7.9 Hz, H_{3pyr}); 8.84-8.76 (m, 2H, $H_{4pyr/7phen}$); 8.72 (dd, 1H, *J* = 8.3, 1.2 Hz, H_{4phen}); 8.37-8.29 (br, 1H, H_{5pyr}); 8.24-8.14 (m, 2H, $H_{5/6phen}$); 8.03-7.96 (m, 2H, $H_{9phen/3phen}$); 7.89 (m, 1H, H_{8phen}); 6.88 (d, 2H, *J* = 8.5 Hz, H_{ph}); 6.65 (d, 2H, *J* = 8.5 Hz, H_{ph}); 3.61 (s, 1H, CH_2);

UV-Vis (CH_3CN) λ_{max} (ε_{max}/$dm^3\,mol^{-1}\,cm^{-1}$): 274 (49 600), 399 (15 500) nm.

The corresponding chloride complex was obtained by anion metathesis, eluting the corresponding PF_6 solid through a Dowex® resin ion exchange column and eluting with ultrapure water. The resulting aqueous solution containing the complex, as a chloride salt was freeze dried overnight to give rise to a yellow/green dry solid. For all final complexes obtained as PF_6 salts, the exchange for the respective Cl salt was carried out in the same way.

ΔΔ,ΛΛ- $[Rh_2(L_{azo})(phen)_2Cl_4]Cl_2$

Positive-ion ESI (10 ev, H_2O): *m/z* (%) 538 $[Rh_2(L_{azo})(phen)_2Cl(MeOH)_3]^{2+}$ (100), 1076 $[Rh_2(L_{azo})(phen)_2Cl(MeOH)_3]^{+}$ (20).

UV-Vis (H_2O) λ_{max} (ε_{max}/dm^3 mol^{-1} cm^{-1}): 228 (50 033), 274 (38 100), 357 (11 266), 388 (12 033), 555 (2500) nm.

2.10.8 ΔΛ-$[Rh_2(L_{azo})(phen)_2Cl_4](PF_6)_2$ (2)

Positive-ion ESI (5 ev, CH_3CN): *m/z* (%) = 543 $[Rh_2(L_{azo})(phen)_2Cl_4]^{2+}$ (100), 1086 $[Rh_2(L_{azo})(phen)_2Cl_4]^{+}$ (10), 1231 $[Rh_2(L_{azo})pPhen)_2Cl_4][PF_6]^{+}$ (10).

Elemental analysis calcd (%) for $[Rh_2(C_{23}H_{18}N_6)(C_{12}H_8N_2)_2Cl_4(PF_6)_2]$: C:41.0; H:2.5; N:10.2; found: C:40.9; H:2.5; N:10.2.

^{1}H-NMR (400 MHz, CD_3CN, 25 °C, TMS): δ= 9.82-9.77 (m, 2H, H_{2phen}/$_{6pyr}$); 9.05 (d, 1H, *J* = 7.0Hz, H_{3pyr}); 8.79 (m, 3H, $H_{4pyr/7/4phen}$); 8.34-8.29 (br, 1H, H_{5pyr}); 8.21-8.10 (m, 3H, $H_{5/6phen}$ and H_{3phen}); 7.98 (m, 1H, H_{9phen}); 7.86 (m, 1H, H_{8phen}); 6.89 (d, 2H, *J* = 8.5 Hz, H_{ph}); 6.65 (d, 2H, *J* = 8.5Hz, H_{ph}); 3.60 (s, 1H, CH_2);

UV-Vis (CH_3CN) λ_{max} (ε_{max}/dm^3 mol^{-1} cm^{-1}): 274 (66 400), 399 (20 800) nm.

ΔΛ-$[Rh_2(L_{azo})(phen)_2Cl_4]Cl_2$

Positive-ion ESI (10 ev, H_2O): *m/z* (%) 538 $[Rh_2(L_{azo})(phen)_2Cl(MeOH)_3]^{2+}$ (100), 1076 $[Rh_2(L_{azo})(phen)_2Cl(MeOH)_3]^{+}$ (20).

UV-Vis (H_2O) λ_{max} (ε_{max}/$dm^3\ mol^{-1}cm^{-1}$): 227 (57 533), 275 (40 900.0), 357 (10 733), 392 (12 266), 556 (1566) nm.

2.10.9 Synthesis of $[Rh_2(L_{azo})(bpy)_2Cl_4](PF_6)_2$

$[Rh(DMSO)(bpy)Cl_3]$ (0.200 g, 0.45 mmol) and L_{azo} (0.034 g, 0.09 mmol) were suspended in a mixture of propanol:water (2:1) (70 ml) and refluxed for a period of 40 minutes. The starting orange solution becomes light brown and after 15 minutes of reflux the solution becomes green and is left refluxing for 25 minutes more. The reaction mixture was cooled down to room temperature and the complex precipitated as a PF_6 salt by addition of a concentrated aqueous solution of NH_4PF_6. The resulting dark green precipitate was washed with 1 ml of water to remove the excess of salt and dried with diethyl ether (2 ml). The complex was re-dissolved in a minimum amount of acetonitrile and precipitated with diethyl ether (0.090 g).

Positive-ion ESI (5 eV, CD_3CN): *m/z* (%) 518 $[Rh_2(L_{azo})(bpy)_2Cl_4]^{2+}$ (100), 1036 $[Rh_2(L_{azo})(bpy)_2Cl_4]^{+}$ (10).

2.10.10 Separation of the Isomers by Preparative HPLC

The isomers were separated using the same HPLC method as for the previous complexes. The final method utilises a reverse phase C_{18} preparative column and starts with a mixture of water (0.01% TFA): acetonitrile (0.01% TFA) (85:15) that runs for a period of 5 minutes, after which time the ratio of (0.01% TFA) is increased to 30% over a period of 20 minutes, staying at (70:30) water (0.01% TFA):acetonitrile (0.01% TFA) for a period of 15 minutes and finally going back to the initial ratio of 85:15 and running for 5 minutes.

Retention time for ΔΔ,ΛΛ-$[Rh_2(L_{azo})(bpy)_2Cl_4](PF_6)_2$ **(3)**: 21.7 minutes.

Retention time for ΔΛ-$[Rh_2(L_{azo})(bpy)_2Cl_4](PF_6)_2$ **(4)**:: 22.9 minutes.

2.10.11 ΔΔ,ΛΛ-$[Rh_2(L_{azo})(bpy)_2Cl_4](PF_6)_2$ (3)

Positive-ion ESI (5 eV, CH_3CN): *m/z* (%) = 518 $[Rh_2(L_{azo})(bpy)_2Cl_4]^{2+}$ (100), 1036 $[Rh_2(L_{azo})(bpy)_2Cl_4]^{+}$ (10).

Elemental analysis calcd (%) for: $[Rh_2(C_{23}H_{18}N_6)(C_{10}H_8N_2)_2Cl_4(PF_6)_2]$: C:38.9; H:2.6; N:10.5 found: C:39.0; H:2.8; N:10.3.

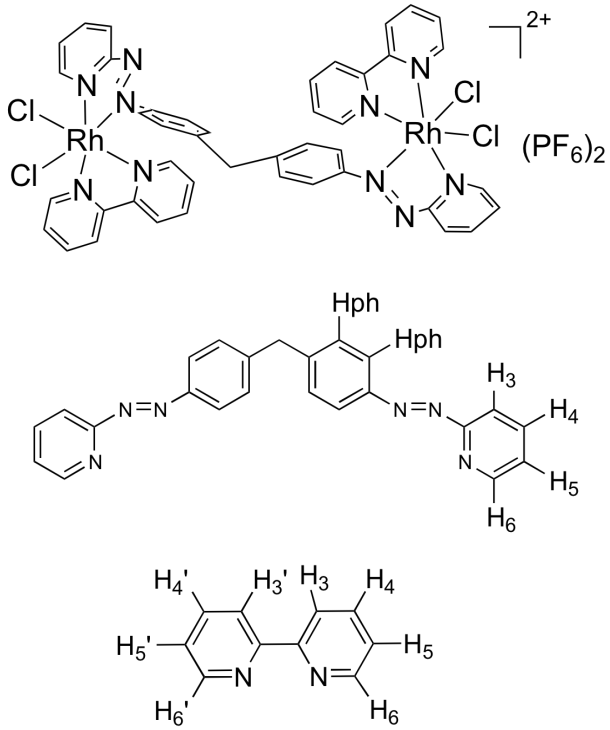

^{1}H NMR (400 MHz, CD_3CN, 25 °C, TMS) δ= 9.67 (d, 1H, *J* = 5.4 Hz, H_{6pyr}); 9.48 (d, 1H, *J* = 5.8 Hz H_{6bpy}); 8.99 (d, 1H, *J* = 7.5 Hz, H_{3pyr}); 8.75 (td, 1H, *J* = 8.0, 1.6 Hz H_{4pyr}); 8.41 (d, 1H, *J* = 7.4 Hz, H_{3bpy}); 8.31-819 (m, 4H, $H_{5pyr}/H_{4/4'/3bpy}$); 7.72 (m, 1H, H_{5bpy}); 7.67 (d, 1H, *J* = 5.8 Hz, $H_{6'bpy}$); 7.57 (m, 1H, H_{8bpy}); 7.03 (d, 2H, *J* = 8.5 Hz, H_{ph}); 6.96 (2H, d, *J* = 8.5 Hz, H_{ph}); 3.88 (s, 1H, CH_2);

UV-Vis (CH_3CN) λ_{max} (ε_{max}/dm^3 mol^{-1} cm^{-1}): 250 (42 320), 390 (13 520) nm. nm.

ΔΔ,ΛΛ-$[Rh_2(L_{azo})(bpy)_2Cl_4](Cl)_2$

Positive-ion ESI (10 eV, H_2O,): *m/z* (%) = 514 $[Rh_2(L_{azo})(bpy)_2Cl(CH_3OH)_3]^{2+}$ (100), 498 $[Rh_2(L_{azo})(bpy)_2Cl(CH_3OH)_2]^{2+}$ (40), 505 $[Rh_2(L_{azo})(bpy)_2(CH_3OH)_3(H_2O)]^{2+}$ (30) 512 $[Rh_2(L_{azo})(bpy)_2(CH_3OH)_4]^{2+}$ (5).

UV-VIS (H_2O) λ_{max} (ε_{max}/dm^3 mol^{-1} cm^{-1}): 248 (18 200), 311 (14 333), 386 (7 666), 590 (900) nm.

2.10.12 ΔΛ- $[Rh_2(L_{azo})(Bpy)_2Cl_4](PF_6)_2$ (4)

Positive-ion ESI (5 ev, CH_3CN): *m/z* (%) = 518 $[Rh_2(L_{azo})(bpy)_2Cl_4]^{2+}$ (100), 1036 $[Rh_2(L_{azo})(Bpy)_2Cl_4]^{+}$ (10).

Elemental analysis calculated (%) for $[Rh_2(C_{23}H_{18}N_6)(C_{10}H_8N_2)_2Cl_4(PF_6)_2]$: C:38.9; H:2.6; N:10.5 found: C:39.2; H:2.5; N:10.9.

UV-Vis (CH_3CN) λ_{max} (ε_{max}/dm^3 mol^{-1} cm^{-1}): 250 (50 312), 390 (18 230) nm. nm.

^1H NMR (400 MHz, CD_3CN, 25 °C, TMS) δ= 9.68 (d, 1H, *J* = 5.4 Hz, H_{6pyr}); 9.51 (d, 1H, *J* = 5.8 Hz H_{6bpy}); 8.89 (d, 1H, *J* = 7.5 Hz, H_{3pyr}); 8.75 (td, 1H, *J* = 7.9, 1.6 Hz H_{4pyr}); 8.39 (d, 1H, *J* = 7.4 Hz, H_{3bpy}); 8.33-8.23 (m, 4H, $H_{5pyr/}H_{4/4'/3bpy}$); 7.79 (m, 1H, H_{5bpy}); 7.66 (d, 1H, *J* = 5.8 Hz, $H_{6'bpy}$); 7.57 (m, 1H, $H_{5'bpy}$); 7.04 (d, 2H, *J* = 8.5 Hz, H_{ph}); 6.95 (d, 2H, *J* = 8.5 Hz, H_{ph}); 3.88 (s, 1H, CH_2);

ΔΛ- $[Rh_2(L_{azo})(bpy)_2Cl_4]Cl_2$

Positive-ion MS (10 eV, H_2O): *m/z* (%) = 514 $[Rh_2(L_{azo})(bpy)_2Cl(CH_3OH)_3]^{2+}$ (100), 498 $[Rh_2(L_{azo})(bpy)_2Cl(CH_3OH)_2]^{2+}$ (40), 505 $[Rh_2(L_{azo})(bpy)_2(CH_3OH)_3(H_2O)]^{2+}$ (30)
512 $[Rh_2(L_{azo})(bpy)_2(CH_3OH)_4]^{2+}$ (5).

UV-VIS (H_2O) λ_{max} (ε_{max}/dm^3 mol^{-1} cm^{-1}): 247 (15 666), 313 (12 300), 396 (8 000), 590 (566) nm.

2.10.13 Synthesis of Ligand (L_{azpy})[14]

The ligand was synthesized using a modified literature procedure[14] to avoid the use of benzene as solvent. 2- Nitrosopyridine (0.247 g, 2.29 mmol) and aniline (0.214 g, 2.30 mmol) were stirred for 24 hours in 4 ml of dichloromethane with 1 drop of glacial acetic acid. The red/orange solution was evaporated to dryness in vacuum. A red oil was obtained which after some days standing crystallized into red needle-shaped crystals (0.551 g, 78%).

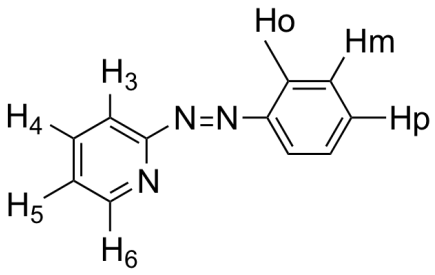

Positive-ion EI (30 eV, $CHCl_3$,): *m/z* (%) = 206 [L_{azpy} + Na^+] (100), 184 [L_{azpy} + H^+] (25).

^{1}H NMR (300 MHz, CD_3CN, 25 °C, TMS): δ = 8.72 (ddd, 1H, *J* = 4.8, 1.8, 1.0 Hz, H_6); 8.04-7.97 (m, 3H, H_o /H_4); 7.76 (dt, 1H, *J* = 8.1, 1.0 Hz, H_p); 7.65-7.60 (m, 3H, H_3/H_m); 7.52 (ddd, 1H, *J* = 7.4, 4.8, 1.0 Hz, H_5).

^{1}H NMR (300 MHz, CD_3OD, 25 °C, TMS): δ = 8.69 (ddd, 1H, *J* = 4.8, 1.8, 1.0 Hz, H_6); 8.09 (ddd, 1H, *J* = 8.1, 7.5, 1.8 Hz, H_4); 8.05-7.98 (m, 2H, H_o); 7.91-7.87 (m, 1H, H_p); 7.89 (d, 1H, *J* = 8.1Hz, H_3), 7.64-7.54 (m, 4H, H_p/H_m/H_5)

UV-Vis (CH_3OH) λ_{max} (ε_{max}/dm^3 mol^{-1} cm^{-1}): 223 (11 000), 319 (17 566), 350 (8066) nm.

^{13}C NMR (100 MHz, CD_3CN, 25 °C, TMS): δ = 149.5 (C_6), 138.6 (C_4/C_o), 132.3 (C_3), 129.5 (C_m), 128.7 (C_5), 125.5 (C_{py}),123.1 (C_4/C_o), 120.3 (C_{ph}), 113.4 (C_p).

2.10.14 Synthesis of *cis*-[Rh(L_{azpy})(phen)Cl_2](PF_6) (5)

[Rh(DMSO)(phen)Cl_3] (0.071 g, 1.52 mmol) and L_{azpy} (0.028 g, 1.52 mmol) were suspended in a mixture of propanol:water (2:1) (25 ml) and heated under reflux for a period of 90 minutes. The solution rapidly changed from orange/red to very strong bright green upon refluxing. The reaction mixture was cooled to room temperature and the complex precipitated as a PF_6 salt by addition of a concentrated aqueous solution of NH_4PF_6. The resulting light green precipitate was washed with 1 ml of water to remove the excess of salt and dried with diethyl ether (2 ml). The complex was re-dissolved in a minimum amount of acetonitrile and precipitated with diethyl ether to afford a dry light green solid (0.105 g, 49%). The complex was used as obtained without requirement of further purification.

Crystals suitable for X-ray diffraction measurements were obtained by slow diffusion of ether into an acetonitrile solution of pure sample of complex.

Positive-ion ESI (30 eV, CH_3CN): *m/z* (%) = 536 [Rh(L_{azpy})(phen)Cl_2]$^+$ (100);

Elemental analysis calcd (%) for $[Rh(C_{11}H_9N_3)(C_{12}H_8N_2)Cl_2(PF_6)]$: C:40.5, H:10.3, N:2.5, found C:40.5; H:10.1, N:2.4;

UV-Vis (CH_3CN) λ_{max} (ε_{max}/ $dm^3\ mol^{-1}\ cm^{-1}$): 227 (45 230), 274 (33 133), 357 (10 400), 375 (9 985) nm;

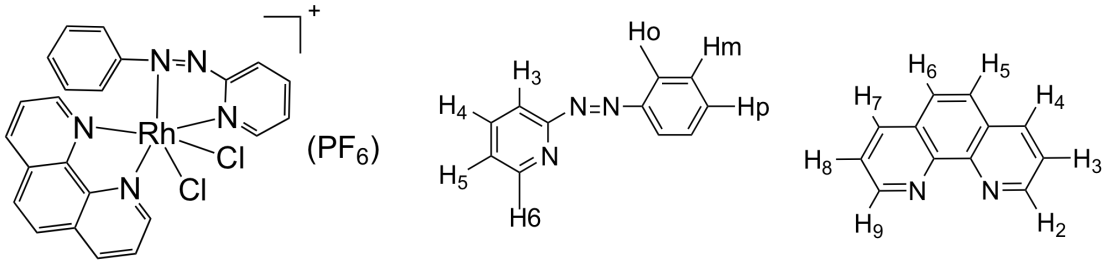

^1H NMR (500 MHz, CD_3CN, -20 °C, TMS): δ= 9.75 (m, 2H, H_{2phen}/H_{6pyr}); 9.04 (d, 1H, *J* = 7.9 Hz, H_{3pyr}); 8.87 (d, 1H, *J* = 8.3 Hz, H_{4phen}); 8.79 (m, 2H, H_{7phen}/ H_{4pyr}); 8.33 (t, 1H, *J* = 6.3 Hz, H_{5pyr}); 8.23 (AB $_{system}$, 2H, $H_{5/6phen}$); 8.15 (dd, 1H, *J* = 8.3, 5.4 Hz, H_{3phen}); 7.99 (d, 1H, *J* = 5.4 Hz, H_{9phen}); 7.84 (dd, 1H, *J* = 8.3, 5.4 Hz, H_{8phen}); 7.33 (t, 1H, *J* = 7.4 Hz, H_p); 7.07 (t, 2H, *J* = 7.9 Hz, H_m); 6.97 (d, 2H, *J* = 7.9 Hz, H_o);

^{13}C NMR (100 MHz, CD_3CN, 25°C, TMS): δ = 152.7 (C_{2phen}/C_{6pyr}), 152.1 (C_{9phen}), 140.6 (C_{4phen}) , 140.4 ($C_{4pyr}/C_{4phen}/C_{7phen}$),127.0 ($C_{8phen}$);

cis-$[Rh(L_{azpy})(phen)Cl_2]Cl$

Positive-ion ESI (10 eV, H_2O): *m/z* (%) 532 $[Rh(L_{azpy})(phen)Cl_2(MeOH-H)]^+$ (100), 536 $[Rh(L_{azpy})(Phen)Cl_2]^+$ (70).

UV-Vis (H_2O) λ_{max} (ε_{max}/$dm^3\ mol^{-1}\ cm^{-1}$): 227 (33 200), 257 (7 366), 274 (25 266), 357 (10 400), 375 (7 633) nm.

2.10.15 Synthesis of *cis*-[Rh(L_{azpy})(bpy)Cl_2](PF_6) (6)

[Rh(DMSO)(bpy)Cl_3] (0.105 g, 0.24 mmol) and L_{azpy} (0.044 g, 0.24 mmol) were suspended in a mixture of propanol:water (2:1) (40 ml) and heated under reflux for a period of 90 minutes. The solution rapidly changed from orange/red to very strong bright green upon refluxing. The solution was kept under reflux for a period of 90 minutes. The reaction mixture was cooled down to room temperature and the complex precipitated as a PF_6 salt by addition of a concentrated aqueous solution of NH_4PF_6. The resulting light green precipitate was washed with 1 ml of water to remove the excess of salt and dried with diethyl ether (2 ml). The complex was re-dissolved in a minimum amount of acetonitrile and precipitated with diethyl ether to afford a dry light green pure solid (0.106 g, 44%). The complex was used as obtained without requirement of further purification.

Crystals suitable for X-ray diffraction measurements were obtained by slow diffusion of ether into an acetonitrile solution of the complex.

Positive-ion ESI (30 eV, CH_3CN): *m/z* (%) 512 [Rh(L_{azpy})(bpy)Cl_2]$^+$ (100);

Elemental analysis calcd (%) for [Rh($C_{11}H_9N_3$)($C_{10}H_8N_2$)Cl_2(PF_6)]: C:38.3, H: 2.6, N: 10.6 found: C: 38.5, H: 2.4, N:10.5.

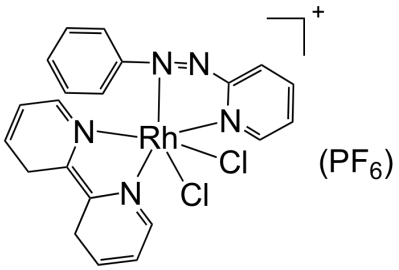

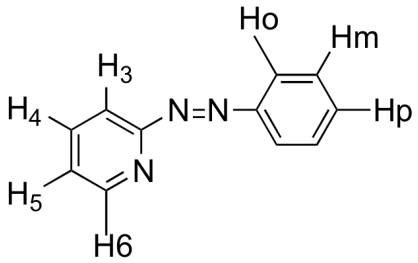

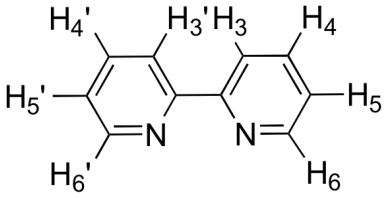

^{1}H NMR (400 MHz, CD_3CN, 25 °C, TMS): δ= 9.68 (d, 1H, *J* = 5.0 Hz, H_{6pyr}); 9.55 (d, 1H, *J* = 5.8, H_{6bpy}), 9.00 (d, 1H, *J* = 8.0 Hz, H_{3pyr}); 8.75 (td, 1H, *J* = 8.0, 1.5 Hz, H_{4pyr}); 8.41-8.27 (m, 5H, $H_{4'/4bpy/}H_{3bpy/3'bpy}H_{5pyr}$); 7.83 (m, 1H, H_{5bpy}); 7.65 (d, 1H, *J* = 5.8 Hz, $H_{6'bpy}$); 7.56 (m 1H, $H_{5'bpy}$); 7.50 (brt, 1H, *J* = 7.4 Hz, H_p); 7.27 (brt, 2H, *J* = 7.9 Hz, H_m); 7.10 (d, 2H, *J* = 7.9 Hz, H_o);

UV-VIS (CH_3CN) λ_{max} (ε_{max}/dm^3 mol^{-1} cm^{-1}): 227 (27 033), 312 (12 833), 361(7900), 565 (833) nm.

^{13}C NMR (100 MHz, CD_3CN, 25 °C, TMS): δ = 152.7 (C_{2phen}/C_{6pyr}), 152.1 (C_{9phen}), 140.6 (C_{4phen}) , 140.4 (C_{4pyr}/C_{4phen}/C_{7phen}),127.0 (C_{8phen});

cis-[Rh(L_{azpy})(bpy)Cl_2]Cl

Positive-ion ESI (10 eV, H_2O,): *m/z* (%) 512 $[Rh(L_{azpy})(bpy)Cl_2)]^+$ (100), 508 $[Rh(L_{azpy})(bpy)Cl$ (MeOH-2H)$]^+$ (50).

^1H NMR (400 MHz, CD_3OD, 25 °C, TMS): δ= 9.70 (d, 1H, *J* = 5.0 Hz, H_{6pyr}); 9.61 (d, 1H, *J* = 5.8, H_{6bpy}), 9.09 (d, 1H, *J* = 7.6 Hz, H_{3pyr}); 8.78 (td, 1H, *J* = 8.0, 1.5 Hz, H_{4pyr}); 8.53 (m, 2H, $H_{3bpy/3'bpy}$); 8.29 (m, 3H, $H_{5pyr/}H_{4/4'bpy}$); 7.88 (m, 1H, H_{5bpy}); 7.75 (d, 1H, *J* = 5.8 Hz, $H_{6'bpy}$); 7.60 (m, 1H, $H_{5'bpy}$), 7.45 (brt, 1H, *J* = 7.5 Hz, H_p); 7.24 (brt, 2H, *J* = 7.9 Hz, H_m); 7.13 (d, 2H, *J* = 7.9 Hz, H_o);

UV-VIS (H_2O) λ_{max} (ε_{max}/dm^3 mol^{-1} cm^{-1}): 235 (19 666), 313 (13 566), 375 (8 266), 590 (566) nm.

2.10.16 Synthesis of $[Rh_2(L_{azo})_2Cl_4](PF_6)_2$

$RhCl_3.3H_2O$ (0.139 g, 0.53 mmol) and ligand (0.200 g, 0.53 mmol) were heated under reflux in a mixture of propanol:water (2:1) (100 ml) for 20 minutes. The final dark yellow/green solution was filtered hot to remove the black insoluble polymer. The filtrate was then cooled to room temperature and poured into a concentrated aqueous solution of NH_4PF_6 (20 ml, 0.064 g, 0.39 mmol) and stirring for 10 minutes to allow complete precipitation of the solid. The precipitate was then filtered, and washed with 5 ml of water to remove excess of salt and re-dissolved into a minimum amount of acetonitrile and flashed precipitated with diethyl ether to give a dry green/yellow solid (0.225 g).

Positive-ion MS (5 eV, CH_3CN): *m/z* (%) = 552 $[Rh_2(L_{azo})_2Cl_4]^{2+}$ (100), 1104 $[Rh_2(L_{azo})_2Cl_4]$ (15).

Elemental analysis calcd (%) for $[Rh_2(C_{23}H_{18}N_6)_2Cl_4(PF_6)_2]$ C: 39.6, H: 2.6, N: 12.1; found C: 39.5, H: 2.6, N: 12.1.

2.10.17 Separation of the Isomers by Preparative HPLC

The isomers were separated using the same HPLC method as for the previous complexes. The final method utilises a reverse phase C_{18} preparative column and starts with a mixture of water (0.01% TFA): acetonitrile (0.01% TFA) (85:15) that runs for a period of 5 minutes, after which time the ratio of (0.01% TFA) is increased to 30% over a period of 20 minutes, staying at (70:30) water (0.01% TFA):acetonitrile (0.01% TFA) for a period of 15 minutes and finally going back to the initial ratio of 85:15 and running for 5 minutes.

Retention time for $[Rh_2(L_{azo})_2Cl_4](PF_6)_2$ **(7)**: 27.3 minutes.
Retention time for $[Rh_2(L_{azo})(_2Cl_4](PF_6)_2$ **(8)**:: 28.4 minutes.

$[Rh_2(L_{azo})_2Cl_4](PF_6)_2$ (7)

Positive-ion ESI (5 eV, CH_3CN): *m/z* (%) = 552 $[Rh_2(L_{azo})_2Cl_4]^{2+}$ (100), 1104 $[Rh_2(L_{azo})_2Cl_4]$ (15), 1249 $[Rh_2(L_{azo})_2Cl_4](PF_6)^+$ (10)

Elemental analysis calcd (%) for $[Rh_2(C_{23}H_{18}N_6)_2Cl_4(PF_6)_2].2H_2O$ C: 38.6, H: 2.8 N: 11.7; Found C:38.1, H:2.3, N:11.4

^1H NMR (400 MHz, CD_3CN, 25 °C, TMS): δ= 9.53 (d, 1H, *J* = 5.5 Hz, H_6), 8.99 (t, 2H, *J* = 8.1 Hz, $H_{3/3'}$), 8.76 (td, 1H, *J* = 8.6, 7.1Hz, H_4), 8.59 (td, 1H, *J* = 7.8, 6.3 Hz, $H_{4'}$), 8.28-8.24 (m, 1H, H_5), 7.90 (d, 1H, *J* = 5.5 Hz, $H_{6'}$), 7.86-7.80 (m, 1H, $H_{5'}$), 7.74 (d, 2H, *J* = 8.6 Hz, H_{ph}), 7.36 (dd, 4H, *J* = 8.6, 2.8 Hz, $H_{ph/ph'}$), 7.21 (d, 2H, *J* = 8.6 Hz, $H_{ph'}$), 4.21(s, 2H, CH_2).

UV-VIS (CH_3CN) λ_{max} (ε_{max}/dm^3 mol^{-1} cm^{-1}): 408 (58 750) nm.

$[Rh_2(L_{azo})_2Cl_4]Cl_2$ (7)

Positive-ion ESI (10 eV, H_2O): *m/z* (%) = 515 $[Rh_2(L_{azo})_2MeOH(H_2O)_2]^{2+}$ (100), 506 $[Rh_2(L_{azo})_2MeOH(H_2O)]^{2+}$ (60), 497 $[Rh_2(L_{azo})_2MeOH]^{2+}$ (25).

UV-VIS (H_2O) λ_{max} (ε_{max}/dm^3 mol^{-1} cm^{-1}): 392 (16 166) nm.

$[Rh_2(L_{azo})_2Cl_4](PF_6)_2$ (8)

Positive-ion ESI (5 eV, CH_3CN): *m/z* (%) = 552 $[Rh_2(L_{azo})_2Cl_4]^{2+}$ (100), 1104 $[Rh_2(L_{azo})_2Cl_4]$ (10), 1249 $[Rh_2(L_{azo})_2Cl_4](PF_6)^+$ (10)

Elemental analysis calcd (%) for $[Rh_2(C_{23}H_{18}N_6)_2Cl_4(PF_6)_2]$ C: 38.6, H: 2.8, N: 11.7; Found C:38.4, H:2.5, N:11.7.

^1H NMR (400 MHz, CD_3CN, 25 °C, TMS): δ= 9.53 (d, 1H, *J* = 5.5 Hz, H_6), 9.01-8.93 (m, 2H, $H_{3/3'}$), 8.76 (td, 1H, *J* = 7.8, 1.6 Hz, H_4), 8.59 (td, 1H, *J* = 7.8, 1.6 Hz, $H_{4'}$), 8.31-8.21 (m, 1H, H_5), 7.88 (d, 1H, *J* = 5.3 Hz, $H_{6'}$), 7.86-7.82 (m, 1H, $H_{5'}$), 7.74 (d, 2H, *J* = 8.6 Hz, H_{ph}), 7.41 (d, 2H, *J* = 8.6 Hz, H_{ph}), 7.33 (d, 2H, *J* = 8.6 Hz, $H_{ph/ph'}$), 7.18 (d, 2H, *J* = 8.6 Hz, $H_{ph'}$), 4.23 (s, 2H, CH_2).

UV-VIS (CH_3CN) λ_{max} (ε_{max}/dm^3 mol^{-1} cm^{-1}): 405 (60 606) nm.

$[Rh_2(L_{azo})_2Cl_4]Cl_2$ (8)

Positive-ion ESI (10 eV, H_2O): *m/z* (%) = 515 $[Rh_2(L_{azo})_2MeOH(H_2O)_2]^{2+}$ (100), 506 $[Rh_2(L_{azo})_2MeOH(H_2O)]^{2+}$ (60), 497 $[Rh_2(L_{azo})_2MeOH]^{2+}$ (25).

UV-VIS (H_2O) λ_{max} (ε_{max}/dm^3 mol^{-1} cm^{-1}): 390 (25 666.7) nm.

2.10.17 Synthesis of $[Rh(L_{azpy})_2Cl_2](PF_6)$ (9)

$RhCl_3.3H_2O$ (0.100 g, 0.38 mmol) and ligand (0.139 g, 0.76 mmol) were refluxed in a mixture of propanol:water (2:1) (60 ml) for 3 hours. The final dark green solution was filtered hot to remove the black insoluble polymer. The filtrate was then cooled down to room temperature and poured into a concentrated aqueous solution of NH_4PF_6 (20 ml, 0.064 g, 0.39 mmol) and left stirring for 10 minutes to allow complete precipitation of the solid. The precipitate was then filtered, washed with 5 ml of water to remove excess of salt, re-dissolved into a minimum amount of acetonitrile and precipitated with diethyl ether to give a dry green/yellow solid (0.200 g, 30%)

Elemental analysis calcd (%) for $[Rh(C_{11}H_9N_3)_2Cl_2(PF_6)]$ C: 38.6, H: 2.6, N: 12.3; found C: 38.7, H: 2.7, N: 12.3.

UV-VIS (CH_3CN) λ_{max} (ε_{max}/dm^3 mol^{-1} cm^{-1}): 363 (24 470) nm.

Positive-ion ESI (30 eV, CH_3CN): *m/z* (%) = 539 $[Rh(L_{azpy})_2Cl_2]^+$ (100).

^1H NMR (400 MHz, CD_3CN, 25 °C, TMS): δ= 9.52 (d, 1H, *J* = 5.5 Hz, H_{6pyr}), 8.78 (d, 1H, 7.6 Hz, H_{3pyr}), 8.61 (td, 1H, *J* = 7.8, 1.5 Hz, H_{4pyr}), 8.12-8.10 (br, 1H, H_5), 7.60 (t, 1H, *J* = 8.0 Hz, H_p), 7.42 (t, *J* = 8.0 Hz, 2H, H_m), 7.28 (d, 2H, *J* = 7.6 Hz, H_o).

2.10.18 Synthesis of $[Rh_2(L_{azo})_3](NO_3)_6$ (10)

$Rh(NO_3)_3.xH_2O$ (0.010 g, 0.035 mmol) and L_{azo} (0.013 g, 0.035 mmol) were heated under reflux under argon in a mixture of propanol:water (2:1) (60 ml) for 20 minutes. The mixture of solvents was previously degassed for 30 minutes in a schlenk under stirring. The strong dark orange solution was cooled to room temperature filtered to remove the insoluble polymeric material and evaporated to dryness. The nitrate salt complex was taken into a minimum amount of methanol and precipitated with diethyl ether to afford a dark orange/brown compound (0.055 g, 16%).

Elemental analysis calculated (%) for $[Rh_2(L_{azo})_3](NO_3)_6.N_4O_{16}$ C: 40.9, H: 2.7, N: 19.4; Found C:38.0, H:2.7, N:19.3.

Positive-ion ESI (5 eV, CH_3CN): *m/z* (%)= 670 $[Rh_2(L_{azo})_3]^{2+}$ (100), 1340 $[Rh_2(L_{azo})_3]^{+}$ (15), 1402 $[Rh_2(L_{azo})_3](NO_3)$ (2).

^1H NMR (400 MHz, MeOD, 25 °C, TMS): δ = 8.84 (dd, 1H, *J* = 5.3, 1.1 Hz, H_{6pyr}), 8.43 (td, 1H, *J*= 8.0, 1.6 Hz, H_{4pyr}), 8.25 (d, 1H, *J* = 8.0 Hz, H_{3pyr}), 8.09 (d, 2H, *J* = 8.4 Hz, H_{ph}), 7.94 (ddd, 1H, *J*= 7.5, 5.4, 1.0 Hz, H_{5pyr}), 7.58 (d, 2H, *J* = 8.4 Hz, H_{ph}), 4.29 (s, 1H, CH_2).

UV-VIS (MeOH) λ_{max} (ε_{max}/dm^3 mol^{-1} cm^{-1}): 387 (37 766), 420 (34 833), 530 (12 633).

UV-VIS (H_2O) λ_{max}/nm, (ε_{max}/dm^3 mol^{-1} cm^{-1}): 385 (33 333), 413 (33 266), 510 (12 800) nm.

2.10.19 Synthesis of $[Rh(L_{azpy})_3](NO_3)_3$ (11)

$Rh(NO_3)_3.xH_2O$ (0.010 g, 0.035 mmol) and L_{azpy} (0.019 g, 0.105 mmol) were heated under reflux under argon in a mixture of propanol:water (2:1) (60 ml) for 20 minutes. The mixture of solvents was previously degassed for 30 minutes in a schlenk under stirring. The strong dark orange solution was cooled down to room temperature and evaporated to dryness. The nitrate salt complex was taken into a minimum amount of methanol and precipitated with diethyl ether to afford a dark orange/brown compound (0.050 g, 58%).

Positive-ion ESI (5 eV, MeOH): *m/z* (%) = 531 $[Rh(L_{azpy})_2]^+(NO_3)$ (100), 469 $[Rh(L_{azpy})_2]^+$ (40)

UV-VIS (H_2O) λ_{max} (ε_{max}/dm^3 mol^{-1} cm^{-1}): 332 (27 766), 408 ^{sh} (15 033), 520 (2 933) nm.

^1H NMR (400 MHz, MeOD, 25 °C, TMS): δ = 8.85 (d, 1H, *J* = 4.3 Hz, H_{6pyr}), 8.49 (td, 1H, *J* = 8.0, 1.4 Hz H_{4pyr}), 8.22 (d, 1H, *J* = 8.0 Hz, H_{3pyr}), 8.11 (d, 2H, *J* = 7.0 Hz, H_o), 7.91 (dd, 1H, *J* = 7.0, 5.5 Hz, H_{5pyr}), 7.68 (m, 3H, $H_{p/m}$).

2.11 References

[1] B. M. Zeglis, V. C. Pierre, J. K. Barton, *Chem. Commun.* **2007**, 4565.

[2] F. P. Pruchnik, P. Jakimowicz, Z. Ciunik, J. Zakrzewska-Czerwinska, A. Opolski, J. Wietrzyk, E. Wojdat, *Inorg. Chim. Acta* **2002**, *334*, 59.

[3] M. A. Scharwitz, I. Ott, Y. Geldmacher, R. Gust, W. S. Sheldrick, *J. Organomet. Chem.* **2008**, *693*, 2299.

[4] M. J. Hannon, C. L. Painting, A. Jackson, J. Hamblin, W. Errington, *Chem. Commun.* **1997**, 1807.

[5] G. I. Pascu, A. C. G. Hotze, C. Sanchez-Cano, B. M. Kariuki, M. J. Hannon, *Angew. Chem., Int. Ed.* **2007**, *46*, 4374.

[6] U. Schatzschneider, J. K. Barton, *J. Am. Chem. Soc.* **2004**, *126*, 8630.

[7] M. Harlos, I. Ott, R. Gust, H. Alborzinia, S. Wolfl, A. Kromm, W. S. Sheldrick, *J. Med. Chem.* **2008**, *51*, 3924.

[8] A. C. G. Hotze, B. M. Kariuki, M. J. Hannon, *Angew. Chem., Int. Ed.* **2006**, *45*, 4839.

[9] E. C. Taylor, *J. Org. Chem.* **1982**, *47*, 552.

[10] C. Das, A. K. Ghosh, C. H. Hung, G. H. Lee, S. M. Peng, S. Goswami, *Inorg. Chem.* **2002**, *41*, 7125.

[11] A. K. Ghosh, P. Majumdar, L. R. Falvello, G. Mostafa, S. Goswami, *Organometallics* **1999**, *18*, 5086.

[12] S. Swavey, K. J. Brewer, *Inorg. Chem.* **2002**, *41*, 6196.

[13] K. Kalyanasundaram, M. Gratzel, M. K. Nazeeruddin, *J. Phys. Chem.* **1992**, *96*, 5865.

[14] R. A. Krause, K. Krause, *Inorg. Chem.* **1980**, *19*, 2600.

[15] U. McDonnell, J. M. C. A. Kerchoffs, R. P. M. Castineiras, M. R. Hicks, A. C. G. Hotze, M. J. Hannon, A. Rodger, *Dalton Trans.* **2008**, 667.

[16] E. C. Constable, M. J. Hannon, *Inorg. Chim. Acta* **1993**, *211*, 101.

[17] J. Lacour, C. Ginglinger, F. Favarger, S. TorcheHaldimann, *Chem. Commun.* **1997**, 2285.

[18] J. G. Planas, D. Prim, E. Rose, F. Rose-Munch, D. Monchaud, J. Lacour, *Organometallics* **2001**, *20*, 4107.

[19] J. J. Jodry, J. Lacour, *Chem. Eur. J.* **2000**, *6*, 4297.

[20] M. J. Hannon, V. Moreno, M. J. Prieto, E. Moldrheim, E. Sletten, I. Meistermann, C. J. Isaac, K. J. Sanders, A. Rodger, *Angew. Chem., Int. Ed.* **2001**, *40*, 880.

[21] T. Yutaka, M. Kurihara, K. Kubo, H. Nishihara, *Inorg. Chem.* **2000**, *39*, 3438.

[22] D. F. Zigler, J. Wang, K. J. Brewer, *Inorg. Chem.* **2008**, *47*, 11342.

[23] E. L. Menon, R. Perera, M. Navarro, R. J. Kuhn, H. Morrison, *Inorg. Chem.* **2004**, *43*, 5373.

[24] A. C. G. Hotze, E. P. L. van der Geer, H. Kooijman, A. L. Spek, J. G. Haasnoot, J. Reedijk, *Eur. J. Inorg. Chem.* **2005**, 2648.

[25] H. Caldararu, K. Dearmond, K. Hanck, *Inorg. Chem.* **1978**, *17*, 2030.

[26] L. J. Childs, *Supramolecular assemblies based on imine and azo chemistry, PhD Thesis*, University of Warwick, Coventry, **2002**.

Chapter 3

DNA Binding Studies

3.1 Introduction

This chapter aims to explore the DNA binding properties of the complexes synthesized in chapter 2, using different spectroscopic techniques and gel electrophoresis. For these studies it was important that each complex had good solubility in water and this was achieved for all the complexes obtained as PF_6 salts (**1**, **2**, **3**, **4**, **5**, **6**, **7** and **8**) by ion exchange to the respective chloride salt using Dowex ion exchange columns. In case of complex **10** the final nitrate salt already exhibited high water solubility and it was used as obtained. The complexes exhibited good stability in water at room temperature. UV-Vis spectra were recorded each 30 minutes during a period of 12 hours and no significant differences were observed. The MS of the chloride salt in water for each complex **1** to **8** was carried out, however it was not possible to obtain ^{1}H-NMR spectra for the chloride salt of the single and double stranded complexes, once when the complexes were dissolved in D_2O they formed a gel (example can be seen from picture in Figure 3.1), which didn't allow the molecule to tumble on the NMR timescale, giving rise to a very broad unique band or to a completely flat line spectrum. Gelating by a supramolecular helicate like complex that does not bear surface functional groups is as far as we know unprecedented. This may be related to the presence of the coordinated chloride ligands in each di-nuclear complex. Although this happens in aqueous conditions for NMR this does not affect the solutions of the

complexes used for DNA binding studies since the concentration needed for ^{1}H-NMR spectra is at least four times higher than the one used for DNA binding studies (CD and LD).

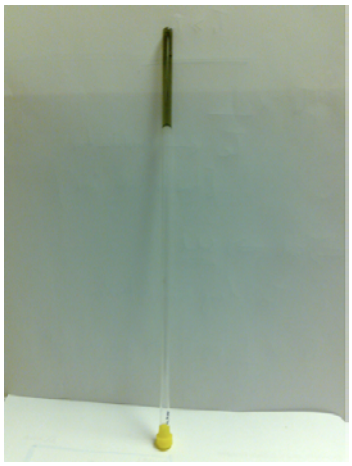

Figure 3.1- NMR tube containing complex **1** in D_2O, upside down exemplifying the formation of the "solid gel" formed between the complex and D_2O.

For the mononuclear complex **6**, the chloride salt could be analyzed by ^{1}H-NMR spectroscopy although the peaks were broader than in the ^{1}H-NMR spectra of the PF_6 salt in CD_3CN. This can be explained by the fact that when **6** is added to D_2O, although there was still the formation of a dense solution, it is not as dense compared with the di-nuclear complexes.

3.2 Circular Dichroism (CD)

Circular Dichroism (CD) is a widely used spectroscopic technique which allows a rapid characterization of nucleic acids and their complexes with bound proteins or drug molecules at relatively low sample concentration (micromolar scale). [1, 2]

CD is based on the use of circular polarized light and how it interacts with matter. The electric field vector rotates around the propagation direction forming a helix in the space during the propagation process (Figure 3.2). When the helix is left or right handed oriented the circular polarized light is referred to as left or right handed light. Chiral molecules, whose mirror images are not superimposable, absorb the left and right handed circularly polarized light differently.

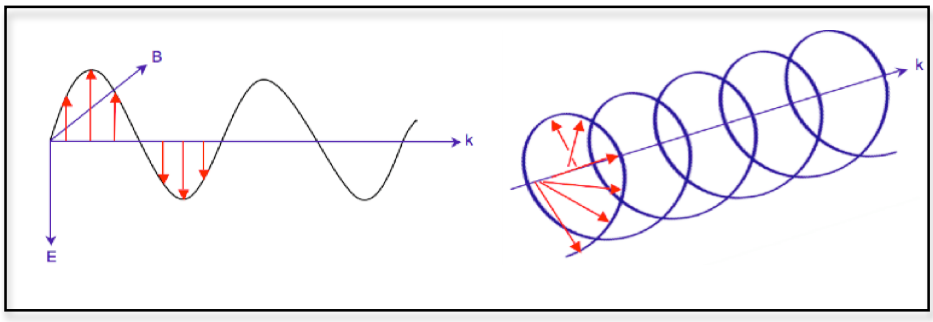

Figure 3.2 Representation of a linearly (left) and circularly polarized light (right) of electromagnetic radiation. The k vector indicates the direction of propagation and the arrows indicate the direction of the electric field vector (E).[1]

The difference in the absorbance (A) between the left (A_l) and the right (A_r) circularly polarized light is measured as a wavelength function and gives rise to a CD signal according to the equation below.

$$CD = A_l - A_r$$

In the case of DNA, CD spectroscopy is very useful to give information regarding its structural conformation. The chirality of the DNA molecule is due to the chiral centres of the carbons of the ribose in the phosphate backbone, which per se do not produce any detectable transitions and therefore have no CD signal. However, the nucleotides of DNA have CD signals, which are induced by the adjacent chiral deoxyribose. The CD signal of DNA is due to the transitions associated with the bases in the UV region of the spectrum, but at the same time it depends on the orientation and distance of the bases, which makes it possible to detect different DNA conformations. DNA can exist in three double helical forms, B-, A- or Z-DNA (as Discussed in Chapter 1) and indeed each of them has a different characteristic CD signal in the UV region. The CD spectrum of the B-DNA extracted from calf-Thymus (ct) is shown in Figure 3.3.

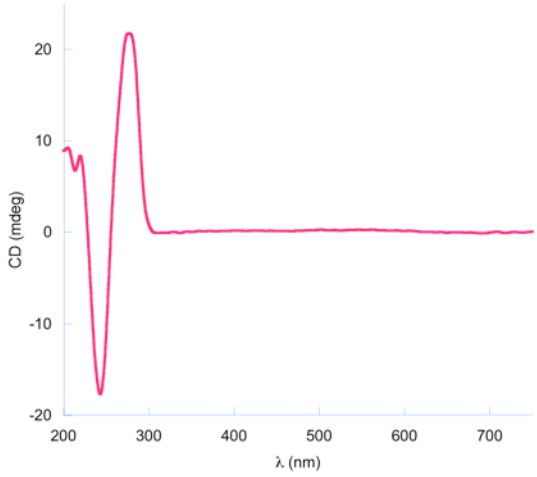

Figure 3.3 CD Signal of 300 μM ct-DNA (base pairs-bp).

The CD spectrum of ct-DNA is characterized by having a positive band centred at 280 nm followed by a negative band at 245 nm and an intersection point at the UV absorption maximum (260 nm). Over 300 nm the DNA does not have any CD signal.

Nonchiral drug molecules (molecules that lack handedness and thereby optical activity) have no CD signal. However, when bound to DNA, nonchiral molecules often give rise to a CD spectrum due to an induced CD signal (ICD) resulting from the chiral environment around the molecule.[1, 2] This effect allows the DNA-synthetic agent interactions to be probed and in addition the binding mode (s) by which the drug molecule targets the DNA.

3.3 UV-Visible ct-DNA Titrations with Rh(III) Complexes

UV-Vis ct-DNA (300 μM) titrations were carried out using complexes **1** to **6** (Figure 3.4). Spectra show no significant changes in the region between 300-500 nm upon addition to ct-DNA. The absorbance variation is linear (shown on respective plots of Abs *vs*. concentration of complex) with the increase of concentration of complex suggesting that the structure of each complex remains unchanged on the interaction with ct-DNA. The absorbance relating to the ligands of the complexes is clearly visible at 260 nm, changing the shape of the DNA spectrum in this region, with an increase in the band intensity while the titration experiment progresses.

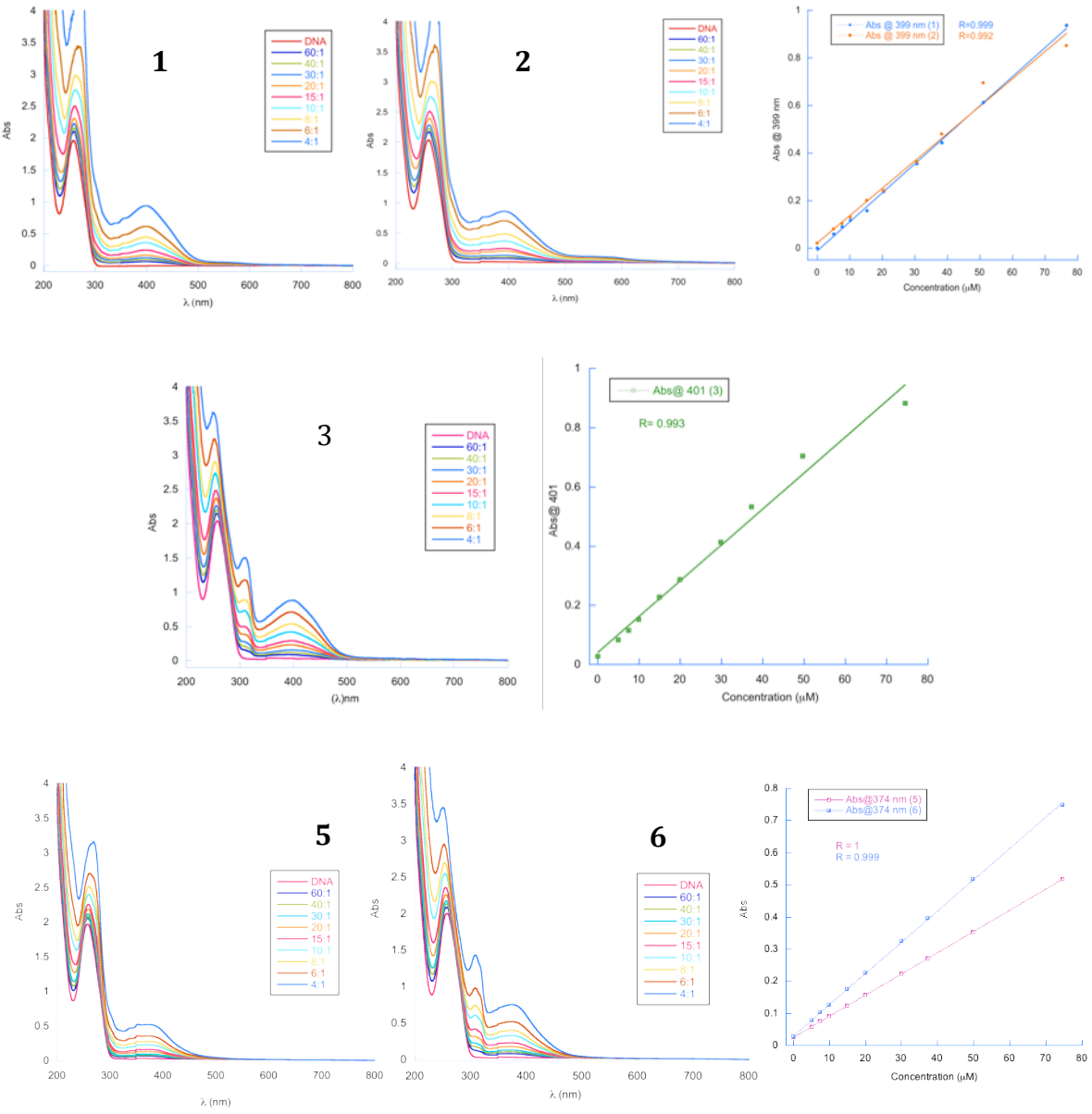

Figure 3.4 UV-Vis of 300 μM ct-DNA in 20 mM NaCl and 1 mM $Na(CH_3)_2AsO_2.3H_2O$ (pH 6.8) with increasing concentration of complexes **1** to **6** and respective plots of Abs *vs.* Concentration of complex. The legends show ct-DNA:complex ratios.

The same experiments were carried out for the Rh(III) di-nuclear double stranded complexes (**7** and **8**) using ct-DNA (300 μM). Once more no changes in the structure of the complexes are detectable by UV-Vis spectroscopy while the titration experiment

progresses, with the absorbance variation being linear with the increase of the amount of the complex (Figure 3.5).

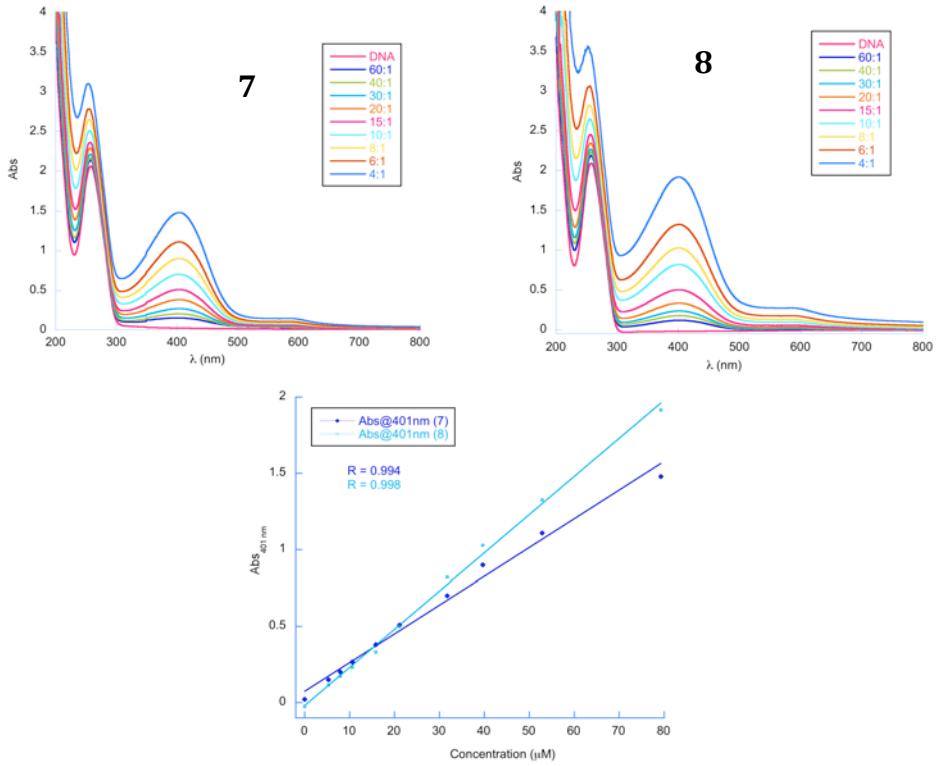

Figure 3.5 UV-Vis of 300 μM ct-DNA in 20 mM NaCl and 1 mM $Na(CH_3)_2AsO_2.3H_2O$ (pH 6.8) with increasing concentration of complexes **7** and **8** (top) and respective plots of Abs *vs.* Concentration of complex (bottom). The legends show ct-DNA:complex ratios.

The UV-Vis titrations were carried out two times: one during the CD titration process, every time the complex was added, a UV-Vis scan was run before the CD scan; and another one using the same stock of ct-DNA and complex solution but this time the titration was processed straight away. No differences between the two titrations were observed. The fact that no changes on the UV-Vis spectra were observed, and no band shifting was registered for any complex, may suggest that the interactions between the complexes and DNA should be of supramolecular nature rather than of coordinative nature, at least during the time of a complete CD titration (~ 6h at room temperature).

The UV-Vis titration of ct-DNA (80 μM) with **10** (Rh(III) di-nuclear triple stranded) shows that the triple stranded helicate structure is retained and as more complex is added the change in the absorbance is linear (Figure 3.6). This is expected for this complex due to the saturated helicate structure, which does not have any vacant coordination sites for covalent interactions with the DNA. Therefore it is expected that the interactions are mainly of supramolecular nature as in the Fe(II) and Ru(II) triple stranded analogues.[3-5]

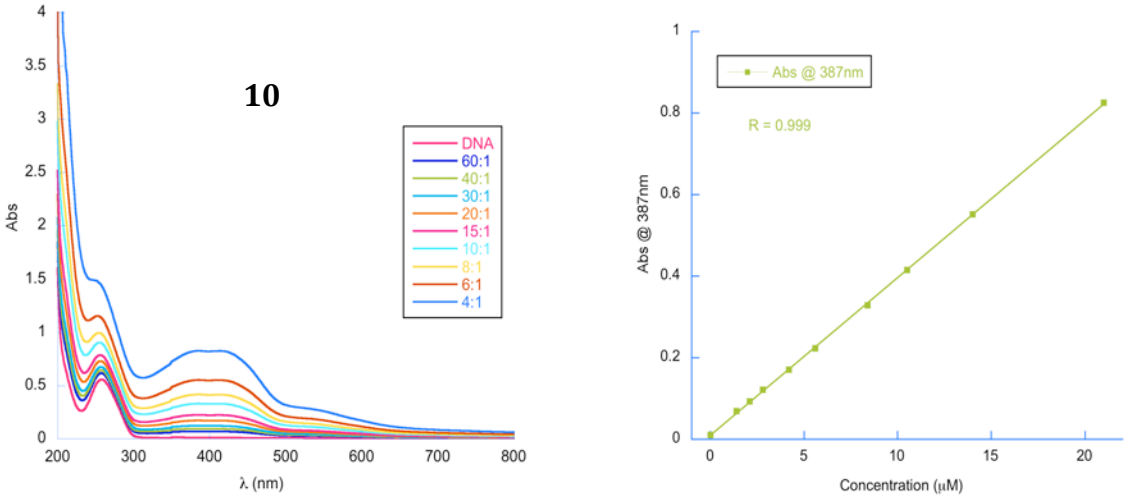

Figure 3.6 UV-Vis of 80 μM ct-DNA in 20 mM NaCl and 1 mM $Na(CH_3)_2AsO_2.3H_2O$ (pH 6.8) with increasing concentration of complexes **10** and respective plot of Abs *vs.* Concentration of complex. The legends show ct-DNA:complex ratios

3.4 CD ct-DNA Titrations with Rh(III) Complexes

To carry on exploring the binding affinities of the complexes with ct-DNA, UV-Visible absorbance circular dichroism (CD) was used. The experiments have been carried out with calf thymus DNA (ct-DNA) in aqueous solution with NaCl (20 mM) and sodium cacodylate buffer (1 mM) pH 6.8, with a constant concentration of ct-DNA (300 μM). For complex **10** (Rh(III) triple stranded complex) the ct-DNA concentration used was 80 μM: due to the high charge of the complex even at low ratios of DNA:complex dark orange/brown strands of DNA-complex aggregates were formed when using higher DNA concentrations.

None of the complexes studied showed intrinsic CD signals, in this way any CD signal that occurs in the spectroscopic regions of the complexes are therefore a result of the interaction between the complexes and ct-DNA.[6]

3.4.1 CD ct-DNA Titrations with Rh(III) Complexes (1 to 6)

Titrations of the ct-DNA (300 μM) with increasing amounts of complexes **1** and **2** led to ICD signals in the complex region with positive bands at 330 nm and 450 nm, which confirms the compound binding to ct-DNA (Figure 3.7). Although both complexes exhibit bands for induced signals, the induced band at 450 nm is stronger for **2** than for **1**. Plotting of the ICD at 450 and 330 nm for **1** and **2** (Figure 3.8, data normalized to 1 at 4:1 loading) show that they have very similar behaviour towards ct-DNA.

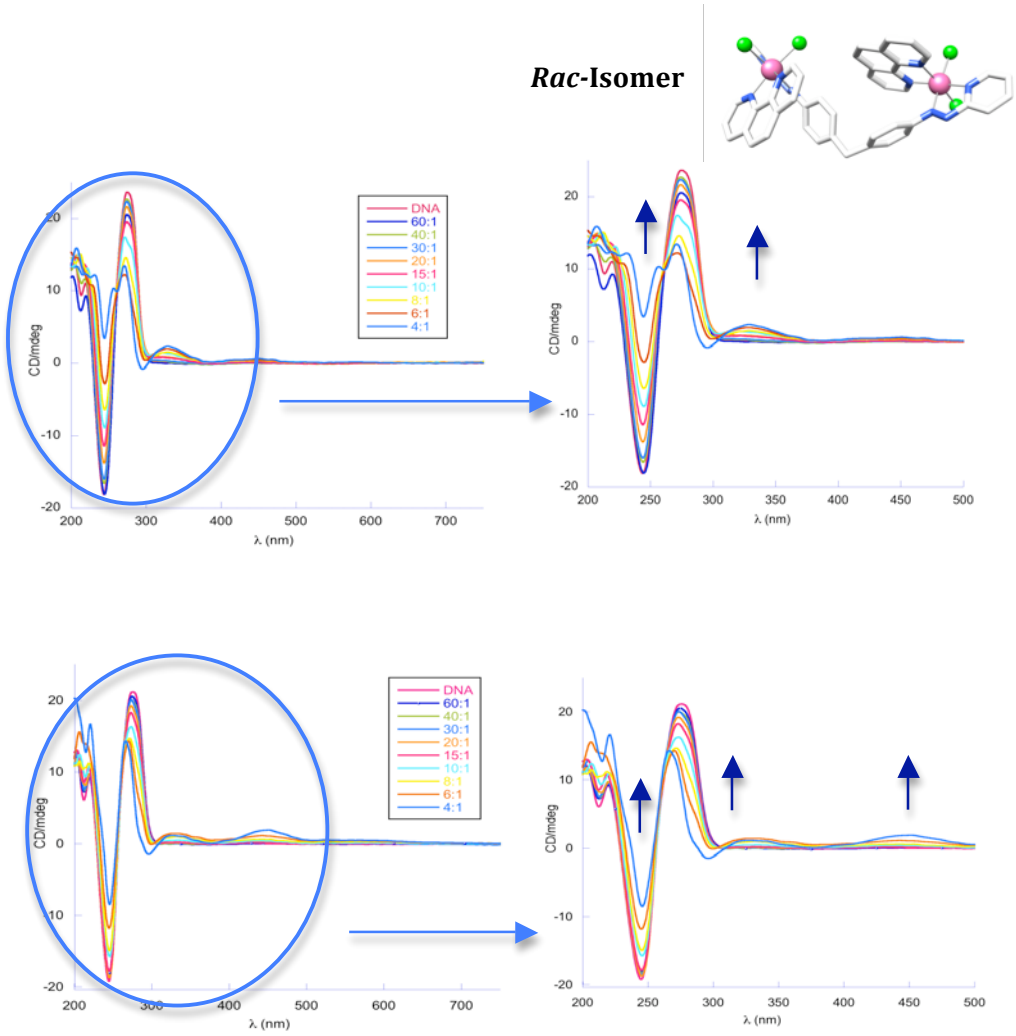

Figure 3.7 CD of 300 μM ct-DNA in 20mM NaCl and 1 mM $Na(CH_3)_2AsO_2.3H_2O$ (pH 6.8) with increasing concentration of complexes **1** (Top) and **2** (Bottom); The legends show ct-DNA:complex ratios.

The DNA region between 200-300 nm, is expected to be affected both by any change in DNA CD but also by overlapping ICD bands from the complex in the same region. Nevertheless, the absence of signature signals of other DNA forms and the retention of the B-DNA signature indicates that DNA retains its B-conformation when the complexes bind.

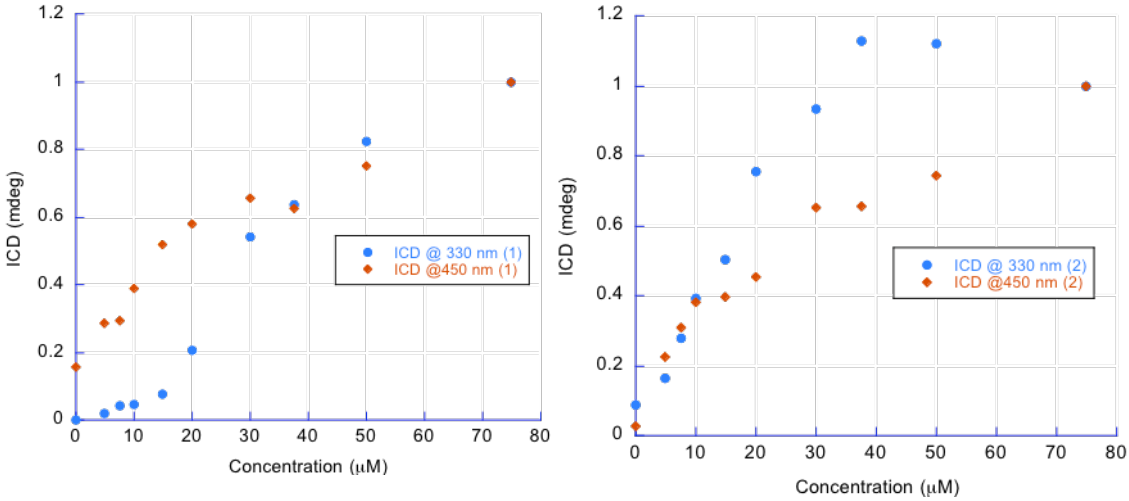

Figure 3.8 Plotting of ICD signal for **1** and **2** vs. complex concentration extracted from the DNA titrations with the respective complexes.

Although during the UV-Vis titration experiment the MLCT band of the complexes **1** and **2** remained centred at 399 nm, without any shift observed, the ICD signal appears in different regions of the spectrum (330 nm and 450 nm). The absorption band of the complexes in the visible region of the absorption spectra is fairly broad being extended from 300 to 500 nm and in the CD experiment in this case, it seems that there are specific transitions at 330 and 450 nm that are optically active under circular polarized light which maybe be overlapping in the UV-Vis spectra.

When analysing the CD spectrum of complex **5** (Figure 3.9), the Rh(III) mononuclear analogue of **1** and **2**, the effect of the complex on DNA is much reduced compared with the di-nuclear analogues; no effect can be observed in the MLCT region of the complex

and in the B-DNA region no significant changes are observed with the B-DNA conformation being retained.

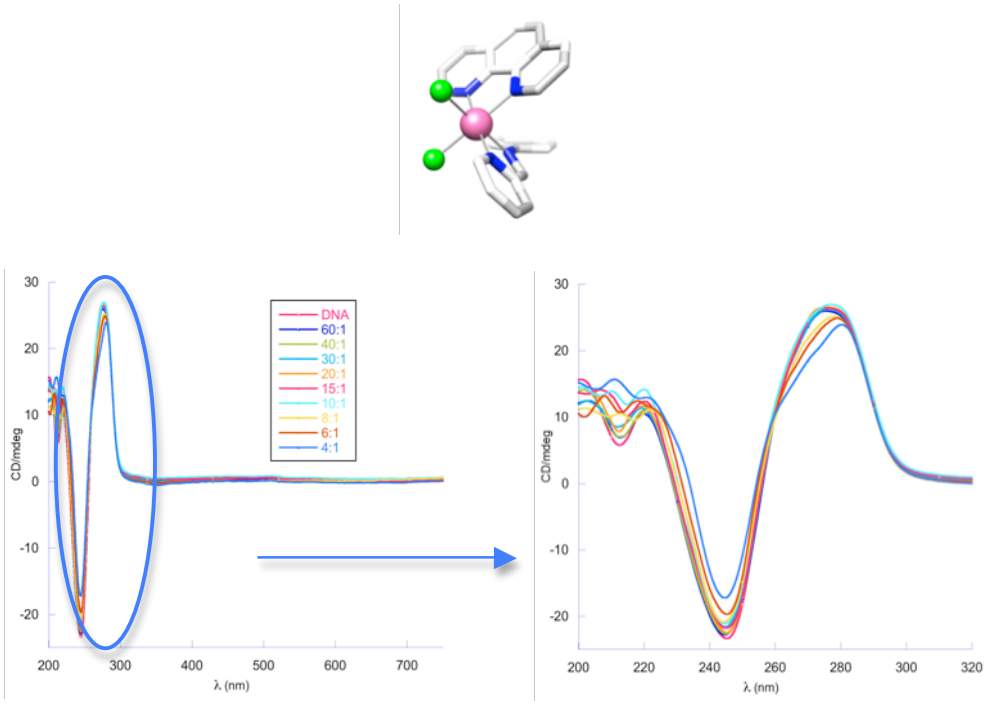

Figure 3.9 CD of 300 μM ct-DNA in 20mM NaCl and 1 mM $Na(CH_3)_2AsO_2.3H_2O$ (pH 6.8) with increasing concentration of complexes **5.** The legends show ct-DNA:complex ratios.

Titrations of ct-DNA (300 μM) with complexes **3** and **4** were carried out and ICD signals observed at 311 and 439 nm proving that both complexes bind to DNA (Figure 3.10). Interestingly there are considerable differences comparing with complexes **1** and **2**, which bear the phen ligands instead of the bpy ligands. These bpy ones seem to have less effect on DNA, since the ICD signal is less intense for the higher concentrations of complex added comparing with the same ratio DNA:complex for complexes **1** and **2**.

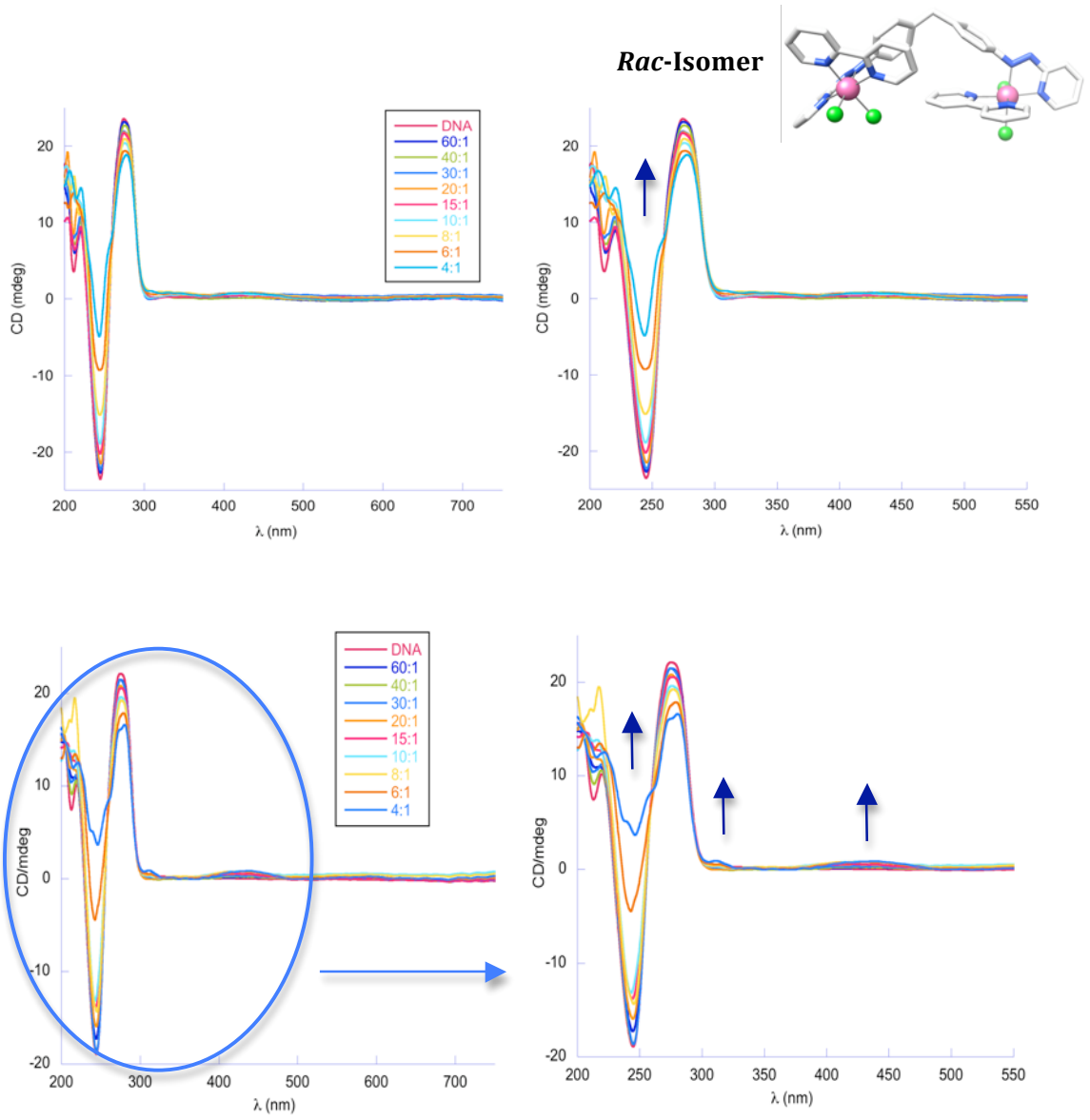

Figure 3.10 CD of 300 μM ct-DNA in 20mM NaCl and 1 mM $Na(CH_3)_2AsO_2.3H_2O$ (pH 6.8) with increasing concentration of complexes **3** (Top) and **4** (Bottom); The legends show ct-DNA:complex ratios.

When comparing the ICD signal of both *meso* isomers of the single stranded complexes with phen ligand and bpy ligands (Figure 3.11), it is clear that there are significant differences with complex **4** showing a weaker ICD for the same ratio DNA:complex. These differences are very interesting as both complexes have the same overall charge (2+) and very similar size and shape. The fact that phen has a bigger

aromatic surface and can behave as an intercalating ligand better than bpy ligand may be one of the reasons why complexes **1** and **2** have better DNA binding affinities when compared with **3** and **4**.

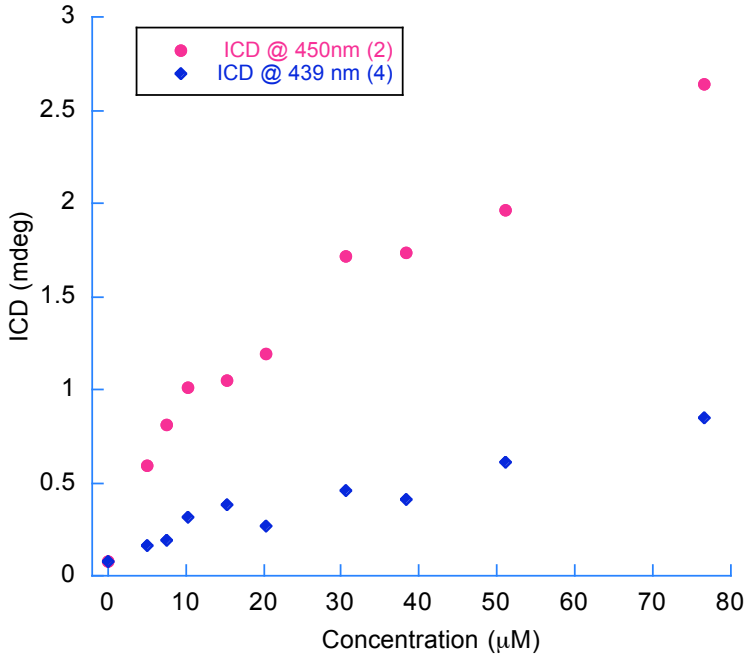

Figure 3.11 Plotting of ICD signal for **2** and **4** vs. complex concentration extracted from the DNA titrations with the respective complexes.

When analysing the CD spectrum of complex **6** (Figure 3.12), the Rh(III) mononuclear complex analogous to **3** and **4**, the effect of the complex on DNA is very weak. The ct-DNA titration with increasing amount of complex shows no ICD signal in the complex region and the DNA region shows the B-DNA form being retained and almost no effect is observed. This result is similar to the DNA titration with complex **5**.

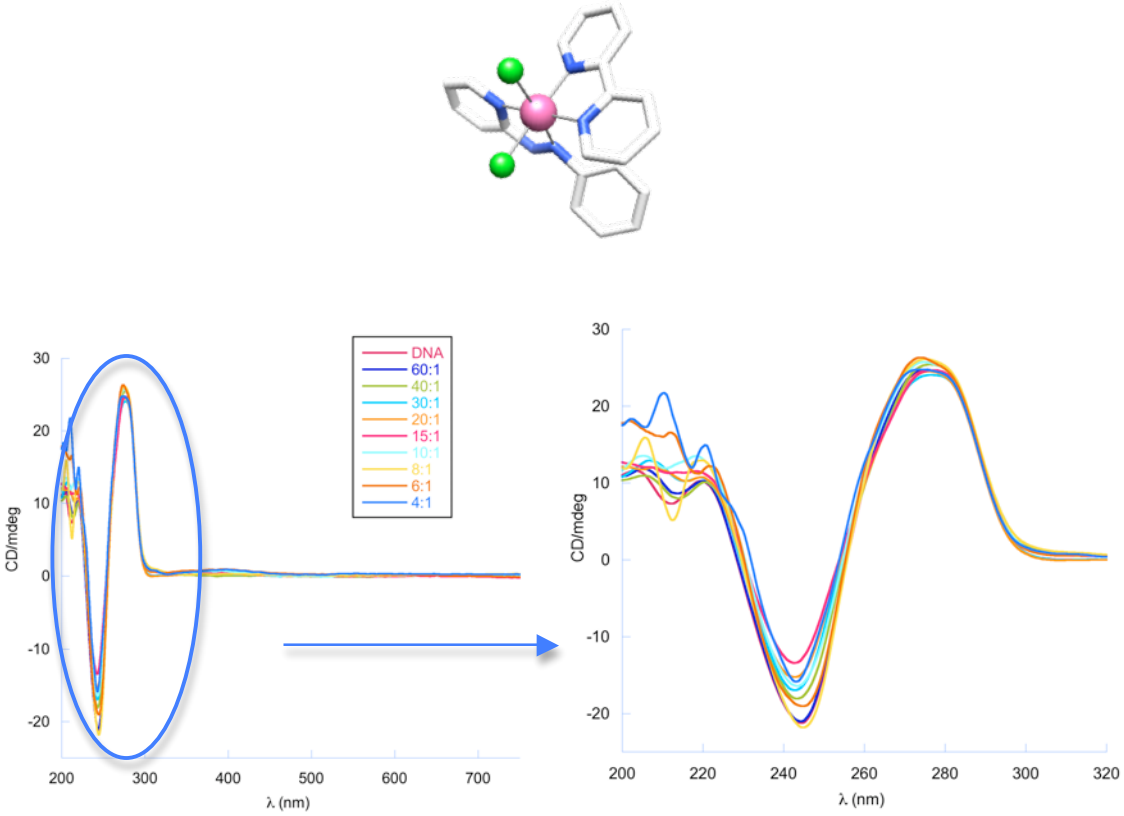

Figure 3.12 CD of 300 μM ct-DNA in 20mM NaCl and 1 mM $Na(CH_3)_2AsO_2.3H_2O$ (pH 6.8) with increasing concentration of complex **6.** The legends show ct-DNA:complex ratios.

3.4.2 CD ct-DNA Titrations with Rh(III) Complexes (7 and 8)

Similar ct-DNA (300 μM) CD titrations were performed using Rh(III) double stranded complexes under the same conditions. Increasing amounts of complexes **7** and **8** led to an induced ICD signal in the complex region with a positive band around 400 nm, which confirms the binding to ct-DNA (Figure 3.13). The B-DNA form is retained although changes are observed upon addition of the complexes to ct-DNA in the UV region. Plotting of the ICD at 400 nm for **7** and **8** (Figure 3.14), show that the second isomer (complex **8**) has clearly better binding effect to ct-DNA when compared with the first

isomer (complex **7**). For the same ratio DNA:complex complex **8** exhibits a higher ICD signal than complex **7**.

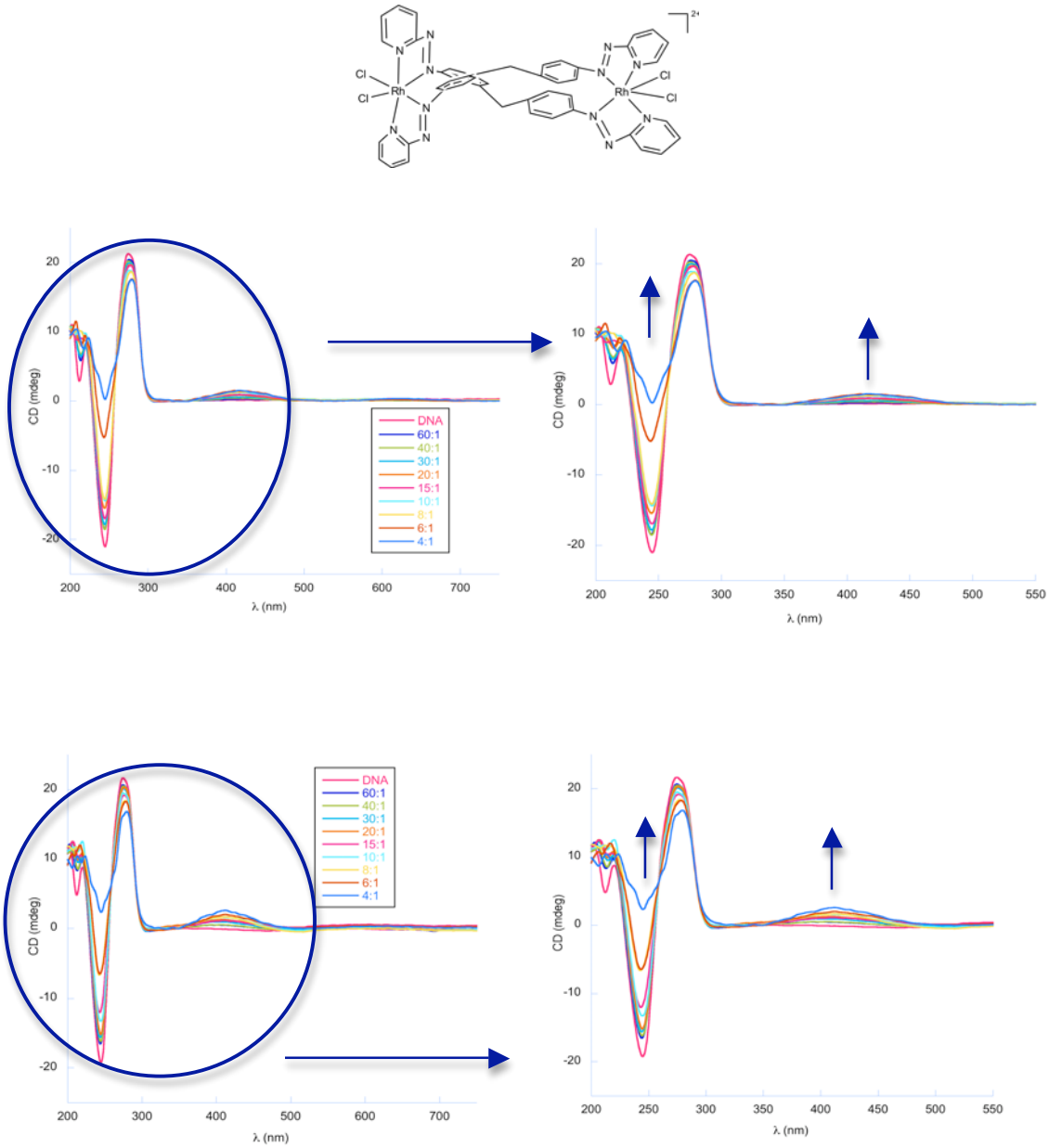

Figure 3.13 CD of 300 μM ct-DNA in 20 mM NaCl and 1 mM $Na(CH_3)_2AsO_2.3H_2O$ (pH 6.8) with increasing concentration of complexes **7** (Top) and **8** (Bottom); The legends show ct-DNA:complex ratios.

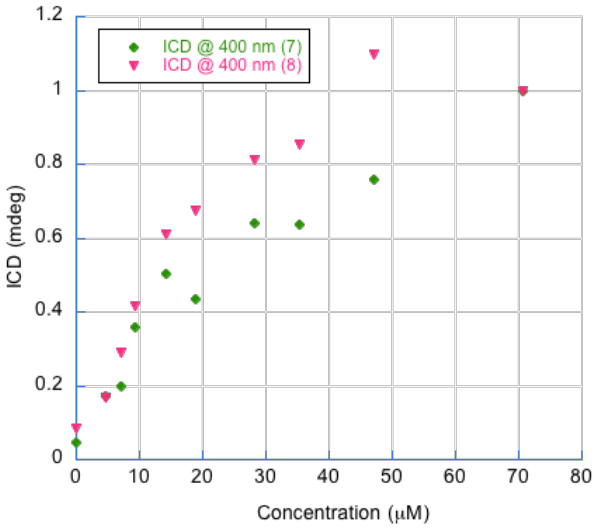

Figure 3.14 Normalized induced CD signal (ICD) at 400 nm for **7** and **8**, data normalized at 4:1 loading.

The fact that during the UV-Vis and CD titrations none of the spectra of the complexes show any shifts of the bands, suggests that the DNA binding interactions are non-covalent under the conditions used for the titration experiments.

3.4.3 CD ct-DNA Titrations with Rh(III) Triple Stranded Complex (10)

As in the UV-Vis titration, the ct-DNA titration (300 μM) with the Rh(III) triple stranded complex **10** was complicated by DNA precipitation at standard conditions. The optimal DNA and complex concentrations achieved were at 80 μM ct-DNA.

Titration of ct-DNA (80 μM) with complex **10** led to the formation of two strong ICD signals in the complex region at 444 nm and 590 nm (Figure 3.15). In addition the B-DNA bands (negative and positive) show hypochromic shifts, as well as small

bathochromic shifts of 5 nm for the negative band at 244 nm and 3 nm for the positive band at 275 nm (Figure 316, Bottom).

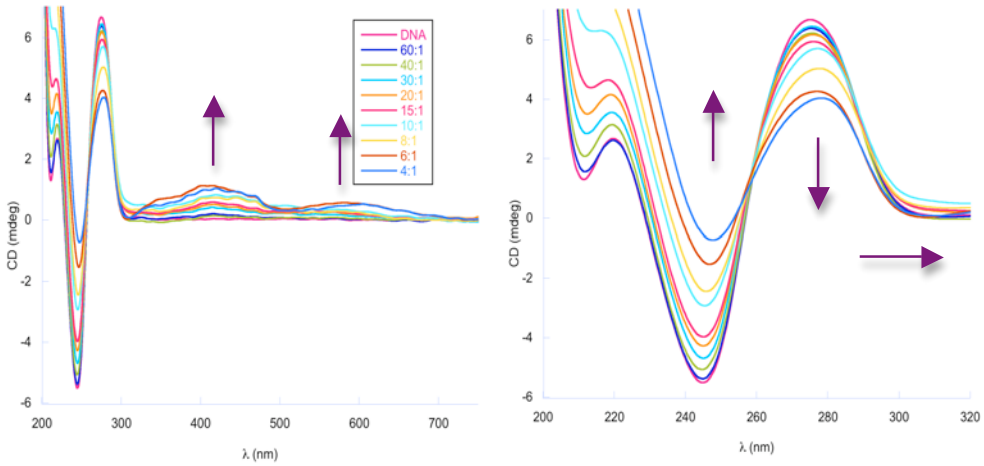

Figure 3.15 CD of 80 μM ct-DNA in 20 mM NaCl and 1 mM $Na(CH_3)_2AsO_2.3H_2O$ (pH 6.8) with increasing concentration of complexes **10**. The legends show ct-DNA:complex ratios.

Although no direct comparisons can be made on this complex with the single and double stranded ones due to the different conditions used for the titrations, it is clear that the complex has a strong effect on B-DNA. The plot of the normalized ICD signal at 444 nm (Figure 3.16, Top) would be consistent with the complex binding to ct-DNA in one single binding mode, which in this case should be of supramolecular nature, in an analogous way to the Fe(II) cylinder which binds into the DNA major groove.

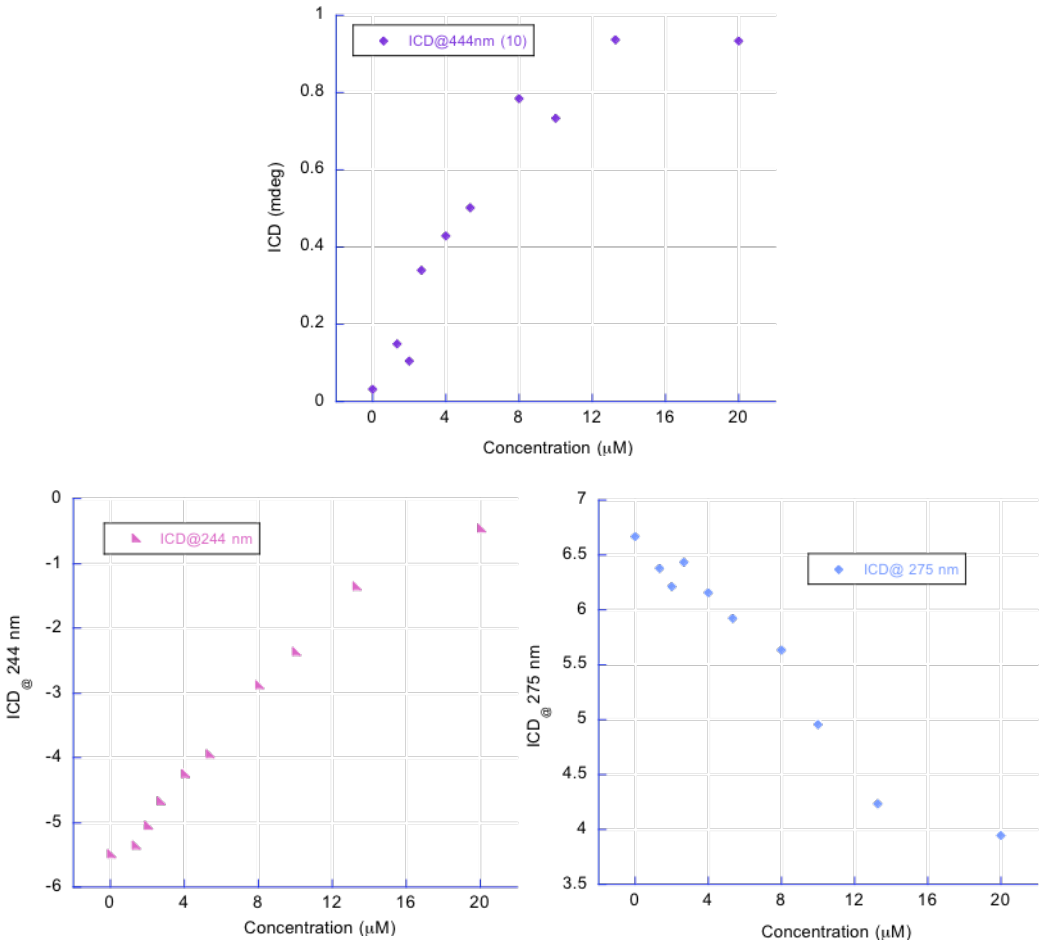

Figure 3.16 (Top) ICD signal (ICD) at 444 nm for **10**; (Bottom) CD signal of DNA at 244 and 275 nm upon addition of complex **10**.

A preliminary estimation of a binding constant (K_b) value for complexes **2**, **7**, **8** and **10** was made using Origin software to plot the ICD signal of the complexes *vs.* concentration and calculated using the methodology and equation reported by Stootman in 2006.[7] The curves of the respective fittings are shown in Appendix A.19-A.22. Table 3.1 shows the values obtained in comparison with the reported values for the Fe(II) and Ru(II) imine cylinders.[8, 9]

Table 3.1 Binding constants K_b (M^{-1}) for Rh(III) complexes.

Complexes	**2**	**7**	**8**	**10**	**Ru(II)[8] cylinder**	**Fe(II)[9] cylinder**
K_b value (M^{-1})	1.46x10^6 (± 0.91) x10^6	1.67x10^4 (±0.67) x10^4	2.39x10^5 (±3.10) x10^5	4.82x10^6 (±3.47) x10^6	5.8x10^7	6x10^7

The weak ICD signal of complexes **3** and **4** did not allow an estimation of a K_b value for these complexes. For complex **1**, a proper fit of the data to the equation was not possible so no value was obtained.

The fact that the Rh(III) complex **10**, the triple helicate, has a lower binding constant in comparison with the Fe(II) and Ru(II) cylinders is unexpected as due to the higher charge a stronger binding would be expected. The K_b value of **10** although higher in comparison with the single ad double stranded Rh(III) dinuclear complexes its order of magnitude is lower than for the Ru(II) and Fe(II) cylinders. These last ones have similar binding, which was expected due to their similar supramolecular structure and overall charge.

3.5 CD Studies with poly [G-C] and poly[A-T]

In order to explore if some of the complexes exhibited any binding preferences between different DNA sequences, CD studies were also carried out using poly[G-C] and poly[A-T]. For these first studies the complexes explored were the two single stranded complexes with phen ligands (**1** and **2**), as these were the ones that have a higher effect on ct-DNA by CD spectroscopy. Also a similar experiment was carried out using one of the double stranded isomers (**8**). The CD studies with poly[G-C] and poly[A-T] were carried out in an analogous way to the ct-DNA titrations. Solutions of the polymers (100 μM, bp) in 20 mM NaCl and 1 mM $Na(CH_3)_2AsO_2.3H_2O$ (pH 6.8) were titrated with increasing concentration of complexes. Four different ratios of DNA: complex were chosen: 60:1, 10:1, 6:1 and 4:1.

Interestingly, CD spectra of complexes **1** and **2** shown in Figure 3.17 show that both complexes may preferentially bind to poly[G-C] rather than poly[A-T] with spectra showing major differences in the DNA region (200-300 nm) for poly[G-C] and almost no effect for poly[A-T]. Additionally, in the complex region (300-500 nm) it is possible to observe an increased ICD signal that confirms the binding of the complexes to poly[G-C]. These results are very interesting and corroborate the idea of the complexes binding in the major groove of DNA since here the GC base pairs are sterically less hindered than in the minor groove.[2] These results are very positive and exciting once they suggest a preference of the complexes for DNA G-C regions, which can open a door for DNA binding selectivity.

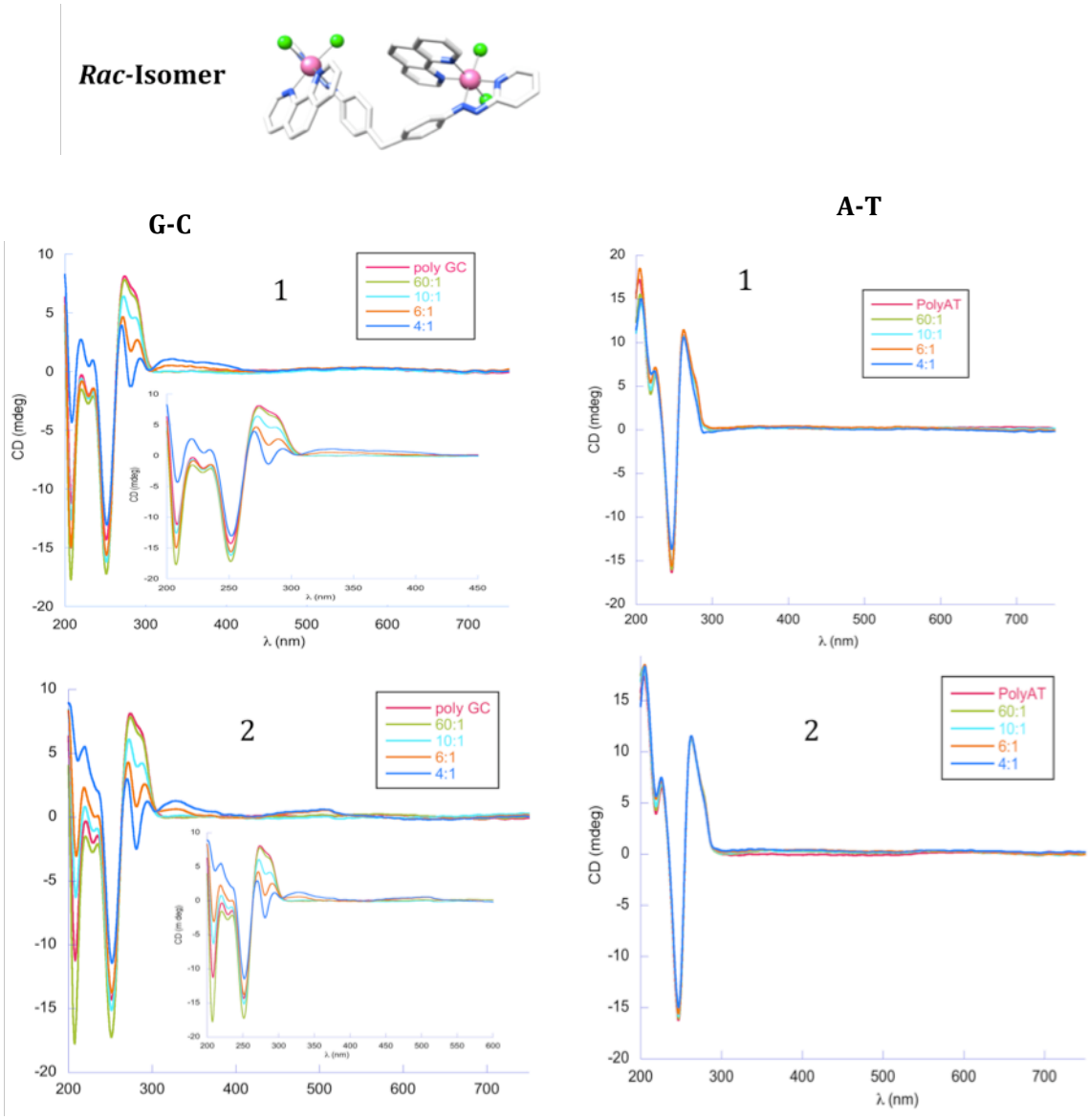

Figure 3.17 CD of 100 μM poly[G-C] (left) and poly[A-T] (right) in 20 mM NaCl and 1 mM $Na(CH_3)_2AsO_2.3H_2O$ (pH 6.8) with increasing concentrations of complexes **1** (top) and **2** (bottom) . The legends show ct-DNA:complex ratios.

A similar study was carried out with the double stranded complexes. For this study, the complex of choice was the second isomer (complex **8**), which was the one that was shown by CD spectroscopy to have a higher effect on ct-DNA. When observing both CD spectra with poly[A-T] and poly[G-C] (Figure 3.18), it is possible to observe that the DNA

region is affected upon interaction with the complex and in the UV region of the complex an ICD signal increases when the concentration of the complex increases. From this is clear that once again the complex may preferentially bind to GC regions rather than AT, although it seems that this effect is much less marked when compared to the same study made for the single stranded isomers, complexes **1** and **2** in Figure 3.17.

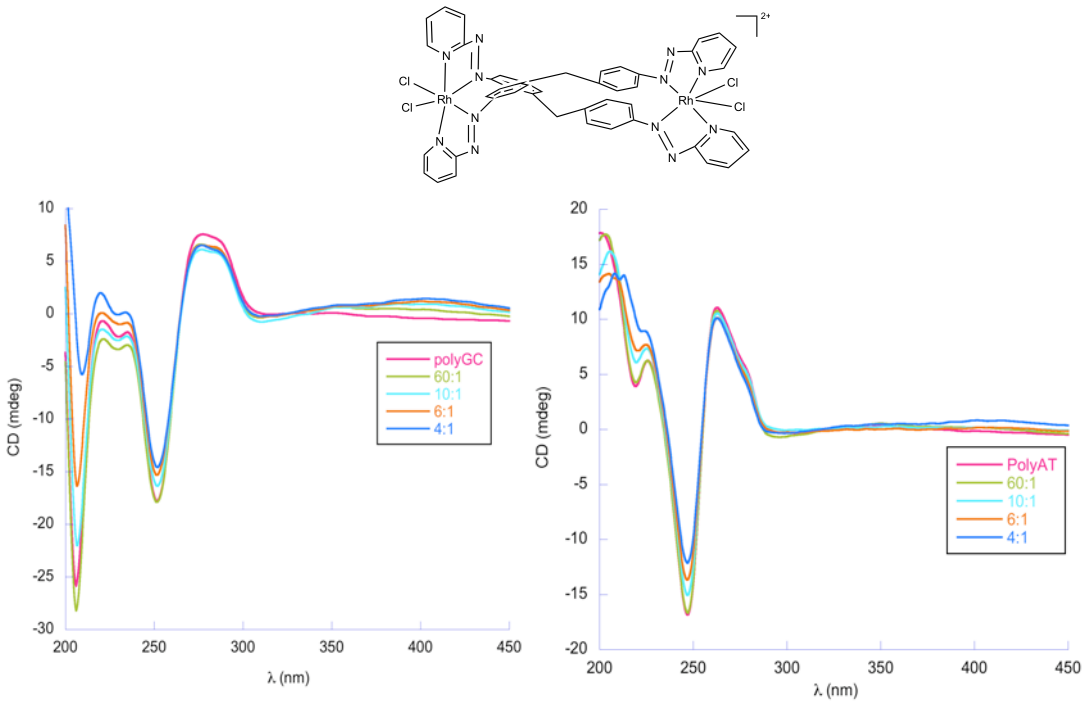

Figure 3.18 CD of 100 μM poly[G-C] (left) and poly[A-T] (right) in 20 mM NaCl and 1 mM $Na(CH_3)_2AsO_2.3H_2O$ (pH 6.8) with increasing concentrations of complexes 8. The legends show ct-DNA:complex ratios.

Although it is noticeable that complexes **1**, **2** and **8** may preferentially bind to G-C rather than to A-T sequences, this effect is not as strong as with ct-DNA. Similar studies made in the past in the Hannon group using the parent cylinder $[Fe_2(L_{im})_3]^{4+}$ suggested that the P enantiomer may prefer the regular sequences of synthetic DNA rather than the random ordered ct-DNA.[10]

3.6 Flow Linear Dichroism (LD)

Linear dichroism (LD) is the difference between the absorption of linearly polarized light both parallel and perpendicular to a chosen plane and can be used to probe the orientation of long molecules like DNA (with a minimum length of approximately 250 base pairs), using a flow Couette cell containing sample being oriented through a viscous drag (Figure 3.19). [1]

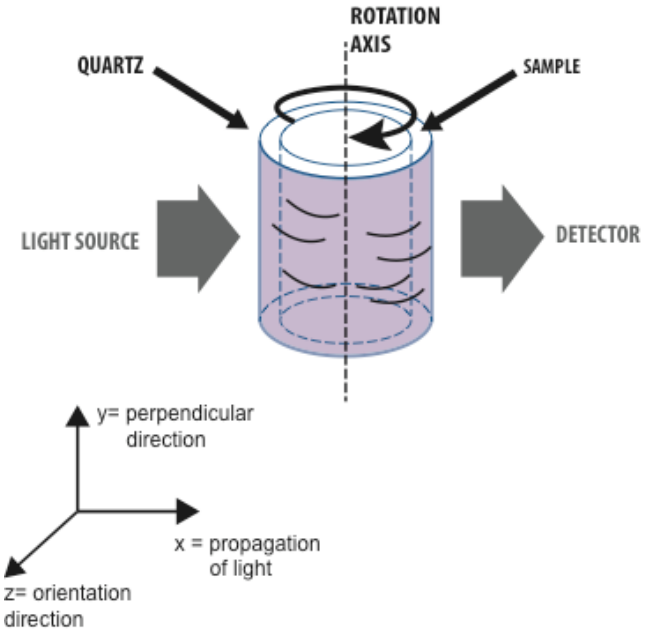

Figure 3.19 Couette flow cell used for LD experiments.

The incident radiation is perpendicular to the rotation axis of the internal cylinder. Strands of long DNA are oriented upon rotation of the internal cylinder. This cell is built with two coaxial cylinders (internal and external) with a gap between them. The linearly polarised light is incident radial to the flow cell and perpendicular to the flow direction. LD signals can be observed for ct-DNA but not for small free molecules. However, if the

molecule binds to the flow oriented ct-DNA and if it does it in a specific orientation it can give rise to an LD signal. If it binds in a random way to DNA it will not show any signal.

3.7 LD ct-DNA Titrations with Rh(III) Complexes

The complexes studied are too small to exhibit any LD signal alone, so any signals arising from the experiment in the spectroscopic region of the complexes after the addition to ct-DNA indicate the binding of the complex to ct-DNA in a specific orientation. The LD titrations were performed using the same conditions as for the CD titrations.

3.7.1 LD ct-DNA Titrations with Rh(III) Complexes (1 to 6)

LD spectra for complexes **1** and **2** show bands in the 300 to 450 nm region of the complexes (Figure 3.20). The signals increase in intensity when increasing the concentration of the complex in the solution proving the binding of the complexes to ct-DNA in a specific orientation(s) and not just randomly. In addition, the negative LD band (220-300 nm) confirms retention of the B-DNA conformation although there are visible structural changes in the ct-DNA since the signal decreases at 260 nm when the concentration of complex added increases. This behaviour of the signal is consistent with a non-intercalative mode, and it can arise from the loss of DNA orientation like DNA coiling or bending.[3, 5] Intercalation of molecules in between the DNA base pairs reduces the flexibility of ct-DNA "stiffening", increasing the magnitude of the LD signal. Although both isomers **1** and **2** coil and bend ct-DNA this effect is not as dramatic as for the iron (II) and ruthenium (II) cylinders.[3, 5] Also, the coiling effect caused by the iron (II)

cylinder with L_{azo} synthesized before in the Hannon group is stronger when compared with these single stranded complexes.[11]

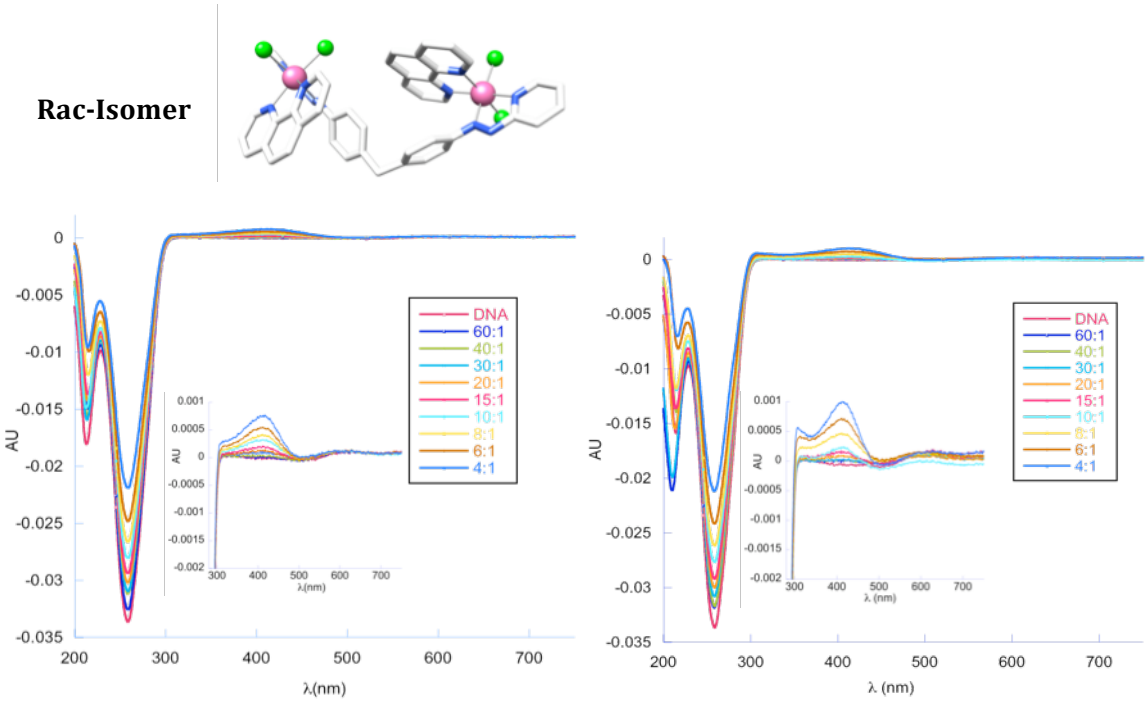

Figure 3.20 LD of 300 μM ct-DNA in 20 mM NaCl and 1 mM $Na(CH_3)_2AsO_2.3H_2O$ (pH 6.8) with increasing concentration of complexes **1** (left) and **2** (right). The legends show ct-DNA:complex ratios.

For complexes **1** and **2** small additions of the complexes to ct-DNA caused immediate changes on the ct-DNA LD band showing that both complexes coil ct-DNA even at low loading (Figure 3.21). These LD studies corroborate what was already observed by CD spectroscopy, with both complexes binding to ct-DNA and inducing a CD signal in the region where the complexes absorb.

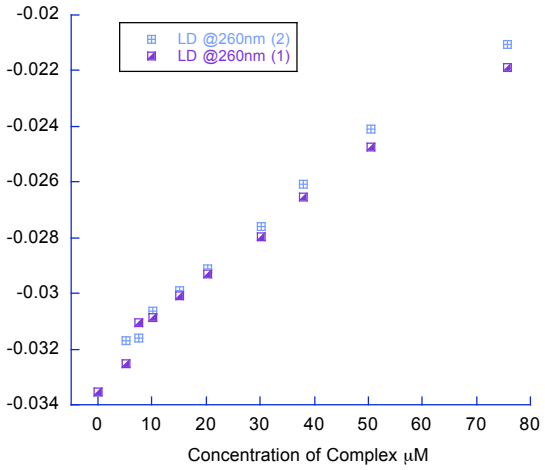

Figure 3.21 Plot of LD signal at 260 nm for complexes **1** and **2**.

For complex **5**, although no LD positive band arises in the complex absorbing region, it is still possible to observe a decrease in the ct-DNA LD band suggesting the coiling and binding of the complex to ct-DNA although in a non specific orientation (Figure 3.21) and less than for complexes **1** and **2**.

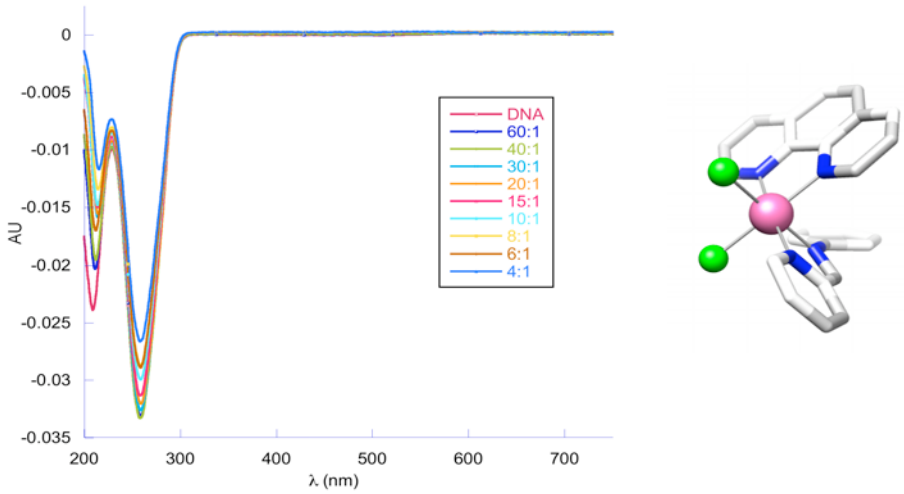

Figure 3.22 LD of 300 μM ct-DNA in 20 mM NaCl and 1 mM $Na(CH_3)_2AsO_2.3H_2O$ (pH 6.8) with increasing concentration of complex **5**. The legends show ct-DNA:complex ratios.

This result is in accordance with previous CD studies for the same complex (see section 3.4.1), with the ct-DNA upon titration with the complex not being affected, no ICD signal was observed and the B-DNA conformation being retained and almost not affected even at high loading of the sample.

A different LD experiment was also carried out using complex **2** (selected because it seemed to show more binding effect with both ct-DNA and poly[G-C]). This time, a fresh solution with a DNA:complex ratio 10:1 was compared with a sample with same ratio DNA:complex that was incubated for a period of 24 hours at 37 °C. The same stock solutions of ct-DNA and complex were used for both experiments. From the LD spectra (Figure 3.23) we can observe a significant decrease of the LD band at 260 nm and an increase in the positive band in the complex region over time, which can be compared with the spectrum for the ratio of 4:1 (DNA:complex) for the fresh titration (Figure 3.20 right).

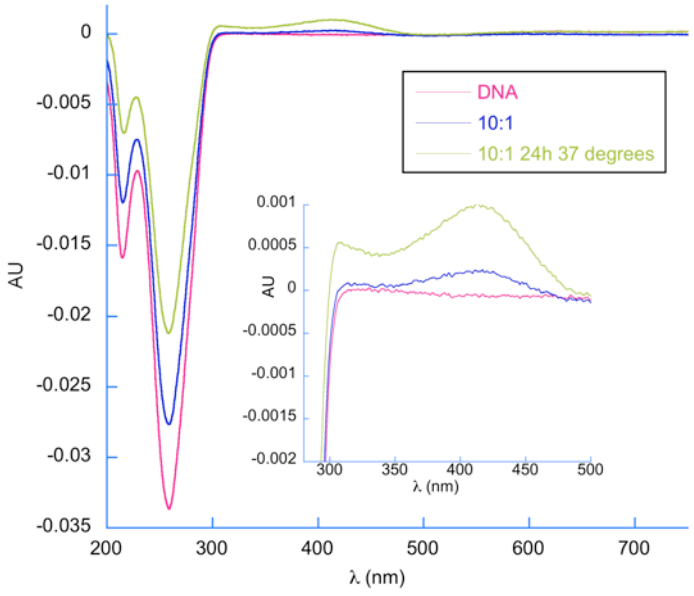

Figure 3.23 LD of 300 μM ct-DNA in 20 mM NaCl and 1 mM $Na(CH_3)_2AsO_2.3H_2O$ (pH 6.8) with complexe **2**, ratio ct-DNA:complex used 10:1.

These results suggest that coordinative binding of the complex to ct-DNA may occur over time in addition to major groove binding and electrostatic interactions, which occur upon a fresh titration of ct-DNA with the complex. The chlorides of the complex can slowly (during the incubation period) be replaced by nitrogens of the bases (possibly guanines). This subsequent binding mode seems to cause more DNA coiling.

LD titrations were carried out under the same conditions for complexes **3** and **4** (single stranded with bpy ligands). The LD spectra of both complexes (Figure 3.24) show an ILD signal band at 300 nm, which is stronger for complex **4**.

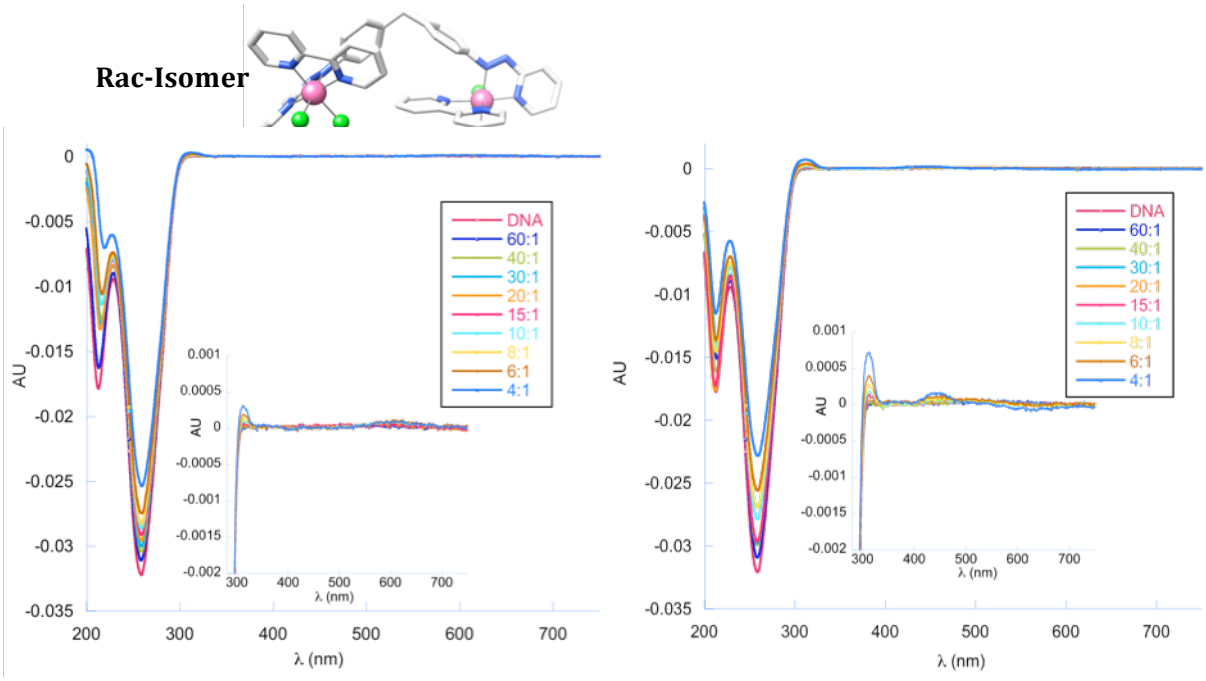

Figure 3.24 LD of 300 μM ct-DNA in 20 mM NaCl and 1 mM $Na(CH_3)_2AsO_2.3H_2O$ (pH 6.8) with increasing concentration of complexes **3** (left) and **4** (right). The legends show ct-DNA:complex ratios.

In addition complex **4** shows a second ILD band, although weak around 450 nm. The ILD signal observed for both complexes, proves the binding to DNA in a specific orientation (s) and not merely randomly. The negative LD band (220-300 nm) confirms retention of the B-DNA conformation. This behaviour of the LD signal again is consistent with a non-intercalative mode, and consistent with the loss of DNA orientation from DNA coiling or bending. Complex **4** appears to cause more ct-DNA coiling than complex **3**. The plot of the LD signal at 260 nm shown in Figure 3.25 suggests that two DNA binding modes might occur for complex **4**.

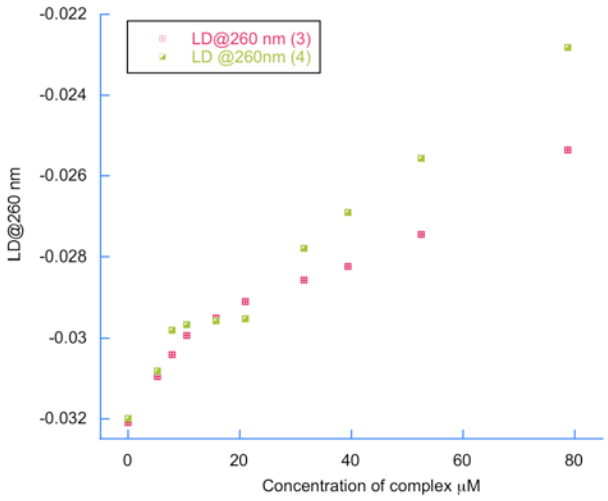

Figure 3.25 Plot of LD signal at 260 nm for complexes **3** and **4**.

The less effect on LD experiments of complexes **3** and **4** in comparison with **1** and **2** (Figure 3.26) is consistent with the bigger effects on the CD of the latter ones.

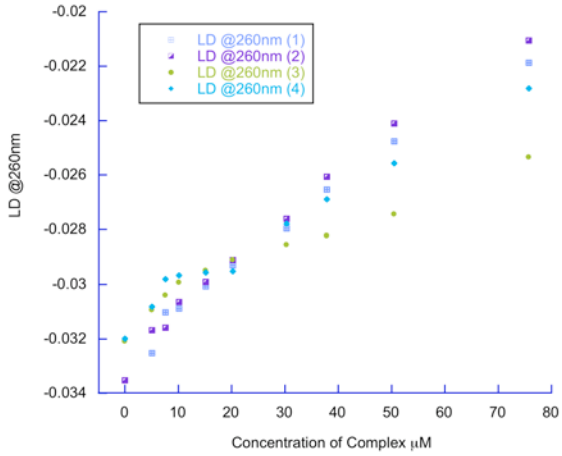

Figure 3.26 Plot of LD signal at 260 nm for complexes **1** and **2**, vs. **3** and **4**.

When analysing the LD spectrum of complex **6** (Figure 3.27), a very low intense LD positive band arises in the complex region, but it is still possible to observe a decrease in the ct-DNA LD band suggesting the coiling and binding of the complex to ct-DNA although in a non specific orientation and clearly this effect is much less than for complexes **3** and **4**. This was expected once the CD titration with **6** showed that ct-DNA was almost not affected by increasing amounts of complex.

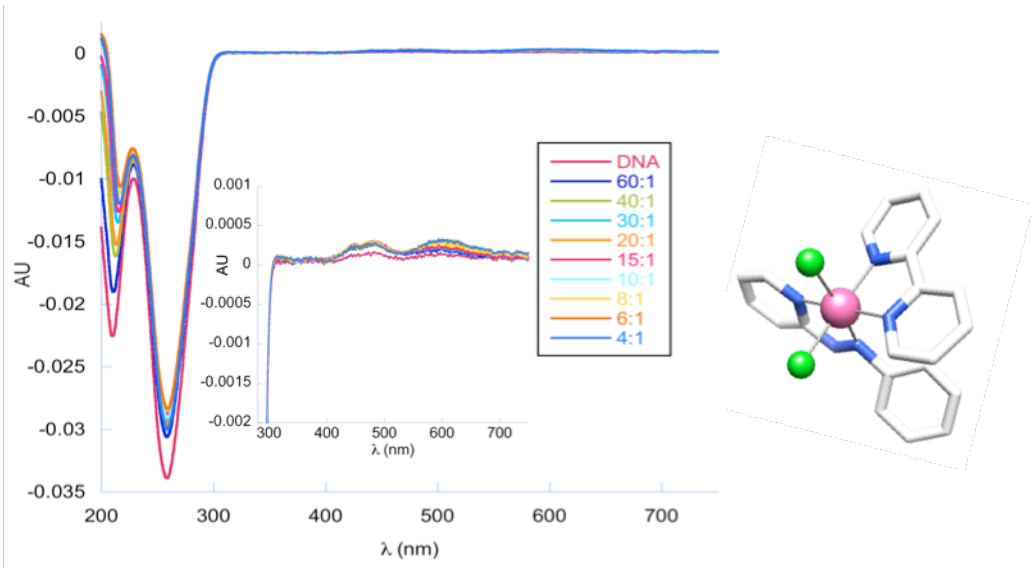

Figure 3.27 LD of 300 μM ct-DNA in 20 mM NaCl and 1 mM $Na(CH_3)_2AsO_2.3H_2O$ (pH 6.8) with increasing concentration of complex **6**. The legends show ct-DNA:complex ratios.

Comparing the LD spectra of both mononuclear complexes **5** and **6**, both spectra are similar. Complex **5** shows a slight bigger decrease of the negative LD band of the ct-DNA at 260 nm suggesting that the complex causes a slightly bigger coiling/bending of the ct-DNA than complex **6**.

Table 3.2, shows a comparison between the percentage values of loss of LD signal when ct-DNA was titrated with each complex **1** to **6** for the highest DNA: complex ratio used (4:1). From this there is a clear difference between the coiling/bending effects of the di-nuclear single stranded complexes in comparison with the mononuclear analogues, with the first ones having a stronger effect. Also, between the different single stranded complexes, the ones with phen ligands (**1** and **2**) seem to cause a higher coiling for the same DNA:complex ratio.

Table 3.2 Comparison of the % of loss of LD signal at 260 nm for complexes **1** to **6** in a DNA:complex ratio of 4:1.

DNA:Complex ratio	% of loss of LD signal at 260 nm after interaction with complexes					
	1	**2**	**3**	**4**	**5**	**6**
4:1	35	37	21	29	20	16

The *meso* isomer of the different complexes (**2** and **4**) has a consistent higher DNA bending effect when compared with the respective *rac* isomer. The complexes with bpy ligands, both di-nuclear and mononuclear, show a constant lower DNA bending effect. Complex **6** seems to be the one causing a smaller ct-DNA bending/coiling effect when compared with the rest of the complexes.

3.7.2 LD ct-DNA Titrations with Rh(III) Complexes (7 and 8)

In the LD experiments made with the double stranded complexes (**7** and **8**) (Figure 3.28), the negative LD band (220-300 nm) confirms that the B-DNA conformation is retained although there are visible structural changes in the ct-DNA once the signal decreases at 260 nm when the concentration of complex added increases. Complex **8**, exhibits a clear higher coiling/bending effect when compared with complex **7** and also shows some ILD signal suggesting that the complex is interacting with ct-DNA in a specific orientation. Figure 3.29 (left) shows the plot of the LD signal at 260 nm on increasing the concentration of the complexes **7** and **8**. Of the di-nuclear complexes **1**-**4**, **7** and **8** the double stranded isomer **8** gives the highest coiling/bending effect. Complex **8** shows to be more effective in bending ct-DNA with 58% of loss of LD signal at 260 nm versus ~ 38% for complex **7** (Table 3.3).

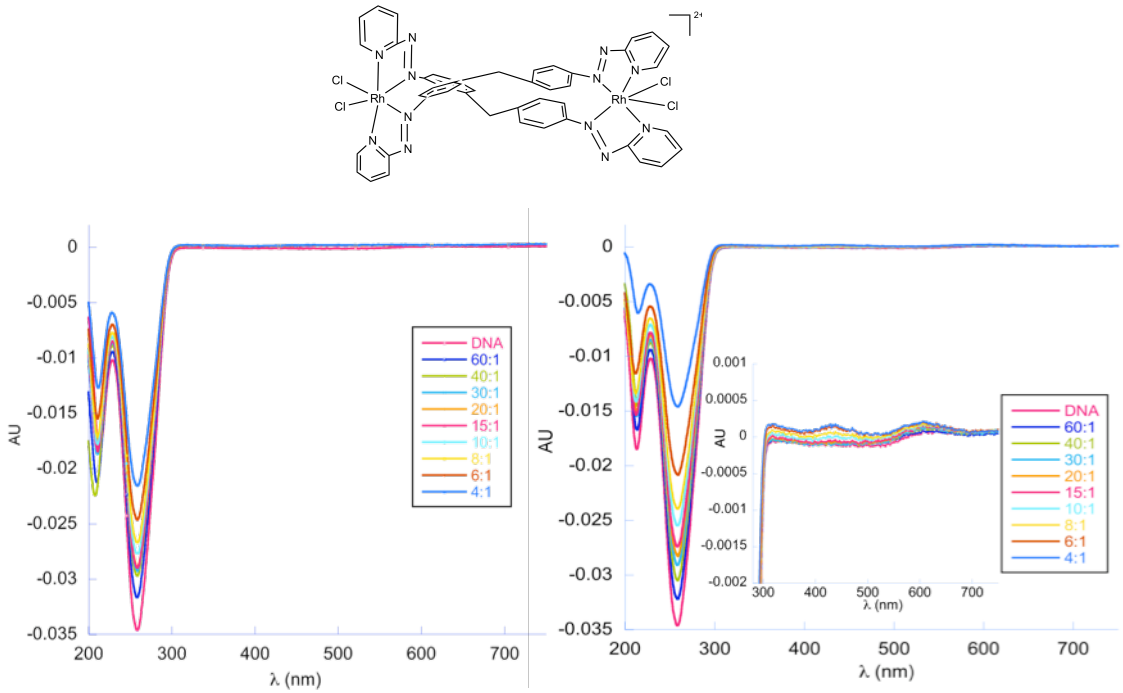

Figure 3.28 LD of 300 μM ct-DNA in 20 mM NaCl and 1 mM $Na(CH_3)_2AsO_2.3H_2O$ (pH 6.8) with increasing concentration of complex **7** (left) and **8** (right). The legends show ct-DNA:complex ratios.

Below the ratio 20:1 all the four complexes (**1**, **2**, **7** and **8**) have very similar behaviour in coiling/bending ct-DNA as shown in Figure 3.29 (right). These results are in accordance with the ones obtained for the complexes when studied by CD spectroscopy. The CD titration for complex **8** showed stronger ICD produced upon addition of complex when compared with complex **7**.

Interestingly, although the coiling effect for these two double stranded isomers is comparable or higher than for the single stranded complexes discussed before, no ILD signal in the complex region is observed for **7** and only a very low intensity ILD is observed for **8**. The data obtained for **7** confirm that the complex is binding to ct-DNA, though do not confirm binding in a specific orientation.

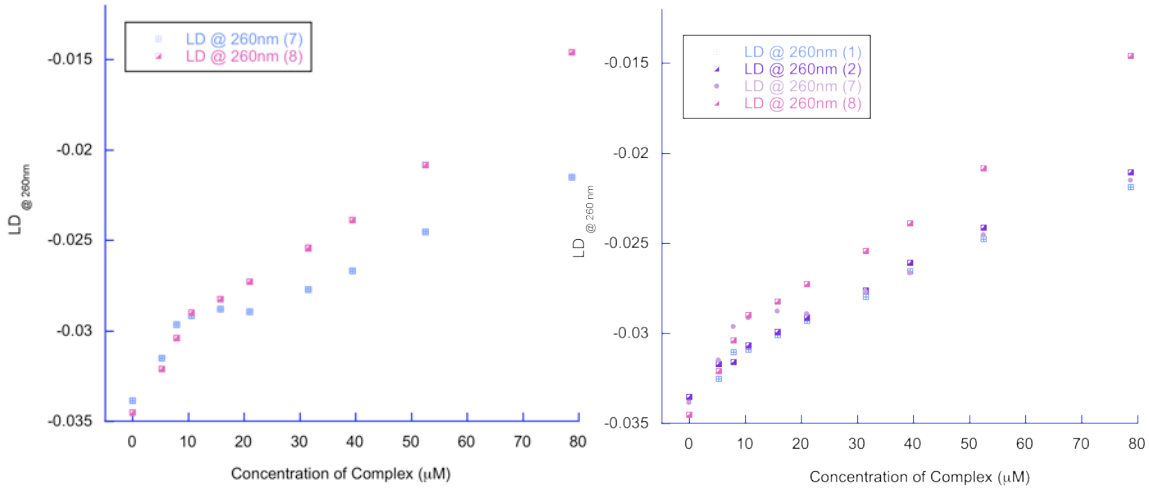

Figure 3.29 (Left) Plot of LD signal at 260 nm for complexes **7** *vs.* **8**. (Right) Plot of LD signal at 260 nm for complexes **1** and **2** *vs.* **7** and **8**.

Table 3.3 Comparison of the % of loss of LD signal at 260 nm for complexes **7** and **8** in a DNA:complex ratio of 4:1.

DNA:Complex ratio	% of loss of LD signal at 260 nm after interaction with complexes	
	7	**8**
4:1	38	58

3.7.3 LD ct-DNA Titrations with Rh(III) Triple Stranded Complex (10)

The LD Titration for the Rh(III) triple stranded complex used the same conditions as used for CD titration of the same complex, using a less concentrated solution of ct-DNA and complex due to precipitation at high concentration. An analogous experiment was carried out with the Fe(II) triple stranded helicate in order to directly compare the binding properties of both complexes. For this, the Fe(II) helicate was synthesized following the literature procedure;[4] synthetic details and characterization can be found in the experimental section 3.9.2.

The titration of 80 μM of ct-DNA with increasing concentration of the Rh(III) complex, caused a dramatic coiling/bending effect on the DNA, with the band of the B-DNA at 260 nm having an intensity decrease of 62% for 4:1 ratio DNA:complex (Figure 3.30, left). Once more, while the LD band of the B-DNA decreases indicating the coiling/bending effect of the complex on ct-DNA, no ILD band is observed in the complex region. This contrasts with the Fe(II) triple helicate which shows an ILD signal in the MLCT region of

the complex with a positive band centred at 550 nm (Figure 3.30, right). The iron cylinder causes more dramatic ct-DNA coiling (90% for 4:1 ratio DNA:complex) (Figure 3.30, bottom) when compared with complex **10**. Nevertheless the Rh(III) complex **10** is still an effective DNA coiling agent. It is noteworthy that the Fe(II) cylinder with L_{azo} is less effective at coiling than the Fe(II) with L_{im} cylinder.[5, 11]

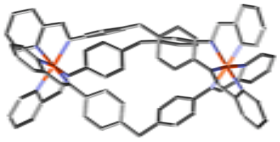

Rh(III) L_{azo} Triple Helicate **Fe(II) L_{im} Triple Helicate**

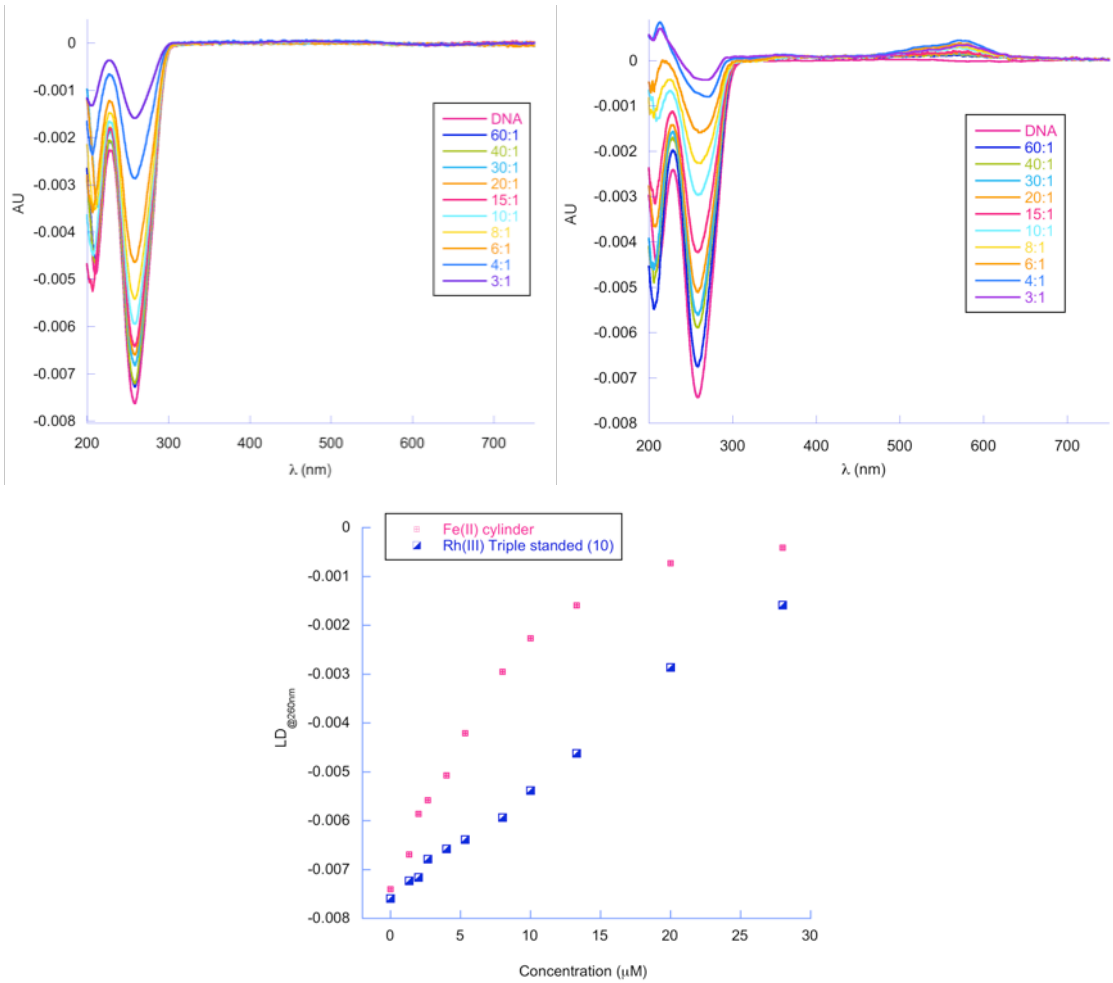

Figure 3.30- LD of 80 μM ct-DNA in 20 mM NaCl and 1 mM $Na(CH_3)_2AsO_2.3H_2O$ (pH 6.8) with increasing concentration of complex **10** (left) and $[Fe_2(L_{im})_3]Cl_2$ (right). The legends show ct-DNA:complex ratios. (Bottom) Plot of LD signal at 260 nm for complexes **10** *vs.* $[Fe_2(L_{im})_3]Cl_2$.

3.8 Gel Electrophoresis Studies

There is ongoing interest in DNA cleavage effects caused by metal complexes with multiple potential applications as structural probes and therapeutic agents.[12-18] Many transition metal complexes that are able to cleave DNA have been reported and special attention has been given to rhodium diimine complexes because of their well known and interesting photocleavage properties.[15]

There are several accepted oxidative mechanisms by which metal complexes target the nucleobases or the sugar functionality and cleave single and double stranded DNA. These mechanisms involve base oxidation by photosensitized singlet oxygen $^1O_2$ and H-atom abstraction from the sugar moiety (Figure 3.31). [19]

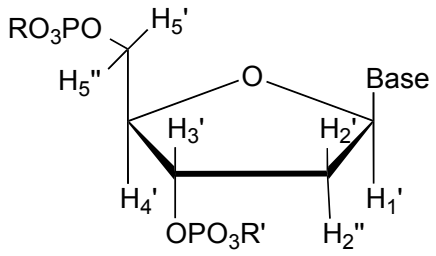

Figure 3.31 Molecular structure of the sugar moiety (deoxyribose).

The abstraction of the H-atom of the sugar may occur through reaction of a photoactivated ligand, generation of a hydroxyl radical or formation of a reactive metal-oxo species. The H-5´ position is the most prone to abstraction by free radicals diffusing along the helix since it is the proton which is most exposed to the solvent in ds-DNA.[13, 17, 19]

The cleavage reactions of plasmid DNA can be monitored using agarose gel electrophoresis. Plasmid DNA can assume three conformations: the supercoiled (sc) which is an intact form and migrates faster in the gel, the circular conformation (oc) which is obtained upon cuttng of one strand (nicking) of the sc form causing its opening to a relaxed circular structure that due to its conformation migrates slower; and finally, if both sc strands are cleaved, a linear (Lin) form will appear in the gel and it will migrate in between the sc and the oc forms (Figure 3.32). Unwinding angles can be quantified by applying the formula:

$$\phi = -18\,\sigma\ /\ r_{(c)}$$

where, ϕ=unwinding angle, σ= superhelicity constant and $r_{(c)}$ = ratio (base:complex bound) where supercoiled and relaxed DNA co-migrate. Plasmid pBR322 was chosen, and using cisplatin, known to unwind the DNA by 13 °, σ was determined to be -0.059.[20]

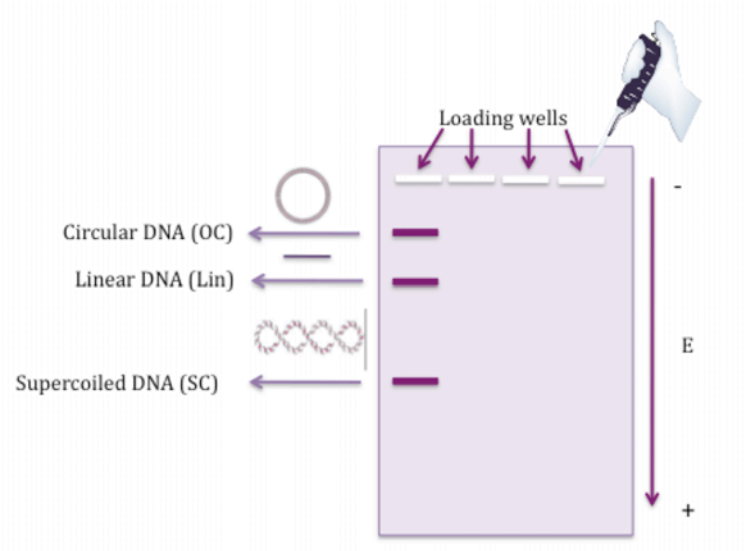

Figure 3.32 Picture exemplifying a Gel electrophoresis experiment using plasmid DNA.

3.8.1 Gel electrophoresis Studies with Complexes (1-6)

In order to assess whether the complexes induced plasmid DNA unwinding and/or cleavage, agarose gel (1%) experiments were carried out with each of the complexes.

Initial experiments were made using complexes **1** and **2** with plasmid DNA (pBR322). Plasmid solutions (100 μM) were incubated with different ratios of the complexes for a period of 2 hours at 37 °C. In order to confirm the stability of each complex at this temperature, UV-Vis spectra were carried out for a period of 2 hours under the same experimental conditions and no significant differences were registered. Table 3.4, shows the ratios of plasmid DNA:complex which were used in the gel electrophoresis experiments.

Table 3.4 Ratios of plasmid DNA (pBR322) and complex used in gel electrophoresis studies.

wells	c	1	2	3	4	5	6
DNA:Complex	DNA	20:1	12:1	8:1	6:1	5:1	3:1

The control plasmid DNA (lane c) contains a mixture of sc form in approximately 80% and oc form in 20%. From Figure 3.33 it is possible to observe that in the presence of both single stranded di-nuclear complexes (**1** and **2**) the sc form starts to run slower from lane 1 with the complexes binding and causing unwinding of the supercoiled DNA.

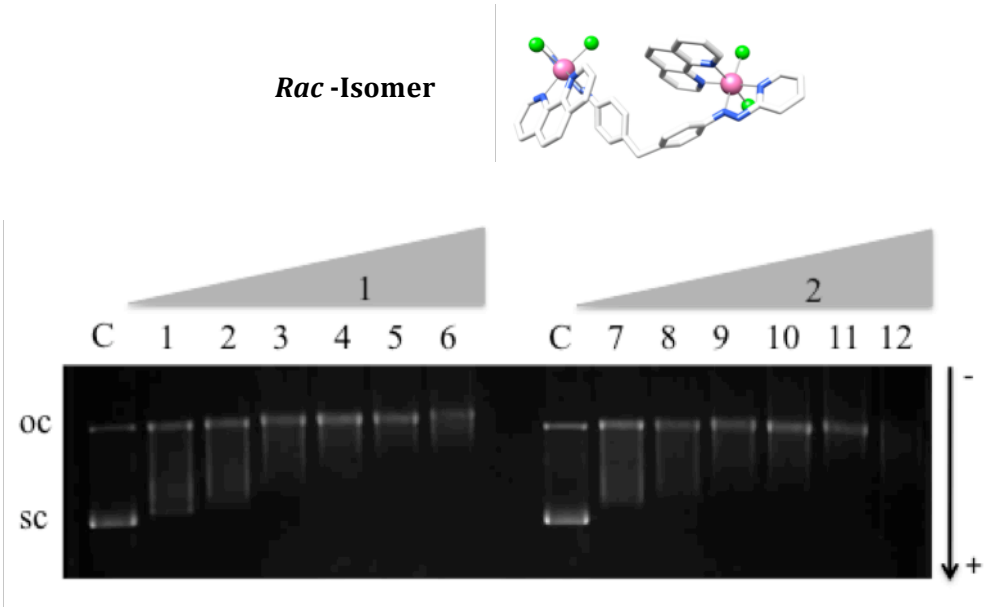

Figure 3.33 Agarose gel (1%) electrophoresis showing the changes in the electrophoretic mobility of the oc and sc forms of pBR322 plasmid DNA incubated for 2 hours at 37 °C with different ratios of complex **1** (lane 1-6) and complex **2** (lanes 7-12). Lane c, pBR322 plasmid DNA in absence of complex (control-c).

In addition, the presence of the complexes induces a decrease in the amount of sc form and the consequent increase of the nicked form (oc). This effect suggests that the complex binds and unwinds sc DNA and can induce single strand break to afford oc DNA. Both complexes have a very similar effect. The same experiment was carried out for the mononuclear analogue (complex **5**) and after two hours incubation of pBR322 with different ratios of **5** it was possible to observe that the presence of the complex had almost no effect on the DNA (Figure 3.34). The differences of binding effect between the di-nuclear and the mononuclear complexes observed by these gel electrophoresis experiments corroborate what was already seen by CD and LD measurements, with complex **5** showing much less binding to ct-DNA.

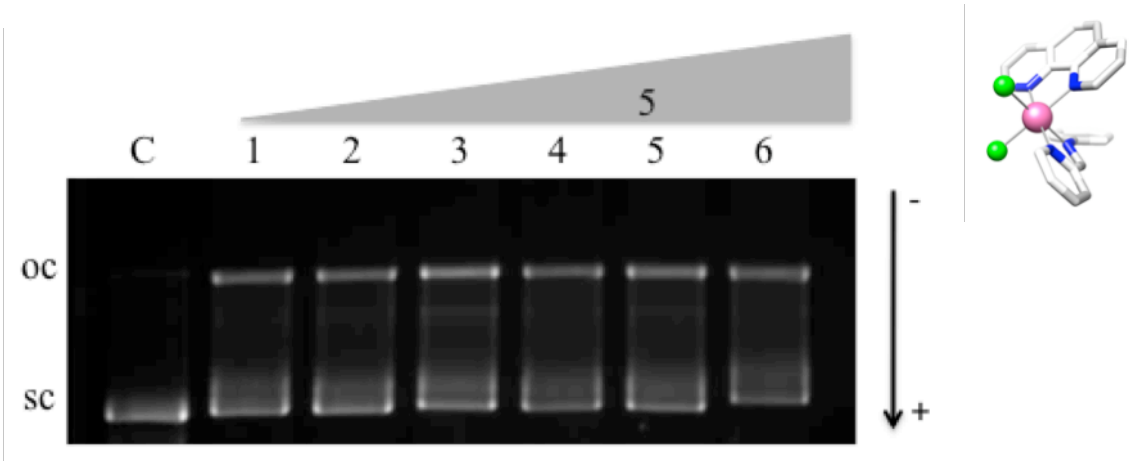

Figure 3.34 Agarose gel (1%) electrophoresis showing the changes in the electrophoretic mobility of the oc and sc forms of pBR322 plasmid DNA incubated for 2 hours at 37 °C with different ratios of complex **5** (lane 1-6). Lane c, pBR322 plasmid DNA in absence of complex (control-c).

To explore any coordinative binding effects, the complexes were incubated with the DNA for 24 hours instead of 2 hours. The ratios of DNA:complex were kept equal and experimental conditions used were the same. From Figure 3.35 is clear that the longer incubation time of **1** and **2** with plasmid DNA resulted in considerable higher cleavage effect compared with the incubation for 2 hours (Figure 3.33). From lanes 1 to 6 in Figure 3.35, the sc band disappears straight away from the lowest concentration of complex used and the oc band increases. For complex **2**, for the lowest concentration of complex (lane 7) the sc band could still be observed although with the slower mobility. On increasing the concentration of complex from lanes 8 to 11 this band was no longer observed. The major differences between this experiment and the 2 hours incubation experiment was the appearance of the new band with mobility between the sc and the oc forms, which was attributed to the linear form of plasmid DNA (lin). This band could easily be seen for complex **1** from lanes 1 to 5 and for complex **2** from lanes 8 to 11. The

photodamage effect was especially marked for the highest concentrations of complexes (lanes 6 and 12) where all the bands disappeared. Doing the same experiment with complex **5**, no linear DNA band was observed nor did the sc band disappear, although when compared with the gel of Figure 3.34 there was an increase of the amount of oc form of DNA from lanes 1 to 6 and a decrease in the amount of sc form. The stability of the three complexes in aqueous solution for periods of 24 hours at 37 °C was confirmed by UV-Vis spectroscopy with all three complexes being stable and no decomposition being observed.

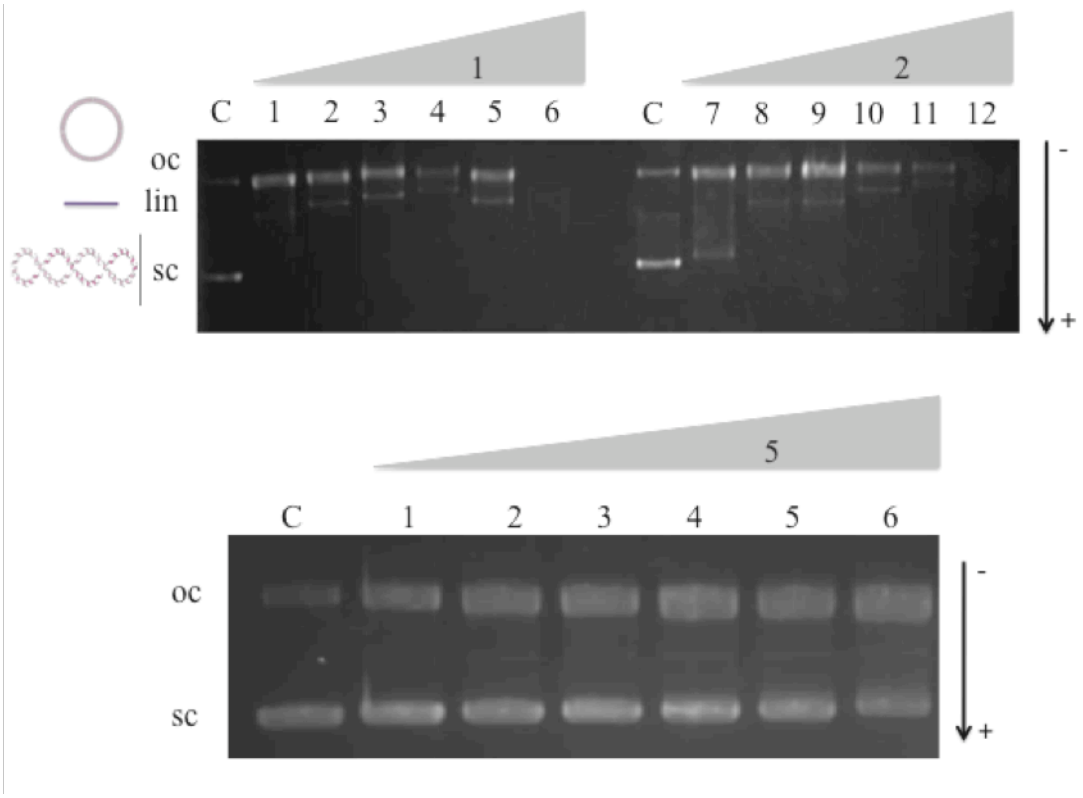

Figure 3.35 Agarose gel (1%) electrophoresis showing the changes in the electrophoretic mobility of the oc and sc forms of pBR322 plasmid DNA incubated for 24 hours at 37 °C (Top) with different ratios of complex **1** (lane 1-6) and complex **2** (lanes 7-12); (Bottom) with different ratios of complex **5** (lane 1-6). Lane c, pBR322 plasmid DNA in absence of complex (control-c).

A similar experiment was carried out with complexes **1** and **2**, in total dark conditions. The samples were prepared, incubated for 2 hours at 37 °C and run in the gel

in a dark room (data shown in A.23). From the gel is possible to see that although some DNA unwinding is observed for both isomers the effect is much less than when comparing with the samples, which were prepared and ran in the gel under normal sunlight conditions. This data might suggest that light is of importance for the DNA cleavage process to be more effective.

Complexes **3** and **4**, were similarly incubated with pBR322 for 2 hours at 37 °C. The agarose gel (1%) after staining (Figure 3.36) shows complex **4** to cause more DNA unwinding with the increased mobility of the sc band in comparison with complex **3**. Lane 12 shows disappearance of the sc form of the plasmid DNA and an increase of the amount of the oc form with slower mobility of the same band. The fact that complex **4** seems to affect the DNA more is consistent with CD and LD experiments. Comparing **3** and **4** with **1** and **2** reveals that complexes **1** and **2** exhibit a stronger DNA unwinding effect.

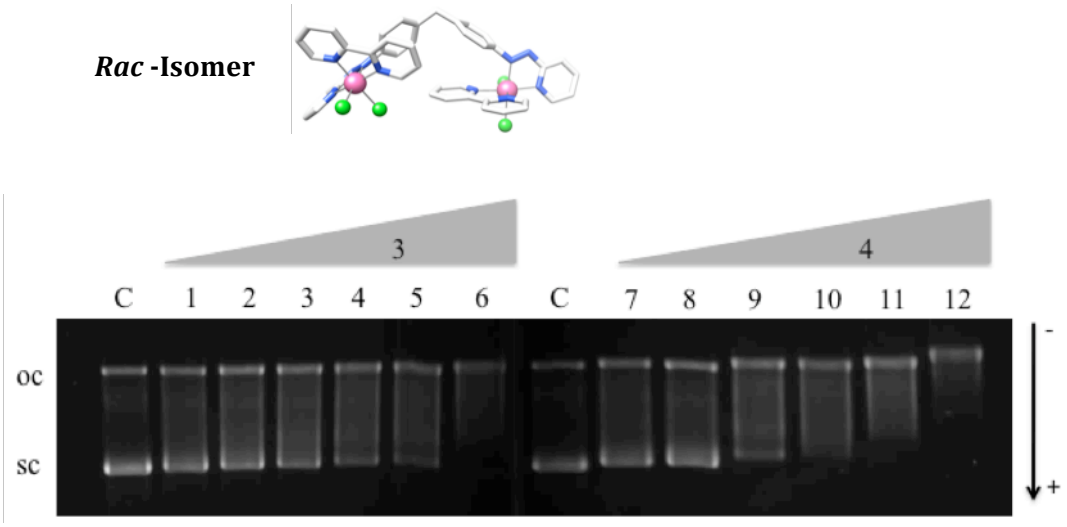

Figure 3.36 Agarose gel (1%) electrophoresis showing the changes in the electrophoretic mobility of the oc and sc forms of pBR322 plasmid DNA incubated for 2 hours at 37 °C with different ratios of complex **3** (lane 1-6) and complex **4** (lanes 7-12); Lane c, pBR322 plasmid DNA in absence of complex (control-c).

Complex **6** exhibits a similar effect to complex **5**, with almost no effect on plasmid DNA (Figure 3.37); a slight retardation of the sc band is observed for the highest ratio DNA:complex (lane 6) as well as an small increase on the oc form.

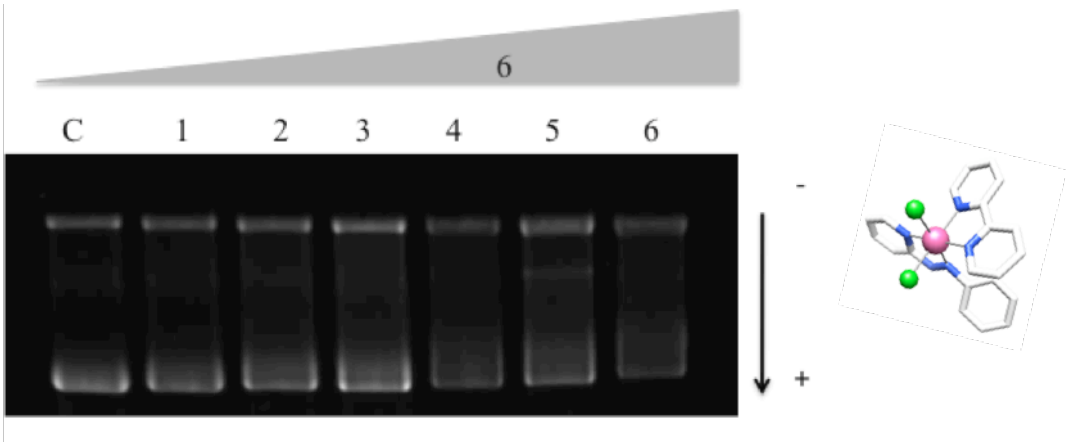

Figure 3.37 Agarose gel (1%) electrophoresis showing the changes in the electrophoretic mobility of the oc and sc forms of pBR322 plasmid DNA incubated for 2 hours at 37 °C with different ratios of complex **6**. Lane c, pBR322 plasmid DNA in absence of complex (control-c).

The 24 hours incubation experiment using **3** and **4**, revealed the complexes to cleave plasmid DNA with significant differences when compared with the same experiment carried out only for 2 hours. Once more complex **4** has a greater effect. From lanes 1 to 6 and 7 to 12 (Figure 3.38) it is possible to observe the nicking of the DNA, with the amount of oc increasing when the concentration of the complex bound to plasmid DNA increases. Interestingly, it is suggested that complex **4**, after 24 hours incubation is able to cleave both DNA strands with appearance of a linear form of DNA from lane 9, which is not evident for complex **3**. The mononuclear analogue, complex **6**, shows an increase on the unwinding of DNA with a retardation of the sc band more marked when compared with the 2 hours incubation with a consecutive increase of the oc form.

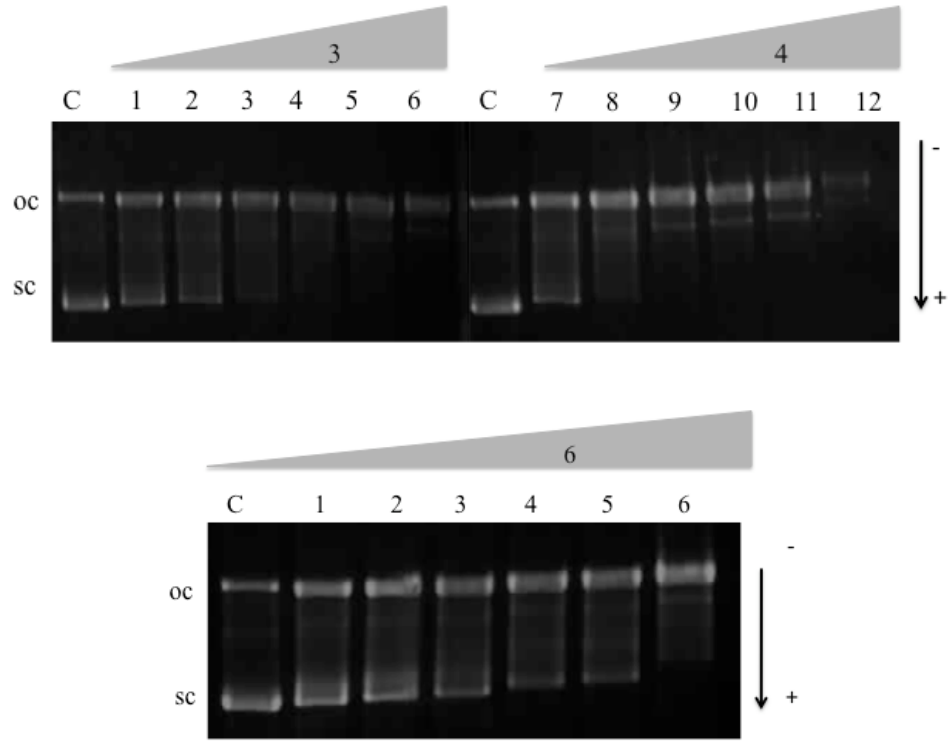

Figure 3.38 Agarose gel (1%) electrophoresis showing the changes in the electrophoretic mobility of the oc and sc forms of pBR322 plasmid DNA incubated for 24 hours at 37 °C (Top) with different ratios of complex **3** (lane 1-6) and complex **4** (lanes 7-12); (Bottom) with different ratios of complex **6** (lane 1-6). Lane c, pBR322 plasmidDNA in absence of complex (control-c).

Table 3.5 shows the values of the unwinding angles for complexes **1** to **6** after 2 hours incubation of each of them with pBR322 at 37 °C. The dinuclear single stranded complexes show higher unwinding angles when compared with cisplatin, which is reported to unwind plasmid DNA by 13 °.[20] The mononuclear complex **5** has a slightly lower unwinding angle when compared with cisplatin while complex **6** is less effective. Complexes **3** and **4** show unwinding angles inferior to cisplatin but more interesting is the big difference in comparison with **1** and **2**, corroborating the spectroscopic results obtained before; complexes **1** and **2** affecting the ct-DNA by CD and LD more strongly than **3** and **4**.

Table 3.5 Unwinding angles (Φ) calculated for complexes **1** to **6** after 2 hours at 37 °C incubation with pBR322.

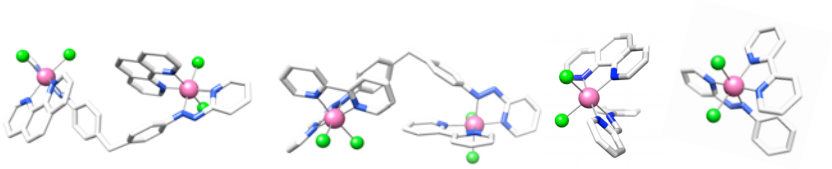

Complexes	**1** ***rac***	**2** ***meso***	**3** ***rac***	**4** ***meso***	**5**	**6**	**cisplatin**
Φ values (°)	30	35	10	11	10	6	13

3.8.2 Gel Electrophoresis Studies with Complexes 7 and 8

The gel in Figure 3.39 (top) shows that both double stranded complexes **7** and **8**, after 2 hours incubation are able to cleave plasmid DNA. For complex **8**, the sc form disappears straight away from the second concentration used (lane 8) and there is a subsequent increase of the oc form of DNA. From lane 10 it is almost impossible to observe any DNA bands, either because of complete fragmentation or because the complex is bound to DNA, making intercalation of the stain ethidium bromide more difficult and therefore preventing the subsequent UV visualization. The same happens for complex **7** in lane 6.

After 24 hours of incubation of the complexes with pBR322 (Figure 3.39 bottom), it is evident that both complexes are able to double cleave plasmid DNA; from lanes 1 and 7 the existence of linear form of DNA is clear. On increasing the concentration of the complex, from lanes 4 to 6 and 10 to 12, the interaction of the complex with DNA

becomes stronger and once more it becomes harder to visualize the bands after staining of the agarose gel.

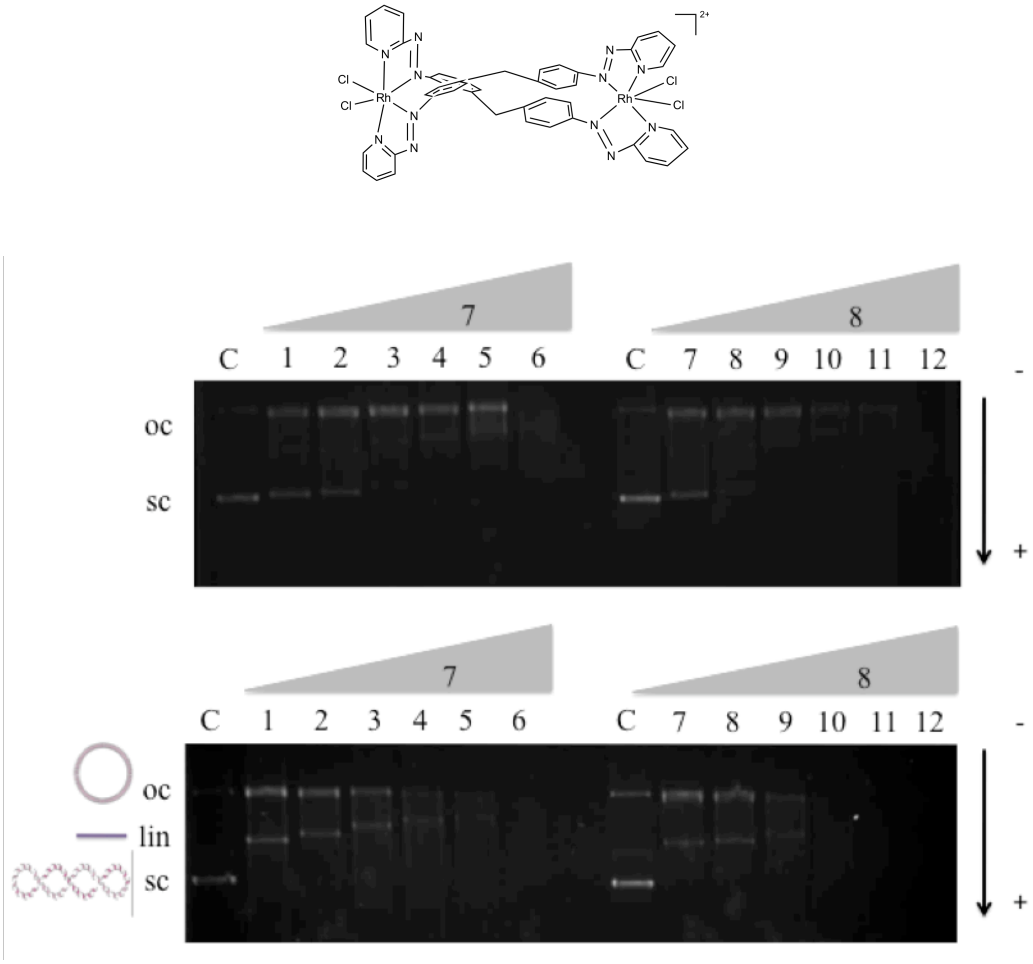

Figure 3.39 Agarose gel (1%) electrophoresis showing the changes in the electrophoretic mobility of the oc and sc forms of pBR322 plasmid DNA incubated for 2 hours at 37 °C (Top) with different ratios of complex **7** (lane 1-6) and complex **8** (lanes 7-12); (Bottom) pBR322 plasmid DNA incubated for 24 hours at 37 °C with different ratios of complex **7** (lane 1-6) and complex **8** (lanes 7-12); Lane c, pBR322 plasmid DNA in absence of complex (control-c).

3.8.3 Gel Electrophoresis Studies with Complex 10

At low concentrations of the triple stranded complex, it is possible to distinguish oc and sc bands in the gel. As the concentration of the complex increases, the mobility of the sc form of plasmid DNA decreases and there is an increase of the amount of the oc form suggesting some cleavage (Figure 3.40). This shows that the complex is binding and unwinding structure of the DNA, decreasing the mobility of the sc band. Although it is apparent that an increase in the concentration of complex results in an increase in DNA binding, this is less effective than for the Hannon's Fe(II) and Ru(II) triple helicates which unwind pBR322 with angles of 27 ° and 13 ° respectively.[21] The value of the unwinding angle for complex **10** could not be calculated, as the oc and sc bands did not co-migrate for the concentrations used in these experimental studies. As regarding the other Rh(III) complexes presented, it seems that complex **10** is less effective in unwinding plasmid DNA although CD and LD studies showed that the complex strongly coils ct-DNA.

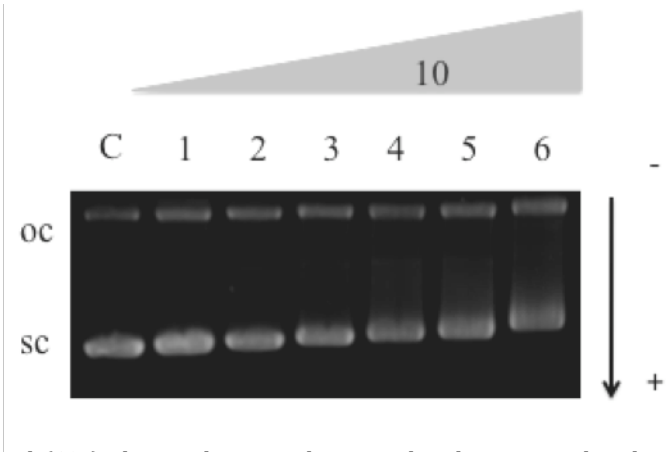

Figure 3.40 Agarose gel (1%) electrophoresis showing the changes in the electrophoretic mobility of the oc and sc forms of pBR322 plasmid DNA incubated for 2 hours at 37 °C with different ratios of complex **10** (lane 1-6); Lane c, pBR322 plasmid DNA in absence of complex (control-c).

3.9 Studies with Mononucleotide Models

In order to further study how the different isomers bind to DNA and verify if they can coordinatively bind to DNA, interactions with model nucleobases were studied. Preliminary studies involved the use of complexes **1** and **2** (single stranded with phen ligands) and the different nucleobases: guanosine 5'monophosphate (5'-GMP) and 9-ethylguanine (Figure 3.41).

ESI-MS was used to investigate the interaction since the ^{1}H-NMR spectra of the complexes in D_2O could not be obtained (gel formation).

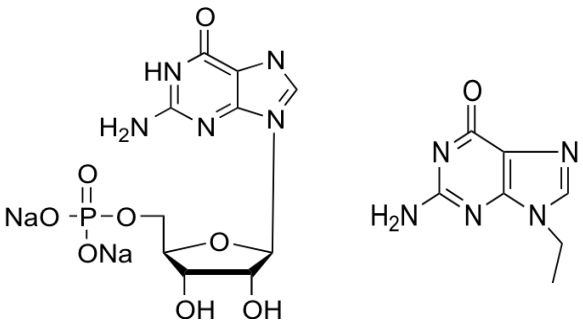

(5'-GMP) **(9-EG)**

Figure 3.41 Structure of DNA model nucleobases 5'-GMP and 9EG.

Complexes **1** and **2** were incubated with four equivalents of nucleobase in 1 mM TAA buffer (pH 7.0) at 37 °C. An ESI-MS spectrum of each complex in the presence of base was recorded at time 0, 2, 24 and 48 hours. ESI–MS confirm that adducts are formed for the two isomers after 24 hours of incubation at 37 °C. Both complexes showed the same behaviour and presented the same adduct patterns. Similar experiments carried out using sodium cacodylate buffer did not prove effective, perhaps because of buffer interference with ESI.

The spectra at time 0 hours and 2 hours show no peaks that can suggest the covalent binding of the nucleobase to the complex. At these times only doubly charged peaks $[M_2(L_{azo})_2X_4]^{2+}$ of the complexes were observed, although with some replacement of the chloride ligands with methanol (the solvent used to spray the sample in the MS-ESI). After 24 hours of incubation, although the major peaks are still those of the starting complex, small doubly charged peaks started to appear at higher *m/z* values. After 24 hours small fragments with *m/z* 671 $[Rh_2(L_{azo})(phen)_2(5'\text{-GMP})\text{-}4H^+]^{2+}$, 687 $[Rh_2(L_{azo})(phen)_2(5'\text{-GMP})(H_2O)+4H^+]^{2+}$, 694 $[Rh_2(L_{azo})(phen)_2Cl(5'\text{-GMP})+H^+]^{2+}$ appeared in the ESI-MS of complexes **1** and **2** suggesting the covalent binding of the complex to the 5'-GMP, by coordination of guanine N7 replacing a chloride ligand.
No changes were observed in the ESI-MS after 48 hours with no increase of the peaks already existent or new fragments formed (data shown in A.24-A.27).

The same experiment was carried out for one of the mononuclear complexes. The ESI-MS of complex **5** after incubation with the nucleobase exhibited no adducts between complex and nucleobase. The ESI-MS of the complex remained the same during the 48 hours.

Although efforts were made to prepare an adduct using a different nucleobase (9EG) under the same conditions, no adducts were observed by ESI-MS.

Nevertheless these studies with 5-GMP confirm that coordinative binding of the nucleobases to complexes **1** and **2** is possible lending support to the observations on complexes with ct-DNA by CD, LD and gel electrophoresis.

3.10 Conclusions

DNA binding studies were performed by CD and LD spectroscopy and gel electrophoresis, using ct-DNA and the Rh(III) complexes.

CD studies with **1** and **2** showed that both complexes bind to DNA with similar effect inducing a CD signal in the visible region (330 and 450 nm) although without affecting the B-DNA conformation. This effect is much reduced when comparing with the mononuclear analogue, complex **5**, which does not induce any CD signal in the complex region but produces minor changes in the DNA absorbance with the B-DNA conformation being retained. In addition CD studies with poly[G-C] and poly[A-T] sequences suggested that **1** and **2** might prefer GC rich sequences compared to AT, however the effect is less marked when compared with ct-DNA. The LD spectra of **1** and **2**, show that both complexes are able to bend/coil ct-DNA to similar extend. Positive ILD bands in the 300-500 nm region confirm the binding of the complexes to ct-DNA in a specific orientation and not randomly, and probably to the DNA major groove. The LD spectrum of **5**, shows that the complex is still able to coil and bend ct-DNA although to a lesser extent than **1** and **2**.

MS studies made with DNA mononucleotide models confirm that coordinative binding might occur after 24 hours incubation: complexes **1** and **2** with 5-GMP showed peaks of base-complex adducts.

The CD spectra of complexes **3** and **4**, show that the complexes bind to ct-DNA without affecting the B-DNA conformation and showing ICD signals in the 311 and 439 nm region. The CD spectrum of complex **6**, the mononuclear analogue, shows that the complex has practically no affinity towards ct-DNA, with the DNA absorbing region

almost not being affected and no appearance of an ICD signal in the visible region of the spectrum. LD studies on these complexes support the observations made by CD spectroscopy, with both di-nuclear (**3** and **4**) being able to coil and bend ct-DNA in a specific orientation (confirmed by the ILD positive bands). On the other hand complex **6**, in a similar way to **5**, shows a small amount of DNA coiling and bending although in the LD spectra of **6** it is possible to observe a slight ILD signal suggesting that the interaction of the complex with the DNA occurs in a specific orientation.

Complexes **1** and **2** exhibit stronger DNA binding affinities by CD and LD when compared with **3** and **4** while the mononuclear complexes **5** and **6** seem to have very similar effects between them.

Gel electrophoresis studies corroborated the results obtained with the spectroscopic methods. Complexes **1**, **2**, **3** and **4** are able to unwind and cleave plasmid DNA. 24 hours incubation experiment led to formation of linear DNA (double strand cleavage) although **1** and **2** have stronger effect. Unwinding of plasmid DNA is much reduced for complexes **5** and **6**.

CD and LD spectra of the di-nuclear double stranded complexes (**7** and **8**) show that both complexes are able to bind strongly to ct-DNA causing it to bend/coil with **8** exhibiting a stronger effect than **7**. Complex **7** has a very similar coiling/bending effect on ct-DNA, while **8** definitely has a stronger effect. Both di-nuclear complexes (single and double stranded) have same overall charge and the differences observed suggest that structure, together with different geometry of the complexes, is of high importance for the DNA binding affinities. Also, CD studies with **8** and poly[G-C] and poly[A-T] suggested that the complexes might prefer GC but once again, like with **1** and **2**, the interaction is less marked than with ct-DNA.

Gel electrophoresis studies with **7** and **8** show that both complexes singly cleave plasmid DNA and after 24 hours incubation linear DNA is observed.

Complex **10** (di-nuclear triple stranded complex) binds strongly through a single binding mode to ct-DNA with the CD spectrum showing a strong positive ICD signal in the MLCT region and with the B-DNA conformation being retained although strongly affected. The LD spectrum shows that the complex is an effective DNA coiling agent with 62% of DNA LD signal lost. According to the estimated K_b value, this complex shows the higher value when compared with the single and double stranded dinuclear Rh(III) complexes, as expected due to the increased overall charge and different structure, however the value is lower than for the parent Fe(II) and Ru(II) cylinders.

The interesting differences in the DNA binding affinities found between the complexes encouraged the work presented in the next chapter (Chapter 4) in which the aim is to explore how the DNA binding affinities relates to the biological activity of the complexes in cancer cell lines.

3.11 Experimental

3.11.1 Materials

Ultrapure water (18.2 MX, Fisher) was used in all Circular and Linear dichroism experiments, electrophoresis gel and for the 5'-GMP experiments. Poly[G-C], Poly[A-T] and ct-DNA (highly polymerised) were purchased from Sigma–Aldrich and were dissolved in water without any further purification. Stock solutions of the different DNA polymers were kept frozen until the day of use. The DNA concentrations of those stocks were determined by UV–Vis measurements using the known molar-extinction coefficient of ε_{258} = 6600 mol^{-1} dm^3 cm^{-1} per DNA base for ct-DNA, ε_{258} = 6600 mol^{-1} dm^3 cm^{-1} per DNA base for Poly[A-T] and ε_{258} = 8400 mol^{-1} dm^3 cm^{-1} per DNA base for Poly [G-C]. Stock solutions of 1 M NaCl and 100 mM sodium cacodylate buffer (pH 6.8) were prepared and together with ct-DNA stock, were used to obtain final solutions of ct-DNA 300 μM, NaCl 20 mM and sodium cacodylate 1 mM. Commercially available Tris acetate–EDTA (TAE, from Fisher) working buffer was used for gel electrophoresis of pBR322 plasmid DNA purchased from New England Biolabs.

3.11.2 CD Experiments

For CD experiments, spectra were collected in cuvettes of 1 cm (750–200 nm region) pathlength, using a Jasco J-715 spectropolarimeter. Spectroscopic titrations were performed from which CD absorption spectra were recorded. For each titration three solutions were prepared: solution A of ct-DNA (300 μM or 80 μM), NaCl (20 mM) and sodium cacodylate buffer (10 mM); stock solution B of complex in water (500 μM or 170

μM); stock solution C of ct-DNA (600 μM or 160μM), NaCl (40 mM) and sodium cacodylate buffer (20 mM). First solution A was recorded to have the CD spectrum of DNA without complex. Then the titration was performed decreasing the DNA:complex ratio from 60:1 to 4:1 by adding aliquots of solution B. For each volume of solution B, the same volume of solution C was added to ensure that the concentration of ct-DNA, NaCl and sodium cacodylate remained unaltered.

3.11.3 Flow LD Experiments

Flow LD spectra were collected using a flow Couette cell (Krometek) in a Jasco J-715 spectropolarimeter adapted for LD measurements. Long molecules, such as DNA can be orientated in a flow Couette cell. The flow cell consists of a fixed outer cylinder and a rotating solid quartz inner cylinder, separated by a gap of 0.5 mm, giving a total pathlength of 1 mm. The titration was identical to that described for the CD experiment.

3.11.4 Gel Electrophoresis Experiments

The electrophoresis experiments were carried out using gel trays of 210 x 150 mm with a 15-toothed comb to produce the sample wells. An Electrophoresis Power Supply-EPS 301 system was used as a constant voltage supply set to 120 V and 300 mA. The gel was prepared by warming up 2 g of agarose (from USB Corporation) in 1x Tris acetate buffer (1xTAE, which was obtained by dilution of 100 ml of 10 x TAE, supplied by SIGMA, in 1 L of water). The same 1 x TEA buffer was used as a working buffer. The solutions to analyze were prepared in a volume of 16 μl containing: 96.3 μM pBR322

plasmid DNA, where required and different concentrations of complexes (from 50 μM stock solution in water) to obtain solution with different plasmid:complex ratio. The solutions were incubated for 2 and 24 hours at 37 °C and then 4 μl of loading buffer (30% glycerol and 0.25% bromophenol blue in ultra pure water) was added. Sixteen microlitres of each solution were loaded and the samples ran for 2 hours and 20 minutes. After electrophoresis the gel was stained for 60 minutes in 400 ml of 1 x TEA buffer containing an ethidium bromide solution ($1\mu g.ml^{-1}$). The gel was visualized using an UVtec -uvipro platinum system. The gel bands were integrated using ImageJ [†]software and values plotted using KaleidaGraph 4.0 software.

3.11.5 DNA Model Nucleobases Experiments

ESI-MS Nucleotide binding studies: 5'-GMP and 9EG were purchased for Sigma-Aldrich, stored at 4°C in a dessicator and used without any further purification. They were dissolved in 1 mM TAA buffer (pH 7.0) before each experiment. Fresh solutions of complexes in 1 mM TAA buffer (pH 7.0) were used. The stock solution of base was (4 mM) and of complex (0.5 mM). The solutions were mixed to have a final ratio base:complex of 4:1 in a final volume of 100 μl. The solutions were incubated for 48 hours at 37 °C in the dark. ESI-MS spectra were taken of freshly prepared mixtures of base plus complex and after 2, 24, 48 hours. The optimal ESI (+) conditions for observing the peaks of the complexes and complex plus base were found to be a cone voltage of 10 eV using methanol as a spray solvent.

[†] **ImageJ Software**, National Institutes of Health, USA.

3.11.6 Synthesis of the Fe (II) Triple Helicate $[Fe_2(L_{im})_3](PF_6)_4$[22]

The L_{im} and the racemic and $[Fe_2(L_{im})_3](PF_6)_4$ were synthesized according to literature procedures.[22] Three equivalents of L_{im} and 2 equivalents of iron (II) chloride were heated under reflux in methanol for 2 hours. The resulting purple colored solution was cooled to room temperature and the respective PF_6 salt of the complex was re-precipitated from a saturated methanolic NH_4PF_6 solution. The purple precipitate of $[Fe_2(L_{im})_3](PF_6)_4$ was isolated by filtration and abundantly washed with methanol.

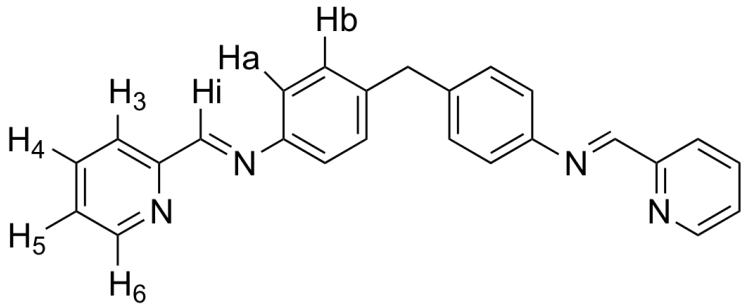

Figure 3.41- Chemical structure of L_{im}.

Positive-ion ESI (30 eV, CH_3CN): *m/z* (%) 311 $[Fe_2(L_{im})_3]^{4+}$(100), 421 $[Fe_2(L_{im})_3F]^{3+}$(10), 462 $[Fe_2(L_{im})_3(PF_6)]^{3+}$ (20).

^{1}H-NMR (300 MHz, CD_3CN, 25 °C, TMS): δ = 8.87 (s, 1H, H_i), 8.51 (d, 1H, *J* = 7.7 Hz, H_3), 8.36 (t, 1H, *J* = 7.7 Hz, H_4), 7.72 (t, 1H, *J* =7 .7 Hz, H_5) 7.31 (d, 1H, *J* = 4.8 Hz, H_6), 6.90 (br, 2H, $H_{a/b}$), 5.48 (br, 2H, $H_{a/b}$), 3.99 (s, 1H, CH_2).

Exchange of counter anion from PF_6^- to Cl^- was obtained by treating $[Fe_2(L_{im})_3](PF_6)_4$

with ion exchange resin (Dowex® 1X8 chloride form, 100-200 mesh, supplied by Sigma-Aldrich) in water. The resulting purple solution was freeze dried.

^{1}H-NMR (300 MHz, D_2O, 25 °C, TMS): δ = 8.89 (s, 1H, H_i), 8.44 (d, 1H, *J* = 7.7, H_3), 8.27 (t, 1H, *J* = 7.7 Hz, H_4), 7.58 (t, 1H, *J* = 6.6 Hz, H_5), 7.27 (d, 1H, *J* = 5.5 Hz, H_6), 7.10 (br, 2H, $H_{a/b}$), 6.60 (br, 2H, $H_{a/b}$), 3.89 (s, 1H, CH_2).

3.12 References

[1] B. N. A. Roger, *Circular and Linear Dichroism*, Oxford University Press, **1997**.

[2] M. Eriksson, B. Norden, *Drug-Nucleic Acid Interactions* **2001**, *340*, 68.

[3] G. I. Pascu, A. C. G. Hotze, C. Sanchez-Cano, B. M. Kariuki, M. J. Hannon, *Angew. Chem., Int. Ed.* **2007**, *46*, 4374.

[4] I. Meistermann, V. Moreno, M. J. Prieto, E. Moldrheim, E. Sletten, S. Khalid, P. M. Rodger, J. C. Peberdy, C. J. Isaac, A. Rodger, M. J. Hannon, *Proc. Natl. Acad. Sci. U. S. A.* **2002**, *99*, 5069.

[5] M. J. Hannon, V. Moreno, M. J. Prieto, E. Moldrheim, E. Sletten, I. Meistermann, C. J. Isaac, K. J. Sanders, A. Rodger, *Angew. Chem., Int. Ed.* **2001**, *40*, 880.

[6] M. A. Galindo, D. Olea, M. A. Romero, J. Gomez, P. del Castillo, M. J. Hannon, A. Rodger, F. Zamora, J. A. R. Navarro, *Chem.Eur. J.* **2007**, *13*, 5075.

[7] F. H. Stootman, D. M. Fisher, A. Rodger, J. R. Aldrich-Wright, *Analyst* **2006**, *131*, 1145.

[8] J. Malina, M. J. Hannon, V. Brabec, *Chem.Eur. J.* **2008**, *14*, 10408.

[9] J. C. Peberdy, J. Malina, S. Khalid, M. J. Hannon, A. Rodger, *Journal of Inorganic Biochemistry* **2007**, *101*, 1937.

[10] I. Meistermann, *DNA Major Groove Recognition by Supramolecular Helicates, PhD.Thesis*, University of Warwick, Coventry, **2001**.

[11] M.Pascu, *Supramolecular architectures: using shape to encode aggregation or function, PhD.Thesis*, University of Birmingham, Birmingham, **2007**.

[12] P. K. L. Fu, P. M. Bradley, C. Turro, *Inorg. Chem.* **2003**, *42*, 878.

[13] R. E. Holmlin, J. A. Yao, J. K. Barton, *Inorg. Chem.* **1999**, *38*, 174.

[14] A. A. Holder, D. F. Zigler, M. T. Tarrago-Trani, B. Storrie, K. J. Brewer, *Inorg. Chem.* **2007**, *46*, 4760.

[15] S. Swavey, K. J. Brewer, *Inorg. Chem.* **2002**, *41*, 6196.

[16] J. Talib, D. G. Harman, C. T. Dillon, J. Aldrich-Wright, J. L. Beck, S. F. Ralph, *Dalton Trans.* **2009**, 504.

[17] T. W. Johann, J. K. Barton, *Philosophical Transactions of the Royal Society of London Series a-Mathematical Physical and Engineering Sciences* **1996**, *354*, 299.

[18] J. Toneatto, R. A. Boero, G. Lorenzatti, A. M. Cabanillas, G. A. Arguello, *Journal of Inorganic Biochemistry* **2010**, *104*, 697.

[19] C. J. Burrows, J. G. Muller, *Chem.Rev.* **1998**, *98*, 1109.

[20] S. F. Bellon, J. H. Coleman, S. J. Lippard, *Biochemistry* **1991**, *30*, 8026.

[21] J. Malina, M. J. Hannon, V. Brabec, *Nucleic Acids Res.* **2008**, *36*, 3630.

[22] M. J. Hannon, C. L. Painting, A. Jackson, J. Hamblin, W. Errington, *Chem. Commun.* **1997**, 1807.

Chapter 4

Biological Activity and PCR Studies of Rh(III) complexes

4.1 Introduction

As discussed previously in chapter 1 the parent cylinders with Fe(II) and Ru(II) metal centers both exhibited cytotoxic activity in different cancer cell lines. The iron cylinder shows activity comparable with carboplatin and further biological tests showed that it is not mutagenic or genotoxic, which represents a big advantage over cisplatin. More exciting is the cytotoxicity exhibited by the dinuclear double stranded Ru(II) complexes synthesized by Hotze that showed activity comparable to cisplatin in both breast and ovarian cancer cell lines with some isomers exhibiting activity ten times higher than cisplatin. The fact that these dinuclear unsaturated helicates exhibited higher activity than the saturated triple helicates corroborates the design concept that incorporating coordinative DNA binding as well as the cylinder architectures might lead to enhanced biological activity.

For this reason it was pertinent to investigate and evaluate the cellular activity of the newly synthesized rhodium (III) complexes. For these studies, two different cancer cell lines were chosen, MDA-MB-231 (breast) and A2780 (ovarian), and MTT assays were carried out to measure the IC_{50} values for each complex.

These biological studies were made in a direct collaboration with Victoria Sadovnikova and Laura Rowley from the Hannon Group and all the experiments were performed in the School of Biosciences of University of Birmingham†.

4.2 Cytotoxic activity by MTT Assay

The most common method to study the cytotoxicity of a new compound is to measure its half maximal inhibitor concentration (IC_{50}) value. This is a measure of the concentration of a drug needed in order to inhibit a certain biological process by half. In a specific case for a complex, the respective IC_{50} value is the complex concentration needed to reduce by half the viability of cancer cells. The lower the IC_{50} of a drug, the higher the cytotoxic activity. The cell lines MDA-MB-231 and A2780 were treated with complexes **1**, **2**, **5** and **6** (Figure 4.1) and cisplatin as a control drug used as a standard for further comparisons.

† Due to the limit access to the School of Biosciences facilities I could not be directly involved undertaking each of the MTT assays for the determination of the IC_{50} values alone but I was able to follow and participate in the procedure several times to become familiar and to further understand the results present herein.

***cis*-[Rh(L_{azpy})(phen)Cl_2]Cl (5)**

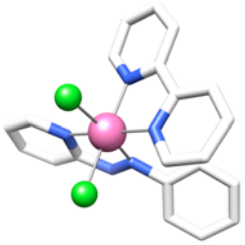

***cis*-[Rh(L_{azpy})(bpy)Cl_2]Cl (6)**

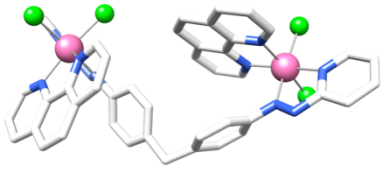

***rac*-[Rh_2(L_{azo})(phen)$_2Cl_2$]Cl_2 (1) and *meso*-(2, not shown)**

Figure 4.1 Molecular structure of the complexes used for MTT assay.

Complexes **7** and **8** (Figure 4.2) were tested only in the MDA-MB-231 cell line. Further IC_{50} values in other cancer cell lines are ongoing but no further results were available at the conclusion of this thesis.

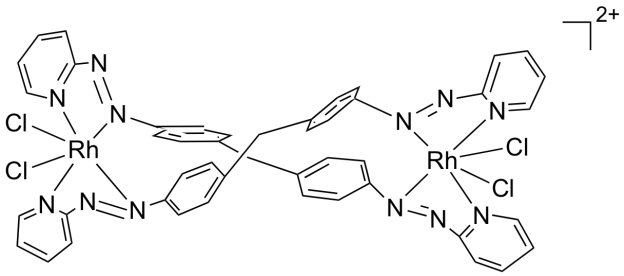

Rh_2(L_{azo})$_2Cl_4$]Cl_2 (7 and 8)

Figure 4.2 Chemical structure of the complexes used for MTT assay.

Cell growth and details of the incubation of the complexes with each cell line are described in the experimental section (4.6.2 and 4.6.3). IC_{50} values were calculated by a colorimetric test, MTT assay.[1] The MTT yellow reagent (3-(4,5-dimethylthiazol-2-yl)-2,5-diphenyl-2H-tetrazolium bromide) is reduced to purple formazan by the mitochondrial reductase in the living cells (Scheme 4.1).

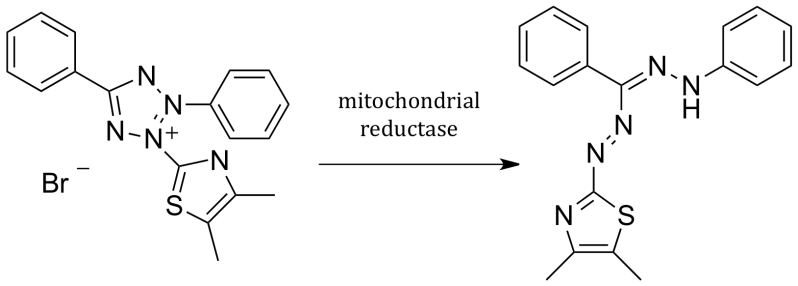

Scheme 4.1 Reduction of the MTT reagent to formazan by the mitochondrial reductase in living cells.

Upon treatment of each cell line with the complexes, MTT reagent is added and upon 2 hours of incubation, UV-Vis detection measures the quantity of formazan formed which is proportional to the amount of living cells after treatment with the complexes.

4.3 IC_{50} for Rhodium (III) Complexes 1, 2, 5, 6, 7 and 8

The stability of the complexes **1**, **2**, **5** and **6** in aqueous medium was recorded over the time period of the cell tests (72 hours), at 37 °C in order to verify if the compounds remained stable in solution over this period. For this, UV-Vis spectroscopy was used with spectra recorded every 30 minutes for 72 hours at 37 °C. Figure 4.3 shows UV-Vis spectra of aqueous solution of the complexes carried out fresh and after incubation.

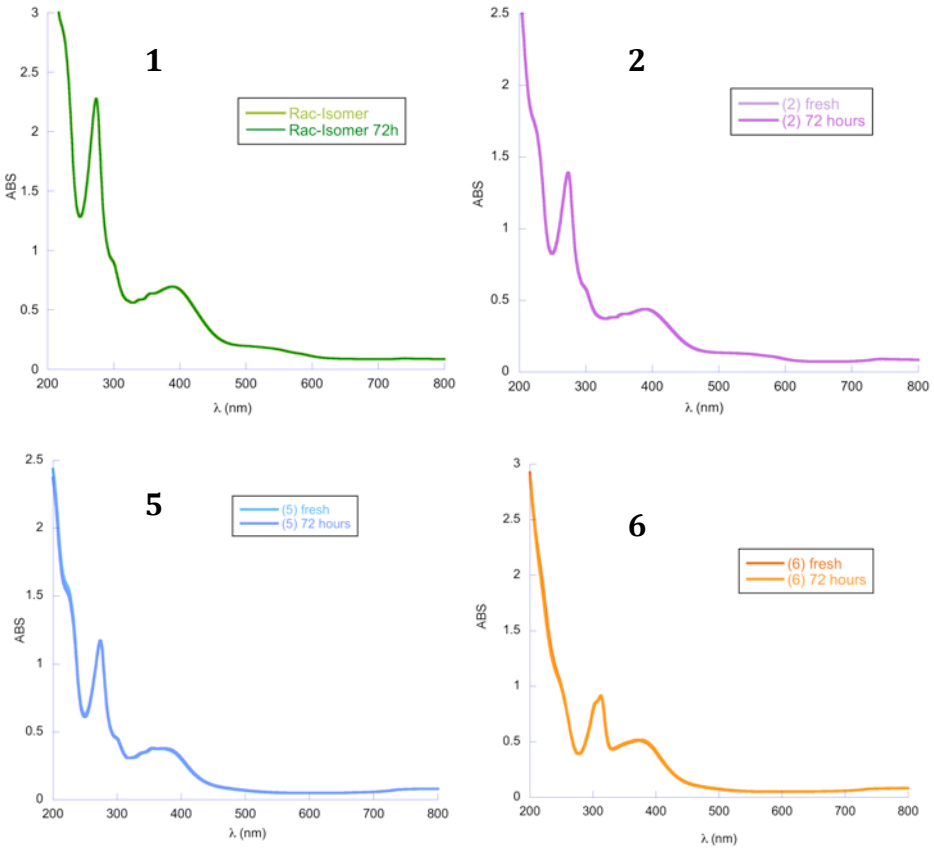

Figure 4.3 UV-Vis spectra of complexes **1**, **2**, **5** and **6** in water. Spectra of freshly made solutions and after 72 hours at 37 °C.

From the spectra above is clear that all four complexes, remain stable throughout the 72 hours period under these conditions.

Complexes **7** and **8** were also evaluated for their stability properties in aqueous medium for 72 hours at 37 °C. UV-Vis spectra of fresh solutions and after incubation can be observed in Figure 4.4.

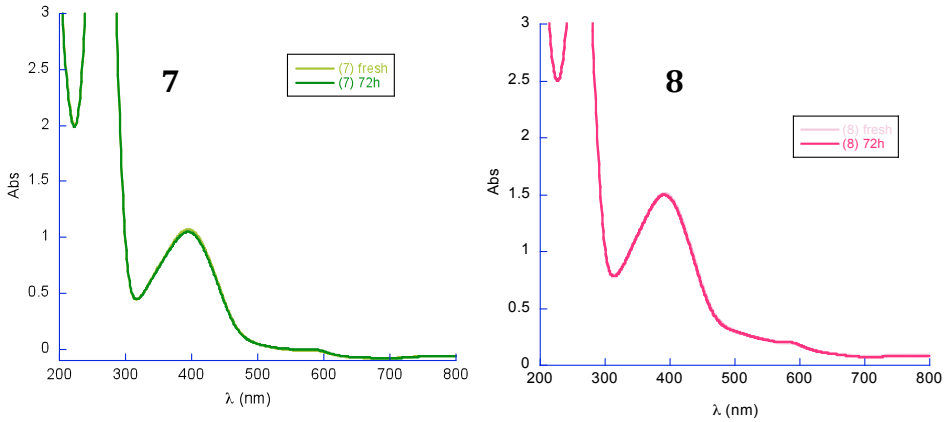

Figure 4.4 UV-Vis spectra of complexes **7** and **8** in water. Spectra of freshly made solutions and after 72 hours at 37 °C.

The two human cancer cell lines (MDA-MB-231 and A2780) chosen for these studies were treated with complexes **1**, **2**, **5** and **6** and cisplatin. Table 4.1 and Chart 4.1 report the IC_{50} values measured for the four complexes in μM. The first important result is that both dinuclear Rh(III) single stranded complexes (**1** and **2**) exhibit similar cytotoxic activity against the breast cancer cell line although less than cisplatin. These result is in accordance with the DNA binding studies showing that both complexes have very similar effect on B-DNA and also both are able to cleave plasmid DNA to the same extent, with complex **2** being slightly more effective than **1**. When the ovarian cancer line (A2780) was tested neither complex was active.

Chart 4.1 IC_{50} (μM) values for complexes **1** and **2**, **5, 6** and cisplatin.

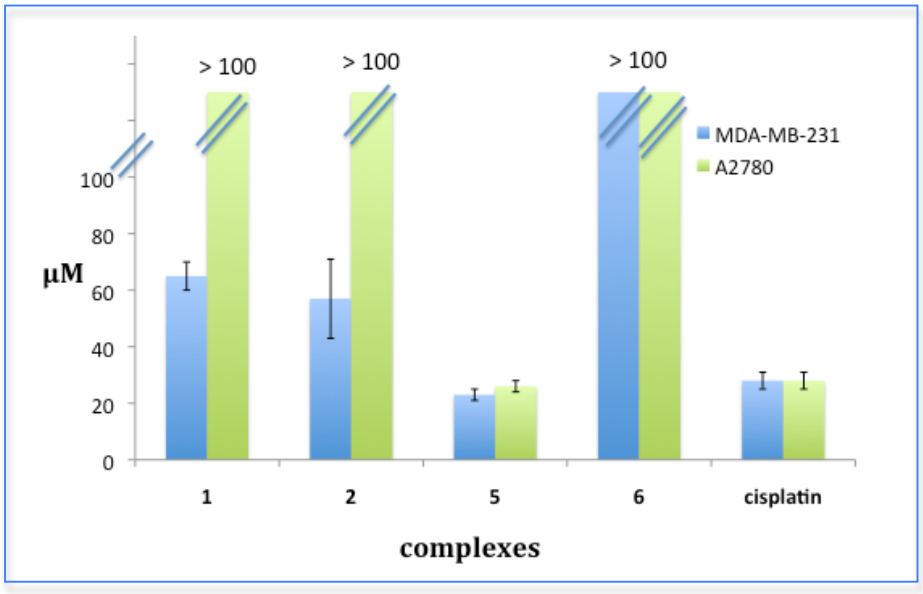

The most surprising result is the cytotoxic activity observed for complex **5**, the mononuclear analogue of **1** and **2**. This complex shows a very similar activity in both cell lines tested with activity equivalent to cisplatin. These results are somewhat unexpected as the DNA binding studies of this complex using CD and LD (chapter 3, section 3.4.1, 3.7.1) showed that the complex almost did not have a significant effect on DNA when compared with the dinuclear analogues. In addition, gel electrophoresis studies showed that **5** did not cause as much plasmid DNA unwinding as **1** and **2** (chapter 3 section 3.8.1). This may suggest that this complex has a different mode of action to cisplatin, perhaps with DNA not the only biological target. In fact, recent reports show that DNA may indeed not be the only target for several metal complexes and that other cellular targets and modes of actions may be responsible for biological activity of some Rh(III) organometallic complexes.[2, 3]

It is possible that the smaller size and charge (1^+) of this complex, in comparison with the dinuclear analogues, may allow the complex to be more readily taken up into cells than the *rac* and *meso* dinuclear isomers with 2^+ charge. Nevertheless this would require further investigations to confirm it. Recent reports from Farrell and co-workers show that increasing the charge can enhance the cellular accumulation and thereby cytotoxicity in some systems.[4] Reports from Hannon and co-workers showed that the 4^+ dinuclear single stranded complex $[Ru_2(L_{im})(bpy)_4]^{4+}$ is inactive against several different cancer cell lines tested while the parent cylinder $[Ru_2(L_{im})_3]^{4+}$ (similar size, same charge) is active against A2780 and T47D with IC_{50} of 72 and 53 μM respectively.[5]

Table 4.1 IC_{50} (μM) values for complexes **1** and **2**, **5, 6** and cisplatin.

Complexes	IC_{50} (μM)	
	MDA-MB-231	**A2780**
1	65 ± 5	>100†
2	57 ± 14	>100
5	23 ± 2	26 ± 2
6	>100†	>100
cisplatin	26 ± 3	28 ± 3

† Due to comparisons with cisplatin a maximum concentration of 100 μM was tested for all complexes. Therefore above this value compounds are classed as inactive and an accurate IC_{50} value cannot be calculated.

Complex **6**, the mononuclear complex with a bpy ligand instead of the phen (**5**) was inactive in both cell lines, with IC_{50} values always over 100 μM. The fact that **5** and **6** have such similar molecular structures yet so different cytotoxicity is interesting.

There is precedent for the size of the polypyridyl ligand, which is directly correlated with lipophilicity of a complex, to play a crucial role in the bioactivity.[2, 6, 7] Sheldrick and co-workers showed how increasing the size of the polypyridyl ligand the IC_{50} values of Rh(III) complexes decreased, with bpy complexes exhibiting activity 10 times lower than phen complexes.[8, 9] Cationic metal complexes with lipophilic properties may diffuse across the plasma membrane within the cells. In this case for complex **5**, the presence of the coordinated phen ligand will increase the lipophilicity of the complex in comparison with **6**, and this may be of high importance for the cytotoxicity exhibited by this complex.

The MDA-MB-231 cancer cell line was chosen for the preliminary cytotoxicity tests with the double stranded Rh(III) complexes. The cell line was treated with the complexes and, once again, with cisplatin as control and for standard comparisons. Table 4.2 reports the IC_{50} values measured for the two complexes in μM.

These first studies indicate that both complexes have high similar IC_{50} values and in case of complex **7**, is non-active towards the cancer cell line studied. Comparing with the dinuclear single stranded complexes **1** and **2**, and taking in consideration the same overall charge (2^+) it strongly suggests that the structure may be of importance for the biological activity. When comparing with the analogous Ru(II) double stranded helicates (discussed in chapter 1) it seems that the Rh(III) ones exhibit less cytotoxicity although

with the proviso that the cancer cell lines tested for the Ru(II) complexes are different from the ones studied for the rhodium complexes so far.

Table 4.2 IC_{50} (μM) values for complexes **7** and **8** and cisplatin.

Complexes	**IC50 (μM)**
	MDA-MB-231
7	>100
8	96 ± 3
cisplatin	37 ± 3

4.4 PCR Studies for Double Stranded Rh (III) Complexes (7 and 8)

The success with the original metallo-supramolecular cylinders has been remarkable. Together with their DNA binding affinities and the ability to bind in the centre of the 3WJs, recently reported work showed that the Ru(II) cylinder is capable of inhibiting DNA polymerase transactions *in vitro* at low concentration (0.1 μM) with the cylinder completely blocking the PCR at a concentration of 1.5 μM.[10]

Several metal complexes have been studied for their anticancer function, and this has been related to the interference in the DNA transcription process. This effect may occur either by the metal compound binding to the RNA polymerase or to the double stranded DNA template. In the case of binding to double stranded DNA template, a stabilization of the double helix is observed which prevents the strand separation that is an essential step in transcription process. Turro and co-workers showed, for example, that rhodium intercalating complexes containing phen and quinone diimine ligands (Figure 4.5) are able to inhibit the transcription and that this phenomenon is related to the ability of the complexes to stabilize double stranded DNA.[11]

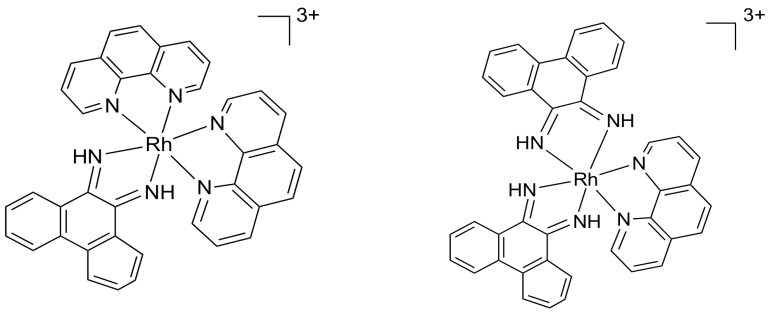

Figure 4.5 Structures of $Rh(phen)_2(phi)^{3+}$and $Rh(phi)_2(phen)^{3+}$.

In addition the dinuclear Rh(II) carboxylates (discussed in Chapter 1) inhibit replication by interacting directly with the enzyme T7-RNA polymerase.[12-14]

To probe whether a compound is able to affect DNA transactions *in vitro*, PCR has been used as an useful tool which provides a similar set of conditions to DNA transactions. In an analogous way, it is a DNA replication process involving DNA polymerase and it is a quick and easy way to obtain preliminary results about the interaction of a complex with DNA during its replication process.

Taking this in to consideration, we were interested in investigating whether our new Rh(III) double stranded complexes were able to inhibit the DNA transactions *in vitro* using PCR.

These studies were carried out in collaboration with Cosimo Ducani from Hannon group and the experiment run in the School of Biosciences of University of Birmingham†.

4.4.1 Polymerase Chain reaction (PCR)

The Polymerase chain reaction (PCR) is a useful, practical and very elegant technique that mimics the amplification of double stranded DNA *in vitro* and has been widely used in many areas of molecular biology.[15] The DNA to be amplified is denatured into single strands and annealed to oligonucleotide primers that are oriented in a way so that when is extended by the DNA polymerase the new synthesized strands will overlap. A scheme

† Although the experiment was carried out by Cosimo, I was able to follow and participate during the full duration of the procedure to become familiar with the technique and to further understand the results present herein.

of the process for the first cycle of PCR is shown in Figure 4.6. These three steps (denaturation, annealing and extension) are repeated several times, which results in an exponential accumulation of strands corresponding to the sequence between the priming sites.[15]

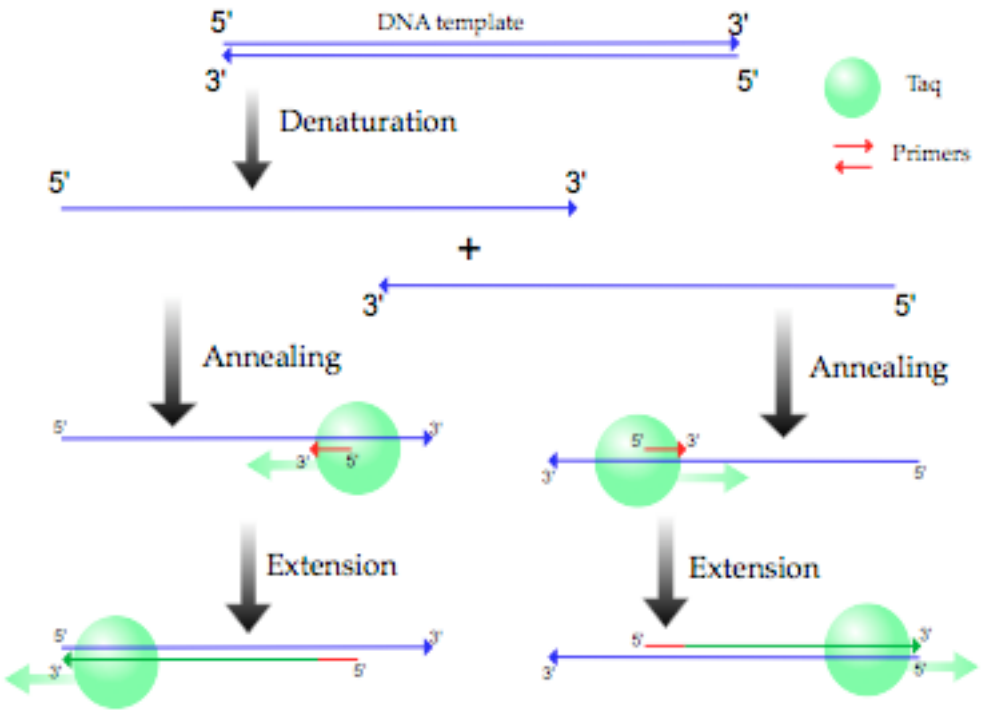

Figure 4.6 Principle of the Polymerase chain reaction (PCR) amplification scheme, representation of the first cycle.

After demonstrating by CD, LD and gel electrophoresis techniques that complexes **7** and **8** are able to bind to DNA and cleave plasmid DNA, we decided to investigate whether these interactions could prevent DNA transactions *in vitro*. PCR reactions were performed using a plasmid pUC19 as substrate and two specific primers together with a Taq DNA polymerase and the four natural deoxynucleotides (A, T, C, G), plus increasing concentrations of complexes **7** and **8**. Agarose gel electrophoresis of the PCR products

after 35 cycles, followed by ethidium bromide staining and UV visualization, showed a single DNA product of the predicted length (Figure 4.7). Details of the procedure are presented in the experimental section 4.6.4.

Excitingly, both rhodium double stranded complexes **7** and **8** affected DNA amplification reducing drastically the intensities of the product bands. Although these results show that both isomers are able to inhibit the PCR in a similar way is possible to observe that complex **8** inhibits the reaction at lower concentration when compared with **7** (Figure 4.7). From lane 5 and 6 there are still visible product bands, which are not observed for complex **8** in lanes 11 and 12, with complex **8** totally blocking the PCR at a concentration of 1.0 μM.

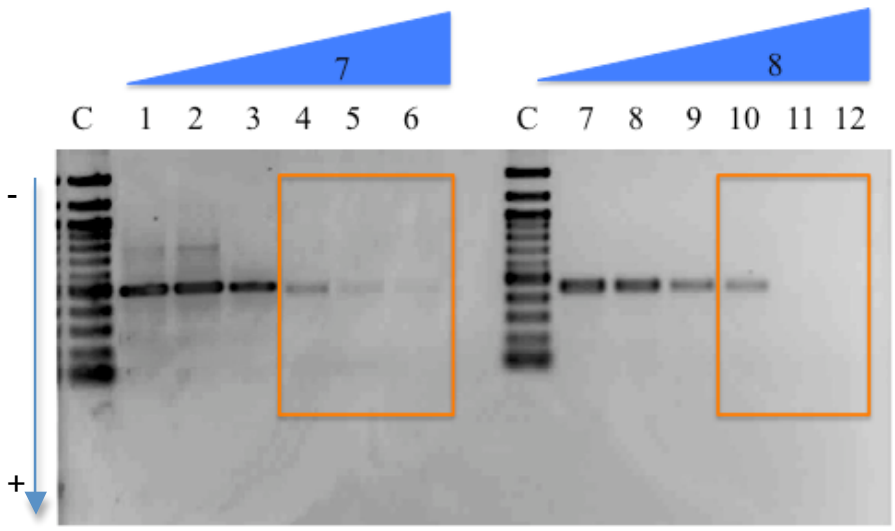

Figure 4.7 Agarose gel 1% after stained with ethidium bromide showing the Inhibition of the PCR by the rhodium complexes **7** and **8**. C) 100 bp oligonucleotide ladders; 1 and 7 are Controls; 2 and 8 complex at 0.1 μM; 3 and 9 complex at 0.3 μM; 4 and 10 complex at 0.5 μM; 5 and 11 complex at 1.0 μM; 6 and 12 complex at 1.5 μM;

This result is in accordance with and supports what was previously discussed in chapter 3 (sections 3.4.2, 3.7.2 and 3.82) where CD (with estimated K_b value being higher for **8** than for **7**), and LD spectra of complex **8** suggest that this isomer has better binding affinities to ct-DNA than complex **7**. This was also corroborated by gel electrophoresis studies. The PCR is inhibited according to the lower intensity of the PCR products and completely blocked at a concentration of 1.0 μM for complex **8** (with total disappearance of the bands at Lanes 11 and 12). These results show that complex **8** has a stronger interaction with the DNA PCR replication process compared to the Ru(II) cylinder.[10] In addition, the covalent binders steroid conjugates synthesized recently in the Hannon group, showed also ability to inhibit (not block) the PCR but at a higher concentration of 25 μM.[16] The double stranded complexes used for this study, inhibit the PCR at lower concentrations than the coordinative steroid binding drugs[16], and totally block it with efficiency comparable with the Ru(II) cylinder.[10] These results suggest that the supramolecular helicate type design (which allows major groove binding interactions) may play an import role for the inhibition of the DNA transactions *in vitro*.

4.5 Conclusions

The cytotoxicity of the new dinuclear Rh(III) single and double stranded complexes **1** and **2**, **7** and **8** and the mononuclear analogues **5** and **6** was evaluated. All complexes were tested for their water stability for a period of 72 hours showing no degradation for this period at 37 °C.

IC_{50} values were determined by an MTT assay and complexes **1** and **2** were found to be active against MDA-MB-231 breast cancer cell lines although with less cytotoxicity than cisplatin. When tested against ovarian cancer cell lines these complexes were shown to be inactive. On the contrary, complex **5**, the mononuclear analogue, is active against the breast and ovarian cancer cell lines tested with activity comparable to cisplatin. This result was very interesting since the complex showed no significant effect on ct-DNA plus, the similar complex **6** (mononuclear with bpy) is inactive towards both cell lines with IC_{50} values over 100 μM. To further investigate and better understand the biological activity of these complexes, assays to determine the IC_{50} value of these complexes in a different cell line are ongoing together with the first studies of the cytotoxicity of complexes **3** and **4** (dinuclear Rh(III) single stranded with bpy).

Preliminary IC_{50} values for the double stranded Rh(III) complexes **7** and **8**, show that the complexes are inactive with values close to or over 100 μM. These results were unexpected given the significant effect of these complexes on ct-DNA. Nevertheless PCR studies showed that these complexes are able to inhibit and block the PCR DNA replication *in vitro* with exciting results comparable with the recent data obtained for the Ru(II) cylinder.

These results should encourage further studies about biological activity of these

complexes and their role in biological systems. Chapter 5 is dedicated to describing further ideas and techniques, which can be applied to more deeply understand the mode of action of the complexes described in this thesis.

4.6 Experimental

4.6.1 Cell Lines and Materials

MDA-MB-231 and A2780 cell lines were obtained from the European Collection of Cell Cultures (ECACC), a Health Protection Agency Culture Collection. Dulbecco`s modified Eagle medium (DMEM) and fetal bovine serum (FBS) were obtained from Invitrogen, UK. Antibiotic antimycotic solution, L-glutamine, trypsin-EDTA, hepes buffer solution, phosphate buffered saline (PBS), MTT (MTT = 3-(4,5-dimethylthiazol-2-yl)-2,5-diphenyl-2H-tetrazolium bromide), dimethyl sulfoxide (DMSO) were purchased from Sigma-Aldrich, UK. Tissue culture flasks, 96 well flat-bottomed microtiter plates (Corning Costar) were obtained from Appleton Woods, UK.

4.6.2 Cell Growth Conditions

MDA-MB-231 human breast cancer and A2780 human ovarian cancer cell lines were grown as monolayers in DMEM medium supplemented with 10% FBS, 1% L-glutamine, 1% Hepes buffer, 1% sodium pyruvate and 1% of antibiotic antimycotic solution. Cells were maintained in the incubator at 37 °C, 5% CO_2 in a humidified atmosphere and regularly checked for absence of contamination.

4.6.3 MTT Assay[1]

Cells were collected from the tissue culture flasks using 1% trypsin-PBS solution. Single cell suspensions were prepared; cells counted using hemocytometer and placed in 96 well microtiter plates at density of 8.000 cells/well and total volume 100 μl/well. Plates with cells were incubated for 24 hours to allow cells to attach to the surface. The

cells were then treated with 5 different concentrations (100 μM, 50 μM, 25 μM, 12.5 μM, 6.25 μM) of synthesized compounds dissolved in fresh mediums and incubated for further 72 hours. After 72 hours of incubation 20 μl of a 5 mg/ml MTT solution in phosphate buffer saline was added to each well of the 96 well plates except three wells of the control and cells were incubated for 2 hours. The medium was carefully removed and 200 μl of DMSO was added to each well of the plate to dissolve the formed purple crystals of formazan. The absorbance was measured 15-20 minutes after the addition of DMSO using a 96-well plate reader (BioRad) at 590 nm.

4.6.4 PCR Experiments

Twelve reaction mixtures were prepared, all containing 1X NH_4 reaction buffer, $MgCl_2$ (1.5 mM), pUC19 plasmid DNA substrate (50 ng, Sigma Aldrich), Taq DNA polymerase (5U; Bioline), dNTPs (3 mM), the primers (0.4 μM each) pUC19F (5'-CGGTGAAAACCTCTGACACA-3') and M13 reverse (5'-CAGGAAACAGCTATGACC-3'; Alta Bioscience). The PCR solutions were incubated for 5 minutes at room temperature with increasing concentrations of complexes **7** and **8**: 0 μM, lanes 1 and 7; 0.1 μM, lanes 2 and 8; 0.3 μM, lanes 3 and 9; 0.5 μM, lanes 4 and 10; 1 μM, lanes 5 and 11; 1.5 μM, lanes 6 and 12. After Taq polymerase activation at 95 °C for 5 min, 35 cycles of PCR were performed as follows: denaturation at 95 °C for 30 s, annealing at 54 °C for 30 s, and synthesis at 72 °C for 5 minutes. A final polymerization step was performed at 72 °C for 5 minutes. The products were loaded on 1.5 % agarose gel and the image was acquired by UV lamp (UVITEC) with the associated software (UVI pro platinum).

4.7 References

[1] T. Mosmann, *J. Immunol. Methods* **1983**, *65*, 55.

[2] G. Gasset, I.Ott, N. Metzler-Nolte, *J. Med. Chem.* **2011**, *54*, 3.

[3] M. A. Scharwitz, I. Ott, Y. Geldmacher, R. Gust, W. S. Sheldrick, *J. Organomet. Chem.* **2008**, *693*, 2299.

[4] J. B. Mangrum, N. P. Farrell, *Chem. Commun.* **2010**, *46*, 6640.

[5] U. McDonnell, J. M. C. A. Kerchoffs, R. P. M. Castineiras, M. R. Hicks, A. C. G. Hotze, M. J. Hannon, A. Rodger, *Dalton Trans.* **2008**, 667.

[6] C. A. Puckett, R. J. Ernst, J. K. Barton, *Dalton Trans.* **2010**, *39*, 1159.

[7] C. A. Puckett, J. K. Barton, *J. Am. Chem. Soc.* **2007**, *129*, 46.

[8] M. Harlos, I. Ott, R. Gust, H. Alborzinia, S. Wolfl, A. Kromm, W. S. Sheldrick, *J. Med. Chem.* **2008**, *51*, 3924.

[9] M. Dobroschke, Y. Geldmacher, I. Ott, M. Harlos, L. Kater, L. Wagner, R. Gust, W. S. Sheldrick, A. Prokop, *ChemMedChem* **2009**, *4*, 177.

[10] C. Ducani, A. Leczkowska, N. J. Hodges, M. J. Hannon, *Angew. Chem. Int. Ed* **2010**, *49*, 1.

[11] P. K. L. Fu, P. M. Bradley, C. Turro, *Inorg. Chem.* **2003**, *42*, 878.

[12] K. Sorasaenee, P. K. L. Fu, A. M. Angeles-Boza, K. R. Dunbar, C. Turro, *Inorg. Chem.* **2003**, *42*, 1267.

[13] H. T. Chifotides, P. K. L. Fu, K. R. Dunbar, C. Turro, *Inorg. Chem.* **2004**, *43*, 1175.

[14] D. T. Odom, C. S. Parker, J. K. Barton, *Biochemistry* **1999**, *38*, 5155.

[15] R. A. Gibbs, *Anal. Chem.* **1990**, *62*, 1202.

[16] C. Sanchez-Cano, M. Huxley, C. Ducani, A. E. Hamad, M. J. Browning, C. Navarro-Ranninger, A. G. Quiroga, A. Rodger, M. J. Hannon, *Dalton Trans.* **2010**, *39*, 11365.

Chapter 5

Conclusions and Future work

5.1 Conclusions

The work described in this thesis aimed to create and study new DNA-binding Rhodium Supramolecular complexes. A key first aim was therefore to design and investigate synthetic procedures for the synthesis of new Rh(III) supramolecular complexes. This target was successfully achieved and Chapter 2 shows the synthesis, purification and characterization of new Rh(III) mononuclear and dinuclear single, double and triple stranded complexes.

In the case of the dinuclear Rh(III) double and triple stranded supramolecular helicates they are the first examples known to date. The L_{azo} was the ligand of choice for the Rh(III) dinuclear complexes since most probably due to its lack of stability, L_{im} did not produce the complexes designed. Comparing with the Ru(II) chemistry, the double stranded complexes are more difficult to prepare: for Ru(II), 5 different isomers were identified and isolated, while for Rh(III) only two isomers were separated (*rac* and a *meso* ββ isomers), although in similar yields to the Ru(II) analogues. The Ru(II) ones, are neutral complexes while the Rh(III) are cationic which makes much more difficult to separate them as a consequence.

For the dinuclear Rh(III) triple stranded complex, much has been achieved. This

complex is obtained rapidly from crude reaction in higher yield and purity when compared with the Ru(II) analogue. Comparing with the Ru(II) this complex is much easier to make. But is harder to isolate pure since, again the higher charge of the complex perhaps makes the purification process much more difficult. Again, this is the first Rh(III) triple stranded supramolecular complex and further investigations and characterization on this complex are required.

In Chapter 3, the DNA binding properties of the complexes were evaluated by CD, LD, UV-Vis spectroscopy using ct-DNA and gel electrophoresis with plasmid DNA. From these data it was possible to conclude that all dinuclear complexes bind to DNA with CD studies for complexes **1**, **2**, **3**, **4**, **7**, **8** and **10** exhibiting an ICD signal in the metal complex region proving that they bind to ct-DNA, and they do it so without affecting the overall B-DNA structure. By contrast, mononuclear complexes **5** and **6** showed nearly no effect towards ct-DNA. Also, LD experiments showed that the dinuclear complexes are effective DNA bending/coiling agents when compared with the mononuclear analogues.

The similar size and structure of the dinuclear complexes to the Fe(II) and Ru(II) cylinders suggest that they might bind to DNA in the major groove. Studies with DNA bases and complexes **1** and **2**, confirmed that coordinative binding might also be an additional binding mode.

Gel electrophoresis studies showed that the single stranded complexes are effective plasmid DNA unwinding and cleaving agents while the double stranded complexes seem to directly cause DNA cleavage. Thus it is demonstrated that incorporation of rhodium into the supramolecular structures does lead to DNA artificial nuclease activity as hoped at the outset of the work. This is therefore an additional to the tool box available and complements the copper(I) double stranded supramolecular

compounds that were previously shown to cut DNA.

Also, by incorporating the metal complex units into the supramolecular structure leads to more dramatic DNA binding than the mononuclear analogues.

In Chapter 4, the biological activity of some of the complexes synthesized was explored. The single stranded dinuclear Rh(III) complexes with phen ligands showed cytotoxic activity against MDA-MB-231 breast cancer cell lines but were inactive towards the ovarian cell line tested (A2780). When the mononuclear complexes were tested, surprisingly, the complex with phen ligand was active with activity comparable to cisplatin in both cell lines while the one with bpy ligand is non-active.

The IC_{50} values for the double stranded complexes (**7** and **8**) are not as dramatic as those of the corresponding ruthenium double stranded ones (some of which are very active indeed) although the cell line tested was different.

5.2 Future work

In this work the synthesis of new different supramolecular Rh(III) complexes with the dinucleating ligand developed by the Hannon group was achieved for the first time.

Although the procedures established allowed the synthesis of the complexes, for example the yields obtained for the double stranded isomers are fairly low. Due their exciting DNA binding features studied in Chapter 3 and to further study their biological activity, improvement of the synthetic procedure and access to quantities of these materials would certainly prove useful. For instance, microwave assisted synthesis under the similar reaction conditions (propanol:water 2:1) might avoid formation of co-contaminant polymeric material. Microwave radiation often overcomes the kinetic inertness of compounds and simplifies the replacement of ligands in the initial complex

avoiding the formation of side products and in the helicate case, polymeric insoluble materials.[1, 2] A growing body of data has been recently reported on microwave synthesis of metal complexes including ruthenium and rhodium dinuclear and mononuclear complexes with improved yields and faster reactions.[2-5] This methodology could probably be also applied to further explore a different synthetic procedure for Rh(III) triple helicate with L_{im}.

Other attempts to grow crystals of the double and triple stranded complexes are of high interest because it would allow to confirm the characterization explored in Chapter 2 of this thesis and to explore the molecular structure in detail.

From a synthetic point of view, an interesting approach of the Rhodium chemistry was the synthesis of a Rh(I) square planar dinuclear double stranded complex. Considering the interaction with DNA, such complex would allow us to explore the difference in the overall structure and final 2+ charge of a saturated double stranded complex in comparison with the unsaturated double stranded Rh(III) with chloride ligands (Figure 5.1). In addition, the study of its biological activity are of interest since Rh(I) complexes are also known for their anticancer activity.[6] A procedure for the synthesis of such complex was established using commercial available $[Rh(COD)Cl]_2$ as a starting material and L_{azo} as the ligand. Reaction conditions involved refluxing in DCM and resulted in a mixture of the desired compound with a considerable amount of polymeric insoluble materials. Lowering the starting material concentrations and performing the reaction at room temperature in DCM resulted in a dark green solution with a minimal amount of polymer. The solution was filtered through celite and the final green solid was precipitated as a PF_6 salt by addition of a concentrated solution of NH_4PF_6 in water.

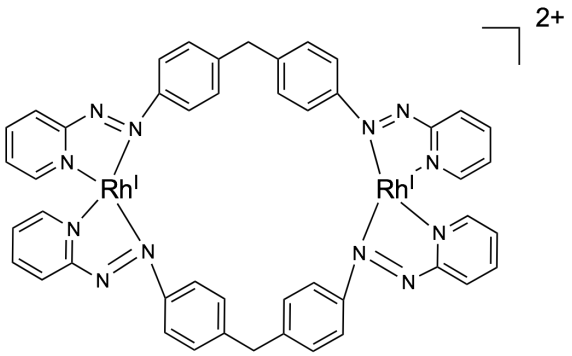

Figure 5.1 Chemical structure of a double stranded Rh(I) supramolecular complex.

The ESI-MS exhibited a doubly charged peak with m/z = 481 corresponding to the species $[Rh_2(L_{azo})_2]^{2+}$. The ^{1}H-NMR in CD_3CN showed a mixture of several isomeric species with the aromatic region showing overlapping peaks. Several attempts to purify this complex using flash chromatography failed. As future work on this complex, HPLC purification/separation should be attempted using the method (or slightly changing it according with the first separation profile) developed for the analogous complexes described in this thesis.

In the chapter 3, CD studies with the single stranded complexes **1** and **2** and with the double stranded **8**, showed that they might preferentially bind to G-C than A-T sites. Although preliminary, these results are quite interesting and they should be considered as a subject for future studies. *DNA footprinting* has been a methodology widely used to explore the selectivity of several metal complexes, in particularly much of the work explored in chapter one done by Barton as co-workers has been on Rh(III) diimine complexes and their different DNA selectivity.[7] Taking into consideration that gel electrophoresis studies presented herein for the single and double stranded Rh(III)

complexes showed that all complexes are able to cleave plasmid DNA (pBR322), DNA *footprinting* studies would be of importance to localize the DNA cleavage site. Also, the results obtained with plasmid DNA and the complexes presented herein should encourage future photocleavage studies to evaluate the DNA damage caused by the compounds.

Coordinative binding of the complexes to DNA should be further investigated. UV-Vis, CD and LD studies with ct-DNA and the complexes changing the experimental conditions, like buffer (without presence of Cl ions which may difficult the coordinative binding to DNA) and incubated samples over a period of 24 hours at 37 °C may provide further information about structural changes of the B-DNA after interaction with the complexes. An experiment run with a single stranded isomer by LD showed a more intense coiling/bending of ct-DNA upon incubation suggesting an additional DNA binding mode (coordinative binding) to the major groove binding.

In chapter 4, the biological activity of some of the complexes synthesized was evaluated. Tests with a different ovarian cancer cell line (SKOV-3) for these complexes are ongoing to try to understand if the complexes have some kind of specificity for breast over ovarian cancer.

In addition to understand more deeply why the mononuclear complex **5** has such a different behaviour in cancer cell lines comparing with **6**, cellular uptake studies are of interest. Inductively coupled plasma mass spectrometry (ICP-MS) and atomic absorption spectroscopy (AAS) are techniques commonly used to explore the cellular uptake of several complexes.[8] Certainly this would allow to further understanding the

mode of action of these two compounds. This technique would be useful as well to study the new isomers of Rh(III) double stranded complexes. Preliminary tests showed that the two isomers have very high IC_{50} values with complex **7** being non-active in MDA-MB-231 cancer cell. Another interesting feature to explore would be to test the complexes in the same cancer cell lines with the use of irradiation. It is known in the literature that for example $[Rh(phen)_2Cl_2]^+$ shows antitumor properties when irradiated with light of a certain wavelength and also that it shows a minimal association with DNA in the dark.[9, 10] Studies with the complexes and DNA and also in cells using light would allow to probe if the compounds could be potential PDT agents.

PCR studies with the double stranded complexes (**7** and **8**) show very promising and exciting results with the complexes blocking the PCR at 1.0 μM concentration. The fact that the complexes exhibited good DNA binding features, the lack of cytotoxicity is unexpected. This fact may be explained by the lack of cellular uptake of the complexes through the cell which in comparison with the analogues Ru(II) (which are neutral) charge may in this case play an important role for the enter of the complexes inside the cell. Nevertheless, the cytotoxic activity of this complexes in different cell lines is an ongoing subject of work, special in A2780 and SKOV-3 cell lines to enable to establish possible structure-activity relationships between this complexes and the single stranded ones and in the future with the Rh(III) triple stranded.

5.3 References

[1] J. Klinowski, F. A. A. Paz, P. Silva, J. Rocha, *Dalton Trans.* **2011**, *40*, 321.

[2] N. A. Ezerskaya, E. S. Toropchenova, I. V. Kubrakova, S. V. Krasheninnikova, T. F. Kudinova, T. A. Fomina, I. N. Kiseleva, *J. Anal. Chem.* **2000**, *55*, 1132.

[3] C. R. K. Glasson, G. V. Meehan, J. K. Clegg, L. F. Lindoy, J. A. Smith, F. R. Keene, C. Motti, *Chem. Eur. J.* **2008**, *14*, 10535.

[4] S. Herrero, R. Jimenez-Aparicio, J. Perles, J. L. Priego, F. A. Urbanos, *Green Chem.* **2010**, *12*, 965.

[5] D. Amarante, C. Cherian, C. Ernmel, H. Y. Chen, S. Dayal, M. Koshy, E. G. Megehee, *Inorg. Chim. Acta* **2005**, *358*, 2231.

[6] G. Gasset, I.Ott, N. Metzler-Nolte, *J. Med. Chem.* **2011**, *54*, 3.

[7] U. Schatzschneider, *Eur. J. Inorg. Chem.* **2010**, 1451.

[8] C. A. Puckett, R. J. Ernst, J. K. Barton, *Dalton Trans.* **2010**, *39*, 1159.

[9] R. E. Mahnken, M. A. Billadeau, E. P. Nikonowicz, H. Morrison, *J. Am. Chem. Soc.* **1992**, *114*, 9253.

[10] T. Mohammad, *Toxicol. in Vitro* **2004**, *18*, 45.

Appendix

A.1- ^{1}H-NMR and COSY of $[Rh_2(L_{azo})(phen)_2Cl_4](PF_6)_2$ (peak 3 from HPLC)

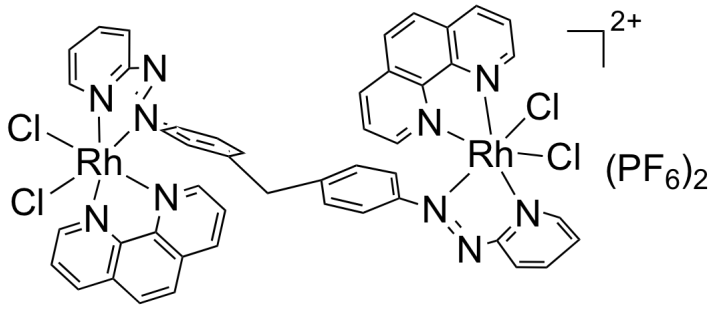

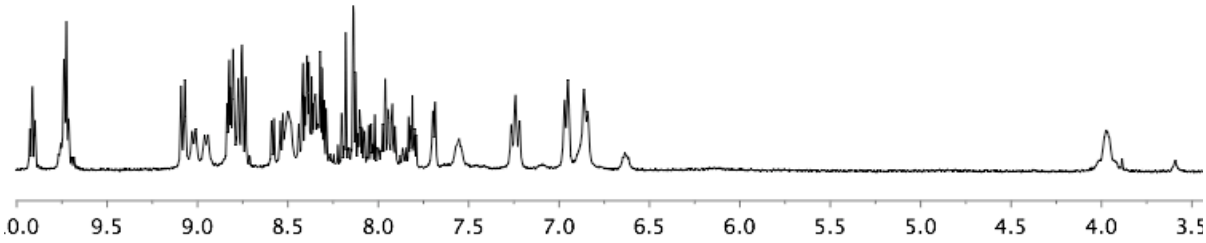

δ/ppm

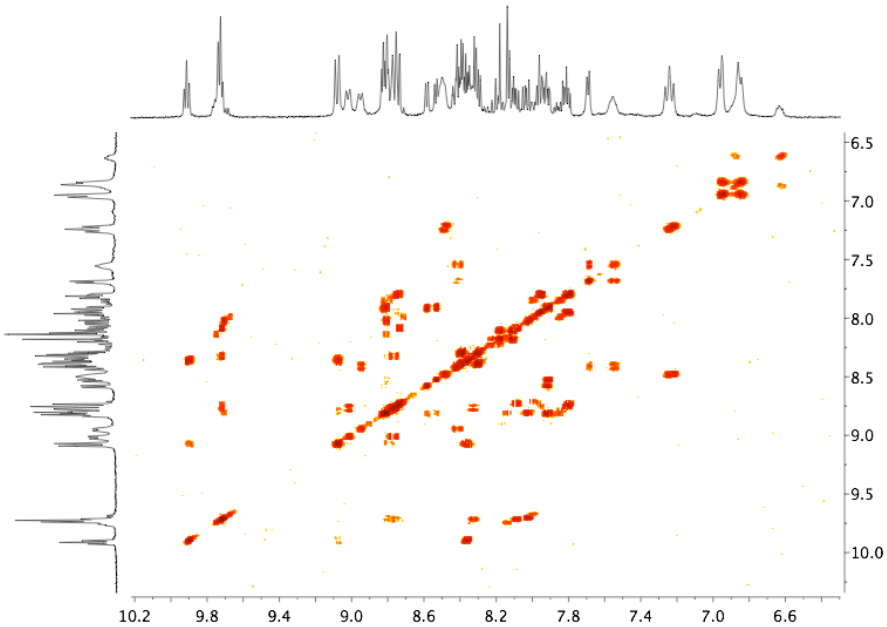

δ/ppm

A.2- Analytical HPLC of $[Rh_2(L_{azo})(phen)_2Cl_4](PF_6)_2$ after preparative separation.

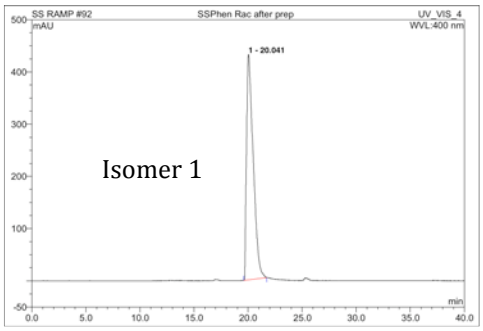

No.	Ret.Time min	Peak Name	Height mAU	Area mAU*min	Rel.Area %	Amount	Type
1	20.04	n.a.	431.917	308.292	100.00	n.a.	BMB
Total:			431.917	308.292	100.00	0.000	

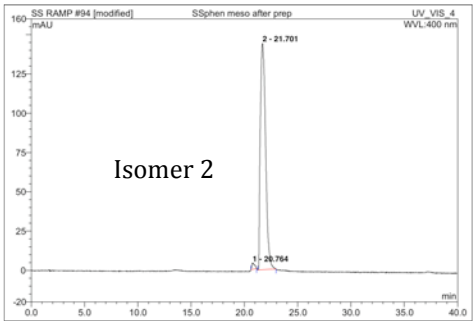

No.	Ret.Time min	Peak Name	Height mAU	Area mAU*min	Rel.Area %	Amount	Type
1	20.76	n.a.	3.976	1.246	1.48	n.a.	BMB*
2	21.70	n.a.	144.121	83.142	98.52	n.a.	BMB
Total:			148.097	84.388	100.00	0.000	

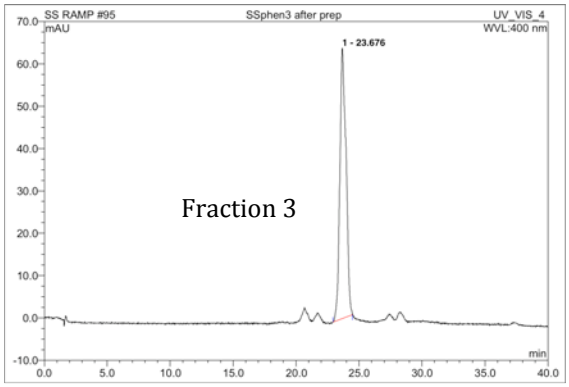

No.	Ret.Time min	Peak Name	Height mAU	Area mAU*min	Rel.Area %	Amount	Type
1	23.68	n.a.	63.984	36.354	100.00	n.a.	BMB
Total:			63.984	36.354	100.00	0.000	

A.3- Table 1- Crystallographic data of complex **5**

	cis-[Rh(L_{azpy})(phen)Cl_2](PF_6) (**5**)	*cis*-[Rh(L_{azpy})(phen)Cl_2](PF_6) Polymorph of (**5**)
Empirical Formula	$C_{23}H_{17}Cl_2N_5Rh$, PF_6	$C_{23}H_{17}Cl_2N_5Rh$, PF_6
M_r	682.20	682.20
T [K]	120(2)	120(2)
Crystal system	Monoclinic	Orthorhombic
Space group	$P\ 2_1/c$	$P\ bca$
Unit Cell Dimensions	a=17.2937(8) Å α=90° b=9.3691(4) Å β=101.245(3)° c=15.8289(6) Å γ=90°	a=32.0286(7) Å α=90° b=8.7051(2) Å β=90° c=35.3828(7) Å γ=90°
V [Å^3]	2515.46(18)	9865.2(4)
Z, Z'	4, 1	16, 2
ρ_{calcd} (Mg/m^3)	1.801	1.837
μ (mm^{-1})	1.024	1.044
Reflections collected	29246	57114
Independent reflections	5755 [R_{int} = 0.0593]	8687 [R_{int} = 0.0648]
Goodness-of-fit on F^2	1.057	1.157
Final R indices [I>2σ(I)]	R_1 = 0.0407, wR_2 = 0.0919	R_1 = 0.0582, wR_2 = 0.1069
R indices (all data)	R_1 = 0.0598, wR_2 = 0.1002	R_1 = 0.0801, wR_2 = 0.1178

A.4- 2D-NMR (COSY) of **5**

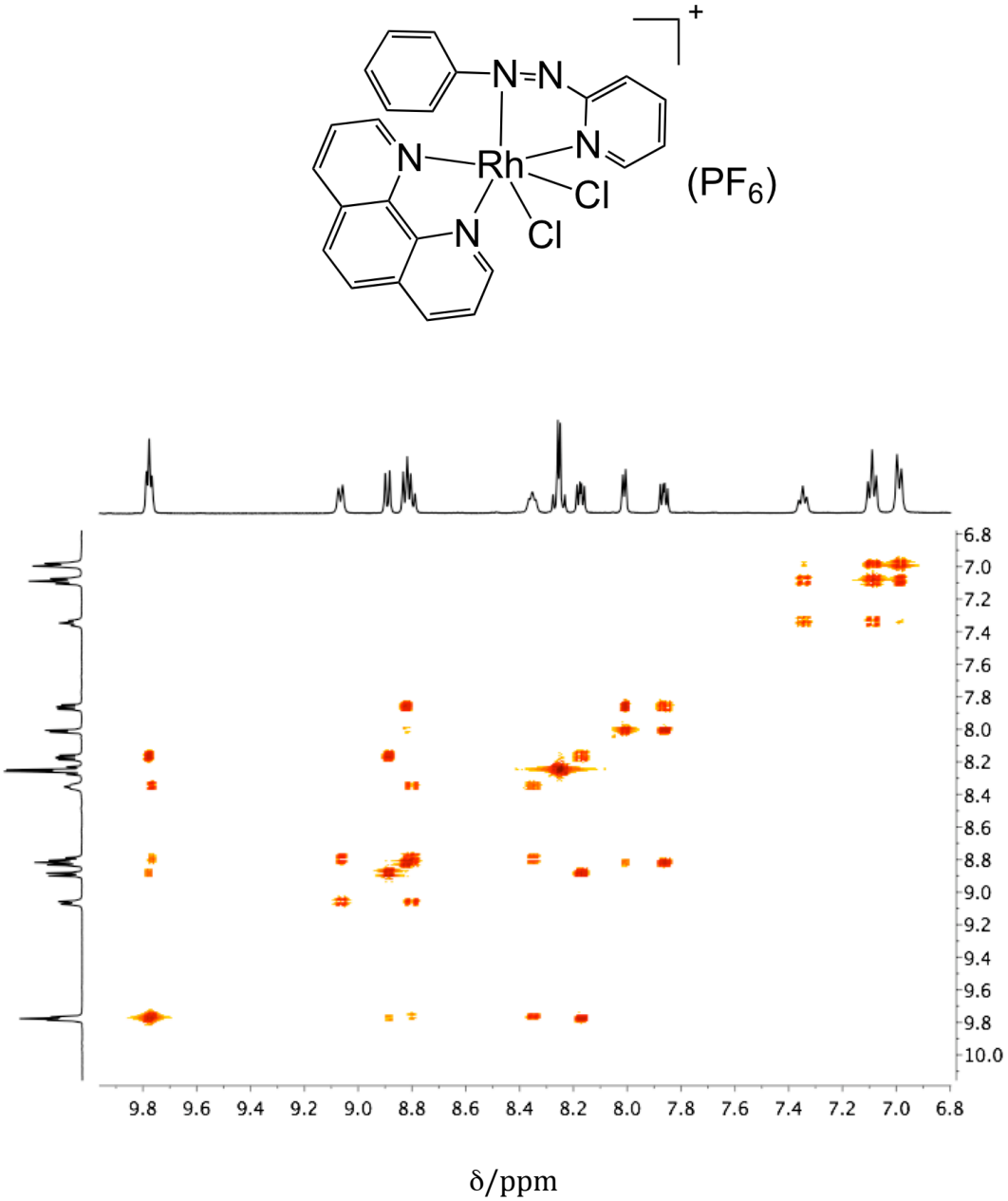

A.5- Table 2- Crystallographic data of complex **6**

	cis-[Rh(L_{azpy})(Bpy)Cl_2](PF_6) (**6**)
Empirical Formula	$C_{21}H_{17}Cl_2N_5Rh$, PF_6
M_r	658.18
T [K]	120(2)
Crystal system	Triclinic
Space group	P -1
Unit Cell Dimensions	a=8.4527(3) Å α=114.024(2)° b=12.1762(3) Å β=94.281(2)° c=13.7877(4) Å γ=108.425(2)°
V [Å^3]	1195.37(7)
Z, Z'	2
ρ_{calcd} (Mg/m^3)	1.829
μ (mm^{-1})	1.073
Reflections collected	17277
Independent reflections	5411 [R_{int} = 0.0591]
Goodness-of-fit on F^2	1.109
Final R indices [I>2σ(I)]	R_1 = 0.0537, wR_2 = 0.1032
R indices (all data)	R_1 = 0.0729, wR_2 = 0.1131

A.6- 2D-NMR (COSY) of **6**

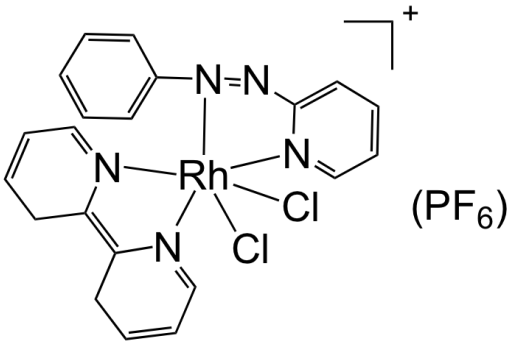

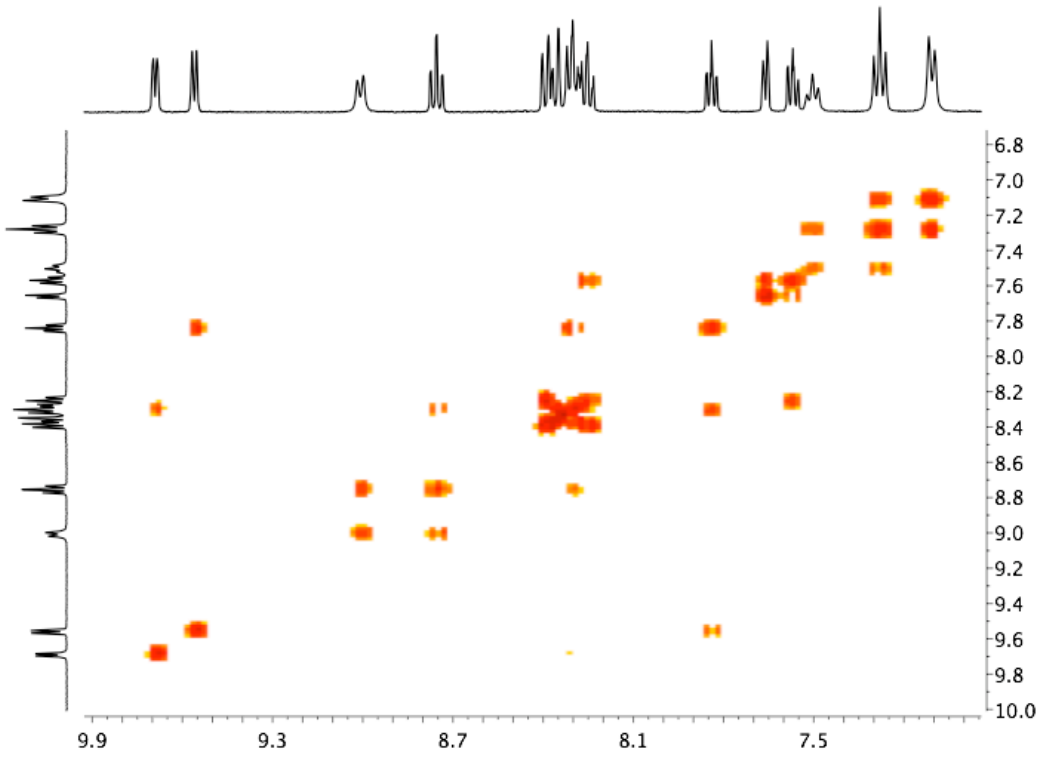

δ/ppm

A.7- 2D-NMR (COSY) of **1**

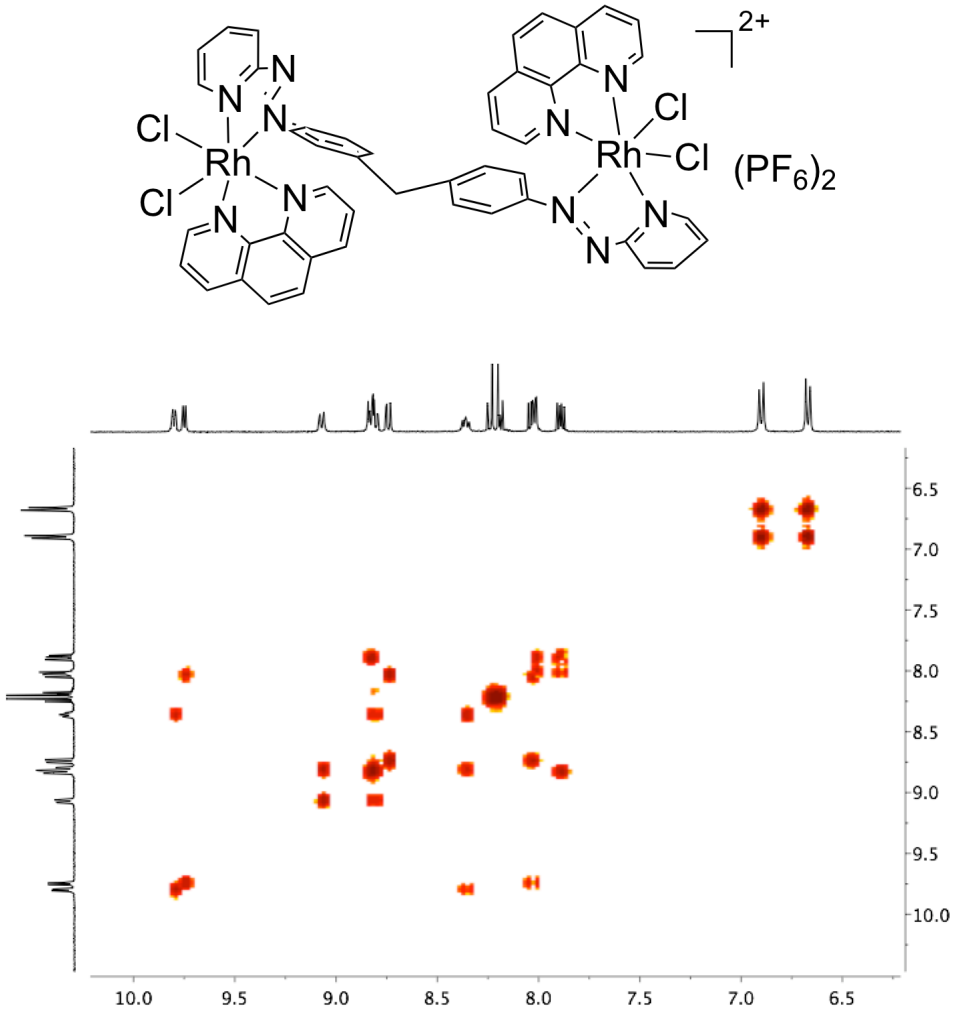

δ/ppm

A.8- 2D-NMR (COSY) of **2**

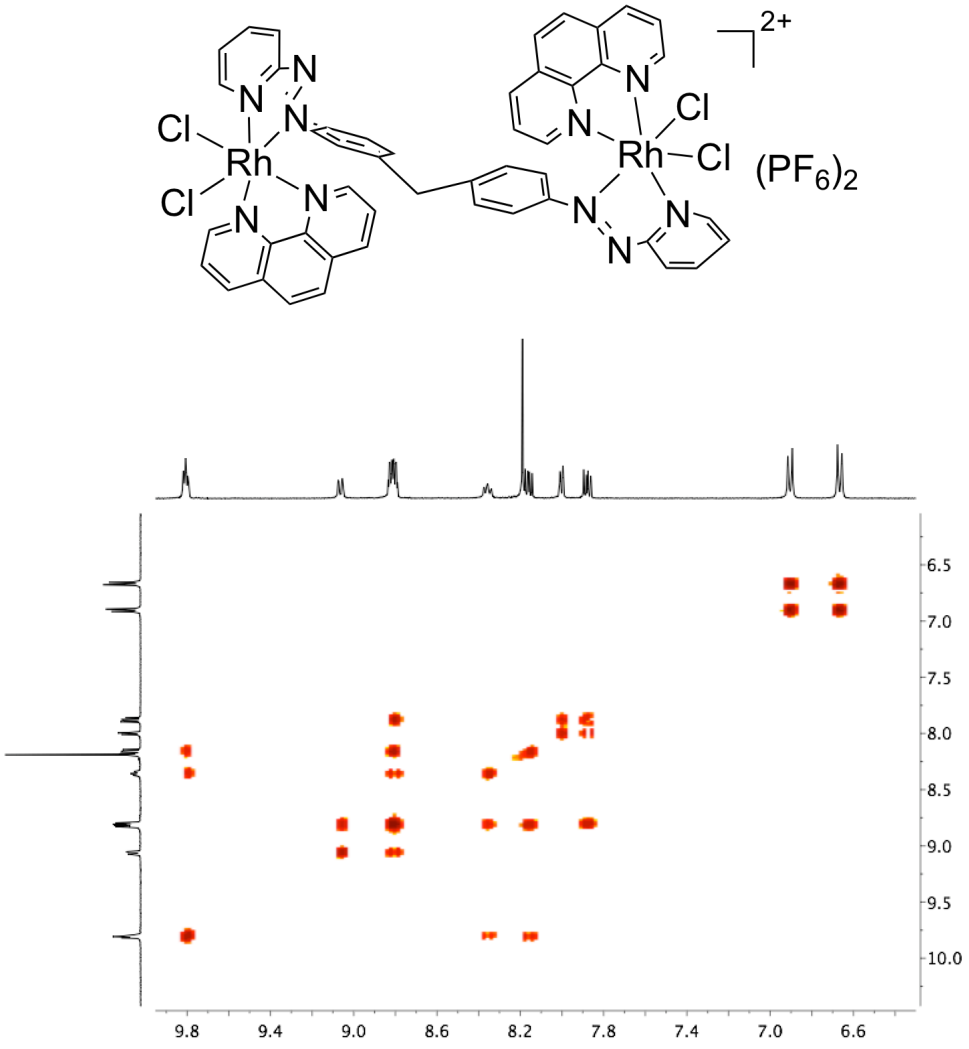

δ/ppm

A.9- Table 3- Crystallographic data of complex **1**

	ΔΔ,ΛΛ - $[Rh_2(L_{azo})(phen)_2Cl_4](PF_6)_2$ (**1**)
Empirical Formula	$C_{47}H_{34}Cl_4N_{10}Rh_2$, 2($PF_6$), 1.5($CH_3NO_2$), 0.5($CH_3N$)
M_r	1488.49
T [K]	120(2)
Crystal system	Monoclinic
Space group	*C 2/c*
Unit Cell Dimensions	a=29.9159(12) Å α=90° b=15.3485(7) Å β=115.153(2)°. c=29.4600(12) Å γ=90°
V [Å^3]	12244.3(9)
Z, Z'	8, 1
ρ_{calcd} (Mg/m^3)	1.615
μ (mm^{-1})	0.853
Reflections collected	48440
Independent reflections	10306 [R_{int} = 0.0962]
Goodness-of-fit on F^2	1.096
Final R indices [I>2σ(I)]	R_1 = 0.1290, wR_2 = 0.2629
R indices (all data)	R_1 = 0.2120, wR_2 = 0.3175

A.10- 2D-NMR (COSY) of **3**

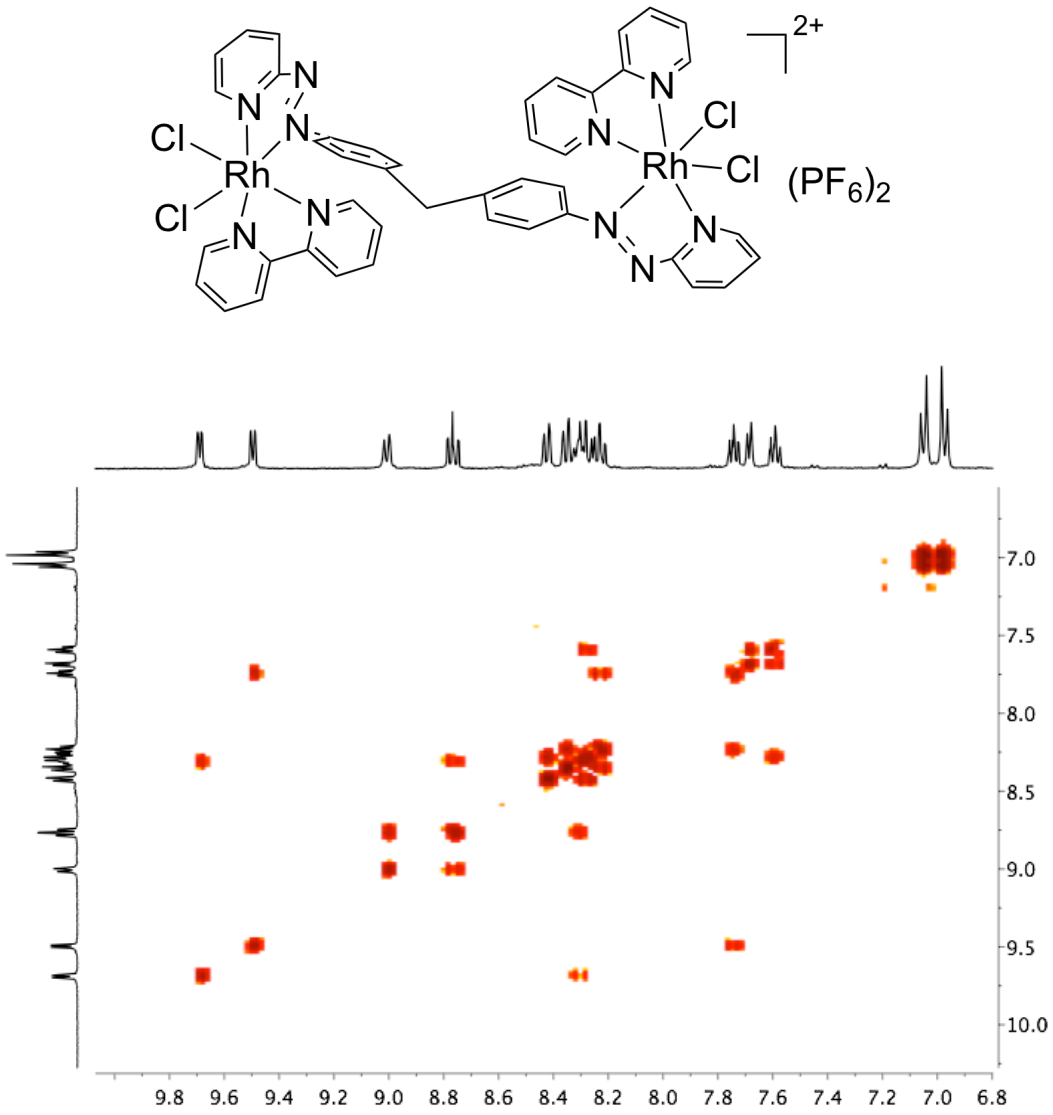

δ/ppm

A.11- 2D-NMR (COSY) of **4**

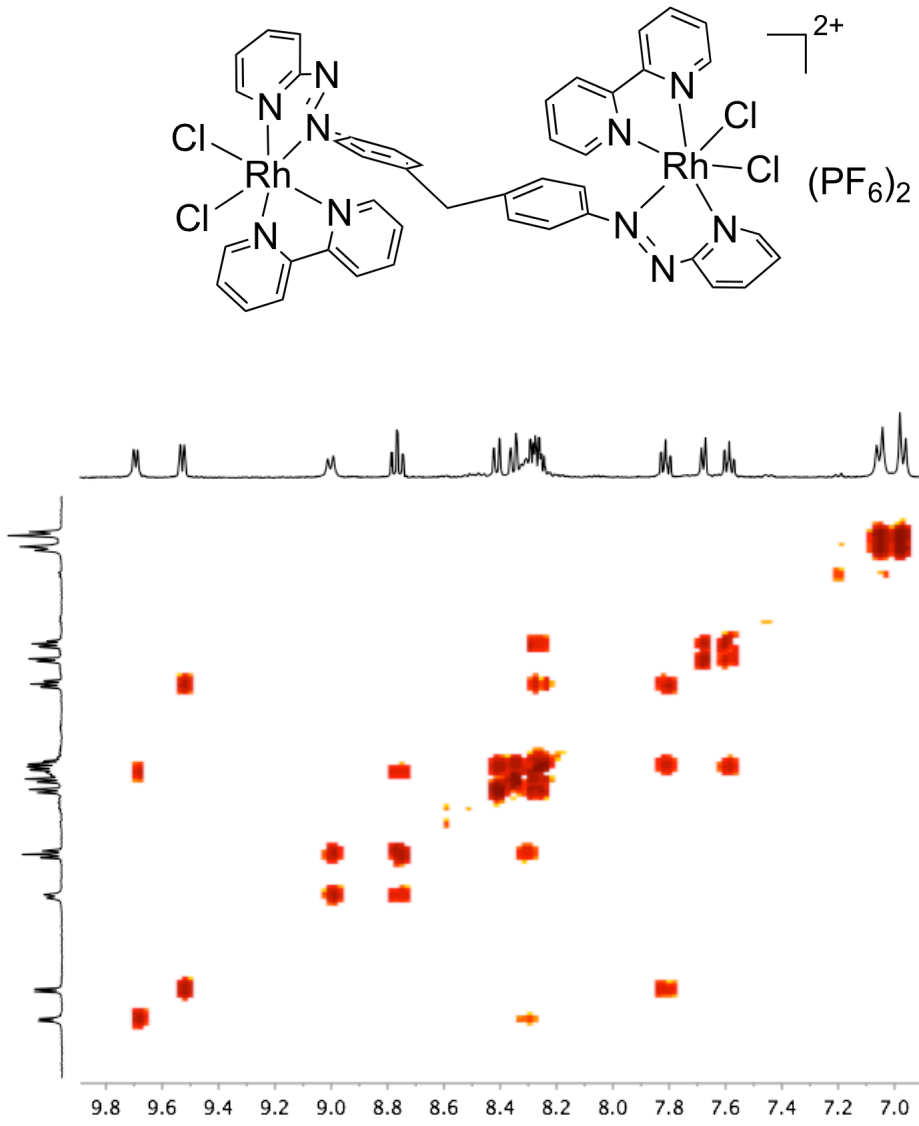

δ/ppm

A.12- Table 4- Crystallographic data of complex **3**

	ΔΔ,ΛΛ - $[Rh(L_{azo})(Bpy)_2Cl_2](PF_6)$ (**3**)
Empirical Formula	$C_{43}H_{34}Cl_4N_{10}Rh_2$, $2(PF_6)$, $3(C_2H_3N)$
M_r	1451.52
T [K]	120(2)
Crystal system	Triclinic
Space group	P -1
Unit Cell Dimensions	a=13.8894(6) Å α=115.750(2) ° b=15.8926(10) Å β=111.773(3) ° c=16.2996(10) Å γ=96.219(3)°
V [Å^3]	2849.0(3)
Z, Z'	2
ρ_{calcd} (Mg/m^3)	1.692
μ (mm^{-1})	0.911
Reflections collected	39523
Independent reflections	9984 [R_{int} = 0.0839]
Goodness-of-fit on F^2	1.191
Final R indices [I>2σ(I)]	R_1 = 0.0807, wR_2 = 0.1348
R indices (all data)	R_1 = 0.1255, wR_2 = 0.1541

A.13- ^{1}H-NMR (300 MHz, 25 °C) in CD_3CN of Fraction 3 of $[Rh_2(L_{azo})_2Cl_4]$

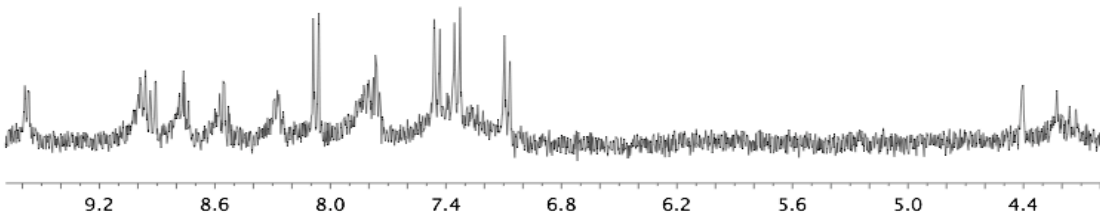

δ/ppm

A.14- 2D-NMR (COSY) of **7**

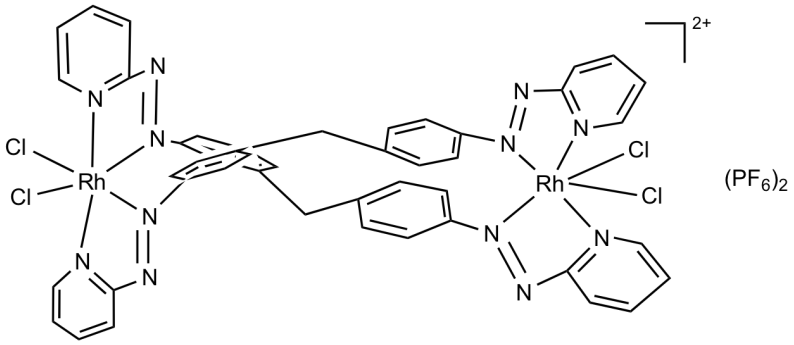

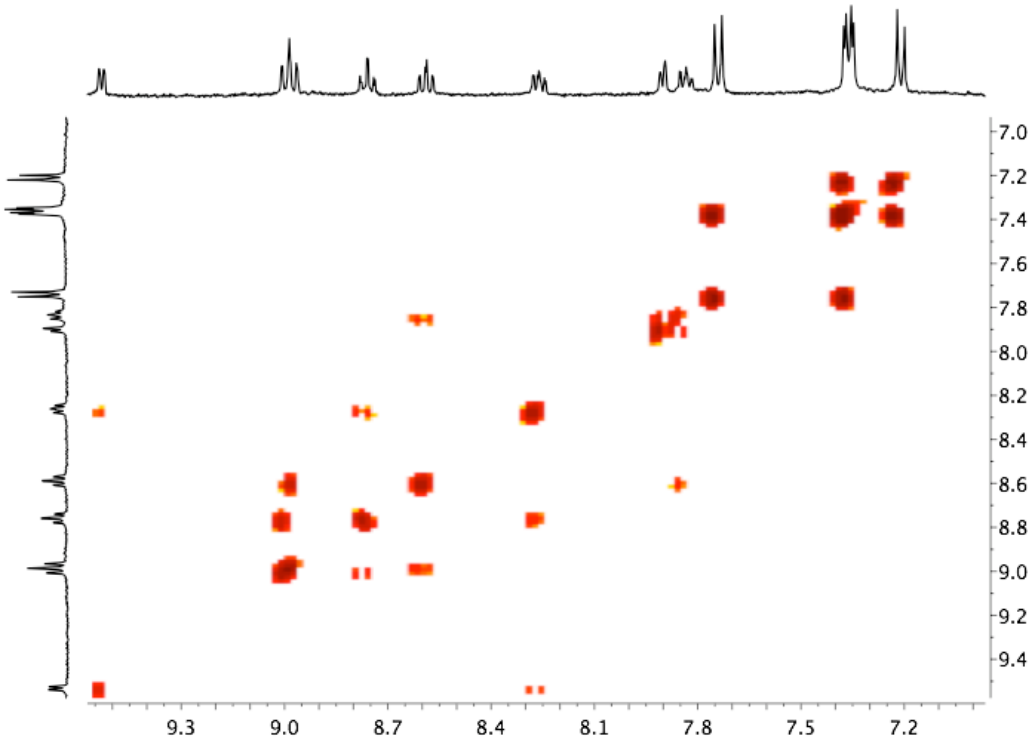

δ/ppm

A.15- 2D-NMR (COSY) of **8**

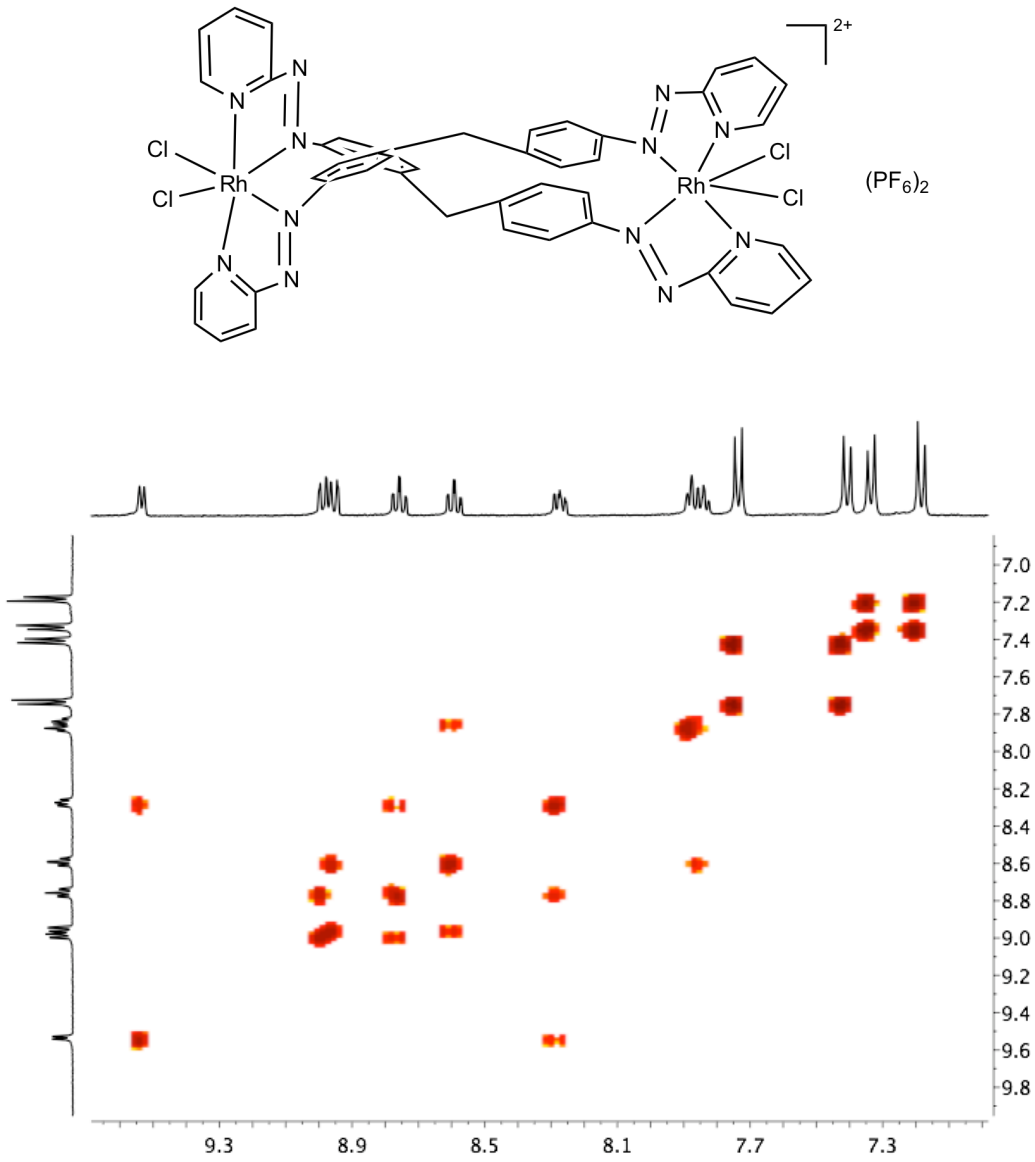

δ/ppm

A.16- 2D-NMR (COSY) of **9**

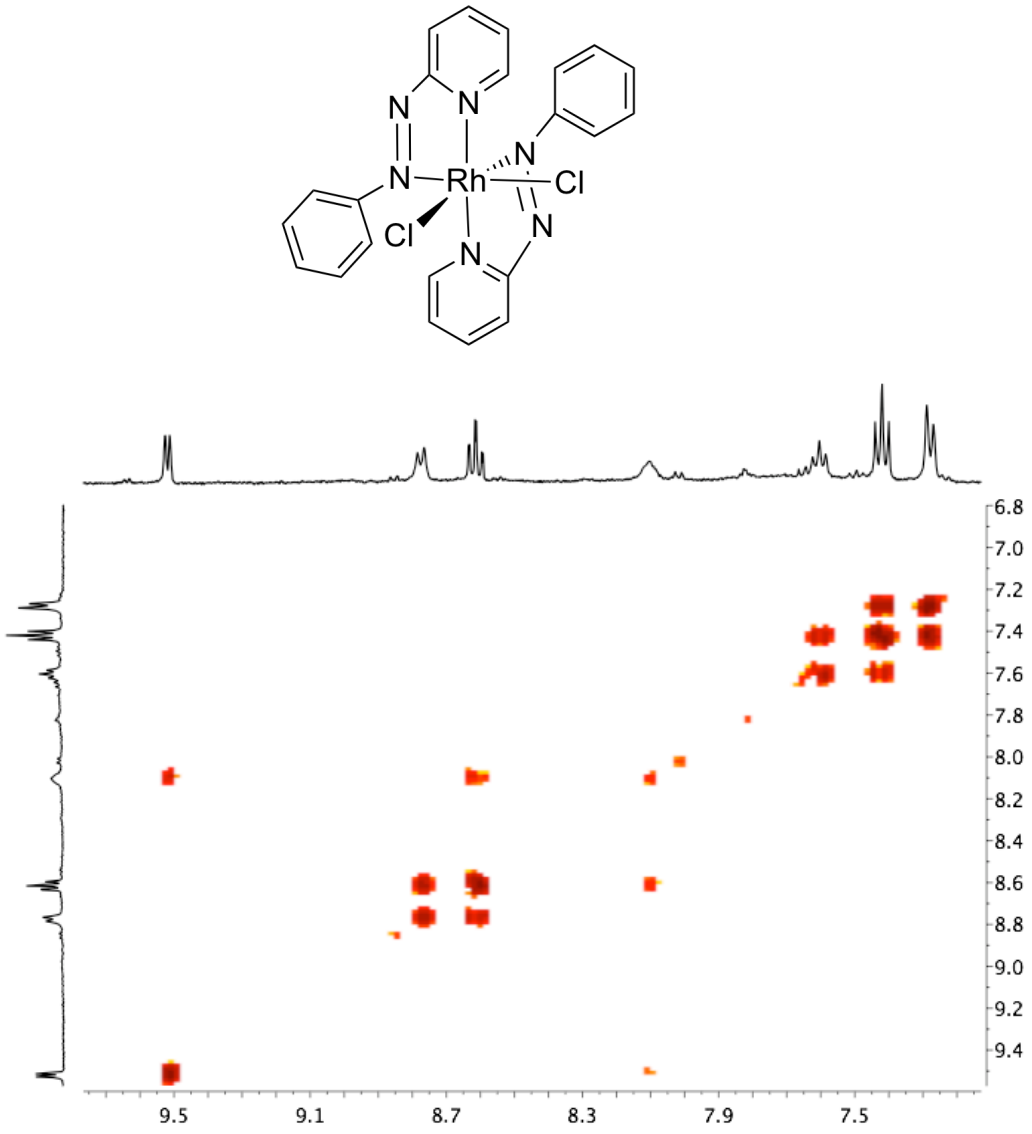

δ/ppm

A.17- 2D-NMR (COSY) of **10**

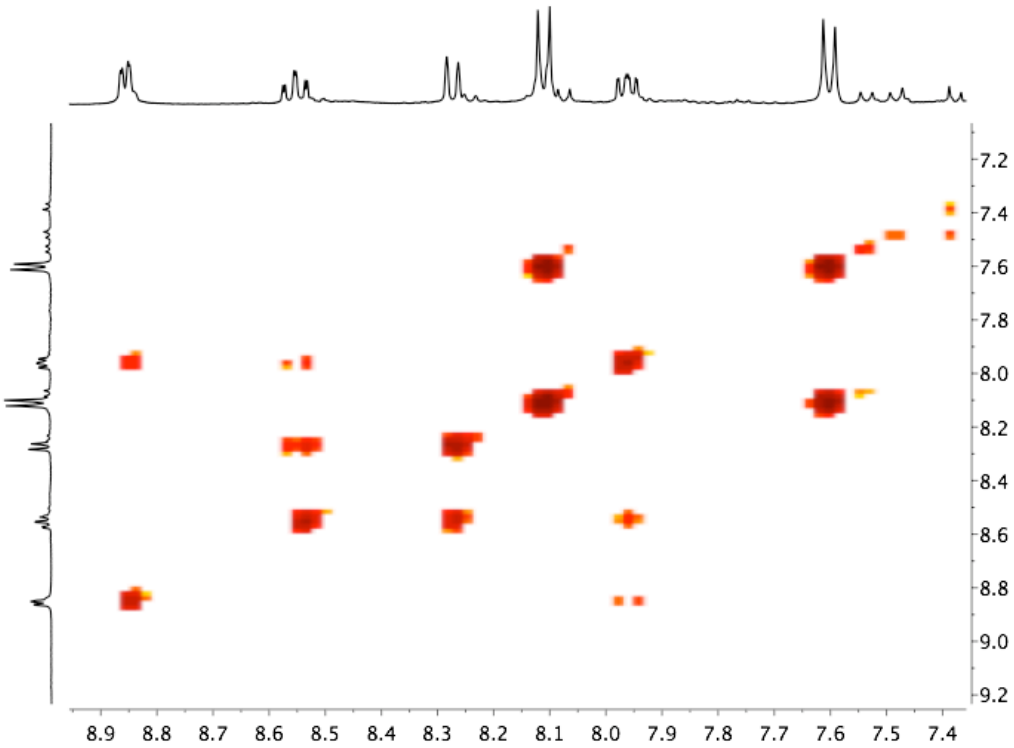

δ/ppm

A.18- 2D-NMR (COSY) of **11**

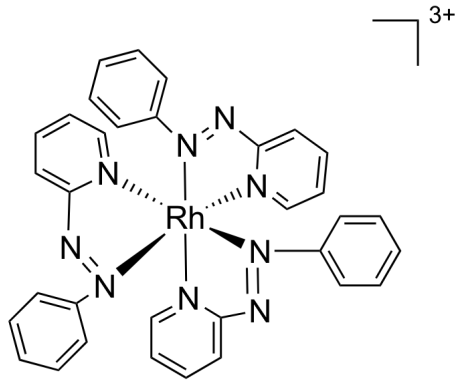

fac

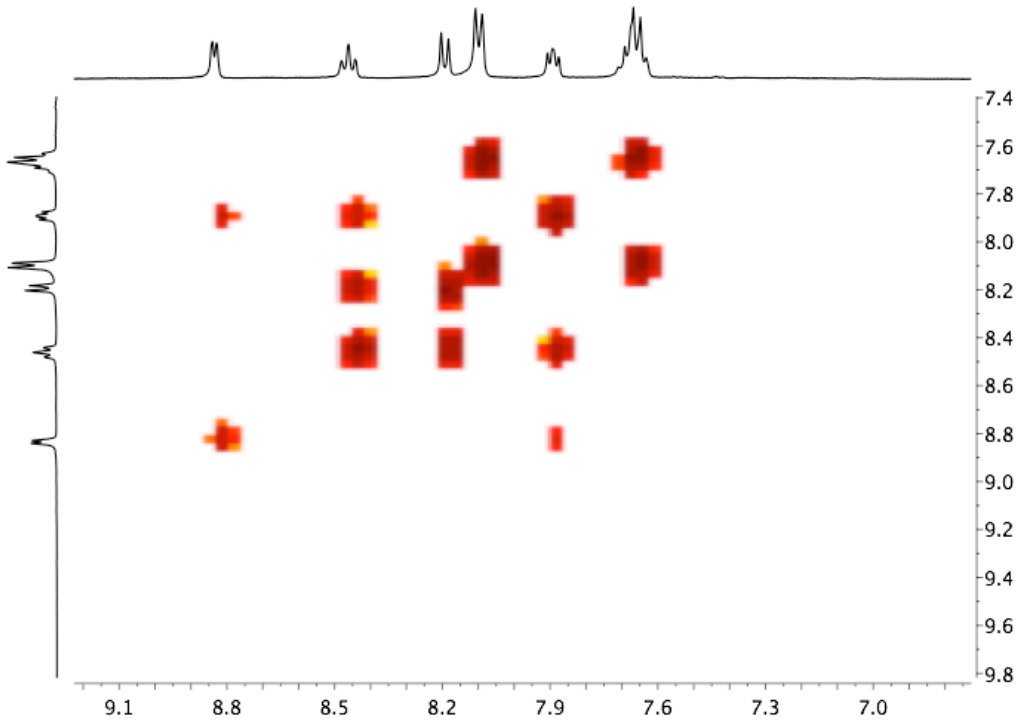

δ/ppm

A.19- Fitting curve for K_b value of complex **2**

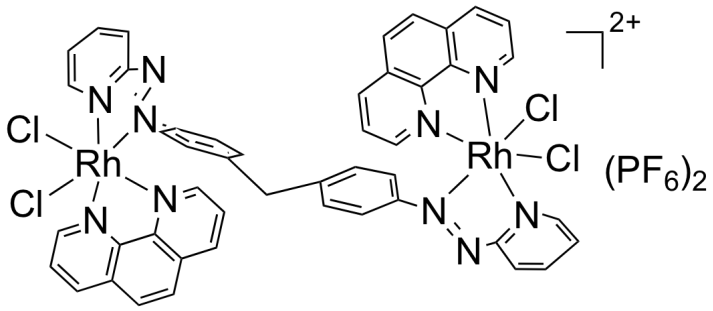

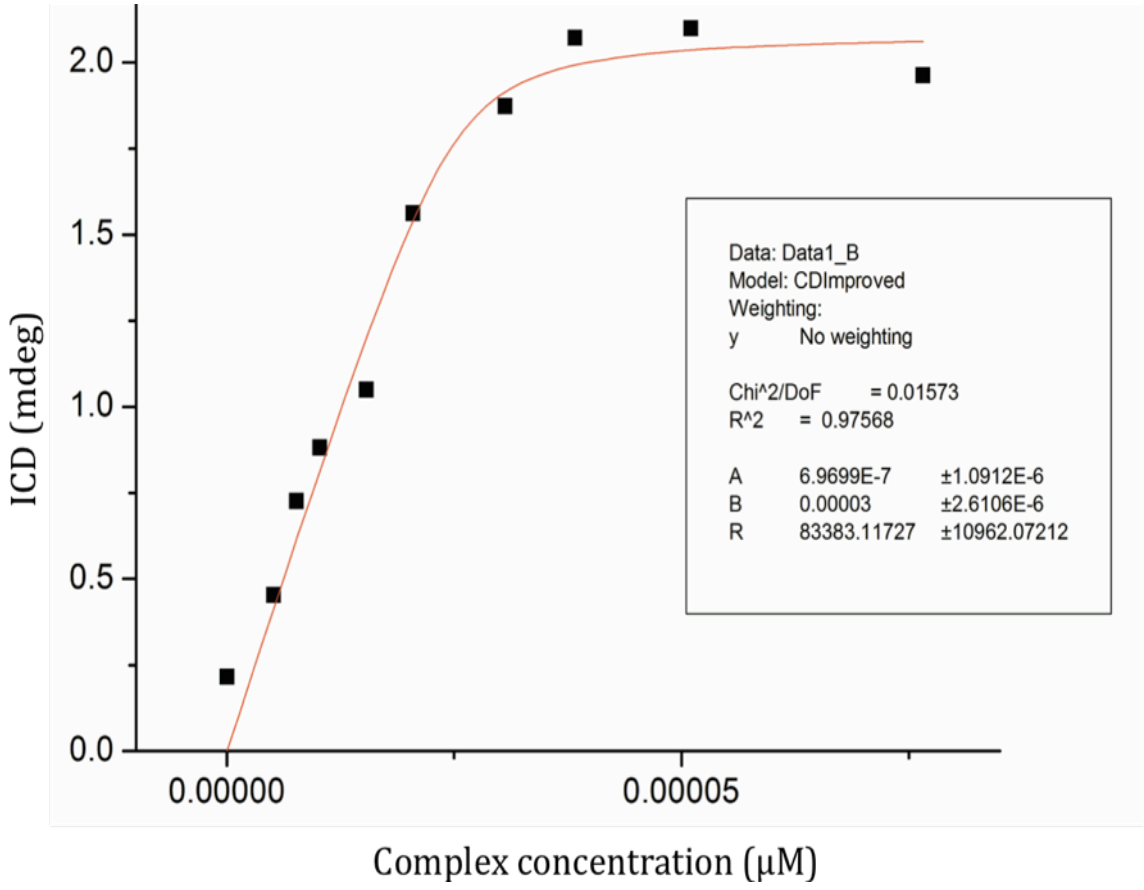

A.20- Fitting curve for K_b value of complex **7**

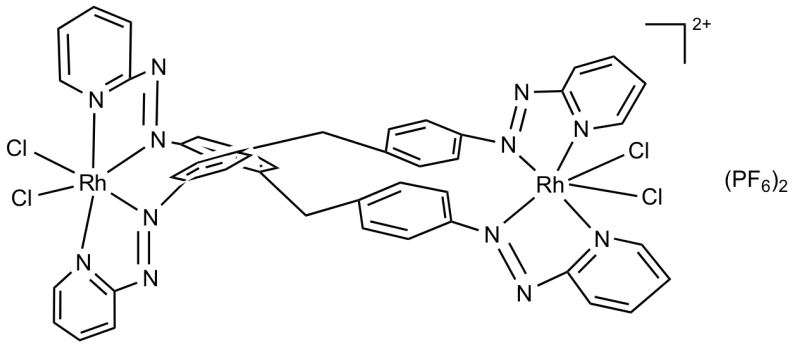

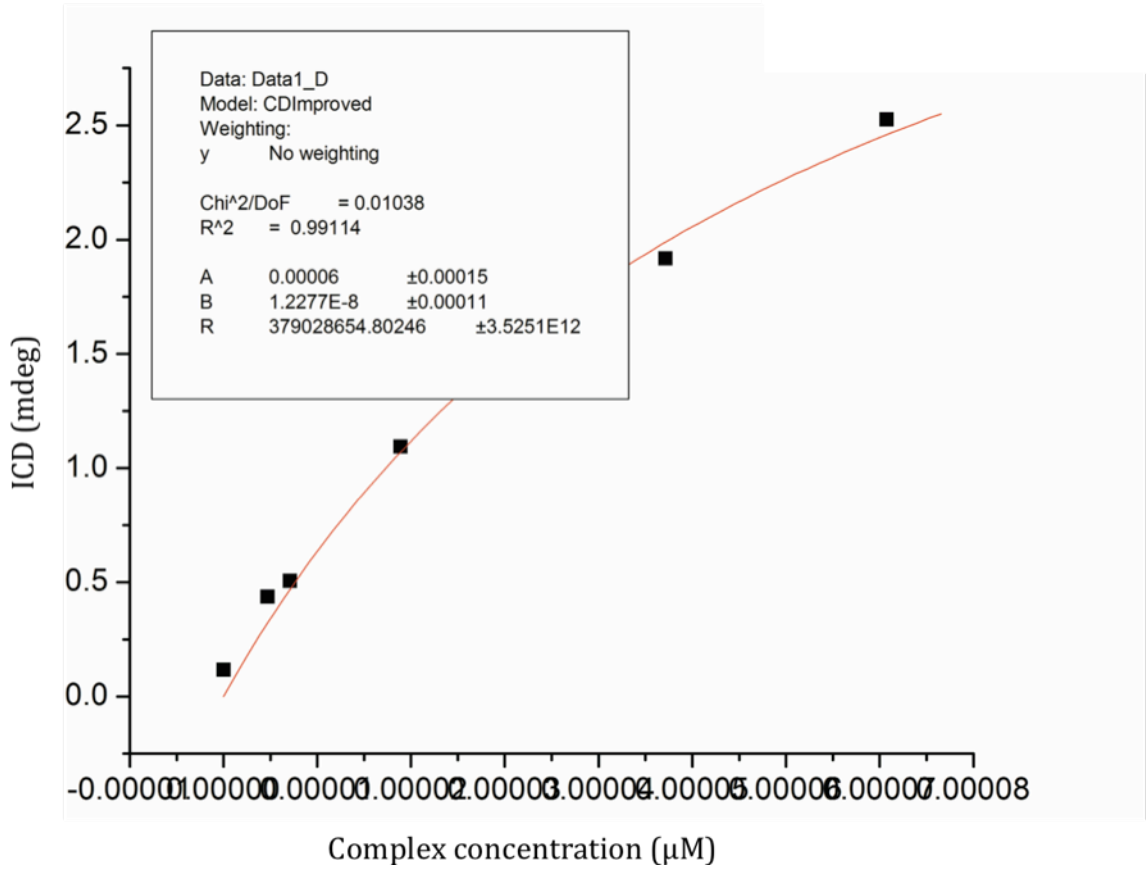

A.21- Fitting curve for K_b value of complex **8**

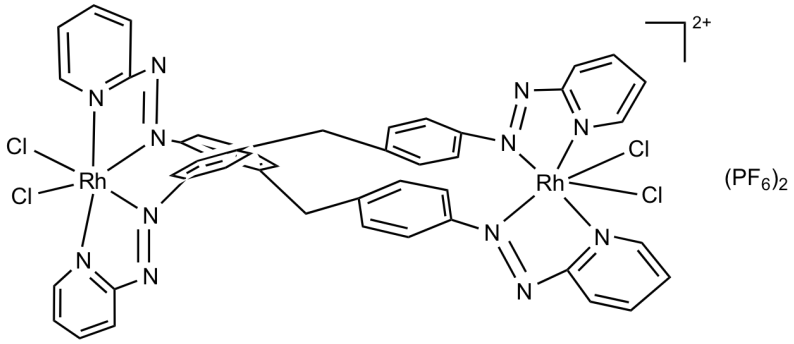

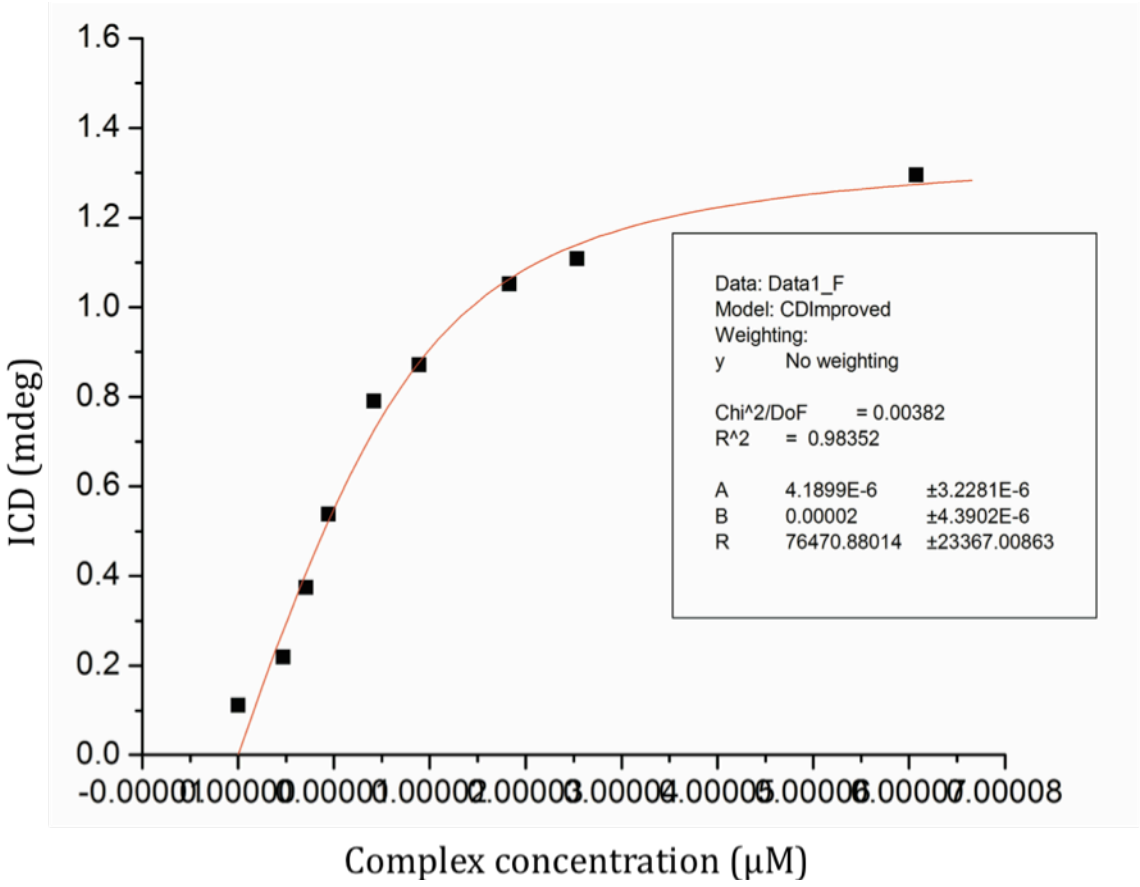

A.22- Fitting curve for K_b value of complex **10**

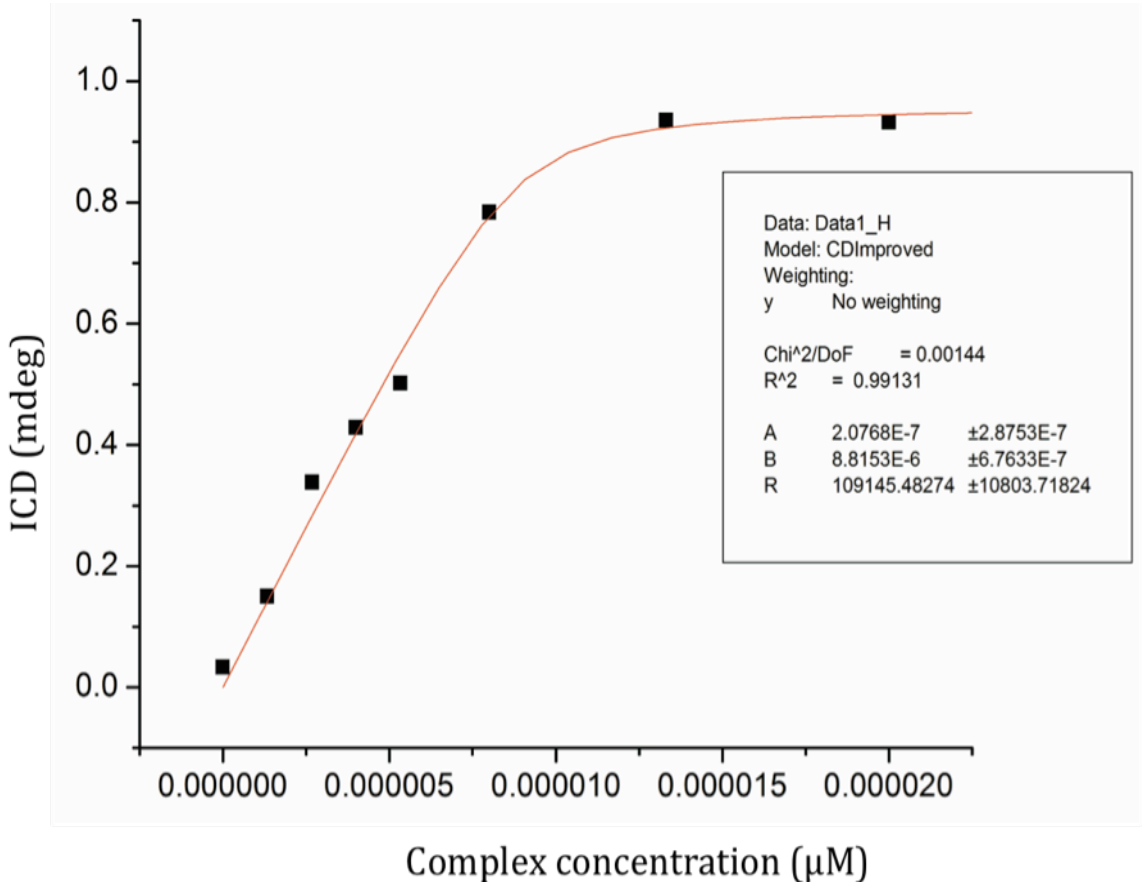

A.23- Electrophoresis Gel of complexes **1** and **2** under dark conditions.

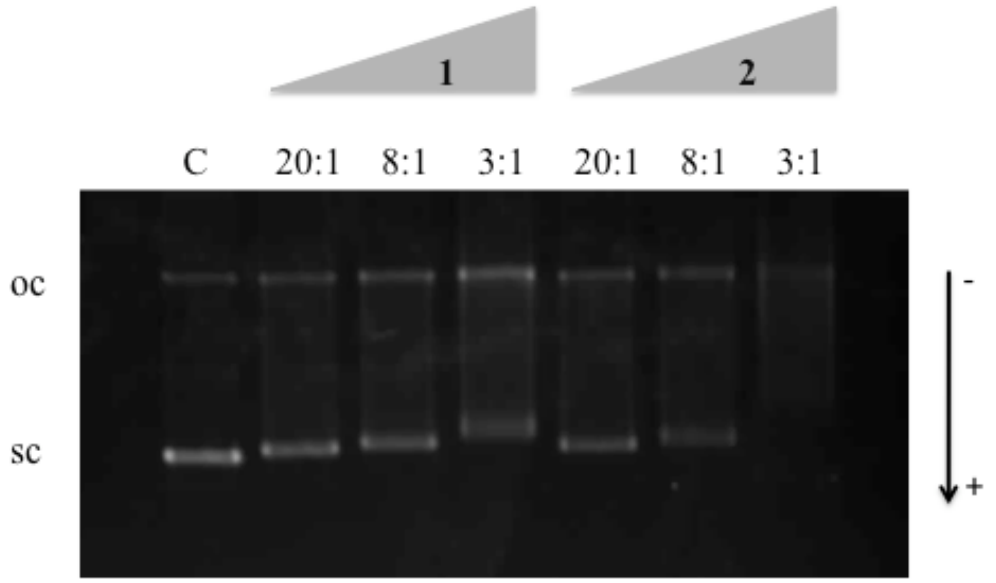

Agarose gel (1%) electrophoresis showing the changes in the electrophoretic mobility of the oc and sc forms of pBR322 plasmid DNA incubated for 2 hours at 37 °C under dark conditions with different ratios of complex **1** and complex **2**. Lane c, pBR322 plasmid DNA in absence of complex (control-c).

A.24- ESI-MS of complex **1**, 0 hours after incubation at 37 °C with 5-GMP (fresh).

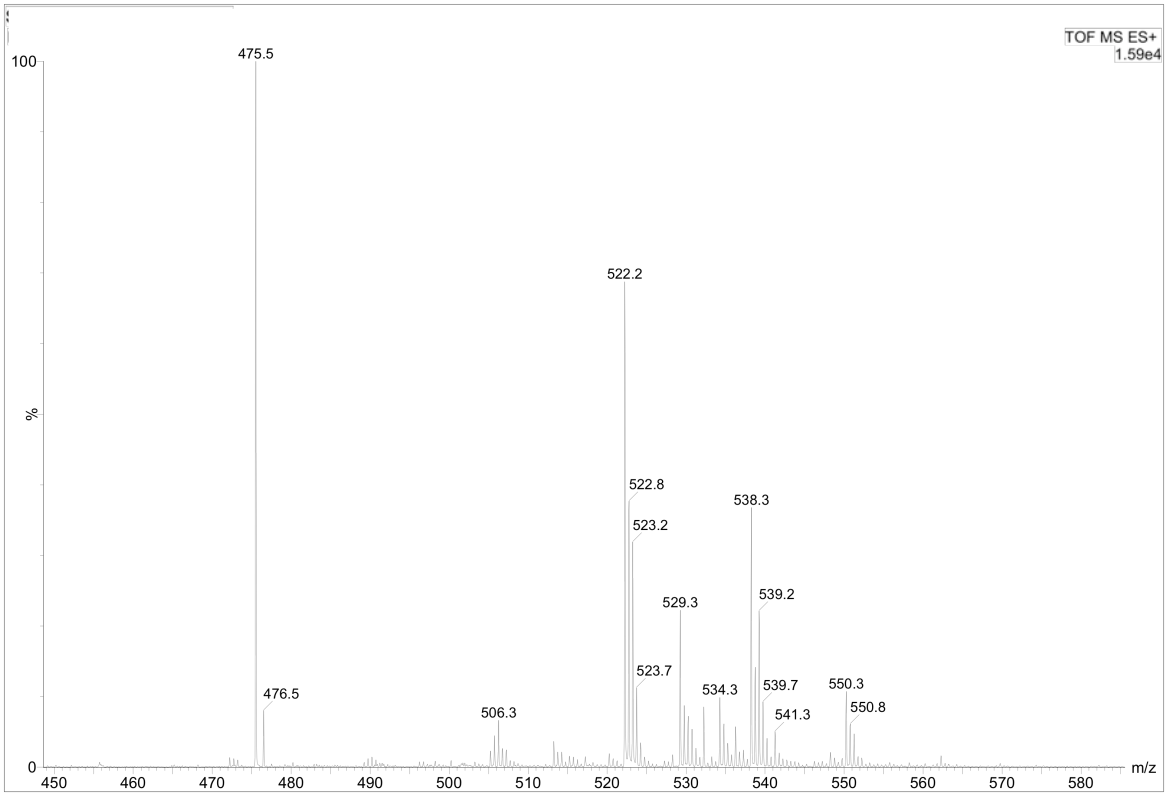

A.25- ESI-MS of complex **1**, 24 hours after incubation at 37 °C with 5-GMP.

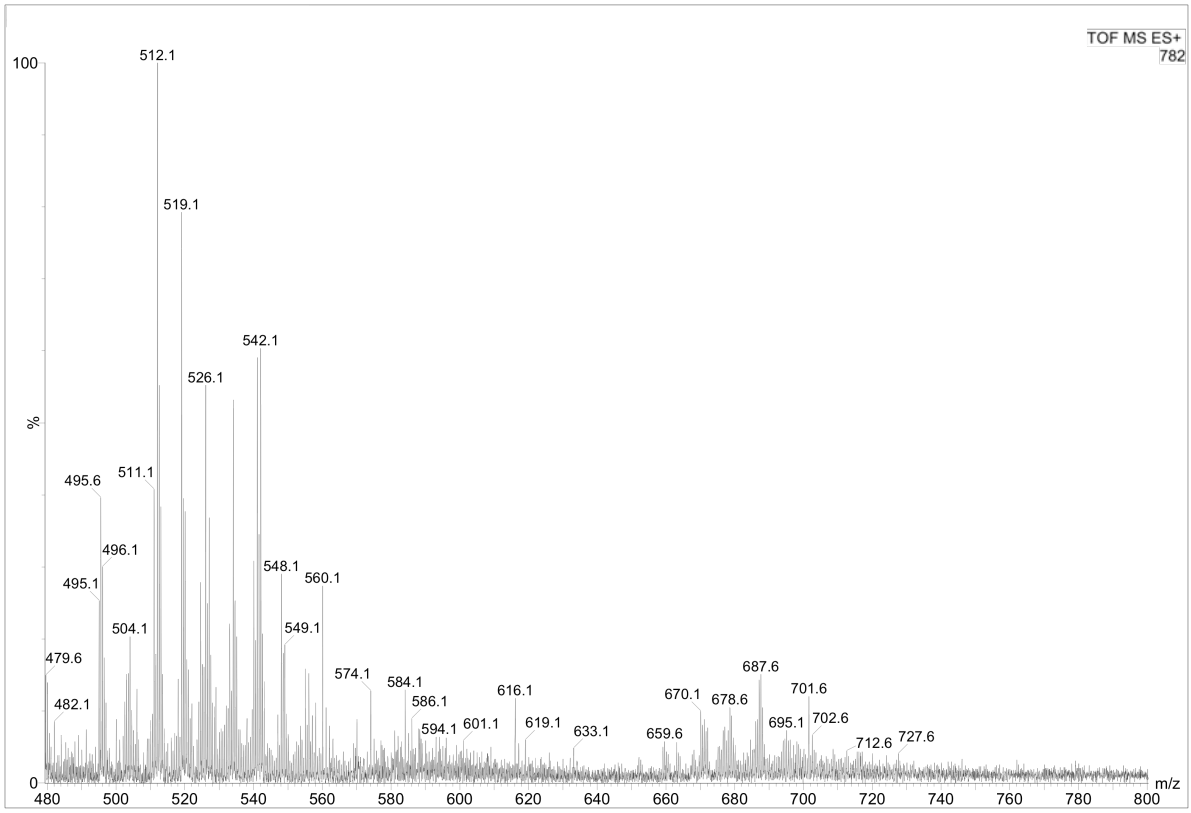

A.26- ESI-MS of complex **2**, 0 hours after incubation at 37 °C with 5-GMP (fresh).

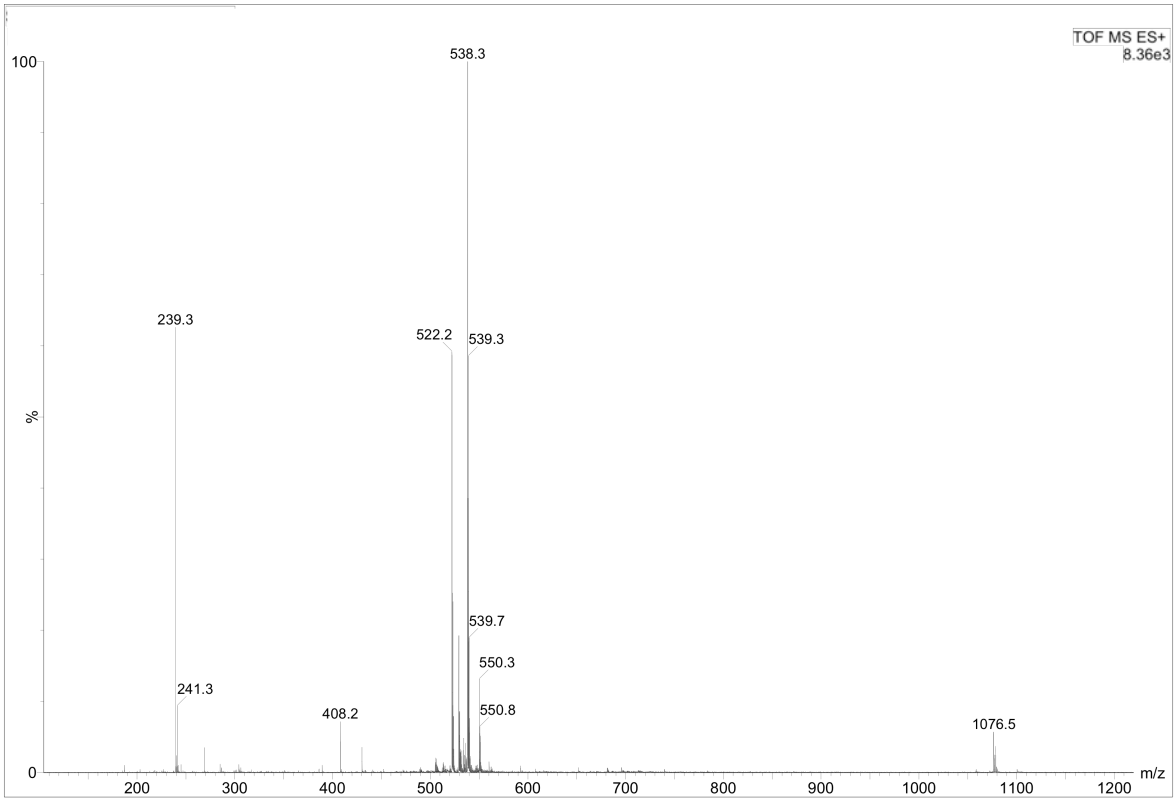

A.27- ESI-MS of complex **2**, 24 hours after incubation at 37 °C with 5-GMP.